



HAL
open science

Evaluation of the impact of a cavity upon an earth dike (analytical and numerical approaches): Application to the Val d'Orléans area (France)

Rafid Alboresha

► **To cite this version:**

Rafid Alboresha. Evaluation of the impact of a cavity upon an earth dike (analytical and numerical approaches): Application to the Val d'Orléans area (France). Other. Université de Lorraine, 2016. English. NNT: 2016LORR0025 . tel-01752229

HAL Id: tel-01752229

<https://hal.univ-lorraine.fr/tel-01752229v1>

Submitted on 29 Mar 2018

HAL is a multi-disciplinary open access archive for the deposit and dissemination of scientific research documents, whether they are published or not. The documents may come from teaching and research institutions in France or abroad, or from public or private research centers.

L'archive ouverte pluridisciplinaire **HAL**, est destinée au dépôt et à la diffusion de documents scientifiques de niveau recherche, publiés ou non, émanant des établissements d'enseignement et de recherche français ou étrangers, des laboratoires publics ou privés.



AVERTISSEMENT

Ce document est le fruit d'un long travail approuvé par le jury de soutenance et mis à disposition de l'ensemble de la communauté universitaire élargie.

Il est soumis à la propriété intellectuelle de l'auteur. Ceci implique une obligation de citation et de référencement lors de l'utilisation de ce document.

D'autre part, toute contrefaçon, plagiat, reproduction illicite encourt une poursuite pénale.

Contact : ddoc-theses-contact@univ-lorraine.fr

LIENS

Code de la Propriété Intellectuelle. articles L 122. 4

Code de la Propriété Intellectuelle. articles L 335.2- L 335.10

http://www.cfcopies.com/V2/leg/leg_droi.php

<http://www.culture.gouv.fr/culture/infos-pratiques/droits/protection.htm>



UNIVERSITE DE LORRAINE
Ecole Nationale Supérieure des Mines de Nancy
Laboratoire GeoRessources
Ecole Doctorale RP2E

THESE
Présentée en vue du grade de
DOCTEUR DE L'UNIVERSITE DE LORRAINE
en Génie Civil-Hydrosystèmes-Géotechnique
Par

ALBORESHA Rafid

**Evaluation of the impact of a cavity upon an earth dike
(analytical and numerical approaches)
Application to the Val d'Orléans area (France)**

**Évaluation de l'impact d'une cavité sur une digue en terre
(approches analytiques et numériques)
Application au cas du Val d'Orléans (France)**

Soutenue publiquement le 26 avril 2016

devant le jury composé de

M. Daniel DIAS	Professeur – Université de Grenoble	Rapporteur
M. Hussein MROUEH	Professeur – Université de Lille	Rapporteur
M. Adel ABDALLAH	Maître de Conférence – Université de Lorraine	Examineur
M. Yves-Laurent BECK	Ingénieur de Recherche – EDF-DT	Examineur
M. Marwan AL HEIB	Ingénieur de Recherche HDR – INERIS	Directeur de thèse
M. Olivier DECK	Professeur – Université de Lorraine	Co-directeur de thèse
M. David MATHON	Ingénieur de Recherche – CEREMA	Invité
M. Philippe GOMBERT	Ingénieur de Recherche – INERIS	Invité

Abstract

The objective of this thesis is to study the interaction mechanisms between a cavity resulting from a karst collapse and a fluvial dike. The question that arises here is to evaluate the potential role of cavities beneath the dikes and their impact on the dike stability in normal and extreme flood conditions. Therefore, the first main point of the present work is to create a method to assess the influence of a dike on the stability of a cavity beneath it. Thereafter the second main point is to evaluate the stability of the dike slope when a cavity appears underneath without taking into account the collapse of the cavity.

To achieve the objectives of the thesis, the dike effect on the cavity stability was investigated by studying the influence of the cavity location relatively to the dike and the interaction mechanisms, in the way to prioritize the geometric and geotechnical parameters for a better evaluation of the risk of dike failure. Numerical and analytical approaches were used. An application is described based on the in situ observations and data for the Val d'Orléans area (France). This area is protected against the Loire's floods by 52 km of earth dikes (levees), in this area, more than 600 karstic sinkholes from 0.5 to 20 m diameter have been identified.

The first results of the analytical method show that the cavity instability can significantly increase when the cavity is located under the centre of the dike, and this can affect the stability of the dike when the cavity is sufficiently close to it. We also show that there is a significant effect of the cavity on the dike slope stability, especially in the saturation state (i.e. during extreme floods): cavity collapse can then contribute to dike collapse.

A nonlinear numerical modeling (2D and 3D) was used to validate the analytical approach, and to highlight the influence of the different geometrical and geotechnical parameters of the dike and the cavity. The results of the numerical modeling confirmed those of the analytical method.

As operational conclusion, the results of the analytical model can be used to help assessing hazard due to the dike collapse taking into account the likelihood of an existing cavity, its position and diameter, and the thickness of the alluvium layer, regarding the data from the Val d'Orléans area.

Keywords: dike, karst, cavity, instability, analytical approach, modeling, Val d'Orléans, France.

Résumé

L'objectif de cette thèse est d'étudier les mécanismes d'interaction entre une cavité résultant d'un effondrement karstique et une digue fluviale. Il s'agit d'évaluer le rôle potentiel des cavités sous les digues et leurs effets sur ces dernières dans des conditions hydrologiques normales et extrêmes. Par conséquent, le premier point est de proposer une méthode pour évaluer l'influence d'une digue sur la stabilité d'une cavité sous-jacente. Le deuxième point concerne la stabilité de la pente de la digue quand une cavité est présente à proximité, sans prise en compte de l'effondrement de la cavité.

Afin d'atteindre les objectifs de la thèse, les influences respectives du positionnement de la cavité par rapport à la digue et des paramètres géométriques et géotechniques ont été étudiées, par des approches analytiques et numériques, pour une meilleure évaluation du risque de rupture de la digue. Une application est proposée, basée sur des observations in situ et des données disponibles pour le secteur du Val d'Orléans (France). Cette zone est protégée des crues de la Loire par 52 km de digues fluviales (les levées), il y a été recensé plus de 600 effondrements karstiques (fontis) de 0,5 à 20 m de diamètre.

Les premiers résultats obtenus par la méthode analytique montrent que l'instabilité de la cavité peut augmenter de manière significative lorsqu'elle est se trouve sous le centre de la digue et que cela peut affecter la stabilité de la digue lorsqu'elle en est suffisamment proche. Nous montrons aussi que le risque d'instabilité de la digue augmente en raison de l'apparition des fontis provenant de l'effondrement de cavités karstiques. Ces résultats indiquent qu'il y a un effet significatif de la cavité sur la stabilité de la pente, surtout dans le cas de matériaux saturés (c'est-à-dire en période de forte crue de la Loire) : autrement dit, l'effondrement de la cavité peut contribuer à la rupture de la digue.

Une modélisation numérique non linéaire (2D et 3D) a été utilisée pour valider l'approche analytique et permettre la compréhension de l'influence des différents paramètres géométriques et géotechniques de la digue et de la cavité. Les résultats de la modélisation numérique ont confirmé ceux de la méthode analytique. Ces derniers peuvent donc être utilisés dans l'évaluation du risque de rupture de la digue en tenant compte de la probabilité d'existence d'une cavité sous-jacente, de sa position, de son diamètre, mais aussi de l'épaisseur de la couche d'alluvions. Les données numériques prises en compte sont celles du Val d'Orléans.

Mots-clés : digue, karst, cavité, instabilité, approche analytique, modélisation, Val d'Orléans.

Acknowledgements

I thank all who in one way or another contributed in the completion of this thesis.

First and foremost, I offer my sincerest gratitude to my supervisor, Dr. Marwan Al Heib, who has supported me throughout my thesis with his patience and knowledge. I attribute the level of my PhD degree to his encouragement and effort and without him this thesis, too, would not have been completed or written.

I take this opportunity to express my deep gratitude to my co-supervisor, Professor Olivier Deck, who gave me greatly thrust to step back for a critical look at my work. His scientific rigor, patience, and valuable advice have allowed this work to succeed.

My thanks also go to Dr. Philippe Gombert for his responses and reflections that not only helped me to better understand the problem of the Karst and its network; but have been very beneficial to the framing of this doctoral research.

The jury of the thesis defense expanded my vision of the issues addressed in my work. I wish to express my sincere thanks to the jury members for their interest in this work and for their contribution to the discussions during the defense. I think of the professor Daniel Dias (the president of the jury) and the professor Hussein Mroueh for allowing me the honor of being the reviewers of my work as well as Dr. Adel Abdallah and Dr. Yves-Laurent Beck for accepting to evaluate the thesis.

Many thanks are due to Professor Thierry Verdel for his welcome in his team GOR, in the laboratory GeoRessources.

I thank my Ph.D. colleagues: (Mimi, Samar, Noémie, Clement, Jamil, Bakri, Jabrane and Thomas), their support and care helped me overcome setbacks and stay focused on my graduate study. I greatly value their friendship and I deeply appreciate their belief in me.

Many thanks are given to the Embassy of French in Baghdad for the provision of this opportunity to finish my graduate study. I thank the faculty of Engineering (in Anbar University) that nominated me to complete my Ph.D. in France. I appreciate the financial support from the Iraqi Ministry of Higher Education and Scientific Research and the administrative support from Campus France that make it possible for me to live and study in France.

Most importantly, none of this would have been possible without the love and patience of my wife (Hadeel) and my two children (Rahaf and Mohammed). I would like to thank all of my family in Iraq (my mother, my father, my two sisters and by brother), for their support all the time so that I can finish my thesis with great pleasure.

Finally, I cannot end the current section of acknowledgments without a thought for administrative staff that spared no effort to contribute. I would particularly like to say a big

thanks to Mrs. Brigitte Siatka who has always given her time to help me in solving administrative problems.

Table of contents

Abstract	3
Résumé	4
Acknowledgements	5
Table of contents	7
List of figures	10
List of tables	16
General introduction	17
Introduction générale	20
Chapter 1:Introduction and literature review	23
1.1 Historical evolution of karst and dikes knowledge.....	23
1.1.1 Karst.....	23
1.1.2 Cavities and sinkholes.....	25
1.1.3 Dikes	27
1.2 Literature review.....	28
1.2.1 Mechanism of karst and cavities collapse	28
1.2.2 Formation and stability of cavities	31
1.2.3 Stability of dikes.....	40
1.3 Geo-risk methodology.....	49
1.4 References.....	52
Chapter 2: The case study (dikes of Val d’Orléans)	58
2.1 The dikes of Val d’Orléans.....	58
2.2 The Val d’Orléans site.....	60
2.2.1 Site presentation.....	60
2.2.2 Geological context	61
2.2.3 Hydrogeological context.....	63
2.3 Sinkholes and subsidence (historical information).....	64
2.4 Mechanical properties of soils.....	67
2.5 Summary.....	69
2.6 References.....	71
Chapter 3: Effect of the dike upon the stability of the cavity	73
3.1 Introduction.....	73
3.2 Analytical approach of cavity collapse.....	73
3.3 Dike effect upon the stability of cavity.....	76
3.4 Calculation of the dike effect	77
3.5 Results analysis and discussion.....	78

3.6	Summary.....	84
3.7	References.....	86
Chapter 4: Effect of cavity upon the stability of the dike slope.....		87
4.1	Introduction.....	88
4.2	Method and objective.....	88
4.3	Slope stability analysis.....	90
4.3.1	The Ordinary method of slices.....	91
4.3.2	Verification of TALREN results.....	94
4.3.3	Initial safety factor of the dike of Val d'Orléans (without cavity).....	96
4.4	Modified method with a cavity underneath the dike	102
4.5	Application to the Val d'Orléans dike: safety factor of slope stability.....	106
4.6	Summary.....	114
4.7	References.....	115
Chapter 5: Numerical modelling (2D and 3D).....		116
5.1	Objective and method.....	117
5.2	General description of the dike of Val d'Orléans model in CESAR-LCPC.....	119
5.3	Slope stability calculation by the c-phi reduction method.....	122
5.3.1	The theoretical bases of the method	122
5.3.2	Slope stability calculation for the dike without cavities	123
5.3.3	Slope stability calculation for the dike with cavities.....	125
5.4	Calculation by standard method.....	126
5.4.1	Effect of the cavity on the slope stability	126
5.4.2	Effect of the dike upon the cavity stability	133
	a-Safety factor criterion.....	128
	b-Vertical displacement criterion.....	136
	c-Plastic strain criterion.....	133
5.5.1	Cavity underneath the centre of the dike	150
5.5.2	Cavity underneath the dike slope	152
5.5.3	Effect of the direction of the cavity.....	153
5.6.1	Cavity stability and collapse shape	156
5.6.2	Cavity effect upon the dike slope stability	159
5.7	Summary.....	160
5.8	References	156
Chapter 6:Expected scenarios due to collapsed cavity underneath a dike.....		163
6.1	Introduction.....	164
6.2	Scenario of isolated karstic caves.....	164
6.2.1	Scenario for one cohesionless alluvium layer.....	165

6.2.2	Scenario for one cohesive alluvium layer	166
6.2.3	Scenario for two alluvium layers	166
6.3	Scenario for cave connected to a karstic conduit.....	167
6.3.1	Scenario for one cohesionless alluvium layer.....	167
6.3.2	Scenario for one cohesive alluvium layer	169
6.3.3	Scenario for two alluvium layers	170
6.4	Water pressure effect and the final form of the cavity collapse	171
6.4.1	Resistance force against the water flow F_f	172
6.4.2	water flow force F	173
6.4.3	Application to the Val d'Orléans case	175
6.5	Summary.....	178
6.6	References.....	179
Chapter 7: General conclusion and perspectives.....		181
7.1	General conclusion.....	182
7.2	Perspectives.....	185
7.1	Conclusion générale.....	186
7.2	Perspectives.....	188
Appendix A: Presentation of UDEC.....		189
Appendix B: Cavities in elastic zone in the numerical model.....		192
Appendix C: The term Lambda in CESAR.....		195

List of figures

Figure 1 Global distribution of major outcrops of karstic terrains (the black zones) of the world (after Ford and Williams 2007).....	24
Figure 2 Map indices presence of karst with the layout of the main rivers, the Val d'Orléans is represented by the small gray rectangle (after the French geological survey BRGM).	24
Figure 3 Classification of sinkholes in karst environment (Waltham et al. 2005).....	25
Figure 4 Classification of subsidence and sinkholes: The pattern of the bedrock indicates the type of rocks in which the different sinkholes are commonly observed; sagging sinkholes in evaporites and the rest in both evaporites and carbonates. Sagging, which refers to progressive downward bending due to lack of basal support, is designated with the more general term subsidence by other authors (Gutiérrez et al. 2014).....	26
Figure 5 Effect of karst sinkholes on several civil structures. a- An aerial view of the damaged a highway in the State of Miranda (Venezuela) 2010 (Photo by Miranda Government/Reuters). b- A collapsed road surface in Guangzhou, Guangdong Province (China) 2008 (Photo by Reuters/China Daily) c- Sinkhole in the main road in Changsha (China), 2012 (photo by Quirky China News / Rex Features). d- Buildings collapse into a sinkhole, Clermont, Florida, USA 2013 (photo by Red Huber/Orlando Sentinel/MCT).	27
Figure 6 Classic two theories to explain the mechanisms of a brutal collapse of cavities. a- Theory of potential erosion. b- Vacuum suction erosion theory (after Waltham and Lu 2007; Parise 2008).....	29
Figure 7 Critical soil layer for sinkhole formation (Chan 1995).....	30
Figure 8 Evolution of a sinkhole (after Beck and Barry 1984).	31
Figure 9 3D Schematic to demonstrate the mechanical condition of a karst collapse. 1 Overlying strata; 2 Limestone; 3 Soil cavity; 4 Karstic cave; 5 Debris; 6 Compression stress and shear stress on the soil arch; 7 Groundwater level; 8 The total atmospheric pressure and additional dead load on the surface; 9 The dead weight of the overlying strata; 10 The total resistance force of collapse; it contains the cohesive strength and interfacial friction of the soil, etc.; 11 Buoyancy force of the soil; 12 Dynamic hydraulic force (according to Zhao et al. 2011).....	34
Figure 10 Mechanical conditions of a limit equilibrium arch of a soil cave. A The mechanical structure of a soil cave can be simplified as a limit equilibrium arch, where F the dynamic hydraulic force; G the deadweight of the cover layer; and P the atmospheric pressure. B The bending moment diagram of the soil arch. C The shearing force diagram of the soil arch (Zhao et al. 2011).....	34
Figure 11 A morphologic model of early sinkhole development based on observations of sinkhole form at Albany, USA (Hyatt et Jacobs 1996).....	35
Figure 12 Mechanism of hydrofracturing theory (a), pore pressure diagrams at the initial moment (b), intermediate stage of downward seepage (c) and final one (d). ΔH : water-table (the level of unconfined water); $\Delta H'0$ and $\Delta H0$: potentiometric level of karst water before and after water head decline; l: the span of a cave (rock void) at the base of karst overburden; h: the thickness of confining bed; t: time of downward seepage. Big arrow and small ones show respectively the propagation of crumbling front and the "shooting" of clay spalls and pieces from the roof of soil void (after Anikeev 1999).....	36

Figure 13 Stability chart, dimensionless stability number $N_c\phi$ with effect of angle of internal friction ϕ and inverted strength profile ($K_0=1-\sin \phi$).....	38
Figure 14 Overflow mechanisms (after Mériaux et al., 2001 cited by Serre, 2005).	42
Figure 15 The scour mechanisms (after Mériaux et al., 2001 cited by Serre 2005 and Keddouri 2011).....	43
Figure 16 Sliding of land side slope mechanism in downstream (after Mériaux et al., 2001 cited by Serre 2005 and Keddouri 2011).	43
Figure 17 Sliding of river side slope mechanism in upstream (after Mériaux et al., 2001 cited by Serre 2005 and Keddouri 2011).	44
Figure 18 Free body diagram for a grain soil in boiling state (after Bendahmane 2004).	45
Figure 19 Phenomenon of seepage erosion (after Pham 2008).....	45
Figure 20 Phenomenon of regressive erosion (Pham 2008).....	46
Figure 21 Phenomenon of cleaning (after Pham 2008).....	46
Figure 22 a-Phenomenon of piping (Pham 2008); b-hydraulic piping in earth dam (Lautrin 2002).....	47
Figure 23 Schematic illustration of the suffosion where the fine grains (light) are present in the pore space (white) of the coarse grains (dark) (after Rosenbrand, 2011).	48
Figure 24 (a) Distribution of failure mechanisms for dike in Hungary in the period 1954–2004 (Nagy and Tóth, 2005). (b) Distribution of identified failure mechanisms for dike in Saxony (Germany) during the August 2002 flood event in the Elbe catchment (Horlacher et al. 2005 cited by Vorogushyn 2009).	49
Figure 25 Sketch showing the adopted methodology of studying dike-cavity interaction.	51
Figure 26 Cross section of Loire dike about 1850 (Source: Media library of Orléans (Médiathèque d’Orléans)) (cited by Orsat 2013).	58
Figure 27 Typical cross sections of a Loire dike nowadays and the evolution of dimensions (d/s: downstream, u/s: upstream). a- oldest unreinforced dike; b- Loire side reinforced dike and c- land side reinforced dike (after Maurin 2012).....	59
Figure 28 Map showing the Val d’Orléans flood zone (grey) and dikes (red) (from: CEREMA).	61
Figure 29 Geological section of the Val d’Orléans (Caudron 1964).	62
Figure 30 A diver inside main conduits of the Val d’Orléans karst system - View taken inside the “Abîme”, one of the springs of Loiret (SSL: The Speleology Underwater Loiret Association, 2004).....	62
Figure 31 Map of alluvial thickness of the Val d’Orléans (sources: SCAN 25® - © IGN Paris - BSS BRGM interpolation "natural neighbors" by ARCGis).	63
Figure 32 Topography of karstic galleries upstream the Loiret’s springs (Boismoreau 2008).	64
Figure 33 Schema shows the difference between the terms sinkhole and subsidence in our work.....	65
Figure 34 Examples of recent karst collapses that occurred in toe of dike in upstream (a), in dike crest (b), on the dike body in downstream (c) and behind the dike, downstream (d) (Gombert et al. 2014).	66
Figure 35 Distribution of collapses and ruptures of dikes in the Val of Orléans (Gombert et al 2014).....	66

Figure 36 Histogram of the distribution of sinkholes (%) with respect to their distance to the Loire (m) (after Orsat 2013).	67
Figure 37 The four dike positions (in red points) that are mentioned in Table 3(after Saussaye and Durand, 2015 and IRSTEA, 2008).	69
Figure 38 Geological cross section and dimensions of the dike in site of Guilly and the soil underneath it. (after IRSTEA).	69
Figure 39 (a) Original karst cave and equilibrium roof arch of the cavity in the soil layer with D diameter (after Keqiang et al. 2004). (b) Mechanical analysis of the soil collapse column above the cavity.	74
Figure 40 Sketch showing main forces that affect the stability of a cavity underneath a dike.	77
Figure 41 Scheme of the dike with different cavity positions (from under toe of the dike until centre of the dike with p is function of the dike above the cavity).	78
Figure 42 Relation between the cavity position (p_i) and the safety factor (SF) in two hydraulic scenarios.	79
Figure 43 Safety factor (SF) due to the effect of the cavity diameter (D) for two cavity positions ($p_i=0$ and $p_i=6$ m) at extreme flooding scenario.	80
Figure 44 Relation between the alluvium thickness H underneath the dike and the critical diameter of cavity $D_{critical}$ for height of dike equals to 6 m.	81
Figure 45 Sinkhole propagation through the body of dike.	82
Figure 46 Safety factor for a cavity under the maximum height of the dike ($p_i=6$ m) in flood state with considering the dike resistance as an additional soil layer.	83
Figure 47 Relation between critical height of alluvium column above the arch of cavity ($h_{critical}$) and the diameter of cavities (D) with height of dike h_d equals 6 m.	83
Figure 48 Critical height of dike (h_d) for different diameter of the cavity ($H=4.5$ m).	84
Figure 49 Types of slope sliding/failures. a. face (slope) failure. b. toe failure. c. base failure (Dinesh 2008).	91
Figure 50 Geometry of Ordinary Method of Slices (after USACE 2003). Where dv and dh are the vertical and horizontal distance respectively between the resultant water force P over the top of the slice and the centre of the slip circle, b is the width of the slice.	92
Figure 51 Forces acting on the slice in ordinary method. a- without water case (dike is dry). b- with water case (after Zhou 2006). W is the weight of the slice, l is the length of the bottom of the slice and ϕ is the angle of the inclination of the bottom of the slice.	93
Figure 52 Sample slope stability problem (SLOPE/W, version 4).	95
Figure 53 Slope stability problem (technical manual of TALREN, version 4).	96
Figure 54 Scheme of the dike and underneath soils properties near Orléans (Maison Vieille, Guilly).	97
Figure 55 The effect of the water content upon the stability of cohesionless soils (sand) (after Nelson 2013).	98
Figure 56 Dike stability - safety factor of slope stability in annual flooding scenario calculations using TALREN	99
Figure 57 Combined effect of degree of saturation and clay content on the angle of internal friction (Al-Shayea 2001).	101

Figure 58 Combined effect of degree of saturation and clay content on the cohesion (Al-Shayea 2001).	101
Figure 59 The result of safety factor of slope stability in flooding (centennial) case calculations in TALREN.	102
Figure 60 Presence a cavity underneath the lowest point of the slip surface, h_s is the vertical distance between the lowest point of the slip surface and the ground surface.	103
Figure 61 Stresses around a circular hole in an isotropic (a) or anisotropic (b) initial stress field.	104
Figure 62 Scheme to clarify the angles used in the calculation of the effect of a cavity on the safety factor.	106
Figure 63 Safety factor (SF) function of the vertical distance between the slip surface and the cavity (d) in a centennial flooding scenario for three different states of the coefficient of lateral earth pressure (K).	109
Figure 64 Safety factor (SF) function of the vertical distance (d) in a flooding scenario (K=0.5).	111
Figure 65 Relation between the critical vertical distance ($d_{critical}$) and the diameter of the cavity (D) according to the results of the Figure 64.	112
Figure 66 Safety factor (SF) function of the diameter of the cavity (D) in a flooding scenario (K=0.5). Values of d were calculated from Equation (4.15).	113
Figure 67 The critical vertical distance ($d_{critical}$), the diameter of the cavity (D) and the safety factor (SF) relation in 3D.	113
Figure 68 Dimensions of the FEM numerical model of the dike of Val d'Orléans, soil and limestone layers.	119
Figure 69 Boundary conditions used for CESAR 2D (u: horizontal and v: vertical displacement) & 3D models (u and v: horizontal and w: vertical displacement).	120
Figure 70 General parameters for the MCNL module calculation in CESAR-V6.	120
Figure 71 Mohr-Coulomb yield surface after strength reduction, c and ϕ are the initial cohesion and friction angle, c_r and ϕ_r are the reduced cohesion and friction angle,	123
Figure 72 Cross section of the dike of Val d'Orléans with finite element dimensions equal to 0.5 m.	124
Figure 73 Isovalues of the plastic strain norm for the dike of Val d'Orléans by using the c-phi reduction method in CESAR with finite element dimensions equal to 0.5 m. The dotted lines refer to the range of potential failure surface, while the red line refers to the failure surface got from the ordinary method (TALREN software).	125
Figure 74 Position of the cavity relative to the dike slope by assuming the same slip surface that the one got from the analytical approach.	127
Figure 75 Plastic strain norm results of a cavity with a 0.5 m diameter, underneath the slope of the dike.	129
Figure 76 Plastic strain norm results of a cavity with a 1 m diameter, underneath the slope of the dike.	130
Figure 77 Plastic strain norm results of a cavity with a 1.5 m diameter, underneath the slope of the dike.	131
Figure 78 Plastic strain norm results of a cavity with a 2 m diameter, underneath the slope of the dike.	132

Figure 79 Positions of the two points used to calculate SF by Mohr circle method.	134
Figure 80 Mohr circle in elastic state with minimum and maximum principal stresses σ_1 and σ_2 , respectively. The envelop of failure for the cohesionless alluvium layer ($c = 0$).	134
Figure 81 Mohr circle in elastic and elasto-plastic states for the point 1 in case of a cavity diameter equal to 2 m underneath the dike.	136
Figure 82 The chosen points used to monitor the vertical displacement.	136
Figure 83 Isovalues of the plastic strain norm for an pre-existed cavity with a 0.5 m.	140
Figure 84 Isovalues of the plastic strain norm for an pre-existed cavity with a 1 m.	141
Figure 85 Isovalues of the plastic strain norm for an pre-existed cavity with a 1.5 m.	142
Figure 86 Isovalues of the plastic strain norm for an pre-existed cavity with a 2 m.	143
Figure 87 Isovalues of the plastic strain norm for a cavity with a 2 m diameter underneath the mid of the dike (the cavity is later than the dike).	144
Figure 88 Effect of the dike presence on the isovalues of the plastic strain norm for a 1 m diameter cavity and different positions away from the dike toe.	147
Figure 89 Relation between the position of the cavity with 1 m of the diameter relative to the dike toe and the vertical displacement due to the dike presence in the crest point of the arch of the cavity.	147
Figure 90 Isovalues of the plastic strain norm of the dike of Val d'Orléans with using the c - ϕ reduction method in CESAR-3D. The dotted lines show the position of potential failure surfaces.	149
Figure 91 Considered shape of the cavity in CESAR/ 3D. D refers to the diameter of the cavity.	149
Figure 92 Isovalues of the plastic strain norm for a longitudinal section of the dike model in CESAR-3D in normal scenario (only half of the 3D model is shown).	151
Figure 93 Isovalues of the plastic strain norm for a longitudinal section of the dike model in CESAR-3D in normal scenario (half of the 3D model is shown).	153
Figure 94 Isovalues of the plastic strain norm for the dike model in CESAR 3D in normal scenario. The cavity is perpendicular to the dike axis (x -axis).	154
Figure 95 Isovalues of the plastic strain norm for the dike model in CESAR-3D in normal scenario. The conduit is perpendicular to the dike axis (x -axis).	155
Figure 96 Instability and failure collapse in the case of inclined surfaces and particle zone.	157
Figure 97 Instability and failure collapse in the case of vertical discontinuities and particle zone.	158
Figure 98 Vertical displacements due to the cavity and the collapse of the dike and the alluvium layer (max. vertical displacement = 5 m, min. vertical displacement = 0 m), the sinkhole on the surface = 2 m.	158
Figure 99 Sinkhole on the head of the dike of Val d'Orléans in area of Jargeau (Dore and Mathon 2011).	159
Figure 100 Isolated karstic cave scenario with one cohesionless soil layer. a- Initial state: formation of the cavity; b- Final state: frustum shape propagation in the cohesionless soil layer and subsidence of the dike head; c- Likelihood of overflow due to the subsidence in flood period. h_a is the height of the cavity arch, c is the cohesion and ϕ is the friction angle of soils.	165

Figure 101 Isolated karstic cave scenario with one cohesive soil layer; a- Initial state: formation of the cavity; b- Final state: cylindrical propagation in the cohesive layers. 166

Figure 102 Isolated karstic cave scenario with two soil layers (with and without cohesion). a- Initial state: formation of the cavity; b- Cylindrical propagation into the cohesive soil layer; c- Final state: frustum shape propagation in the cohesionless soil layer and subsidence of the dike head; d- Likelihood of overflow due to the subsidence in flood period. h_a is the height of the cavity arch, c is the cohesion and ϕ is the friction angle of soils. 167

Figure 103 karstic cave connected to a karstic conduit scenario with one cohesionless soil layer a- Initial state: formation of the cavity; b- Final state: with crammed chimney by the collapsed soil; c- Final state: without collapsed soil in the chimney. 169

Figure 104 Sketch used to illustrate hypothesis of comparison between the volume of collapsed soil V_1 from the chimney and the expected volume to be filled of the karstic conduit underneath the cavity V_2 169

Figure 105 karstic cave connected to a karstic conduit scenario with one cohesive soil layer a- Initial state: formation of the cavity; b- Final state: with crammed chimney by the collapsed soil; c- Final state: without collapsed soil in the chimney. 170

Figure 106 karstic cave connected to a karstic conduit scenario with one cohesionless soil layer; a- Initial state: formation of the cavity; b- Intermediate state: upward progression in the soil layers after the arch falling; c- First expected final state: sinkhole occurrence at the surface of the dike with partially filled chimney by the collapsed soil. d- Second expected final state: sinkhole with opened chimney. 171

Figure 107 The phenomenon of valve closure applied in the karstic conduit. a- Before the collapse of the cavity roof. b- After the collapse of the cavity roof and falling in the conduit. 173

Figure 108 Scheme illustrated the forces that effect upon the collapsed soil mass in the karstic conduit. 173

Figure 109 Considered geometry and properties to assess the force of the water flow on the collapsed soil into a karstic conduit. 175

List of tables

Table 1 Summary of the literature review about the cavity stability in overburden soil.....	38
Table 2 Classification of dikes according to Article R. 214-113 (2007) (in France).....	60
Table 3 Mechanical parameters of the dike and alluvium materials nowadays in the Val d'Orléans with cohesion c and the angle of internal friction ϕ . All boreholes of the tests were taken starting from the head of the dikes.	68
Table 4 Ranges of H/D critical ratio dependent on Figure 44.....	81
Table 5 Results of verification for the example presented in the Figure 4.5.....	95
Table 6 Results of the critical safety factor (SF=1) calculations for the Val d'Orléans dike.	109
Table 7 Mechanical properties of the soil, limestone and the dike materials.....	119
Table 8 Methodology for investigating the dike-cavity interaction in CESAR.	121
Table 9 Results of the safety factor SF of the dike of Val d'Orléans in dry state by using the ordinary method (Fellenius and Bishop) and a numerical method (c-phi reduction method), FE: finite element method, FD: finite difference method.	124
Table 10 Steps to study the effect of the cavity upon the dike slope in CESAR.	127
Table 11 Summary of the numerical calculation results of the cavity effect on the dike slope from CESAR. The plastic strain is in micro-deformation.....	132
Table 12 Results of the safety factor calculation from the Mohr circle method in elastic state. Point 1 & 2 are shown in Figure 79.	135
Table 13 Results of the vertical displacement.	137
Table 14 Steps of calculation to study the effect of the dike upon the cavity stability in CESAR.	138
Table 15 Objectives of the 3D simulations in CESAR and the methods that are used.	148
Table 16 the results of (F/Ff) calculations when the karstic conduit Dk is equal to 1 m (Ff=185 kN).....	177
Table 17 the results of (F/Ff) calculations when the karstic conduit Dk is equal to 1.25 m (Ff=170 kN).....	177
Table 18 Summary of the proposed scenarios and their consequences.....	179

General introduction

The topic of the thesis concerns the vulnerability of dikes located in karst areas. It is based on the case study of the fluvial dikes of the Loire in the Val d'Orléans. These dikes are built on sandy-clay alluvium formation that over the karstified limestones of Beauce. In the Val d'Orléans, almost 600 collapses have been identified on an area of 167 km². Some of these collapses caused severe damages to infrastructures and buildings: if they appear under a dike during a major flood, they can affect the security and the safety of the population, and the economic activities.

The limestone layer which contains caves does not directly correspond to the foundation of the dike because of the intermediate alluvium layer. The presence of a cave in the karstic strata, underneath the dike, contributes to affect the alluvium layer and to weaken the dike foundation: subsidence or sinkhole can thereby affect the dike stability. Slope failures can be minor or they can be significant enough to result in the complete collapse of the dike.

Hydraulic structures including dikes are designed to protect people against flooding. They must be stable against the internal and external loads during the period of services (USACE 2006, CEPRI 2007). The presences of karstic network or cavities created by animals are actually not considered in the stability studies.

The evaluation of the mechanical influence of karstic caves on the dike stability is difficult to quantify (Degoutte 2012) as these natural caves can, because of dissolution and progressive degradation, reach important dimensions like some massive limestone caverns.

Due to the uncertainties relative to the position of the cavities underneath the dike and the limitation of the knowledge relatively to cavity-dike interaction, it is difficult to have a clear idea about the role of these cavities on the dikes stability. Different investigations and actions are carrying out in France to assess the localization and the dimensions of cavities. A database of the historic collapses in Val d'Orléans and their consequences is also considered.

The main objective of this thesis is to perform a mechanical study of the interaction mechanisms between a dike and a cavity formed in alluvial layer. The question that arises here is to evaluate the potential role of the cavities beneath the dikes and their impact on the dike stability in extreme flood and normal conditions. Therefore, the first central issue of the present work is to suggest a methodology to assess the influence of a dike over the stability of a cavity beneath, based on analytical tools. Thereafter, the second main issue is to evaluate the stability of the dike (rotational failure of slope on circular slip surface) when a cavity appears underneath without taking into account the collapse of the cavity. The analytical solution of Kirsch (1898) that addresses the influence of a circular cavity over the stress field was considered to modify the slope failure analysis (Fellenius method) and allow the determination of a safety factor of the dike stability that takes into account the cavity. The validation of the methodology will be investigated through 2D and 3D numerical modellings

and in-situ observations. The objectives of the thesis can be summarized in the following points:

- 1- Study the reverse interaction between the cavity and the dike in term of the mechanism of instability of the cavity and of the dike.
- 2- Identify the main parameters of the cavity that may have a significant influence on the dikes stability.
- 3- Suggest some recommendations to evaluate the effect of cavities upon the stability of dikes.

The scientific steps are based on the state of the art, and on some analytical and numerical tools. The analytical tools offer the main advantage to may be applied in a large area and different situations to allow the risk assessment. Numerical tools have the advantage to understand a more realistic cavity-dike interaction. The in-situ observations are the guarantee of the validation of the obtained analytical and numerical results.

To achieve these objectives, this thesis is composed of seven chapters, they are organized as following:

The chapter 1 presents firstly the historical evolution regarding karst and dikes knowledge. Then, the literature review about the mechanisms and the causes of the cavities collapse and the dike failure is presented. In the end of the chapter, we discuss the geo-risk methodology that is adopted to study the instability hazard and the interaction between cavities and dikes.

The chapter 2 is dedicated to present the case study of this thesis: the geological, hydrogeological and geomechanical characteristics of Val d'Orléans area are described. Then, the configuration of Guilly site is adopted as a case study for our calculation taken into account the data available to validate the methodology (dike-cavity interaction). Parametric studies overcome the limitation and allow the generalization of the developed methodology.

The chapter 3 studies the stability of a cavity with taking into account the effect of an overlying dike. Hence, an existing analytical approach based on the limit equilibrium and limit analysis is improved. The modification of the analytical approach allowed the assessment and the prediction of the risk of collapse due to the cavity position and dike geometry, in term of safety factor. Sensitivity analyses are carried out based on the collected data from in situ observations and data analysis.

The chapter 4 studies the impact of the cavity upon the dike slope stability by using two analytical solutions for the slope stability and the cavity influence. The first is the Fellenius' method (Ordinary method) for the slope stability analysis and the second the Kirsch's solution for the stress variation around a circular hole. Different assumptions were adopted to allow the application of the analytical solution in the case of a circular cavity. The safety factor equations of the slope stability were modified to take into account the modification of stresses induced by the cavity underneath the dike.

The chapter 5 is dedicated to verify the results of the analytical models in the two previous chapters (chapter 3 and 4) by using numerical models. CESAR-V6 (2D and 3D) finite element software is used. The different life steps of the dike were simulated and the evolution of stability and instability were analysed and discussed. Different approaches are discussed to analyse the obtained results of the numerical model (stresses, displacements and plastic deformation strains). The plastic deformation criterion is used as a main failure indicator.

The chapter 6 discusses the several possible scenarios of the influence of the cavity underneath a dike based on the obtained results, the feedback and in-situ observations. These scenarios mainly depend on two factors: the first one is the soil type underneath the dike (cohesive or non-cohesive) and the second one is the connection between the cavity and the karstic conduit. The dike was considered built with a cohesive soil. Several equations are detailed to calculate the water force that act on the collapsed soil mass in the case of a cavity linked with a karstic conduit.

The chapter 7 is devoted to the general conclusion, to discuss the suggested methodology, the operational recommendations to risk assessments and finally the perspective of the thesis.

Introduction générale

Le sujet de recherche de la thèse concerne la vulnérabilité des digues situées en zones karstiques. Il est basé sur l'étude de cas des digues fluviales de la Loire dans le Val d'Orléans. Ces digues sont construites sur une formation d'alluvion sablo-argileux reposant sur les roches calcaires karstifiées de Beauce. Dans le Val d'Orléans, environ 600 effondrements (fontis) ont été identifiés sur une superficie de 167 km². Certains de ces effondrements ont causé des dommages graves à des infrastructures et des bâtiments : s'ils apparaissent sous une digue pendant une inondation majeure, ils peuvent mettre en péril la population et les activités économiques.

La couche de calcaire qui contient les cavités karstiques ne correspond pas directement à la fondation de la digue en raison d'une couche d'alluvion intermédiaire. La présence d'une cavité dans le calcaire, sous la digue, peut affecter la couche d'alluvion et affaiblir les fondations et la stabilité de la digue. Une instabilité des pentes de la digue pourrait être suffisamment importante pour entraîner l'effondrement complet de la digue.

Les ouvrages hydrauliques y compris les digues sont conçues pour protéger les personnes contre les inondations. Ils doivent être stables contre les charges internes et externes au cours de la période de services (USACE 2006, CEPRI 2007). La présence de réseaux ou cavités créées d'origine karstiques ne sont pas réellement pris en compte dans les études de stabilité.

L'évaluation de l'influence mécanique des cavités karstiques sur la stabilité de la digue est difficile à quantifier (Degoutte 2012) dans la mesure où ces cavités naturelles peuvent atteindre des dimensions importantes suite à la mise en œuvre de processus de dissolution et de dégradation progressive.

En raison des incertitudes relatives à la position des cavités en dessous de la digue et de la limitation des connaissances relatives à l'interaction cavité-digue, il est difficile d'avoir une idée claire sur le rôle de ces cavités sur la stabilité des digues. Différentes enquêtes et actions ont été menées en France pour estimer la localisation et les dimensions des cavités. Une base de données des effondrements historiques dans le Val d'Orléans et de leurs conséquences a été réalisée.

Le principal objectif de cette thèse est de réaliser une étude mécanique des mécanismes d'interaction entre une digue et une cavité formée dans la couche d'alluvions. La question qui se pose ici est d'évaluer le rôle potentiel des cavités sous les digues et leur impact sur la stabilité de la digue en situation de crue extrême ou en conditions normales. Par conséquent, la première question centrale de ce travail est de proposer une méthodologie pour évaluer l'influence d'une digue sur la stabilité des cavités, en se basant sur des outils analytiques. Par la suite, la deuxième question principale est d'évaluer la stabilité de la digue quand une cavité apparaît en dessous sans prendre en compte l'effondrement de la cavité. La solution analytique de Kirsch (1898) qui porte sur l'influence d'une cavité circulaire sur le champ de contraintes a été considérée pour modifier l'analyse de la stabilité de la pente (méthode de Fellenius) et

pour permettre la détermination d'un facteur de la stabilité de la digue qui prend en compte la cavité. La validation de la méthodologie sera étudiée par modélisation numérique 2D et 3D et des observations in situ. Les objectifs de la thèse peuvent être ainsi résumés dans les points suivants :

- 1- Étudier l'interaction entre la cavité et la digue en termes de mécanisme d'instabilité de la cavité et de la digue.
- 2- Identification des principaux paramètres de la cavité qui peuvent avoir une influence significative sur la stabilité des digues.
- 3- Suggestions et recommandations pour évaluer l'effet des cavités sur la stabilité des digues.

Les démarches scientifiques sont basées sur l'état de l'art, ainsi que sur certains outils analytiques et numériques. Les outils analytiques offrent l'avantage principal d'être facilement applicables à un grand nombre de situations, permettant de contribuer à l'évaluation des risques. Les outils numériques ont, pour leur part, l'avantage de permettre une meilleure compréhension de l'interaction réelle cavité-digue. Les observations in situ sont la garantie de la validation des résultats analytiques et numériques obtenus.

Pour atteindre ces objectifs, cette thèse se compose de sept chapitres, ils sont organisés comme suit :

Le chapitre 1 présente tout d'abord un ensemble d'informations générales concernant le karst et les digues. Une revue de la littérature relative aux mécanismes et causes de l'effondrement des cavités et à la stabilité des digues est ensuite présentée. Dans la fin du chapitre, nous discutons de la méthode adoptée pour étudier le risque d'instabilité et l'interaction entre les cavités et les digues.

Le chapitre 2 est dédié à la présentation de l'étude de cas : les caractéristiques géologiques, hydrogéologiques et géotechniques du Val d'Orléans sont décrites. Ensuite, la configuration du site de Guilly est adoptée comme cas de référence pour nos calculs. Des études paramétriques permettent alors de généraliser les résultats obtenus.

Le chapitre 3 étudie la stabilité d'une cavité avec prise en compte de l'influence d'une digue située à son aplomb. Une approche analytique basée sur l'analyse limite est proposée. Cette approche analytique permet l'évaluation et la prédiction du risque d'effondrement de la cavité, en termes de facteur de sécurité, en fonction de sa position par rapport à la digue.

Le chapitre 4 étudie l'impact de la cavité sur la stabilité de la pente de la digue en utilisant deux solutions analytiques pour la stabilité de la pente et l'influence de la cavité. La première est la méthode de Fellenius pour l'analyse de stabilité de la pente et la seconde est la solution de Kirsch pour évaluer les variations de contrainte autour d'une galerie circulaire. Différentes hypothèses ont été adoptées pour permettre de combiner les deux approches et estimer l'évolution du coefficient de sécurité de la digue en fonction de la présence d'une cavité.

Le chapitre 5 est dédié à la vérification des résultats des modèles analytiques développés dans les deux chapitres précédents (chapitres 3 et 4) à l'aide de modèles numériques. Le logiciel CESAR-V6 (2D et 3D) basé sur la méthode des éléments finis est utilisé. L'influence de la digue sur la stabilité de la cavité et de la cavité sur la stabilité de la digue est successivement étudiée et discutée. Différents critères sont utilisés tels que les variations de contraintes, les déplacements et les déformations plastiques. Le critère de déformation plastique est utilisé comme indicateur de rupture principale.

Le chapitre 6 discute les différents scénarios possibles de l'influence d'une cavité sur une digue basés sur les résultats obtenus et les observations in situ. Ces scénarios dépendent principalement de deux facteurs : le premier est la nature du sol situé sous digue (cohérent ou non cohérent) et le second est la connexion entre la cavité et le conduit karstique. La digue a été considérée comme formé de sol cohérent. Plusieurs équations sont détaillées pour calculer la force de l'eau qui s'applique sur la masse du sol effondré dans le cas d'une cavité liée à un conduit karstique.

Le chapitre 7 est consacré à la conclusion générale, pour discuter de la méthodologie proposée, les recommandations opérationnelles pour l'évaluation des risques et enfin les perspectives de la thèse.

1.1 Historical evolution of karst and dikes knowledge

1.1.1 Karst

Karst refers to a distinctive terrain that evolves through dissolution of the bedrock. It is therefore associated primarily with limestone, but also with other carbonate rocks (chalk, dolomite) and other soluble rocks (gypsum, salt) (Worthington and Ford 2009, Waltham et al 2005). The origin of the word “karst” can be traced back to several centuries ago in different derivatives of European and Middle Eastern languages, such as the use of “karra” to refer to stone. The region called Kras (between Slovenia and Italy) was the first karstland to receive intensive scientific investigations for its natural characteristics, and hence was viewed as a “classical karstic terrain”. The word, afterward, evolved to karst with the Germans (during the Austro-Hungarian occupation of this country) and typically was used to describe landscape in limestone, dolomite or other soluble material (Huang 2007, Williams 2008).

Typical karstic topography consists of dry streams, sinkholes, caves, enclosed depressions, fluted rock outcrops and large springs (Ford and Williams 1989). Limestone consists mainly of calcite CaCO_3 , formed by the deposition of organisms (shells and corals) or by (bio) chemical precipitation (for example in lakes). Tectonic processes often fracture sedimentary rocks. This process is often rapid, and water entering these cracks gradually dissolves the rocks creating wider and deeper cracks (Forest Practices Branch 2003). The development of karst is largely determined by the water CO_2 content, the geologic processes, the climate factors, the geomorphology and the nature of rocks. Karstic terrains cover around 20% of the whole immersed lands as shown in Figure 1 (Ford and Williams 2007 and 1989).

Karstic features form because water that is slightly acidic from absorbing carbon dioxide from the air and the soil dissolves the bedrock and forms pathways and channels inside. These pathways, called “conduits” or “channels”, are like underground plumbing that carries water from the surface to springs located in valleys. Eventually, these conduits are exposed by erosion and, if large enough, become “caves” (Sturman and Spronken-Smith 2001).

Karst lands cover around 25% of the surface of France (see Figure 2). This is the case of most basins of the Seine and Somme, and a significant portion of the other major basins (Loire, Rhone, Garonne, Rhine, Meuse). Nearly a quarter of linear French rivers, 10,000 km, flows on karst bedrock, including 3,000 km in the context of significant karst index including the Val d'Orléans (Gombert et al, 2014).

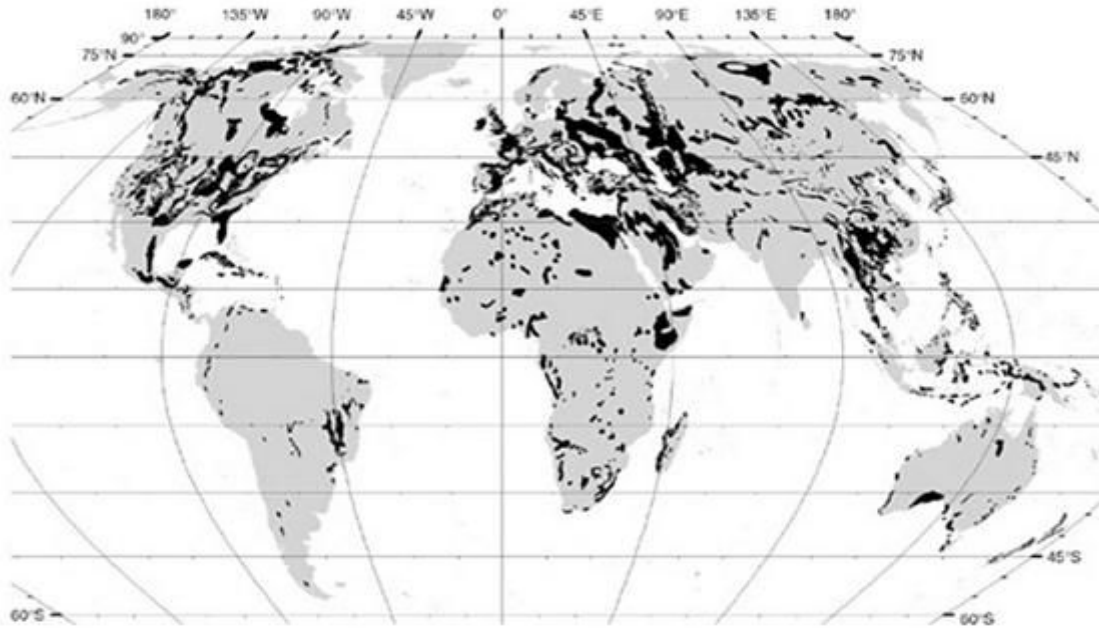


Figure 1 Global distribution of major outcrops of karstic terrains (the black zones) of the world (after Ford and Williams 2007).

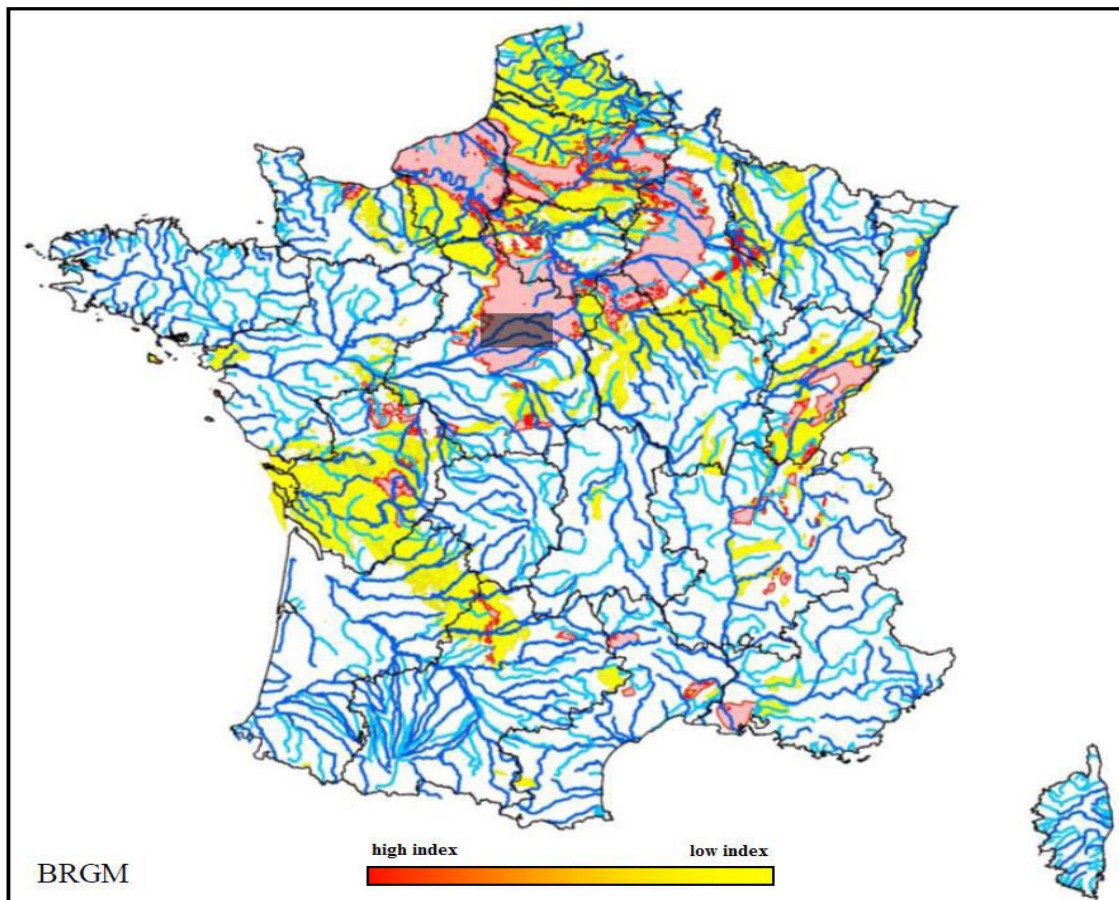


Figure 2 Map indices presence of karst with the layout of the main rivers, the Val d'Orléans is represented by the small gray rectangle (after the French geological survey BRGM).

1.1.2 Cavities and sinkholes

Cavities may appear in rock affected by karstification and cause the subsidence and collapse in upper layers of soils. Sinkhole is considered as a final result when the collapse and propagation of the cavity reaches the surface. According to Waltham et al. (2005), sinkholes can be classified into six types with respect to the mechanisms of the ground failure and the nature of the material that fails and subsides: solution and collapse sinkholes can directly occur in rock, whereas dropout, caprock, suffusion and buried sinkholes occur in the overburden soil layers. Thus, the last three types are named overburden cavities (Figure 3). Gutiérrez et al. (2008) updated the previous classification by dividing the sinkholes into two main groups and by taking into account evaporitic formations (Figure 4): one of them corresponds to solution sinkholes, generated by differential corrosional lowering of the ground surface where karstic rocks are exposed at the surface or merely soil mantled (bare karst). The other group of sinkholes is subsidence sinkholes, which results from both subsurface dissolution and downward gravitational movement (internal erosion or deformation). These sinkholes, that cause the subsidence of the ground surface, are the most important from a hazard and engineering perspective (Gutiérrez et al. 2008, 2014).

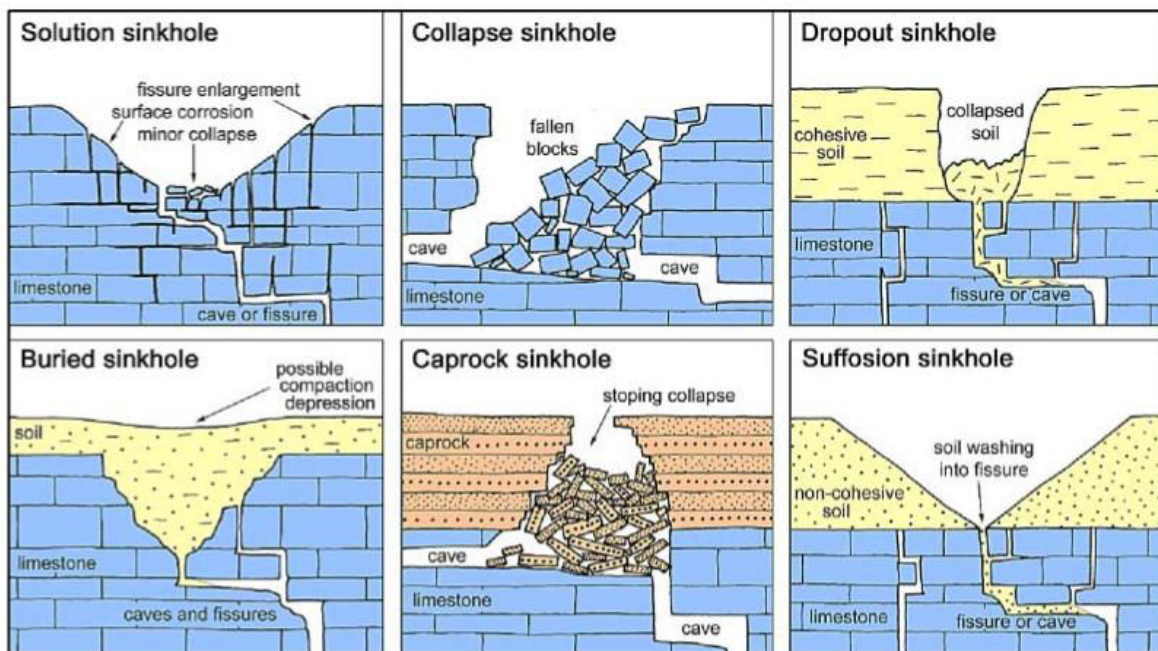


Figure 3 Classification of sinkholes in karst environment (Waltham et al. 2005).

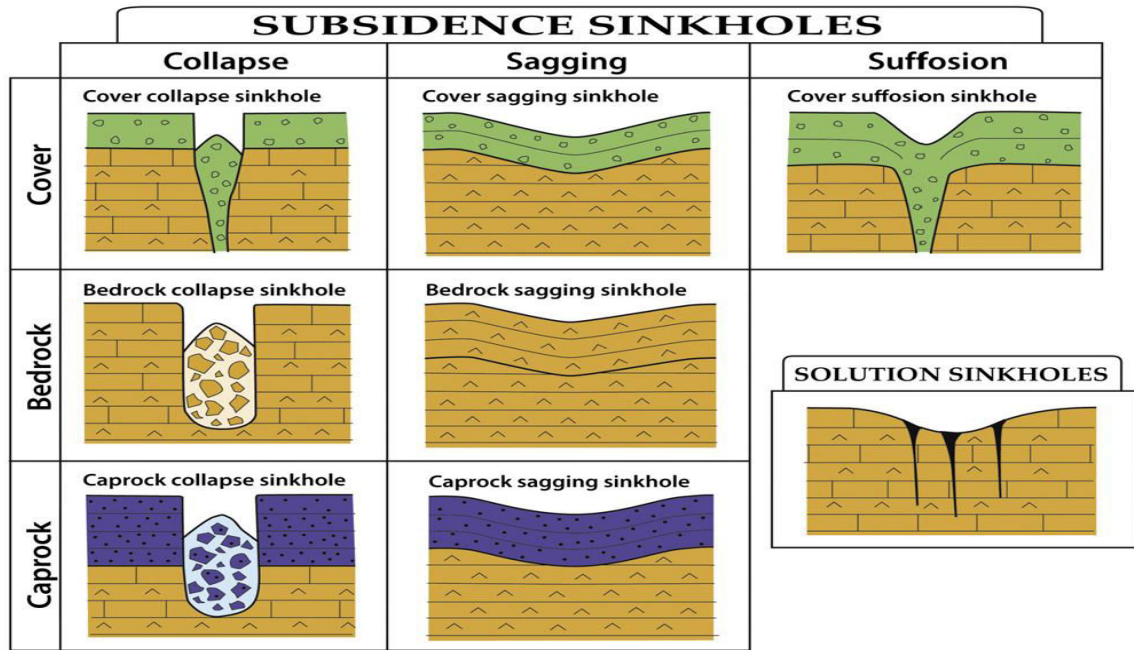


Figure 4 Classification of subsidence and sinkholes: The pattern of the bedrock indicates the type of rocks in which the different sinkholes are commonly observed; sagging sinkholes in evaporites and the rest in both evaporites and carbonates. Sagging, which refers to progressive downward bending due to lack of basal support, is designated with the more general term subsidence by other authors (Gutiérrez et al. 2014).

Some sinkholes are shaped like shallow bowls or saucers whereas others have vertical walls; some hold water and form natural ponds (USGS 2007).

In this work, we focus on the cavities in the superficial formations, which are named in several references by “overburden cavities”. Thus, wherever the word “cavity” is found in next paragraphs and chapters, it refers to “overburden cavity”.

Karst problems worldwide create huge annual costs that are increased due to insufficient understanding of karsts by engineers (Filipponi and Jeannin 2008, Parise et al. 2015). The presence of a cavity underneath civil engineering structures raises concerns about the safety and stability of these structures. Figure 5 shows examples of major sinkhole collapses underneath roads and buildings in different cities around the world. Due to this, we can think that a collapse of a hydraulic structure may cause catastrophic, human, financial and environmental losses. Many hydraulic structures (dams, dikes) around the world are built on karstic foundations. For example, the U.S. Army Corps of Engineers (USACE) has numerous dams built on limestone foundations that are susceptible to karstification (Schaefer 2009). Their failure can be induced by the underground cavities.



Figure 5 Effect of karst sinkholes on several civil structures. (a) An aerial view of the damaged a highway in the State of Miranda (Venezuela) 2010 (Photo by Miranda Government/Reuters), (b) A collapsed road surface in Guangzhou, Guangdong Province (China) 2008 (Photo by Reuters/China Daily), (c) Sinkhole in the main road in Changsha (China), 2012 (photo by Quirky China News / Rex Features), and (d) Buildings collapse into a sinkhole, Clermont, Florida, USA 2013 (photo by Red Huber/Orlando Sentinel/MCT).

1.1.3 Dikes

This work focuses on one of the hydraulic structures which is called dike, and sometimes called flood defense embankment or river levée (Simm et al., 2012). The river dike (or river levée) is defined as “an embankment whose primary purpose is to furnish flood protection from seasonal high water and which is therefore subject to water loading for periods of only a few days or weeks a year” (USACE 2000). The modern word dike or dyke most likely derives from the Dutch word "dijk". Dyke or dike may refer to: a natural or artificial slope or wall to regulate water levels. A dike is called levee (from the French word “levée”) in American English (Ammerlaan 2007). In this work, the word dike is used.

A flood is defined by the French Ministry of Environment as a "submersion (fast or slow) of an area that can be inhabited; it corresponds to the overflow of water" (Lepetit 2002). Stream and river valleys were preferred sites for human habitation for millions of years, most civilizations on the banks of rivers such as the civilizations of Babylon, Egypt and China because such valleys provide drinking water, livestock watering, and irrigation. Soils in river valleys are also among the most fertile that can be found because they are replenished by annual or more or less frequent flooding (Kusky, 2008). For all that reasons, it was important to provide protection for cities and towns by construction dikes that protect people and

property from the river in the flood season, and also in order to increase the height level water for the purpose of navigation.

For the US Army Corps of Engineers (USACE), "all the soil is suitable for the construction of dikes" except the very moist, fine grain or very organic soils. Selection of the type of material is generally based on the availability and proximity to the project area. Maximum slopes for dikes are 1V of 2H, where V and H refer to vertical and horizontal dimensions respectively. Dikes with non-ideal materials such as sand, dams are required to have much shallower side slopes (until 1V to 5H) to prevent damage caused by the infiltration and action of flooding waves (USACE 2000, 2006).

Faced with the risk of flooding, people have always tried to protect themselves against overflowing rivers and streams. They tried to "tame" the rivers to live closer to their surroundings. This protection has been made possible by the gradual construction of dikes.

The construction of dikes was built there more than 3,000 years in Egypt, where a levee system was built along the left bank of the Nile, over more than 1000 km. Civilizations of Mesopotamia and ancient China also built large dike systems (Wei 2012). Like those of the Loire, the oldest dikes still operating today and elevated over time in France date back to the middle ages (Serre 2005, Castanet 2008). There are **8,000** km of dikes that have been identified by the state to this day in France, **5,600** km of them more than a meter tall (CEPRI, 2008).

1.2 Literature review

1.2.1 Mechanism of karst and cavities collapse

In fact, there is no obvious mechanical explaining the karst collapse, but there are several theories to explain the collapse of cavities, and certain conditions must be available in order to collapse occurs.

The collapse of cavities can take different forms: subsidence, sinkhole, etc. The sinkhole is a brutal failure of the ground above a cavity. The cavities can collapse due to natural and/or human factors. In general, the materials change over time and that the cavities have a natural tendency to fill themselves. There are classically two theories to explain the mechanisms of a collapse (Chan 1995, Tharp 1999, Salvati et al. 2002, Keqiang et al. 2004, Zhao et al. 2011).

The first theory is internal erosion, which occurs when the groundwater table is lowered due to natural (drought) or human (pumping) factors; the groundwater velocity increases and the hydraulic gradient becomes steeper. Thus, the groundwater outwashes and erodes the soil cover (overburden) to increase the cavity dimensions at the interface between the bedrock and the soil cover. There are two possible scenarios, depending on the following conditions (Waltham and Lu 2007; Parise 2008):

- If the soil cover is thick enough and has enough strength (high cohesion), a natural balanced arc will be formed in the soil cavity and the cavity will not collapse, if there are no other inducing factors.

- If the soil cover is thin and has poor strength (low cohesion), the soil cavity will continue to enlarge until a collapse occurs (cf. Figure 6-a).

The second theory is the vacuum suction erosion theory, which involves a confined karstic aquifer. When groundwater suddenly falls by large amplitude and the water table drops below the floor of the soil cover, the groundwater will change from confined to unconfined, and a relative vacuum of low air pressure will occur between the water table and the floor of the soil cover as shown in Figure 1.6-b.

According to Chan (1995) the sinkhole will not be formed if the soil next to the slot (karstic cave) does not fall into the cave. Hence, to evaluate the potential sinkhole formation, the first step is to examine the stability of the layer of soil immediately above rock head. From theories of arching (Terzaghi 1943, Tharp 1999), the thickness of this layer is very approximately the width of the slot (Figure 7).

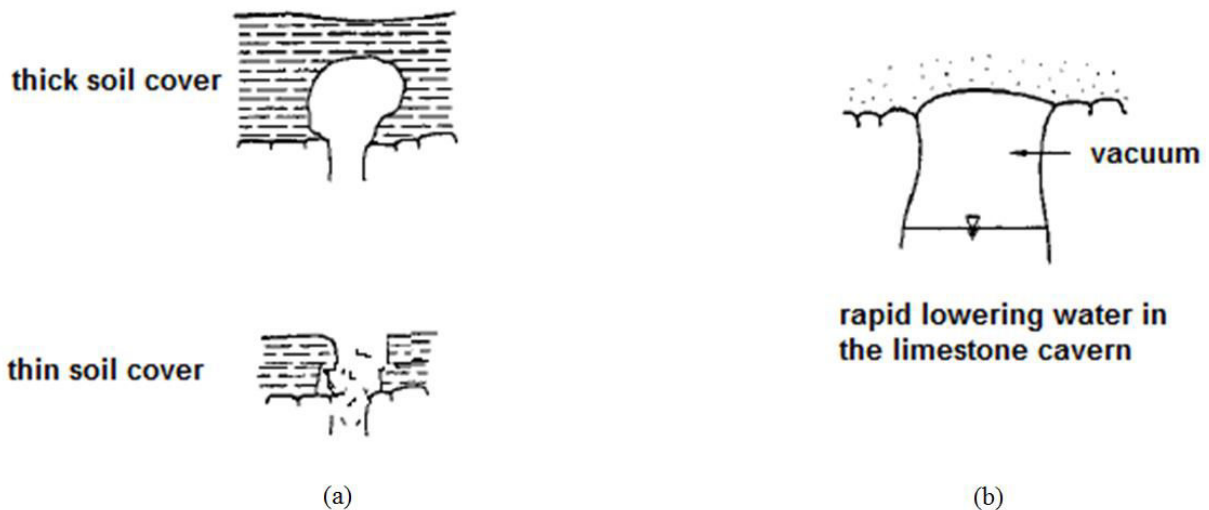


Figure 6 Classic two theories to explain the mechanisms of a brutal collapse of cavities. (a) Theory of potential erosion. (b) Vacuum suction erosion theory (after Waltham and Lu 2007; Parise 2008).

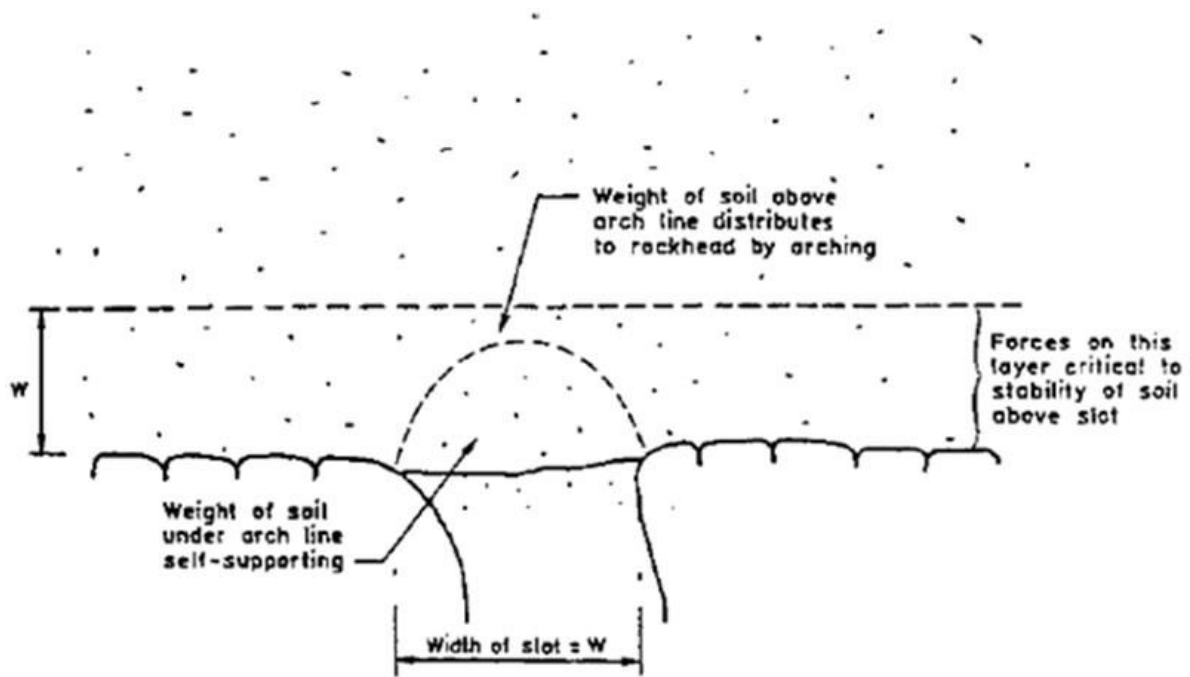


Figure 7 Critical soil layer for sinkhole formation (Chan 1995).

A mechanism of sinkhole formation has been described by Beck and Barry (1984). Piping and collapse of the residual soil above a cavity often result in the formation, upward propagation, and eventual collapse of the void (Figure 8). The state of stress and resulting shear strength of the surrounding will govern the stability of the cavity. Under some combinations of cavity diameter and vertical stress, circumferential stresses may be sufficient to maintain soil stability. One can assess the stability by comparing the vertical stress due to the weight and the shear strength developed on the failure surface (Drumm et al. 1990).

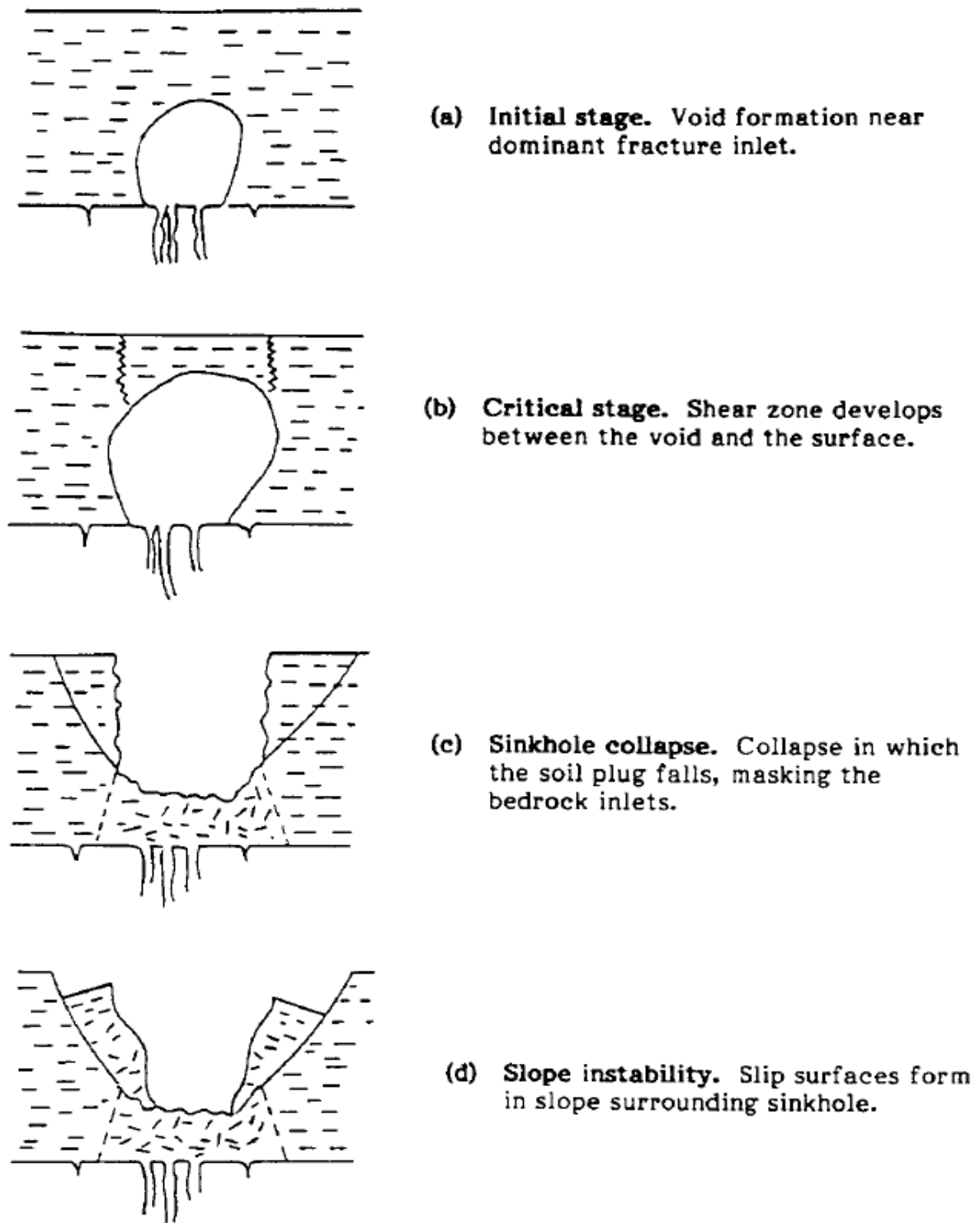


Figure 8 Evolution of a sinkhole (after Beck and Barry 1984).

1.2.2 Formation and stability of cavities

The most available research is descriptive rather than analytical and regarding sinkhole prediction is closely related to particular sites or geology. According to Zhou and Beck (2008), formation of a cavity is probably preceded by formation of a void at the soil/rock

contact by transporting of soil into an opening in the bedrock. Openings in solvable limestone are commonly 10–40 cm in diameter (White et al., 1984). There is commonly a zone of very soft soil just above the rock (Pazuniak 1989, Iqbal 1995, Sowers 1996, Wilson and Beck 1988). This soft zone has also been interpreted as soil that has sloughed into and filled previous soil voids (Sowers 1975, Wilson and Beck 1988). Tensile failure of this layer and perhaps overlying stronger soil will lead to formation of a no-tension cylindrical or dome in the soil (Hodek et al. 1984).

The traditional approach to predict cavity collapse in soil, as opposed to the problem of locating the cavities themselves, has been to use physical modeling and analytical techniques. The stability of soils over cavities was investigated through centrifuge modeling by Craig (1990), Abdulla and Goodings (1996). These centrifuge experiments used idealized cavity configurations, where collapse resulted from the overburden weight alone. Craig (1990) examined the stability of a cylindrical cavity opened up under a two-layered clay sample using two sets of tests. In the first set of tests, overburden weight was gradually increased by increasing the speed of the centrifuge, until the clay layers failed into a preformed cylindrical cavity. In the second set of tests, the centrifuge ran at constant speed while sand was extracted from a void beneath the clay layers. Craig found that the assumption of a simple cylindrical rigid-block failure in the clay was adequate for both sets of tests, providing the ratio of effective overburden depth against cavity diameter was less than unity.

In a similar study, Abdulla and Goodings (1996) investigated the stability of a cemented layer of sand overlying a cylindrical cavity, with and without overburden. They modeled a soil resulting from groundwater extraction in arid regions. The main finding of this study was that the cemented sand layer failed along steeply inclined planes forming a truncated conical section. In thicker cemented layers, however, a compression dome formed with a height of 25–30% of the cavity diameter.

Zhou (1997) demonstrated cavities of 0.2 m in diameter can cause sinkhole collapse in over 15 m thick overburden and the collapse could reach the surface regardless of the thickness of the soil, as long as the karst conduit was not blocked by the collapsed soil. The collapse process ceased every time when the fracture was filled with the soil, and restarted after the filled soil was removed.

Yang and Drumm (1999) analysed stress-strain and indicated the collapse or stability of the cavity is controlled by the relationship between the diameter of the cavity and the thickness of overburden when the cohesion remains constant. For a given value of soil cohesion, the lower bound of the soil cavity diameter and the overburden thickness was described by a power function that is independent of the soil friction angle in cohesive soil. They proposed the following equation to estimate a sort of critical depth (H) for a value of soil cohesion equals to 25 kPa:

$$H = 1.45 D^{1.37} \quad (1.1)$$

H and D are expressed in meters. Where H and D are the height of overburden and diameter of the cavity, respectively. They considered the stable zone is bounded by the line defined by Eq. 1.1. Thus, the height of overburden must be more than H in Eq. 1.1 to be stable.

Zhao et al. (2011) consider that the karst collapse in China depends on several factors: purity of the limestone, degree of karstification, topography, geomorphology, geological structures, covering characteristics and hydrodynamic conditions. They demonstrated that the major cause of most karst collapses in southern China is the rapid change of hydro-climatic conditions which may cause:

-A drastic lowering of the groundwater level, reinforcing the mechanisms of suffosion and / or reducing the load in karst; these would be the main causes of karst collapse in the dry season. In the initial state (Figure 9) and if $G + F_h + P \leq F_a + F_b$, the covering layers of the cave are stable. When the groundwater level declined below the bedrock ($F_b = 0$), if $G + F_h + P \leq F_a$, the covering layers of the cave remain stable; where G is the dead weight of the overlying strata, F_h is dynamic hydraulic force, P is the total atmospheric pressure and additional dead load on the surface, F_a is the total resistance force of collapse, and F_b is buoyancy force of the soil. However, if $G + F_h + P > F_a$, ground fissures and collapse are bound to occur;

-During rain, a sudden increase in saturation in the soil that covers the karst layer, which accelerates the suffosion by increasing the load of the covering 30 to 40% (Figure 10) and a reduction in the cohesion and angle of internal friction of the covering material;

-The extensively distributed red clay is composed of hydrophilic minerals, such as montmorillonite, illite, and kaoline. These minerals are easily disintegrated by groundwater especially in case of repeated cycles of high and low water that create repeated cycles of saturation - desaturation.

-The negative pressure could easily form when groundwater fluctuates during rainfall alternation thus enlarging the soil cavity. This vacuum suction effect would greatly facilitate collapse.

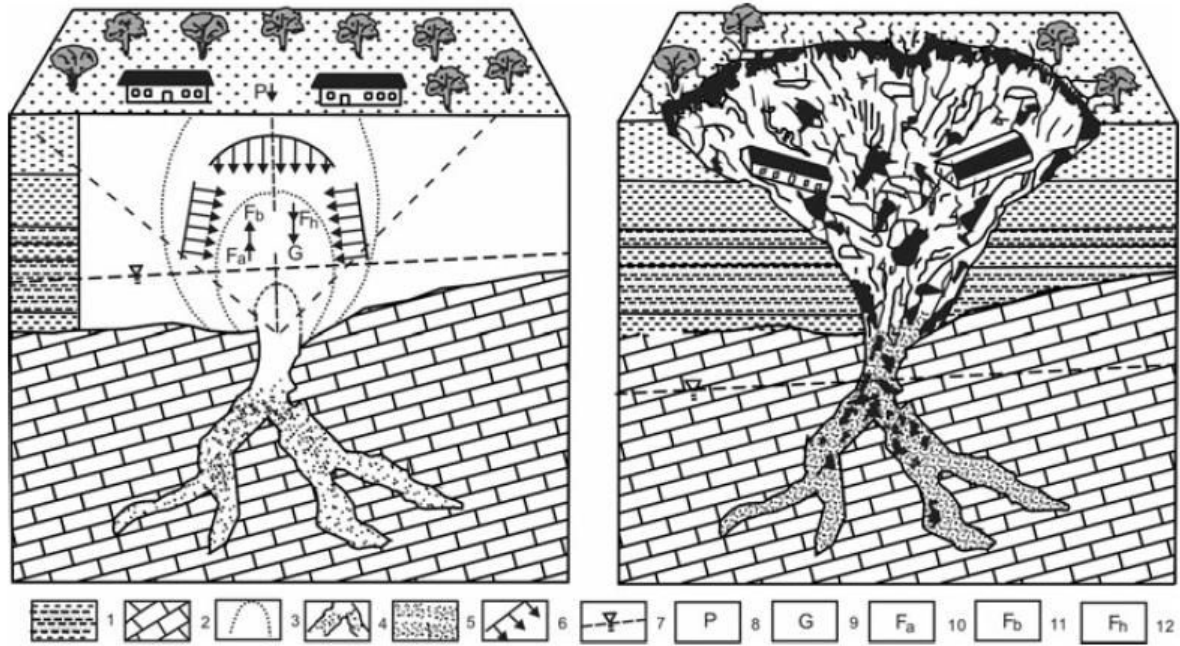


Figure 9 3D Schematic to demonstrate the mechanical condition of a karst collapse. 1 Overlying strata; 2 Limestone; 3 Soil cavity; 4 Karstic cave; 5 Debris; 6 Compression stress and shear stress on the soil arch; 7 Groundwater level; 8 The total atmospheric pressure and additional dead load on the surface; 9 The dead weight of the overlying strata; 10 The total resistance force of collapse; it contains the cohesive strength and interfacial friction of the soil, etc.; 11 Buoyancy force of the soil; 12 Dynamic hydraulic force (according to Zhao et al. 2011).

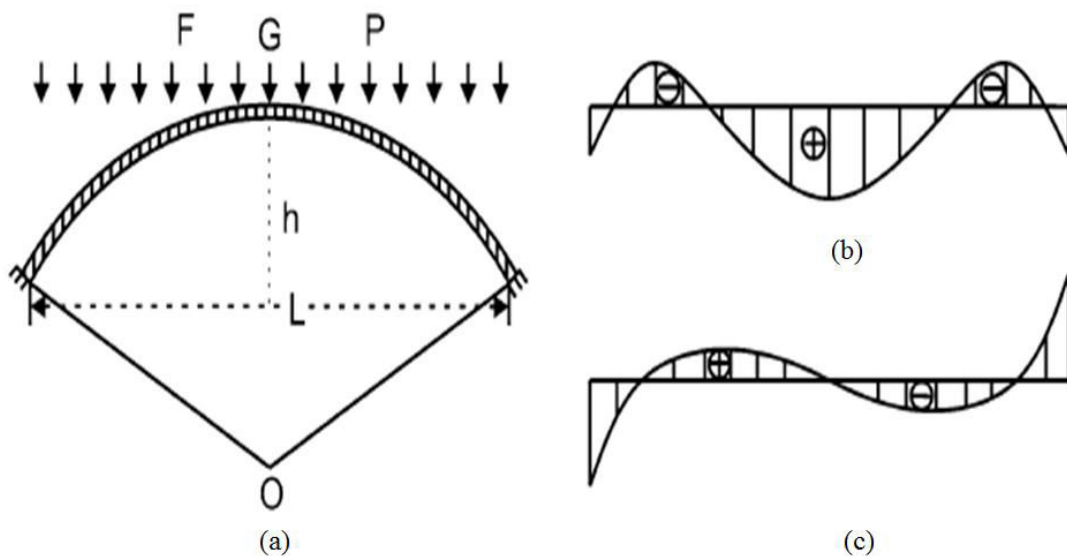


Figure 10 Mechanical conditions of a limit equilibrium arch of a soil cave. (a) The mechanical structure of a soil cave can be simplified as a limit equilibrium arch, where F the dynamic hydraulic force; G the deadweight of the cover layer; and P the atmospheric pressure. (b) The bending moment diagram of the soil arch. (c) The shearing force diagram of the soil arch (Zhao et al. 2011).

Hyatt and Jacobs (1996) examined the distribution and morphology of 312 sinkholes suddenly appeared in the karstic Dougherty Plain at Albany, Georgia (USA) that resulted of flooding of

the Flint River in July 1994. They also evaluated the mode of formation, characterized early stages of the evolution of sinkhole form, and estimated the lowering of the ground surface associated with the development of new sinkholes. They found that 88% of sinkholes occurred inside the limits of flooding, especially in areas of sandy overburden. They presented a descriptive model of the sinkhole form (Figure 11). Sinkholes initiated with the collapse and suffusion of saturated soil arches.

The impact of water on sinkhole formation was analysed by Anikeev (1999) and Sharp (1997, 2003) based on hydrofracturing theory (Figure 12). Anikeev (1999) proposed a simple hydrofracturing criterion that is controlled by the ratio of soil cohesion to the loss of buoyant with considering the case when there is comparatively impervious clay between the bedrock and the main overburden. He found that rapid drawdown in the overburden will induce cracking arches in the clay. A 3 m of drawdown in water level could cause hydrofracturing in soil with cohesion of 25 kPa. While Sharp's numerical analysis indicate that hydrofracturing was unlikely to occur under steady state pore pressure. Transient pore pressure is a more probable cause of failure. In general, the increased load above the soil accompanied with the loss of buoyancy support caused by a rapid drawdown of water table is initially shifted to the pore water. The effect occurs at the perimeter of the soil cavity, where it is manifested in high pore pressures and consequently high pore pressure gradients. If pore pressure exceeds the sum of the radial compressive stress and tensile strength of the soil, hydrofracturing will occur and the cavity will be enlarged. The new free face that results will exhibit the same high gradient. This will result in a progressive failure that may proceed rapidly, accounting for the locally sudden appearance of sinkholes. The critical factor in this example is the rapidity of drawdown. If drawdown were slow enough to allow consolidation without a significant pore pressure transient, sinkhole formation may be slowed down.

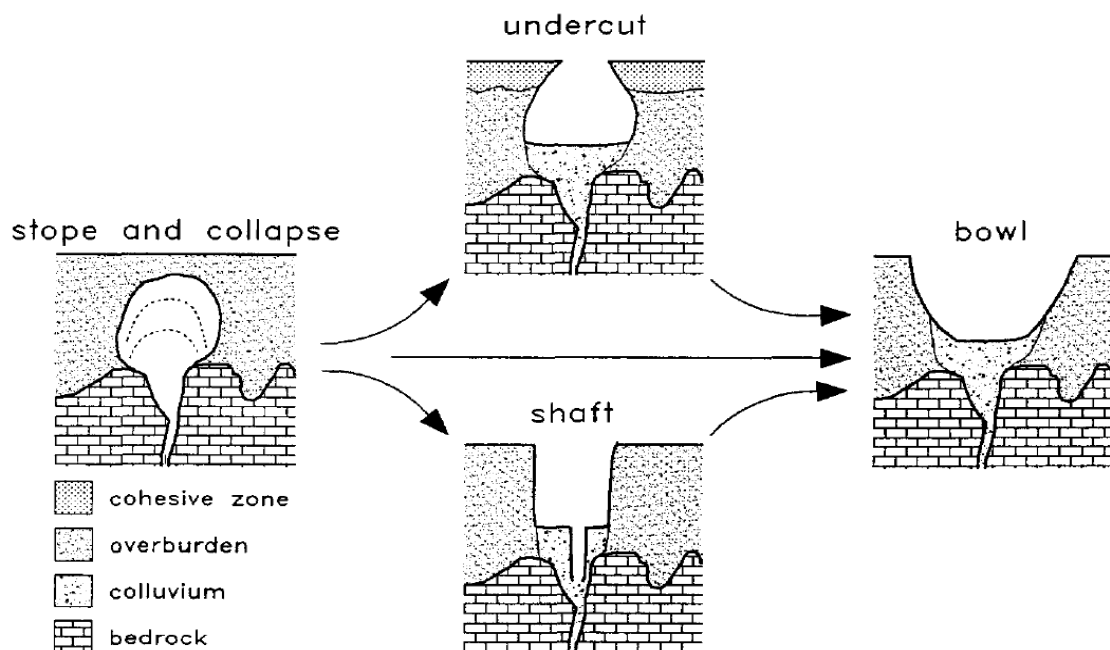


Figure 11 A morphologic model of early sinkhole development based on observations of sinkhole form at Albany, USA (Hyatt et Jacobs 1996).

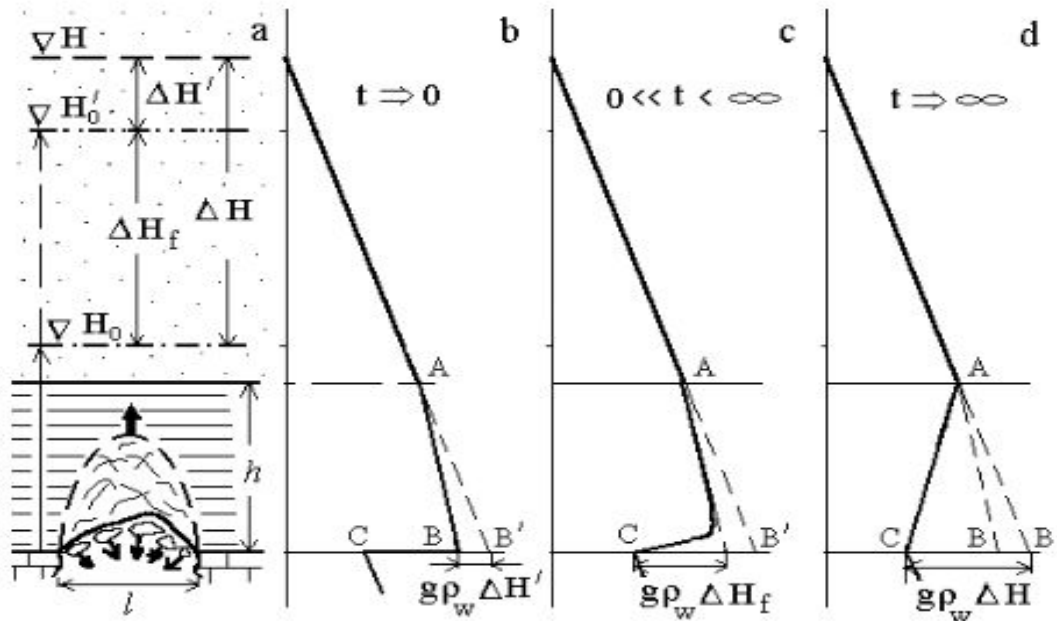


Figure 12 Mechanism of hydrofracturing theory (a), pore pressure diagrams at the initial moment (b), intermediate stage of downward seepage (c) and final one (d). ΔH : water-table (the level of unconfined water); $\Delta H'_0$ and ΔH_0 : potentiometric level of karst water before and after water head decline; l : the span of a cave (rock void) at the base of karst overburden; h : the thickness of confining bed; t : time of downward seepage. Big arrow and small ones show respectively the propagation of crumbling front and the "shooting" of clay spalls and pieces from the roof of soil void (after Anikeev 1999).

There are not many analytical and numerical approaches that deal with failure of soil cavities in literature. Drumm et al. (1990) used classical plasticity theory (Mohr-Coulomb criterion and perfect plasticity) and to evaluate the stability of soils adjacent to a cylindrical cavity and they put analytical model for that. They considered a failure cone with an included angle of $(45-\phi/2)$ (angle with vertical axis) as a first approximation. Their approach applies to the stability of circular excavations. The results confirmed that small cavities are more stable than large cavities for a given overburden thickness. However, for a given cavity diameter, large overburden thicknesses are shown to be more stable than small thicknesses. They explained that these results are contrary to conventional slope stability where stability generally decreases with increasing height. They showed that this difference is the consequence of circumferential stress component in the axisymmetric solution, which may be significant for small-diameter cavities. Their results referred that the stability of the soil is increased due to arching in the circumferential when the thickness of overburden to diameter the cavity ratio (H/D) more than about 40.

Another analytical approach to sinkhole formation was developed by Tharp (1999) who studied the likely expansion of a cavity leading to a sinkhole, including the effects of pore-water pressure changes. Tharp's analysis (1999) began with a linear elastic, isotropic stress field in the soil around a cavity, followed by the development of radial cracks and loss of soil into the cavity. Tharp (1999) concluded that steady-state groundwater conditions should

generally promote stability and that sinkhole formation resulting from rapid drawdown of the water table could be avoided by sufficiently slow lowering.

Augarde et al. (2003) used numerical modelling to study undrained stability of the submerged cavities that lead to sinkhole formation. Finite-element limit analysis techniques are used to obtain upper and lower bound values of a suitable load parameter, which bracket the exact solution. The results are compared with data from literature and derived independently. They neglected the effect of angle of internal friction ($\phi=0$), so their formulas may be used for clay soils. Other numerical analyses were performed by Drumm et al. (2009) to develop a stability chart expressed in terms of a dimensionless stability number and the geometry of a potential cavity in the residual soil (see Figure 13). Shear strength reduction (SSR) method was applied in which the strength parameters were reduced until a convergent solution could no longer be obtained, and the results were used to develop stability numbers. The dimensionless stability number ($N_c\phi$) was in terms of unit weight of soil (γ), height of overburden soil above the cavity (h) and divided by the cohesion of soil (c). The stability charts include the effect of friction angle, and are also developed to allow the investigation of the effect of the inverted strength profile typically observed in karst terrain. In order to include the inverted strength profile in the stability chart, an analysis for the undrained ($\phi =0$) conditions was also performed with the lower 3D/4 portion of the soil profile assigned a reduced cohesion value (c) multiplying it by the inverted strength factor (α). This model is adequate for cohesive soil only because it needs a value of cohesion more than zero in the calculation.

Keqiang et al. (2004) proposed a simple analytical model based on the arch stability combined with the theory of soil-limit equilibrium to evaluate the risk of a sinkhole due to karst cavities due to the dewatering. They considered the collapsed zone above the cavity as soil column and the collapse forces are the weight of this column, deadweight of rainwater, seepage force due to the dewatering and the differential atmospheric pressure in the cavity. While the friction strength surrounding it is considered the resistance force. Then, they assessed the stability of cavities in overburden layers above a karstic stratum by comparing between the collapse forces and the resistance force. The study of karst collapses in Zaozhuang City, China, was performed by applying this analytical model: the results show that the mechanical model generally agreed with the formation mechanisms and the actual stability situation of the observed cavities. The previous literatures are summarized in Table 1 and from them results, we can say:

- H/D ratio can be used as indicator to identify the limit of the cavity collapse.
- The collapsed cavity extends upward either vertically as a vertical column or with an angle as a frustum.

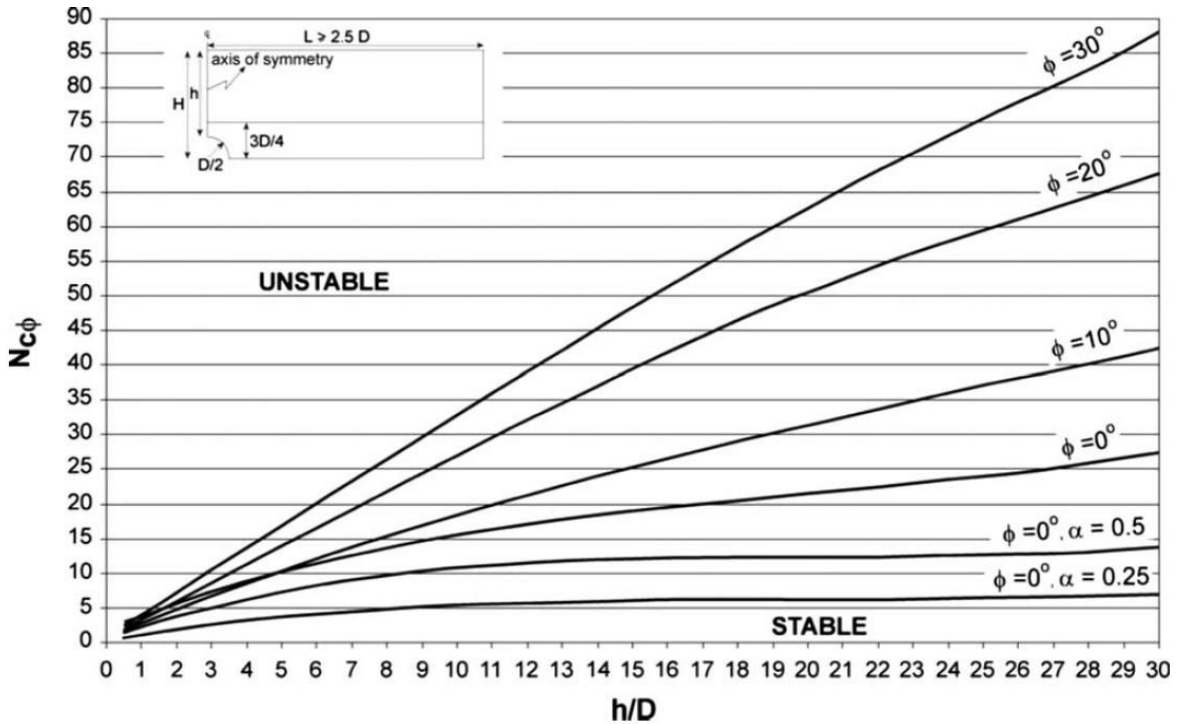


Figure 13 Stability chart, dimensionless stability number $N_{c\phi}$ with effect of angle of internal friction ϕ and inverted strength profile ($K_0=1-\sin \phi$).

Table 1 Summary of the literature review about the cavity stability in overburden soil.

Authors	Theories and methods	Results
Beck and Barry (1984)	Internal erosion theory & soil-limit equilibrium	Describe the sinkhole formation, the cavity in overburden soil above a bedrock formation, upward propagation, and collapse of the cavity.
Craig (1990)	Physical (centrifuge) model	Ratio of effective overburden depth to cavity diameter was less than Unity ($H/D < 1$) for a cylindrical cavity under a two-layered clay.
Drumm et al. (1990)	Analytical analysis (Mohr-Coulomb criterion and perfect plasticity)	A failure cone with an included angle of $(45-\phi/2)$ may be used as a first approximation. The stability of the soil is increased due to arching in the circumferential when H/D more than about 40.
Chan (1995)	Internal erosion theory & soil-limit equilibrium	The minimum thickness of overburden layer that has a stable arch cavity is very approximately the width of the cave.
Abdulla and Goodings (1996)	Physical (centrifuge) model	Dome formed with a height of 25–30% of the cavity diameter in

		thicker cemented layers.
Hyatt and Jacobs (1996)	Bibliographic study	88% of sinkholes occurred inside the limits of flooding, especially in areas of sandy overburden with sinkholes initiated with the collapse and suffusion of saturated soil arches.
Zhou (1997)	Bibliographic study	cavities of 0.2 m in diameter can cause sinkhole collapse and the collapse could reach the surface regardless of the thickness of the soil, if the karstic conduit was not blocked by the collapsed soil.
Sharp (1997,1999, 2003)	Analytical analysis (hydrofracturing theory)	The rapidity of cavity collapse in drawdown area is directly proportional to rapidity of the drawdown and the collapse will occur when pore pressure exceeds the sum of the radial compressive stress and tensile strength of the soil. Steady-state groundwater conditions should generally promote stability.
Yang and Drumm (1999)	Analytical model	The height of overburden must be more than H in following equation to be stable: $H = 1.45D^{1.37}$
Anikeev (1999)	Analytical analysis (hydrofracturing theory)	Rapid drawdown in the overburden will induce cracking arches in the clay. A 3 m of drawdown in water level could cause hydrofracturing in soil with cohesion of 25 kPa.
Augarde et al. (2003)	Numerical model (finite-element)	Study undrained stability of the submerged cavities that lead to sinkhole formation. The exact solution Confined between upper and lower bound values of a suitable load parameter. All their results were for soils had friction angle equals zero.
Keqiang et al. (2004)	Analytical model (theory of soil-limit equilibrium)	Establishing a simple analytical model to compare between the collapse forces and the resistance force that effect the stability of cavities in overburden layers above a karstic stratum in state of dewatering.

Drumm et al. (2009)	Numerical model (finite element)	Stability chart expressed in terms of a dimensionless stability number and the geometry of a potential cavity in the residual soil and it is applicable for cohesive soils.
Zhao et al. (2011)	Bibliographic study	<p>Drastic lowering of the groundwater level would be the main causes of karst collapse in the dry season and a negative pressure could easily form due to groundwater fluctuates thus enlarging the soil cavity and cause the collapse.</p> <p>A sudden increase in saturation in the soil that covers the karst layer, which accelerates the suffosion by increasing the load of the covering 30 to 40%.</p>

1.2.3 Stability of dikes

There different causes of failures are associated to many failure mechanisms that can lead to a breach due to a failure in dike. These mechanisms can occur as a single mode, or a combination of several types of failure modes that act together. The causes of the dike failure in flood time, in general, can be classified into four causes (USACE 2000, Serre 2005, Baars and Kempen 2009) which are overflow, external erosion & scour, slope instability and internal erosion. The classification of failure cases of dike can be explained in more detail in the following:

a- Overflow: The overflow is a flood failure mechanism: during the flood, the water overflows over the dike causing the flow of a water sheet over the structure, and generally quickly leads to the breach, by regressive erosion of the protected land side slope (Figure 14). According to Serre (2005) the erosion realized on the overflow takes place in two phases:

-A phase of progressive erosion: the water flowing over the dike erodes it;

-A tipping phase: the cross section of the dike can no longer resist to the water pressure.

The overflow causes the dike failure when a larger flood than the designed one arises so that the flood level is over the top of dike. It is the consequence of the erosion of the landside slope and crown edge whose material are mainly build with erodible soil.

b- External erosion & scour: The external erosion and scour do not always lead to a breach. This can provide when there is sequence of fluctuations (rising and dropping the surface).

When there is no formation of a breach, however, the degradation may be significant and very dangerous (Mériaux et al., 2001).

The erosion by external failure mechanism consists of a separation of the particles constituting the dike by the current of the river that can erode the dike until it breaks. Other phenomena, such as runoff of rainwater, can also be the cause of the external erosion. The banks of the river side of dikes (upstream), may suffer the effects of water currents, which can cause erosion at the dike toe by scouring as shown in Figure 1.15 (USACE 2000, Serre 2005, Keddouri 2011). Wave action of water currents can form long terraces along the length of the dike slopes. If additional material or bank protection (riprap) is not provided, the embankment will continue to cave as the waves work their way farther into the slope (USACE 2006).

During high water, continuing wave action against a dike slope can erode wide terraces along the length of the dike. This causes scour or breaching along the river ward slope of the dike and reduces the cross sectional area, which can lead to a failure. This type of damage does not typically arise during short storms, especially if the slope has good cover. However, during longer periods of high water, particularly during windy or icy conditions, the damage can develop very rapidly (USACE 2006). Scour corresponds to the external toe erosion of the riverbank and external erosion of the dike body, which combined with the weakening of the mechanical properties (due to saturation of the materials). The toe of dike degrades and sliding occurs in saturated soil (Figure 15). By successive floods, the mechanism leads to the opening of a breach in the dike body (Mériaux et al. 2001).

c- Slope instability: According to Mériaux et al. (2001) and Serre (2005) there are two slope sliding mechanisms:

1- *Sliding of land side slope (in downstream)*, occurring most often during the flood (Figure 16).

Mériaux et al. (2001) showed that this mechanism occurs when three factors come together:

- Profile of narrow dike with strong side slopes (slopes greater than 0.65);
- High piezometric level in the dike due to the absence of drainage and / or to the presence of heterogeneous layers;
- Low compaction of the soils of the dike giving poor mechanical characteristics of dike body materials, or the presence of a sub-consolidated clay layer at the foundation.

These three factors are potentially united in the old breaches zones that have been repaired, however, the reparation has not always been carried out under optimum conditions.

2- *Sliding the river side slope (in upstream)*, occurring during the flood recession. This mechanism, linked to the sub-pressures that develop during the flood period, relates mainly embankment dikes made of clay materials, with steep slopes or too tight riprap. Mériaux et al. (2001) illustrated this mechanism by a schema that shown in Figure 17.

Serre (2005) also added that these previous two mechanisms will not cause a full breach but the dike could not resist the next flood if is not repaired.

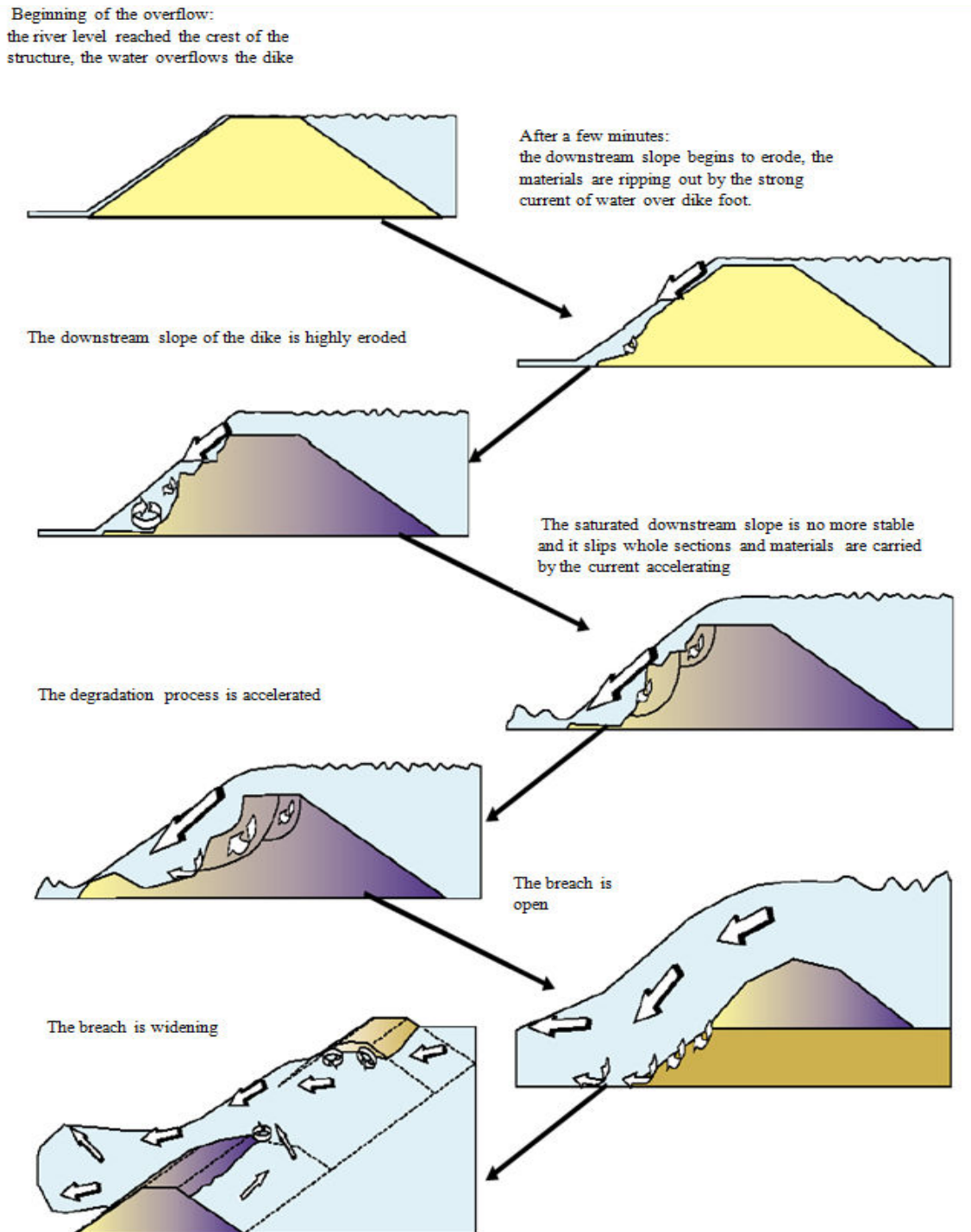


Figure 14 Overflow mechanisms (after Mériaux et al., 2001 cited by Serre, 2005).

The high speed of the water and the vulnerability of banks are the source of erosion of the dike toe.

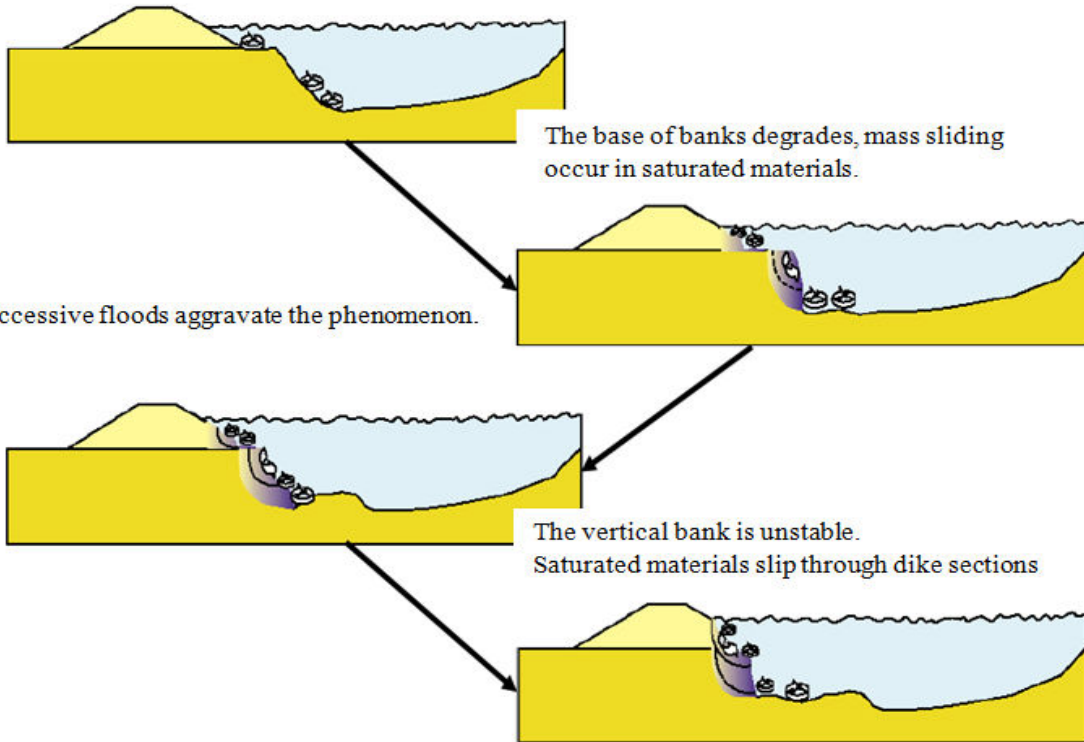


Figure 15 The scour mechanisms (after Mériaux et al., 2001 cited by Serre 2005 and Keddouri 2011).

The saturation of the dike and the rigidity of the slope; causing mass failures sliding slope

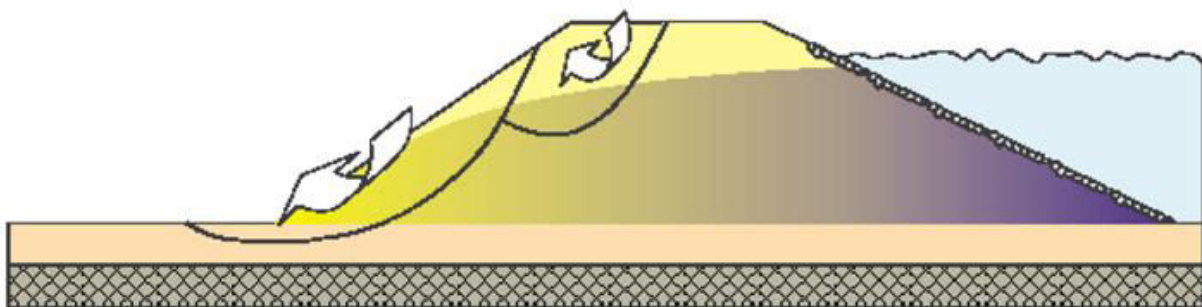


Figure 16 Sliding of land side slope mechanism in downstream (after Mériaux et al., 2001 cited by Serre 2005 and Keddouri 2011).

With the increase in upstream water level and maintaining it at a high rating during a long flood; the dike progressively is saturated.

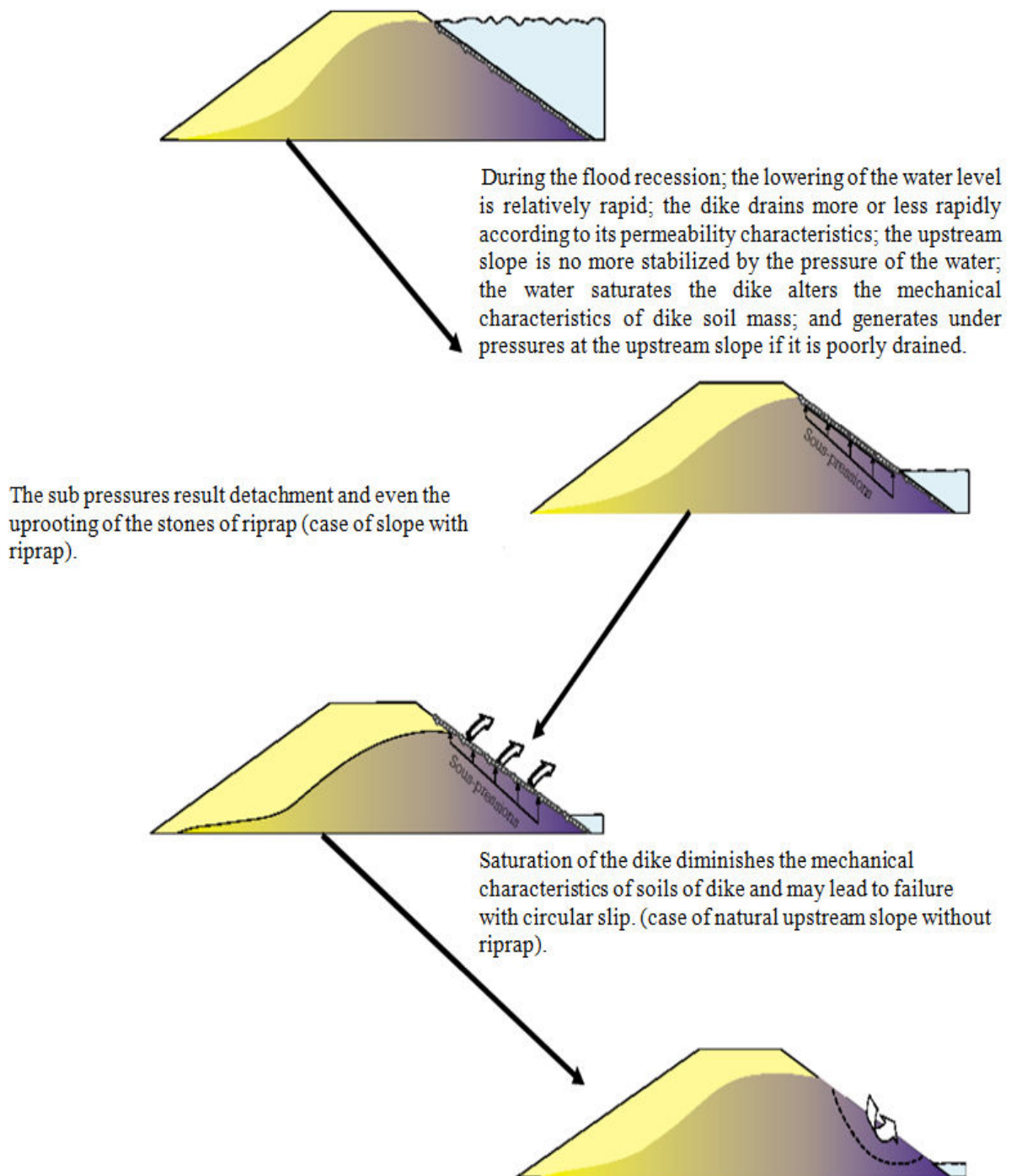


Figure 17 Sliding of river side slope mechanism in upstream (after Mériaux et al., 2001 cited by Serre 2005 and Keddouri 2011).

d- Internal erosion: According to French committee of large dams (CFGB 2002), internal erosion is the main source of incidents of hydraulic earthen works (as dikes).

The internal erosion can be defined as the phenomenon of tearing off and transport downstream of the particles of an embankment or foundation as a result of the action of the flow from the reservoir, river or groundwater. It develops when the two following conditions are fulfilled: the tearing off of soil particles and their transport (Nombré et al. 2015, CFGB 2002).

The mechanisms responsible for internal erosion are complex and depend on several parameters that can be coupled. Even in the laboratory, the identification of the mechanism can be problematic, as interpretations of Skempton and Brogan (1994) which diverges about the same test campaign. In general, the terminology used to characterize internal erosion is variable and depends on the disciplines and researchers. According to the typology of IREX (2003), mentioned by Blais (2005) and other authors in literature (Bendahmane 2004, Keddouri 2011), we can define seven phenomena of detachment of particles and two phenomena of transport.

i. *Phenomenon of detachment off of particles:*

1-Boiling: if water pressure in soil is sufficient to raise a part of the soil, it is said that there is a risk of boiling as shown in Figure 18. Flotation of soil grains due to the hydraulic gradient upward will happen (Bendahmane 2004, Blais 2005, Keddouri 2011).

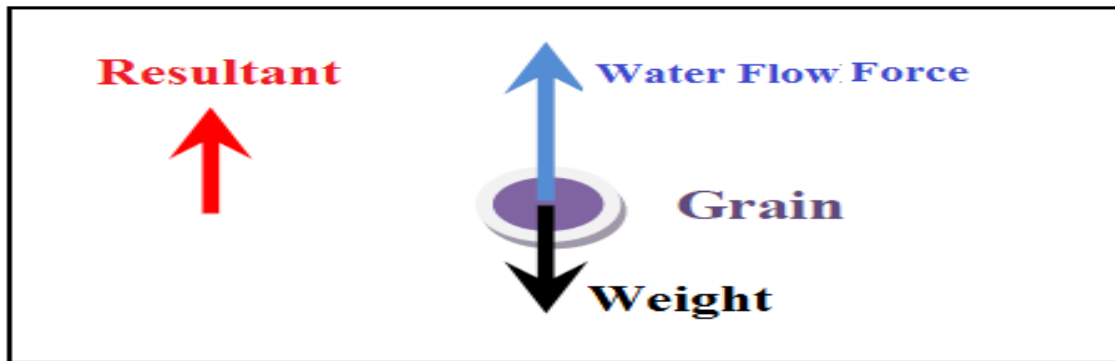


Figure 18 Free body diagram for a grain soil in boiling state (after Bendahmane 2004).

2-Seepage erosion: it corresponds to a particle detachment on the walls of a conduit in the direction of flow when a limit value of the shear generated by the flow is reached (Blais 2005). Water flow performs shear stresses τ due to water-grain friction (Figure 19). If these stresses exceed the critical threshold τ_c , there is detachment off of particles, decreasing the cohesion between the grains and the flow velocity in the pores (Pham 2008, Keddouri 2011).

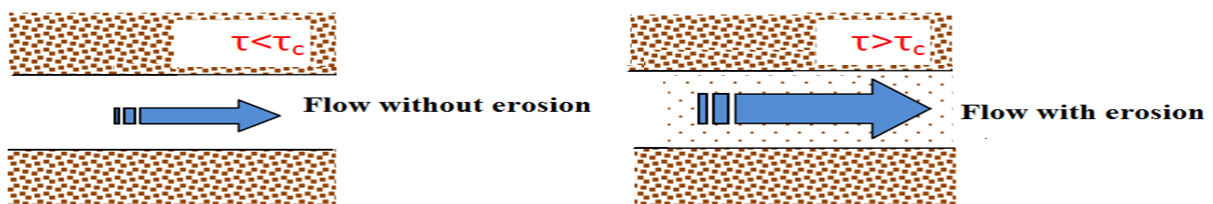


Figure 19 Phenomenon of seepage erosion (after Pham 2008).

3- Regressive erosion: regressive erosion concerns any erosion phenomenon that occurs in a downstream point and continues progressing upstream (Blais 2005). The particles are gradually removed by water flow. This destabilizes the soil structure and increases the hydraulic gradient thereby causing an increase in flow velocity and amplification of the erosion phenomenon (Figure 20). For homogeneous soils this phenomenon develops without limit until the collapse of the soil (Pham 2008).

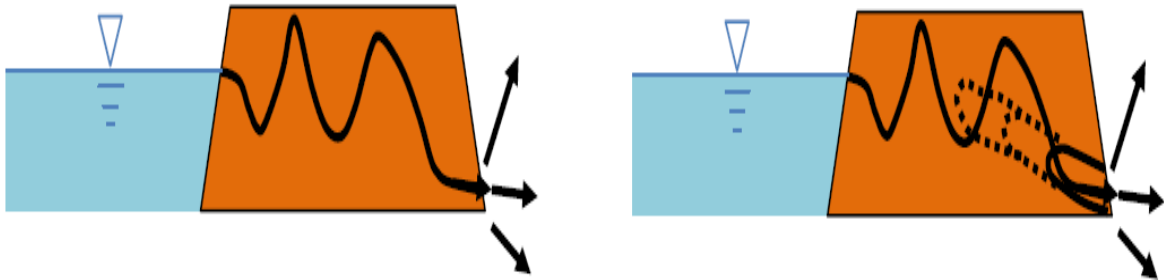


Figure 20 Phenomenon of regressive erosion (Pham 2008).

4- Cleaning: the cleaning and massive displacement of soil trapped under water pressure. This phenomenon occurs when a crack or a karst conduit is filled with clay material, and that the sudden arrival of the water causes displacement of the entire material (Figure 21). This results in the appearance of a cavity or a punctual enlargement of the conduit (Blais 2005, Pham 2008).

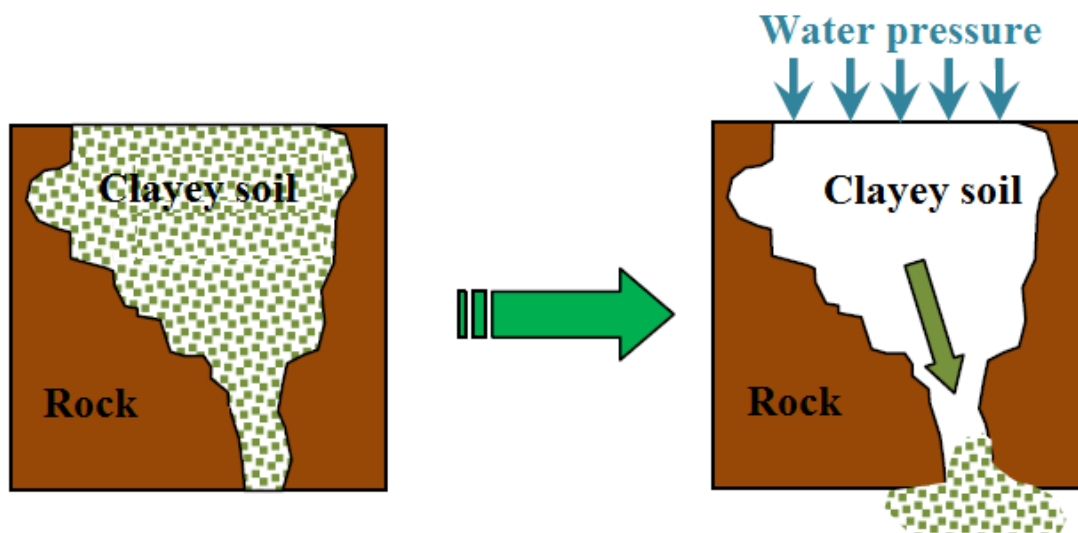


Figure 21 Phenomenon of cleaning (after Pham 2008).

5- Dispersion: the dispersion is a physicochemical process, which tends to disperse the clay platelets, and to generate a decrease in the size of the clay particles of the agglomerates, thereby facilitating migration in a flow. This phenomenon depends on the ionic balance between the fluid and the clay (Blais 2005).

6- Dissolution: the dissolution is not a mechanical, but chemical tearing phenomenon. This phenomenon corresponds to the conversion from a solid state into a liquid state of part of the constituents in a thermal or chemical action. This is reflected by an increase of porosity, and therefore permeability which can promote the occurrence of the internal erosion phenomenon (Garner and Sobkowics 2002).

7- Suffosion by exsolution: it corresponds to the expulsion of air trapped in the earthen structure at it is filled with water. This air trapped is compressed and transported by the flow. The experiments of Garner and Sobkowics (2002) show that the exsolution can cause piping phenomenon.

ii. *Transport phenomenon:*

1- Hydraulic piping: the hydraulic piping appears in a dike when the water flows through it in a preferential way. Along this way there are the weak points affected by erosion (regressive erosion). If these weak points are not surrounded by stable areas limiting their expansion, there is formation of a continuous hole from downstream to upstream, the flow velocity through the structure increases, thereby speeding up the failure process (Lautrin 2002, Blais 2005, Pham 2008). Figure 22 shows examples of piping.

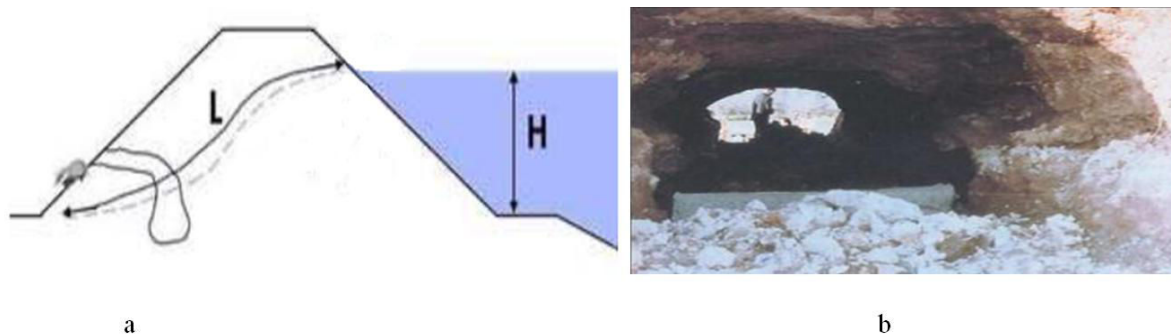


Figure 22 a-Phenomenon of piping (Pham 2008); b-hydraulic piping in earth dam (Lautrin 2002).

2- Suffosion: the term “suffosion” is Russian in origin and was introduced by Pavlov (1898) to describe the process of removal and transport of small soil particles through pores (Khomenko 2006). It is a phenomenon migration of small particles through the body of soil (Rosenbrand 2011). Contrary to the hydraulic piping, suffosion is much slower (see Figure 23). Suffosion may lead to regressive erosion in downstream of the dike, migrating fine particles allowing water to flow more quickly. The filtration through a conduit created by the removal of particles which can quickly lead to piping phenomenon that may result a failure in the dike (Pham 2008, Nombé et al. 2015).

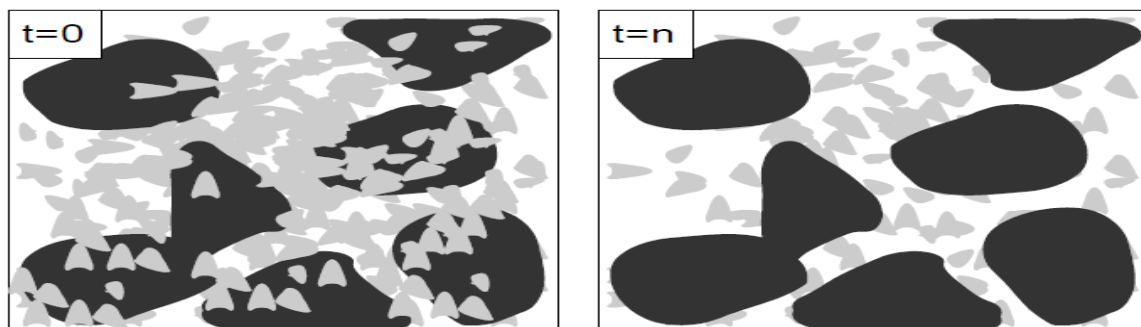


Figure 23 Schematic illustration of the suffosion where the fine grains (light) are present in the pore space (white) of the coarse grains (dark) (after Rosenbrand, 2011).

According to Serre (2005), it has been showed that the internal erosion events on the whole dams and dikes in France during the periods (1970-1997), consisted of 23 piping and 48 suffosions events but only 16 of them concerned the dike against flooding.

Generally, the statistic information about dikes failure is rare. Most of authors mix between the information about earth dams and dikes failure. Nevertheless, the analysis of 117 historical dike failures in the period 1954-2004 in Hungary was carried out by Nagy and Tóth (2005). Overflow is responsible for about 70% of all identified failures in Hungary in the last 50 years (Figure 24-a). The results of the analysis of Hungarian dikes are further supported by recent observations in the Elbe catchment (Saxony). Vorogushyn (2009) mentioned the analysis of responsible failure mechanisms in Saxony (Germany) during the August 2002 flood that is carried out by Horlacher et al. (2005). It is based on 84 identified dike failures and indicates that the dike overflow corresponds to the same percentage that in Hungary (Figure 24-b). However, the most dangerous historical events of dike failure in France were caused by overflow through the flooding periods, as the overflow that happened during flooding on 1846, 1856 and 1866 in Val d'Orléans (Gombert et al. 2014). Lino et al. (1999) showed that the causes of ruptures and breaches of dikes in Val d'Orléans through these three exceptional floods were as the following:

- overflow (66%);
- piping (5%);
- slope instability (10%);
- external erosion (5%) and
- others (14%).

They added, it is likely that some ruptures may have a karst origin.

The probability of presence of internal erosion or cavities underneath the dike remains important and perhaps they cause subsidence or decline in the top of the dike that might result in increasing the probability of overflow in flooding period.

Present work will focus on the presence of the cavity underneath dikes and consider it as a new and additional factor that can threaten the stability of dikes. However, cavities can be adding as one of the internal erosion factors. In this work we try to show the potential impact of the presence of cavities to speed up the other influencing factors on the stability of dikes that we have mentioned above, the effect of its presence upon the slope stability of dike will be studied (see chapter 4).

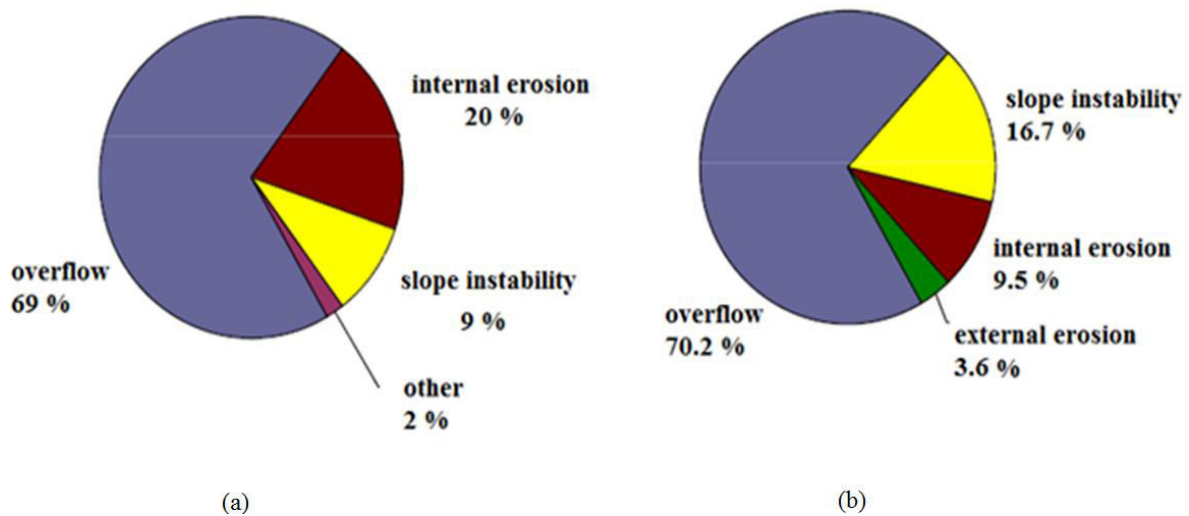


Figure 24 (a) Distribution of failure mechanisms for dike in Hungary in the period 1954–2004 (Nagy and Tóth, 2005). (b) Distribution of identified failure mechanisms for dike in Saxony (Germany) during the August 2002 flood event in the Elbe catchment (Horlacher et al. 2005 cited by Vorogushyn 2009).

1.3 Geo-risk methodology

To study the instability hazard and the interaction between cavities and dikes, we adopt the geo-risk methodology that is illustrated in Figure 25.

Generally, there are several methods allowing studying the interaction between cavities and dikes. The first one is the in situ observations with the collect of the necessary information about the cavities (dimensions, properties, etc.), existing sinkholes or collapses, etc. and the analyse of the data. The second is the analytical methods that may be developed to investigate the stability of dikes and cavities. While, the third one is the numerical methods, which can be used to prove the results of the analytical methods or to calculate more complicated problems which is not possible by analytical method. Each method presents some advantages and limitations. This methodology is based mainly on analytical approaches and verified by numerical modelling. The main advantage of the analytical approaches is that they can be used by engineers to perform and to assess the stability, taking into account the presence of cavities.

The first step of the adopted methodology is the observational method allowing characterising the different components of the system: dike, the soil and the cavity (dimensions, properties and positions) related to the dike. The second step is using an analytical method based on limit equilibrium by taking into account the presence of the dike on the stability of the underneath cavity and to identify the additional risk of sinkhole. The third step first used the analytical approach to evaluate the slope stability of the dike with/without an underneath cavity. Thereafter a numerical method is used to model the problem in two and three dimensions (2D/3D).

In the case of limited and/or uncertain values about the geometrical and geotechnical data, parametric studies must adopt. In this work the parametric studies concern the cavity, the river water level, the caves position underneath the dike and properties of soil (alluvium). The dike slope stability in case of cavities absence was tested by calculating a safety factor. Thereafter, the dike slope stability is re-tested in case of a cavity presence underneath it by using a new approach (analytical method) to take into account the impact of the cavity upon the slope stability.

The developed methodology and tools will be applied on the configuration of Val d'Orléans dikes. The description of the Val d'Orléans will be presented in the next chapter of the thesis.

In conclusion, the mechanical interaction between dike and cavity will be study taking into account the different mechanical and hydromechanical conditions.

1.4 References

- Abdulla, W. A. and Goodings D. J., 1996. Modeling of sinkholes in weakly cemented sand, *Journal of geotechnical engineering*, 122(12), pp 998-1005.
- Ammerlaan P.R.M., 2007. Levees and levee evaluation The Dutch and US practice compared Msc. thesis, Delft University of Technology, Netherlands.
- Anikeev A.V., 1999. Casual hydrofracturing theory and its application for sinkhole development prediction in the area of Novovoronezh Nuclear Power House-2 (NV NPH-2), Russia, in: Beck BF, Pettit AJ, Herring JG (eds.) *Hydrogeology and engineering geology of sinkholes and karst*, Balkema, Netherlands, pp 77–83.
- Augarde C.E., Lyamin A.V., and Sloan S.W., 2003. Prediction of Undrained Sinkhole Collapse, *journal of geotechnical and geoenvironmental engineering*, Vol. 129, No. 3, ASCE, pp 197–205.
- Baars S.V. and Kempen I.M.V., 2009. *The Causes and Mechanisms of Historical Dike Failures in the Netherlands*, Official Publication of the European Water Association (EWA), ISSN1994-8549, 14 pp.
- Bakalowicz M., 1999. *Connaissance et gestion des ressources en eau souterraines dans les régions karstiques*. Guide technique n°3, Lyon, Agence de l'eau Rhône-Méditerranée-Corse, 44 pp.
- Beck Barry F., 1984. Sinkhole Development in Georgia and Florida, U.S.A., and the Founding of the Florida Sinkhole Research Institute in *Proceedings of the Third International Symposium on Land Subsidence*, Venice, Italy. pp 607-616.
- Bendahmane F., Didier M., Alain A. et Pierre T., 2004. *Etude expérimentale de l'évolution par érosion interne des matériaux d'ouvrage hydraulique en terre*. GeM, UMR CNRS 6183, Research Institute of Civil Engineering and Mechanics Saint-Nazaire, France. 9 pp.
- Blais J., 2005. Typologie de l'érosion interne et érosion interne des digues fluviales, *courte revue bibliographique, Ingénieries N° spécial*, pp 65-70.
- Castanet C., 2008. *La Loire en val d'Orléans. Dynamiques fluviales et socio-environnementales durant les derniers 30 000 ans : de l'hydrosystème à l'anthroposystème*. Thèse, Université Paris 1 Panthéon Sorbonne.
- CEPRI (European Centre for Flood Risk Prevention), 2008. *Les digues de protection contre les inondations, Les guides du CEPRI*, 46 pp.
- Chan Y.C., 1995. *Factors affecting sinkhole formation*, Geo report No. 28, Hong Kong, 38 pp.
- Comité Français des Grands Barrages (CFGB), 2002. *Petits Barrages, recommandations pour la conception, la réalisation et le suivi*, Cemagref édition, Coordination : Gérard Degoutte, ISBN 2-85362-551-6, France, 175 pp.

- Craig, W. H., 1990. Collapse of cohesive overburden following removal of support, *Canadian Geotechnical Journal*, 27, pp 355–364.
- Degoutte G., 2012. *Les déversoirs sur digues fluviales*, Quae éditions, SBN-13: 978-2759218851, 181 pp.
- Drumm E.C., Akgun H., Aktürk Ö. And Tutluoglu L., 2009. Stability Charts for the Collapse of Residual Soil in Karst, *journal of geotechnical and geoenvironmental engineering*, DOI: 10.1061/(ASCE)GT.1943-5606.0000066, 7 pp.
- Drumm E.C., Kane W.F. and Yoon C.J., 1990. Application of limit plasticity to the stability of sinkholes, *Engineering Geology*, 29, Elsevier Science Publishers B.V., Amsterdam, pp 213-225.
- Filippini M. and Jeannin P., 2008. Possibilities and Limits to predict the 3D Geometry of Karst Systems within the Inception Horizon Hypothesis, *Geophysical Research Arc Abstracts*, Vol. 10, EGU 2008-A-02825, 2008, EGU General Assembly 2008, 2 pp.
- Ford D.C., and Williams, P.W., 1989. *Karst Geomorphology and Hydrology*: London, Unwin Hyman, 601 pp.
- Ford, D.C., and Williams, P.W., 2007. *Karst Hydrology and Geomorphology*: London, Wiley Chichester, 2nd ed., 576 pp.
- Forest Practices Branch, 2003. *Karst management handbook for British Columbia*, report government publications of province of British Columbia, 69 pp.
- Garner, S.J. and Sobkowicz, J.C., 2002. Internal Instability in Gap-Graded Cores and Filters, *Proceedings of 2002 Annual CDA Conference*, Canadian Dam Association, Victoria, BC, Canada, 10 pp.
- Gombert P., Orsat J., Mathon D., Alboresha R., Al Heib M., Deck O., 2014. Rôle des effondrements karstiques sur les désordres survenus sur les digues de Loire dans le Val d'Orléans (France), *Bull Eng Geol Environ*, 16 pp. DOI 10.1007/s10064-014-0594-8. pp. 125–140.
- Gutiérrez F., Guerrero J., Lucha P., 2008. A genetic classification of sinkholes illustrated from evaporite paleokarst exposures in Spain. *Environ. Geol.* 53, pp 993–1006.
- Gutiérrez F., Parise M., De Waele J., Jourde H., 2014. A review on natural and human-induced geohazards and impacts in karst. *Earth Science Reviews*, 138, pp 61-88.
- Hodek, R.J., Johnson, A.M. and Sandri D.B., 1984. Soil cavities formed by piping. In: *Proc. 1st Multidisciplinary Conf. on Sinkholes*. Balkema, Rotterdam, pp 249–254.
- Horlacher H.B., Bielagk U. and Heyer T., 2005. Analysis of the dike of Bruche at the Elbe and Mulde during the flood of 2002 in the category Sachsen, *Research Report 2005/09*,

- Institute of Hydraulic Engineering and Technical Hydromechanics, Dresden University of Technology, Germany, 82 pp.
- Huang H.H., 2007. Geomorphologic investigations on karst terrain: A GIS-assisted case study on the island of Barbados, M.Sc. Thesis, McGill University, Montreal, 94 pp.
- Hyatt, J.A., and Jacobs, P.M., 1996. Distribution and morphology of sinkholes triggered by flooding following Tropical Storm Alberto at Albany, Georgia, USA: *Geomorphology*, v. 17, pp 305–316.
- Iqbal M.A., 1995. Engineering experience with limestone. In: Proc. 5th Multidisciplinary Conf. on Sinkholes and the Environmental Impacts of Karst. Balkema, Rotterdam, pp 463–468.
- Keddouri A., 2011. Étude des pathologies de la digue d’oued Kreirech wilaya de Djelfa, mémoire de Magister, université Abou Bekr Belkaid, Algérie, ch.1, pp 6-34.
- Keqiang H., Wang B., Zhou D., 2004. Mechanism and mechanical model of karst collapse in an over-pumping area, *Environmental Geology* 46, pp 1102-1105.
- Khomenko V. P., 2006. Suffosion hazard: Today's and tomorrow's problem for cities, IAEG2006 Paper number 577 The Geological Society of London, 8 pp.
- Kusky T. M., 2008. Floods: Hazards of Surface and Groundwater Systems, Facts on File, New York. 144 pp.
- Lautrin D., 2002. Vieillissement et réhabilitation des petits barrages en terre, Cemagref Editions, France, 239 pp.
- Lepetit L., 2002. Etude d’une méthode de diagnostic de digues avec prise en compte du risque liquéfaction. PhD thesis, the doctoral school engineering sciences, Clermont-Ferrand, France.
- Lino M., Mériaux P., Royet P., 1999. Méthodologie de diagnostic des digues appliquée aux levées de la Loire moyenne, CEMAGREF Editions, 223 pp.
- Mériaux P., Royet P. and Folton C., 2001. Surveillance entretien et diagnostic des digues de protection contre les inondations, guide pratique à l'usage des propriétaires et des gestionnaires ; Cemagref, France, 191 pp.
- Nagy L. and Tóth S., 2005. Detailed Technical Report on the collation and analysis of dike breach data with regards to formation process and location factors, Technical report, H-EURA qua Ltd., Hungary, 77 pp.
- Nombré A., Somda E.A., Kabore M., and Millogo F., 2015. Chapter 6, Overtopping and internal erosion on small dams in Burkina Faso Dam Protections against Overtopping and Accidental Leakage, Edited by Miguel Ángel Toledo, Rafael Morán, and Eugenio Oñate CRC Press, eBook ISBN: 978-1-315-68535-9, DOI: 10.1201/b18292-9, pp 83–87.

- Parise M., Closson D., Gutierrez F. & Stevanovic Z., 2015. Facing engineering problems in the fragile karst environment, *Engineering Geology for Society and Territory. Volume 5 - Urban Geology, Sustainable Planning and Landscape Exploitation*. Springer, ISBN 978-3-319-09047-4, p 479-482.
- Parise M., 2008. Rock failures in karst., *Landslides and Engineered Slopes. Proc. 10th International Symposium on Landslides, Xi'an (China), June 30 - July 4, 1*, pp 275-280.
- Pavlov, A.P., 1898. About relief of plains and its change under the influence of subsurface and surface water. *Geosciences*, 5 (3-4), 91-147 (in Russian).
- Pazuniak B.L., 1989. Subsurface investigation response to sinkhole activity at an eastern Pennsylvania site. In: *Proc. 3rd Multidisciplinary Conf. on Sinkholes and the Engineering and Environmental Impacts of Karst*. Balkema, Rotterdam, pp 263–269.
- Pham T. L., 2008. Érosion et dispersion des sols argileux par un fluide, Thèse de doctorat en géotechnique, Ecole nationale des Ponts et Chaussées. France.
- Rosenbrand E., 2011. Investigation into quantitative visualisation of suffusion. PhD thesis, Delft University of Technology, Netherlands.
- Salvati R., Sasowsky I.D., 2002. Development of collapse sinkholes in areas of groundwater discharge, *J Hydrol* 264, 11 pp.
- Schaefer J.A., 2009. Risk evaluation of dams on karst foundations, 29th Annual USSD Conference Nashville, Tennessee, April 20-24, 2009, pp 541-579.
- Serre D., 2005. Évaluation de la performance des digues de protection contre les inondations ; Modélisation de critères de décision dans un Système d'Information Géographique, Ph. D. Thesis, University of Marne-la-Vallée, 2005, 240 pp.
- Sharp T.M., 1997. Mechanics of formation of cover collapse sinkholes. In: Beck BF, Stephenson JB (eds.) *Engineering geology and hydrology of karst terranes*, A. A. Balkema, Netherlands, pp 29–36.
- Sharp T.M., 2003. Cover-collapse sinkhole formation and soil plasticity. In: Beck BF (ed.) *Sinkholes and the engineering and environmental impacts of karst*. Geotechnical Special Publication No.122, American Society of Civil Engineers, Reston, pp 110–123.
- Simm J., Wallis M., Smith P., Tourment R., Veylon G., Deniaud Y., Durand E., McVicker J., and Hersh-Burdick R., 2012. The significance of failure modes in the design and management of levees a perspective from the International Levee, Published in the *Proceedings of the 2nd European Conference on Flood Risk Management, FLOODrisk2012*, Rotterdam, Netherlands, 15 pp.
- Skempton A.W., Brogan J.M., 1994. Experiments on piping in sandy gravels, *Géotechnique*, vol.44 (3), pp 440-460.

- Sowers G.F., 1975. Failures in limestone in humid subtropics. Proceedings American Society Civil Engineers, 101 GT8, pp 771–787.
- Sowers, G.F., 1996. Building on Sinkholes. ASCE Press, New York, 202 pp.
- Sturman A. and Spronken-Smith R., 2001. South Melbourne, Vic.; Auckland The Physical Environment: A New Zealand Perspective, Oxford University Press (OUP). Ch.17, pp 307-325.
- Terzaghi, K., 1943. Theoretical Soil Mechanics. New York: John Wiley & Sons.
- Tharp T.M., 1999. Mechanics of upward propagation of cover-collapse sinkholes, Engineering Geology 52, Elsevier Science B.V., pp 23–33.
- USACE (US Army Corps of Engineers), 2000. Design and Construction of Levees, engineering manual, EM 1110-2-1913, Department of the Army, Washington, DC.
- USACE (US Army Corps of Engineers) 2003, Slope Stability, engineering manual, Appendix c,[online]
http://www.publications.usace.army.mil/Portals/76/Publications/EngineerManuals/EM_1110-2-1902.pdf.
- USACE (US Army Corps of Engineers), 2006. levee owner's manual for non – federal flood control works, the rehabilitation and inspection program public law 84-99, 74 pp.
- USGS (United State Geological Survey), 2007. Sinkholes, Publications Warehouse, report, Fact Sheet 2007-306, 2 pp.
- Vorogushyn S., Merz B. and Apel H., 2009. Development of dike fragility curves for piping and micro-instability breach mechanisms, Nat. Hazards Earth Syst. Sci., 9, Published by Copernicus Publications on behalf of the European Geosciences Union, pp1383–1401.
- Waltham T., Bell F., Culshaw M., 2005. Sinkholes and subsidence, karst and cavernous rocks in engineering and construction, book, Springer, ch.1, 379 pp.
- Waltham, T. & Lu, Z., 2007. Natural and anthropogenic rock collapse over open caves. In M. Parise & J. Gunn (Eds) Natural and anthropogenic hazards in karst areas: recognition, analysis and mitigation. Geol. Soc. London, special publication, 279, pp13–21.
- Wei J., 2012. Great Inventions that Changed the World, book, John Willey & Sons? ISBN: 978-1-118-34273-2, 360 pp.
- White E.L., Aron, G., White, W.B., 1984. The influence of urbanization on sinkhole development in central Pennsylvania. In: Proc. 1st Multidisciplinary Conf. on Sinkholes. Balkema, Rotterdam, pp 275–281.
- Williams P., 2008. World heritage caves and karst; a thematic study, IUCN program on protected areas, World Heritage Studies No.2, Switzerland, 57 pp.

- Wilson, W.L., Beck, B.F., 1988, Evaluating sinkhole hazards in mantled karst terrane. Geotechnical Aspects of Karst Terrains. Geotech. Springer Pub. No. 14, ASCE, New York, 24 pp.
- Worthington S.R.H. and Ford D.C., 2009. Self-Organized Permeability in Carbonate Aquifers, Vol. 47, No. 3, Ground Water, (NGWA) National Ground Water Association, Canada, pp 326–336.
- Yang M.Z., Drumm E.C., 1999. Stability evaluation for siting of municipal landfills in karst. In: Beck BF, Pettit AJ, Herring JG (eds.) Hydrogeology and engineering geology of sinkholes and karst. A.A. Balkema, Netherlands, pp 373–380.
- Zhao H., Ma F., Guo J., 2011. Regularity and formation mechanism of large-scale abrupt karst collapse in southern China in the first half of 2010, Springer, Nat Hazards DOI 10.1007/s11069-011-9888-3, pp 1037-1054.
- Zhou W., 1997. The formation of sinkholes in karst mining areas in China and some methods of prevention. Environ Geol 31(1/2), pp 50–58.
- Zhou W. and Beck B.F., 2008. Management and mitigation of sinkholes on karst lands: an overview of practical applications. Environ. Geol. 55, pp 837–851.

2.1 The dikes of Val d'Orléans

The first dikes against flooding in the Val d'Orléans date back from the 9th century. Called "turcies", they were initially composed of wood and earth and their function was to turn the main stream to allow the cultivation of the valley. Over time and from flooding, these turcies moved closer to the riverbed to win farmlands. They were then reinforced and raised through locally available materials (sandy-clayed alluvium). They were then crowned by roads to link the valley from one end to the other at any time. Their maximum height nowadays is about 8 m above low water datum to a slope of 2/1 (Mathon 2012) (Figure 26).

Depending on their location and their construction history along the river, the dikes do not have the same geometry and structure. The most common type is constructed using a natural soil materials and has no reinforcement element. However, one can also find a reinforced masonry riprap (usually based on wooden piles) in upstream (Loire side), wherever the dike is subjected to the stream action and also downstream (valley side) to eliminate the risk of erosion by submersion (Figure 27). Figure 27 presents three typical dike cross sections (Maurin 2012), from the oldest dike model to the most recent dike type. This figure presents also the foundation section with alluvium and limestone layers.

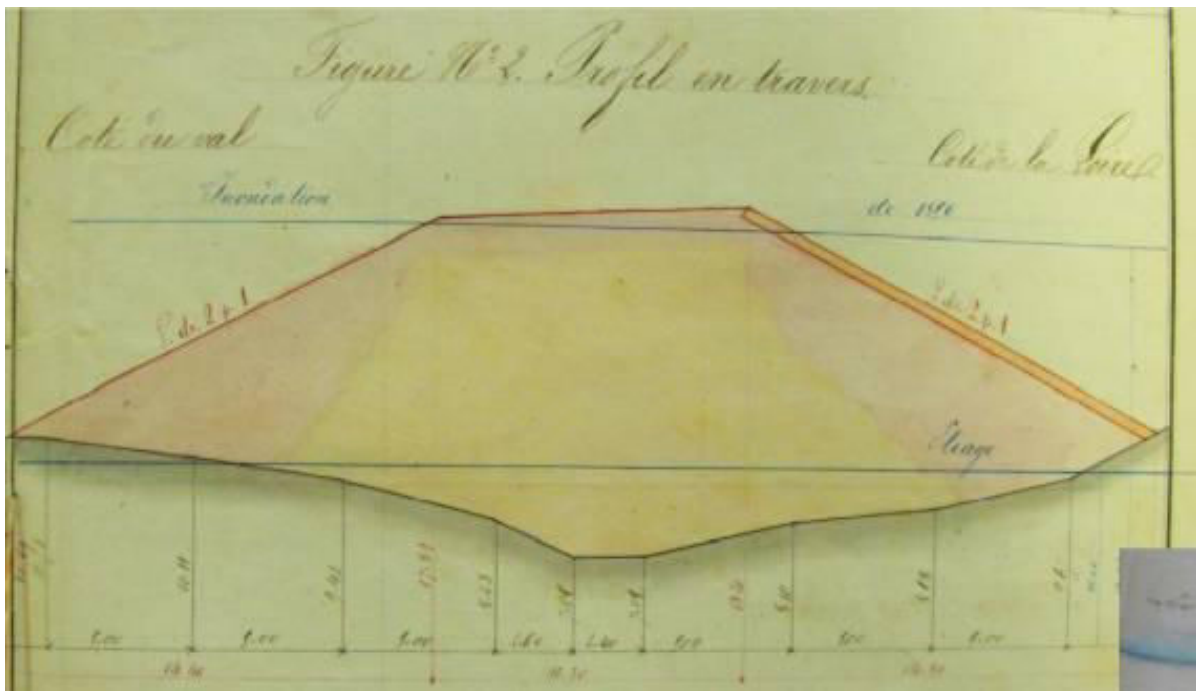


Figure 26 Cross section of Loire dike about 1850 (Source: Media library of Orléans (Médiathèque d'Orléans)) (cited by Orsat 2013).

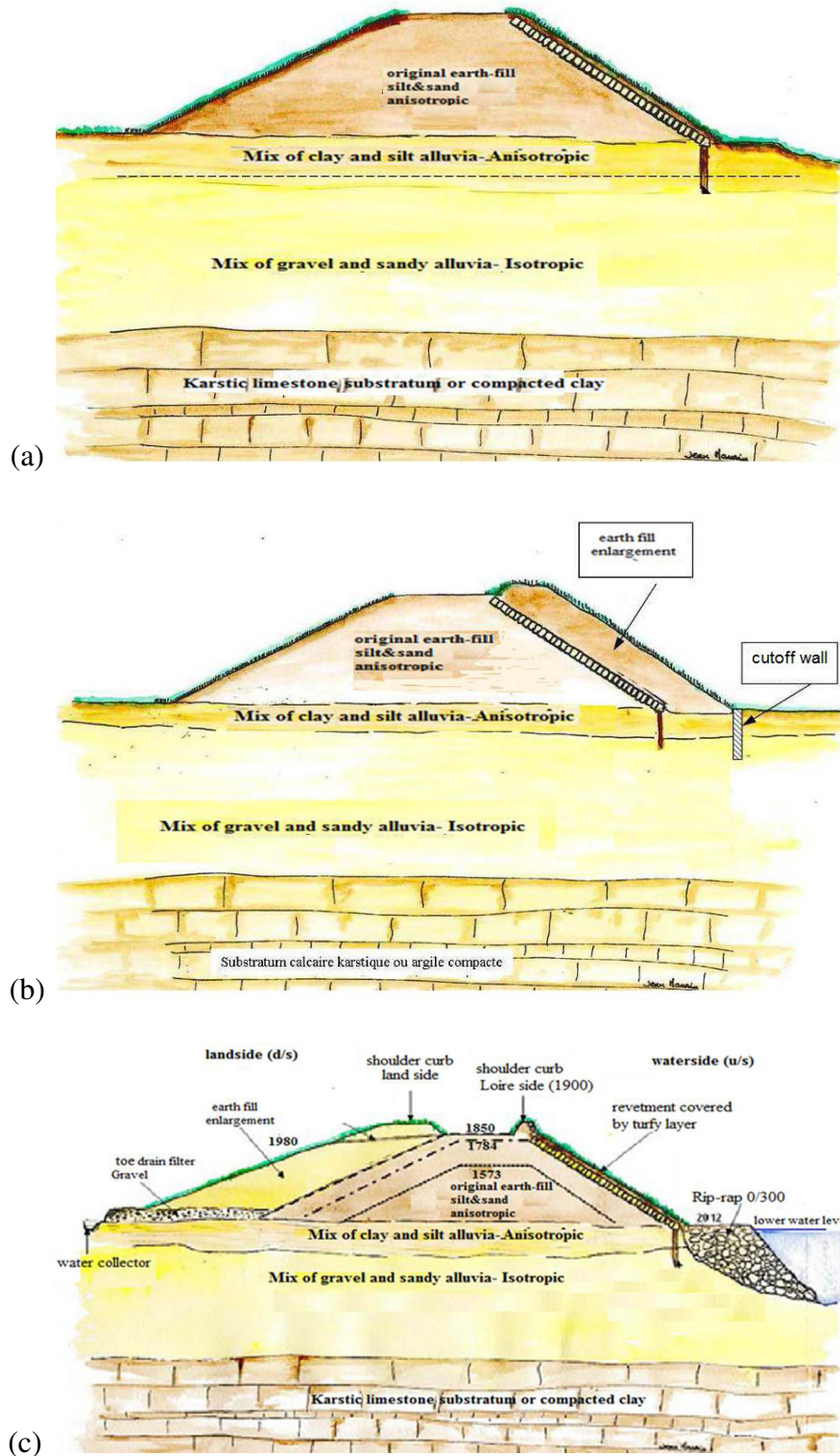


Figure 27 Typical cross sections of a Loire dike nowadays and the evolution of dimensions (d/s: downstream, u/s: upstream). a- oldest unreinforced dike; b- Loire side reinforced dike and c- land side reinforced dike (after Maurin 2012).

In France, the risk assessment study of dikes is mainly based on their classification. The classification of dikes is done according to Article R. 214-113 (2007) of the Code of the Environment, which is based on two criteria: the maximum height of dike structures H in

meters (defined as the greatest height measured vertically between the top of the structure and the natural terrain on the side of the protected area) and the protected population P (number of people) as shows in Table 2. Thus, the dikes of Val d'Orléans are considered in class A, due to their height and the population numbers of the area. The class A is considered as the most dangerous configuration in state of potential breaching through the dike in flood seasons because of negative consequences due to flooding (CEPRI 2008).

Table 2 Classification of dikes according to Article R. 214-113 (2007) (in France).

CLASS	Dike height H (m)	Population in the protected area P
A	$H \geq 1$	and $P \geq 50\,000$
B	$H \geq 1$	and $1\,000 \leq P < 50\,000$
C	$H \geq 1$	and $10 \leq P < 1\,000$
D	either $H < 1$	or $P < 10$

2.2 The Val d'Orléans site

2.2.1 Site presentation

The Loire is the longest and most capricious river in France (1012 km). On its banks, live about 4 million people, including 300,000 that are subject to flooding hazard (Maurin et al., 2012). Since the Middle Age, the protection of people and property against flooding of the Loire is mainly focused on the construction of dikes (levees). Their total length is now about 650 km. According to the recent risk assessment study, 6 billion Euros is the estimated damage that could be caused by the next major flooding as occurred in 1846, 1856 and 1866 (Gombert et al. 2014). The area of the Val d'Orléans is halfway through the river. It covers about 30 km upstream of Orléans up to 5 km downstream, towards the confluence of the Loire with a little river called the Loiret (Figure 28). The area is 1-7 km wide and it is protected against flood by about 50 km of dikes (Maurin J. 2012; Gombert et al. 2014).

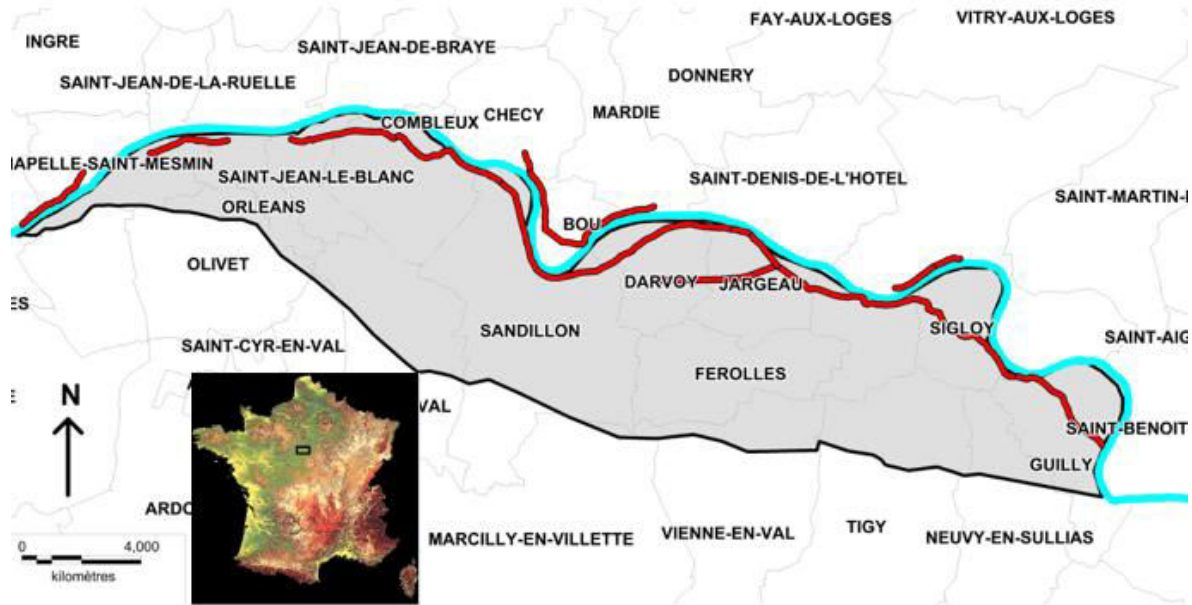


Figure 28 Map showing the Val d'Orléans flood zone (grey) and dikes (red) (from: CEREMA).

During the last centennial floods of the nineteenth century, these dikes collapsed 35 times which led to catastrophic flooding consequences. No further 100-years flood occurred during the twentieth and the beginning of the twenty first centuries and the likely response of these old dikes during future major floods is poorly understood. One important information obtained from the geology investigations in the Val d'Orléans is the presence of 5-15 m of clayed sandy alluvium covering a karstified Tertiary limestone bedrock called Beauce limestone. The limestone bedrock contains karst cavities. The cavity may play a significant role on the dike collapse and vice versa.

2.2.2 Geological context

After leaving Primary terranes of the Massif Central, the Loire crosses the southwestern part of the Paris basin and thus overlaps the Secondary and Tertiary formations between Decize and Angers. It is between Gien and Blois that Loire intersects the Tertiary formation of Beauce limestones. The Val d'Orléans is located in the heart of a relatively shallow dipping synclinal in which Loire and Loiret flow from West to East (see Figure 29). This area is characterized by relatively simple geology: the Loire alluviums are based on a substratum formed by the Beauce limestones (Caudron 1964).

The formation of Beauce limestone has an outcrop area of 10,000 km² (LCPC 1973). This is a relatively heterogeneous formation highly fractured and subjected to an intense karstification (Gutierrez et Binet 2010). Karstification is taking place in its upper part, represented by lacustrine Oligo-Miocene limestones, whose average thickness is estimated around 60 to 80 m. In these specific aquifers, water flows through cracks and fractures in the rock, and by corrosion and erosion, form a multitude of underground conduits are formed, some of them

penetrable by man as shown in Figure 30. The average diameter of the main karstic conduit is about 5 m near the karstic springs of Loiret (Joodi 2009).

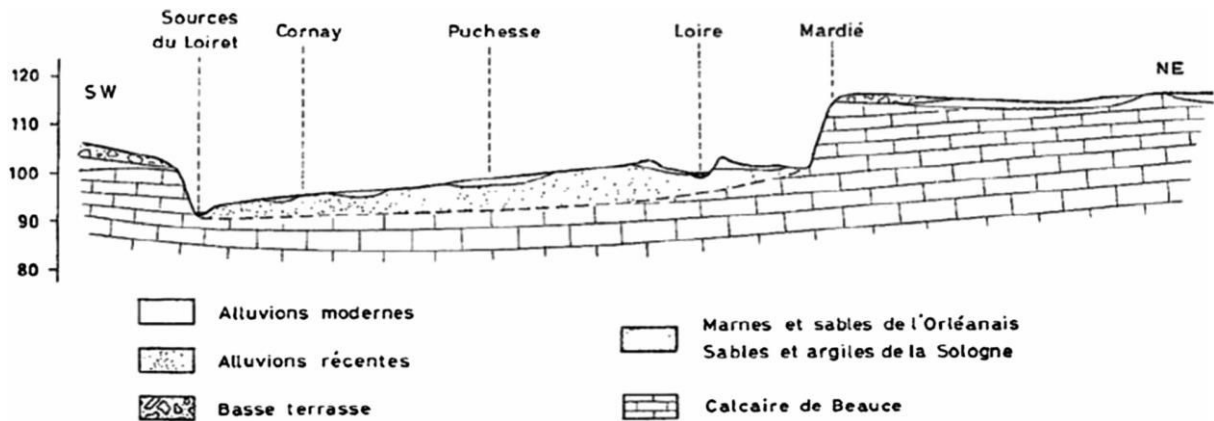


Figure 29 Geological section of the Val d'Orléans (Caudron 1964).



Figure 30 A diver inside main conduits of the Val d'Orléans karst system - View taken inside the "Abîme", one of the springs of Loiret (SSL: The Speleology Underwater Loiret Association, 2004).

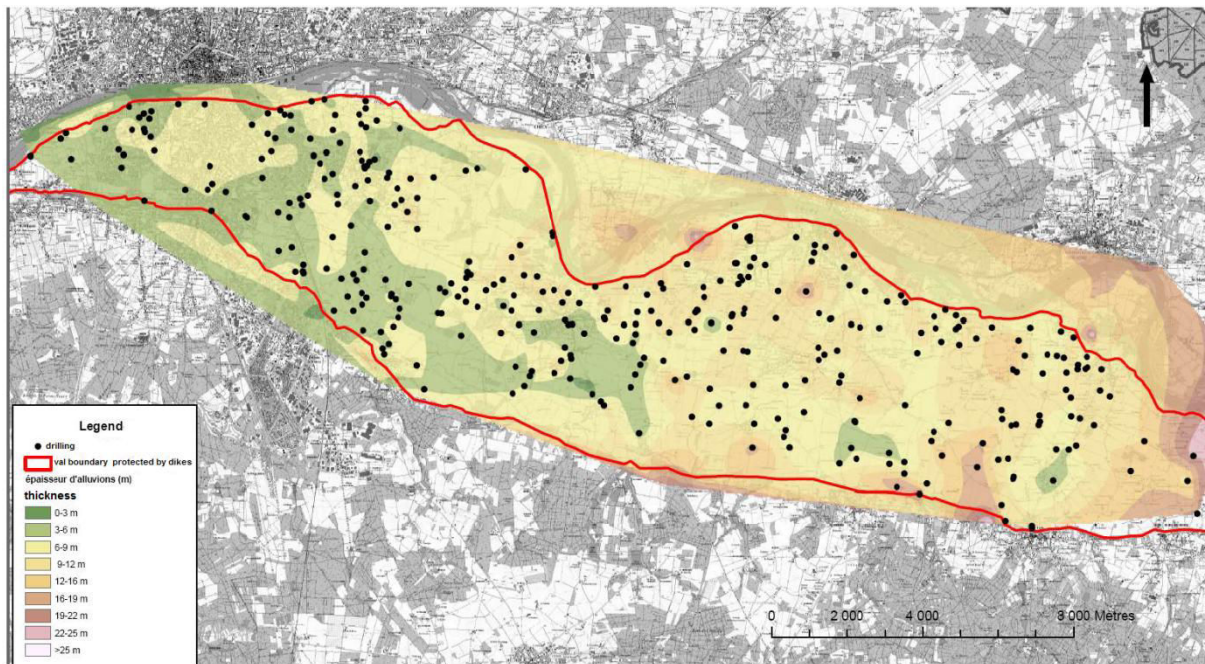


Figure 31 Map of alluvial thickness of the Val d'Orléans (sources: SCAN 25® - © IGN Paris - BSS BRGM interpolation "natural neighbors" by ARCGis).

The overburden of the karstic formation is constituted by 5 to 10 m of Loire's sandy-clayed alluvium with a maximum thickness of 25 m as shown in Figure 31. Generally, the alluvium is organized in two horizons: the upper horizon consists of fine sandy soil associated with silt or clay, while the lower horizon consists of coarser sand, more or less gravelly.

On the tectonic plan, the Beauce limestone are generally tabular but the Val d'Orléans zone corresponds to a broad syncline whose Loire occupies the North flank and Loiret the axis (Figure 29). The limestone is also affected by several major tectonic features that may have influenced the direction of the Loire and of the karstic circulations.

2.2.3 Hydrogeological context

These two formations contain itself an aquifer: the alluvium aquifer is overlying the karstic aquifer. This configuration implies (i) the alluvium aquifer and the karstic aquifer are in hydraulic continuity in this area (Lepiller 2006) and (ii) the water from the Loire enters the karst through numerous sinkholes and circulates until the Loiret's springs, located 15 km downstream. The cumulated average of underground flow is around 12 m³/s, with an average velocity of more than 200 m/h (Guttierez and Binet 2010). These values are characteristic of highly developed karstic conduits as mentioned by the speleologists that have explored the Loiret's springs caves: Boismoreau (2008) draws the map of 4300 m of karstic galleries from 2 to 9 m high, located between 8 and 28 m deep (Figure 32).

Inside the Val d'Orléans, more than twenty boreholes have reached karstic caves between 8 and 28 m deep, with diameter from 0.2 to 4.4 m. Such cave has also been found downstream of our study area, between 20 and 30 m deep, with diameter from 1.50 to 6 m (LCPC 1973).

That means the Beauce limestone is highly karstified in all these areas with some caves that can appear a few meters under the alluvium basis. That means the likelihood to have a karst cavity under the dike can be significant in the Val d'Orléans area.

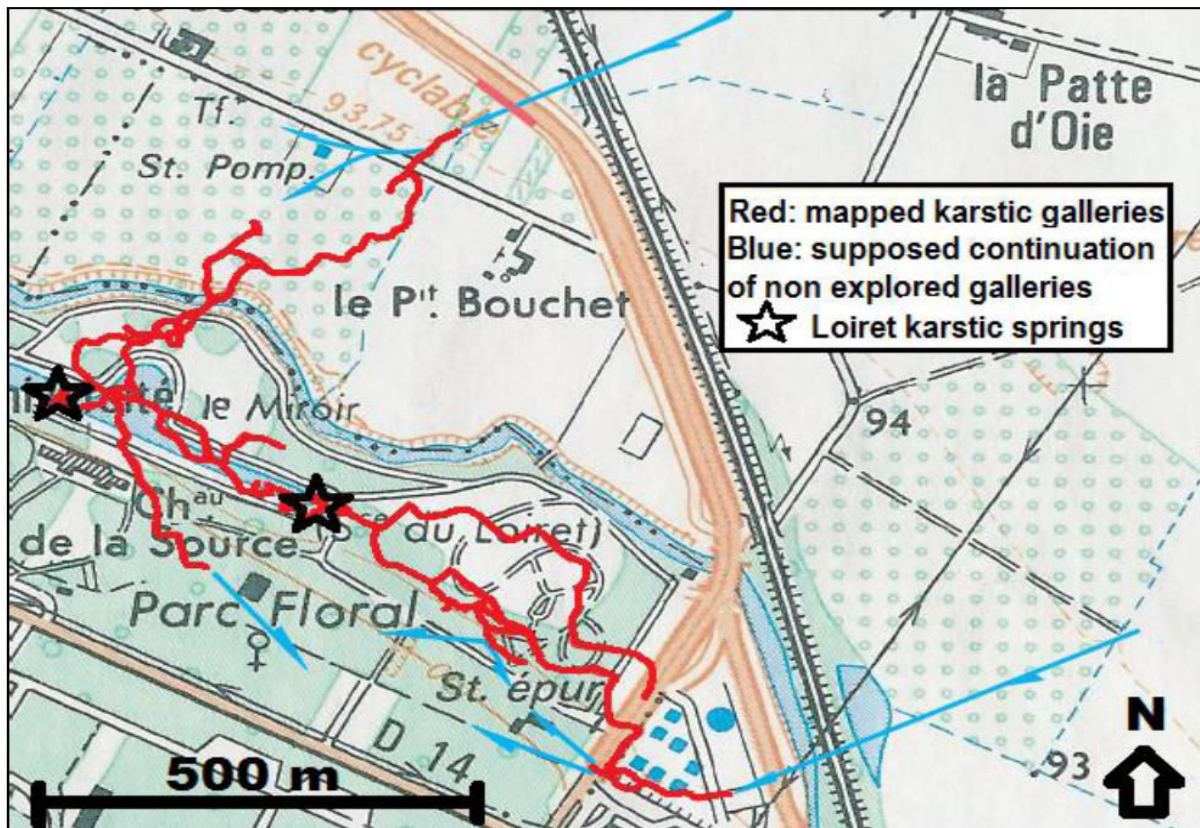


Figure 32 Topography of karstic galleries upstream the Loiret's springs (Boismoreau 2008).

2.3 Sinkholes and subsidence (historical information)

In this work, we distinguished two forms of probable surface consequences of karst cavities underneath the dike; the first expected instability form is the sinkhole, which is a hole or an opened void formed at a land surface (as we defined it in the previous chapter), while the second is the subsidence, which is a soft lowering of the land surface (Figure 33).

In the site of the dike of Val d'Orléans, the two forms of the instability (sinkhole and subsidence) were noted. Sinkholes recently were noted in the toe and head of the dike as illustrated in the Figure 34 (a and b) respectively. Chapter 6 identify the required conditions to get a sinkhole.

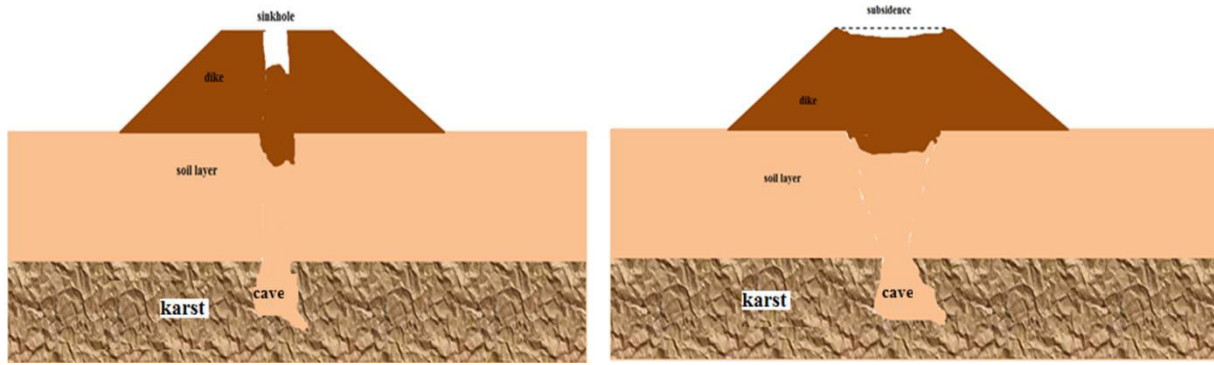


Figure 33 Schema shows the difference between the terms sinkhole and subsidence in our work.

The historic study and the analysis of ancient documents were collected. In the Val d'Orléans, nearly 600 collapses were reported since 1856 on an area of 167 km², representing an average of 3 collapses/km² (Gombert et al. 2014). Their diameter varies from 0.50 to 18 m and 62 % occurred at distance less than 2 km from the Loire (Figure 35), that is to say, close to the dikes.

Statistically, more than 50 collapses must have appeared under the dikes or in their immediate proximity, but only ten of them have effectively been observed (Figure 34). Sinkholes and subsidence probably occur in the region due to the collapse of the karstic caves that are only 10-20 m deep. The analysis of history cases of the dike failure seems to indicate a likelihood of the influence of the karstic cave on the stability of some dikes (see Figure 34 a & b).

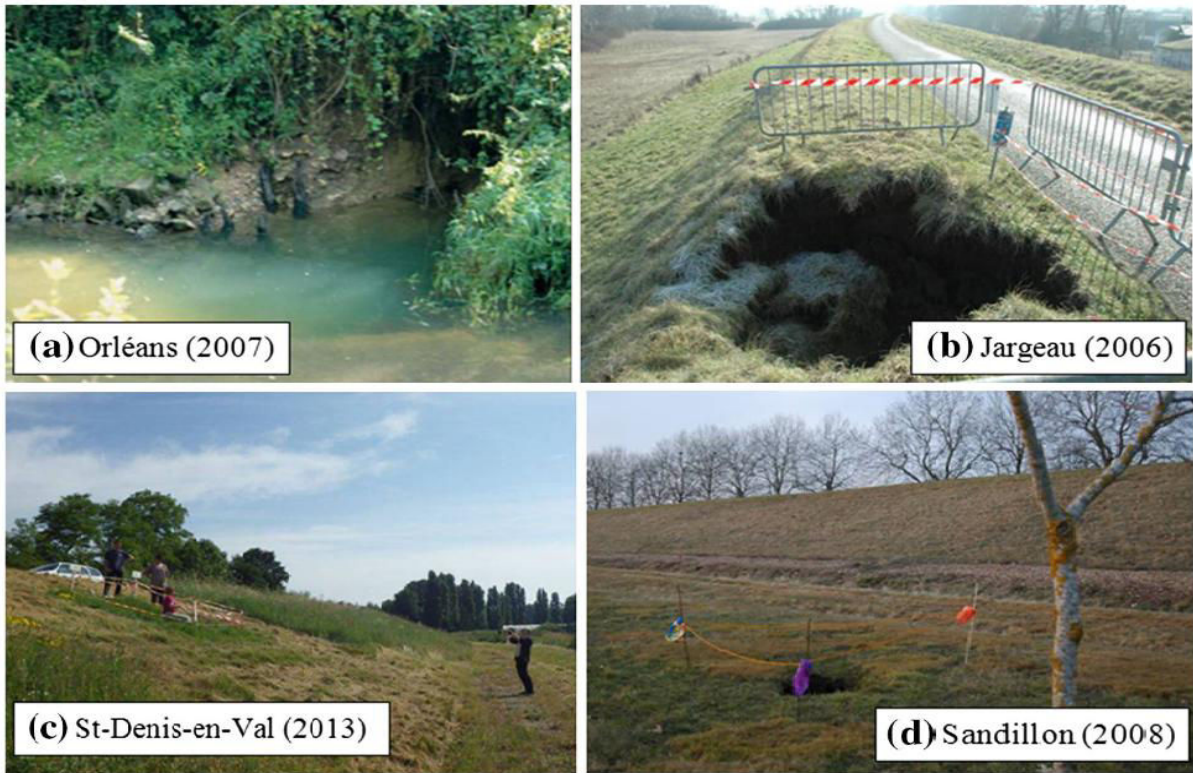


Figure 34 Examples of recent karst collapses that occurred in toe of dike in upstream (a), in dike crest (b), on the dike body in downstream (c) and behind the dike, downstream (d) (Gombert et al. 2014).

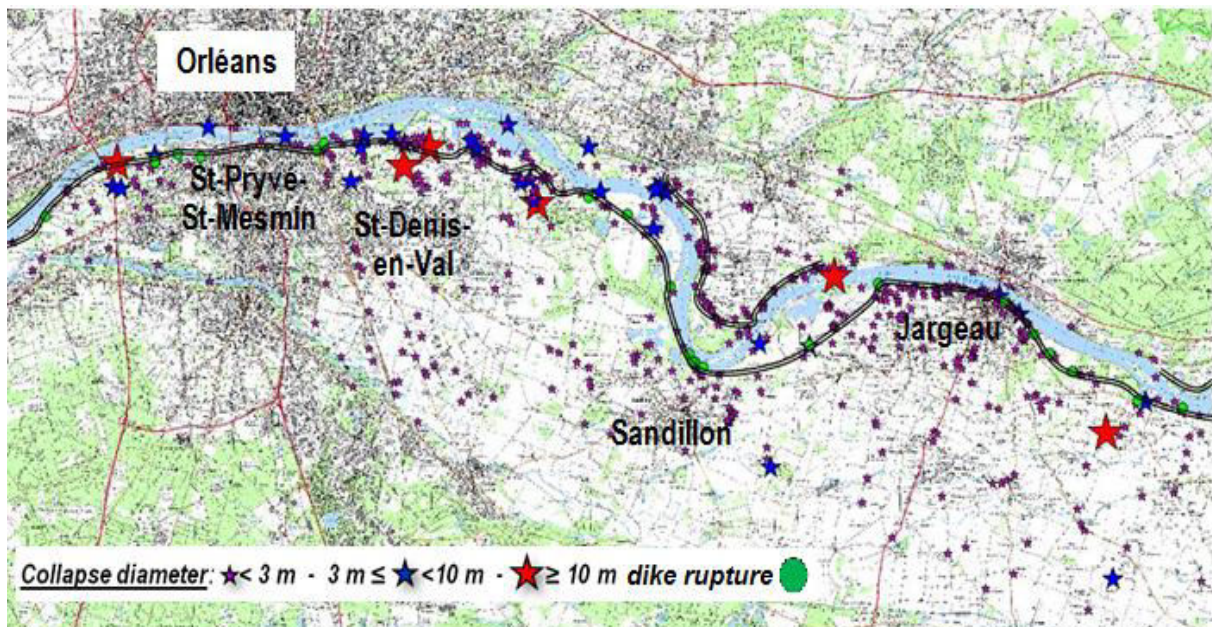


Figure 35 Distribution of collapses and ruptures of dikes in the Val of Orléans (Gombert et al 2014).

A statistical study of the distribution of 473 sinkholes was performed by Orsat (2013). More than 90% of reported sinkholes in this study had surface diameters ranging from 0.5 to 2 m.

She distributed these sinkholes according to their distance from Loire (Figure 37). The distances are considered positive in the left side of the Loire (Val d'Orléans) and negative on the right side. We can note from the histogram in Figure 36 that the density of sinkholes is higher in left side of Loire, and especially in the first 1000 meters where the dikes are built. Thus, if we consider that the sinkholes are the final results of karstic cavities collapses, the study of their effect of on the dike stability appears and reasonable and realistic problematic.

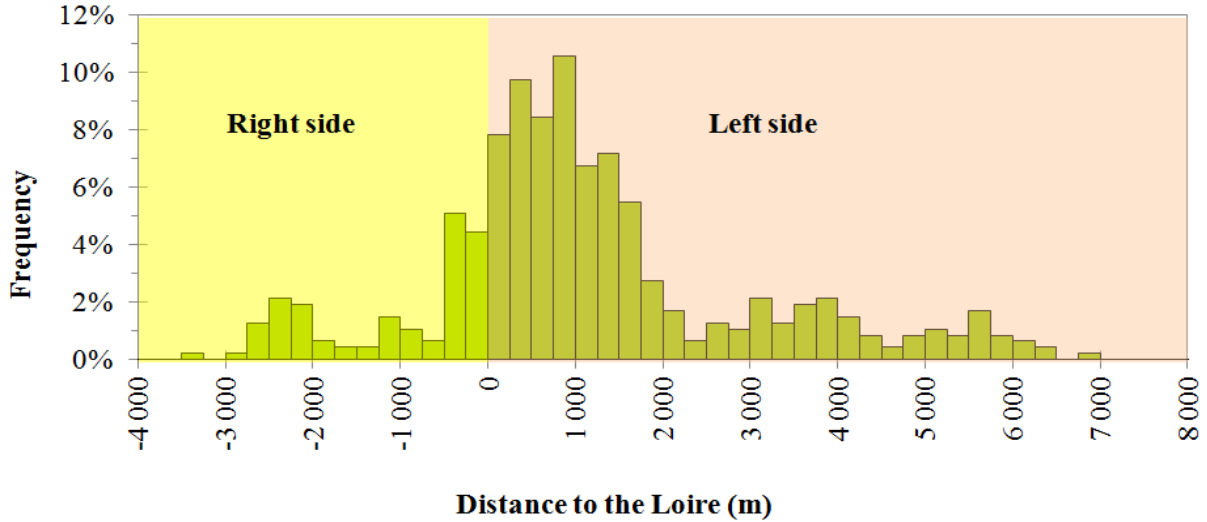


Figure 36 Histogram of the distribution of sinkholes (%) with respect to their distance to the Loire (m) (after Orsat 2013).

2.4 Mechanical properties of soils

The sinkhole occurrence depends on different parameters: soil characteristics, depth and geometry of the cavity, etc. From literature review, the knowledge of mechanical properties of the dike and the alluvium layer is limited. IRSTEA (National Research Institute of Science and Technology for Environment and Agriculture in France) and CEREMA (Study Centre and expertise about the risks, the environment, mobility and development in France) carried out some laboratory tests, the results are summarized in Table 2 for alluvium layer and dike material and the positions of these investigations is shown in Figure 37.. Unfortunately, these investigations do not contain information about the dimensions of the dike cross sections as well as the height of the dike, which cause difficulty to distinguish between soils of the dike from those that belong to the soil underneath it. As a consequence, the dimensions of the dike, which were identified by IRSTEA, were adopted. At last, we used the cohesion c and friction angle ϕ values in Guilly site that are listed in Table 3. However, this dike in site of Guilly was chosen because of the weakest values of cohesion in the both the dike and the soil layer in addition to the thickness of the alluvium layer value is less than the range of average (5-10 m). Thus, the use of the properties that were investigated by IRSTEA, it would make us in safe side of the study (Figure 2.13). Furthermore, the values of soil layer properties in the same site (Guilly) which carried out by CEREMA are used to verify the value of critical diameter of cavities (see chapter 3). The values ($c = 0$ and $\phi = 36^\circ$) were neglected because of the position of investigation is unclear where exactly it is located; in the part of the dike or in

the alluvium layer. Moreover, these values are for layer represent 30 centimetres only which cannot be considered for the entire alluvium layer (or the dike). The depth of karst (limestone) was assumed equal to 10 m in elastic state (Figure 38) and it was taken into account in numerical model only.

Table 3 Mechanical parameters of the dike and alluvium materials nowadays in the Val d'Orléans with cohesion c and the angle of internal friction φ . All boreholes of the tests were taken starting from the head of the dikes.

Site	Depth (m)	Type of soil	c (kPa)	φ (°)	Permeability (m/s)	Source
St-Pryve-St-Mesmin	3.88 - 4.24	clay	0-17	22-25	$2,7 \cdot 10^{-9} - 10^{-7}$	CEREMA (Saussaye and Durand, 2015)
St-Denis-en-Val	2.5 - 3	Silt Sandey clay	21	25	$2,7 \cdot 10^{-9} - 10^{-7}$	CEREMA (Saussaye and Durand, 2015)
Sigloy	5.5-5.9	Silty clay	0-16	21-29	$2,7 \cdot 10^{-9} - 5 \cdot 10^{-5}$	CEREMA (Saussaye and Durand, 2015)
	6.13-6.25	Silty sandy	0	37		
	6.64-7	Clay	0-14	23-33		
	9.66-10	clay	0-32	9-19		
Guilly	4.7-5	Silty sand	0	36	$5 \cdot 10^{-5}$	CEREMA (Saussaye and Durand, 2015)
	11 -11.6	clay	36	16	$2,7 \cdot 10^{-9} - 10^{-7}$	
Guilly	0.5-6	Silt	5	32	Non-determined	IRSTEA, 2008
	6-10.5	Sand slightly clayey sand	0	32		



Figure 37 The four dike positions (in red points) that are mentioned in Table 3(after Saussaye and Durand, 2015 and IRSTEA, 2008).

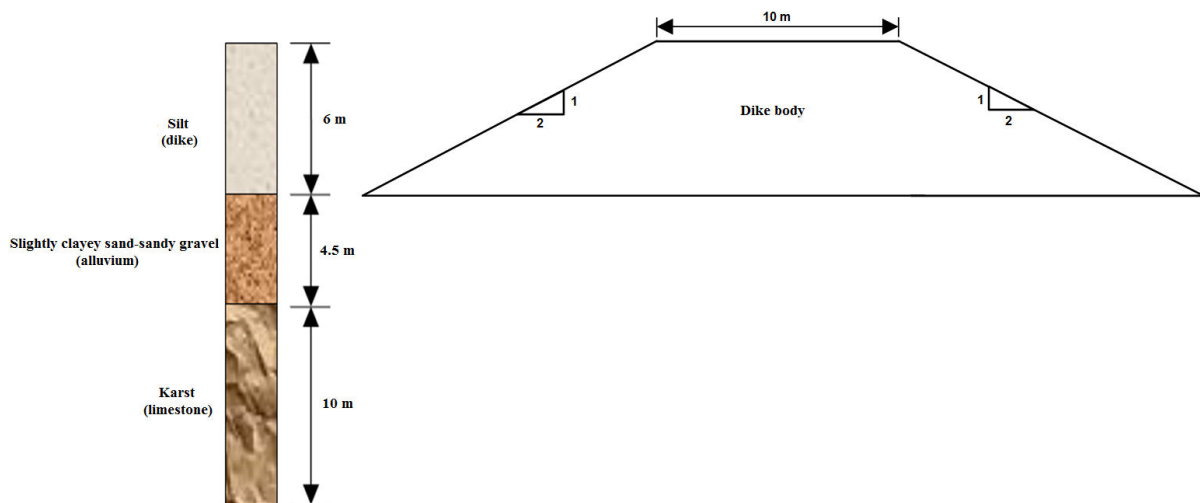


Figure 38 Geological cross section and dimensions of the dike in site of Gully and the soil underneath it. (after IRSTEA).

2.5 Summary

The dikes protect a large territory in the karstic area called “Val d’Orléans”, where the dikes are classified in class A (in the most dangerous important group in France). The data regarding the instability (sinkhole and subsidence) of this area present a real scientific challenge, if we suppose that such instabilities result from the interaction between the cavity and the dike.

In this chapter, we described the geological, hydrogeological and mechanical characteristics of Val d'Orléans area. Then, we decided to use this configuration as a case study for our calculation taken into account the data available for the Guilly site to validate the methodology (dike-cavity interaction).

We noted that there are few quantitative data and investigations about mechanical properties of soil of dike and underneath. We will use the existing data and sensitivity analysis to assess the roles of the alluvium layer, the dimension of the cavity and the presence of the dike in the appearance of subsidence and sinkhole.

2.6 References

- Boismoreau P., 2008. Les sources du Parc Floral, spéléologie Subaquatique Loiret, 10 janvier 2008.
- Caudron M., 1964. Les sources du Loiret: livret guide hydrogéologique (hydrogeological guide book), BRGM.
- CEPRI (European Centre for Risk Prevention Flood), 2008. Les digues de protection contre les inondations, L'action du maire dans la prévention des ruptures, guides of CEPRI, 46 pp.
- Dore L., Mathon D., 2014. Repartition du risque karstique dans le val d'Orléans: approche bibliographique National days of Geotechnical and Engineering Geology JNGG2014 - Beauvais 8-10 July 2014, 11 pp.
- Gombert P., Orsat J., Mathon D., Alboresha R., Al Heib M., Deck O., 2014. Rôle des effondrements karstiques sur les désordres survenus sur les digues de Loire dans le Val d'Orléans (France), Bull Eng Geol Environ, DOI 10.1007/s10064-014-0594-8, pp. 125–140.
- Guttierez A., Binet S., 2010. La Loire souterraine : circulations karstiques dans le Val d'Orléans. Géosciences, Vol. 12, pp 42-53.
- Joodi A., 2009. Apport de l'équation de Brinkman à la modélisation de l'écoulement d'eau et du transport de soluté dans l'aquifère karstique: application au système karstique du Val d'Orléans, PhD thesis, university of Orléans.
- LCPC (central laboratory for roads and bridges), 1973. Le calcaire de Beauce: géologie – hydrogéologie -applications en construction routière et génie civil. C. R. des journées d'études des 8 et 9 juin 1972 à Blois, LCPC, juin 1973.
- Lepiller M., 2006. Val d'Orléans, Aquifères et eaux souterraines en France, tome 1, Roux (éd.), BRGM Editions, pp 200-214.
- Mathon D., 2012. Etude de danger des digues de Loire de classe A - Groupe de travail : karsts et digues, technical notes (version C), 20 pp.
- Maurin J., 2012. Étude de dangers – levée d'Orléans - version 2-1, Non-technical summary, DREAL Centre SLBLB, 16 pp.
- Maurin J., Boulay A., Ferreira P., Tourment R., Beullac B., 2013. Études de dangers des digues de classe A de la Loire et de ses affluents – retour d'expérience, Digues maritimes et fluviales de protection contre les submersions, 2nd National Symposium, Aix-en-Provence, 6 pp.
- Maurin J., Ferreira P., Tourment R., Boulay A., 2012. Niveau de sureté des digues : un outil pour l'évacuation massive du Val d'Orléans en cas de crue majeure de la Loire. European

symposium (anti-flood defences - today's problems), SHF (Evénements extrêmes fluviaux et maritimes), 8 pp.

Orsat J., 2013. Caractérisation de l'impact des réseaux karstiques dans la survenue des désordres sur les digues de classe A du Val d'Orléans, Master-Report 1, Environment Geosciences, University of Lille 1.

Saussaye L. and Durand E., 2015. Levées du Val d'Orléans (45); Investigations géotechniques complémentaires- Complementary geotechnical investigations- CEREMA and DREAL Centre SLBLB- Affaire 2014-c14RB0229/C, 265 pp.

SSL (Spéléologie Subaquatique Loiret), 2004. Le bulletin de la rivière du Loiret – hors série, 8 pp.

Treffot M., 2015. Analyse et modélisation des facteurs de prédisposition à l'effondrement karstique des terrains du Val d'Orléans, Master-Report 2, Université de Strasbourg.

3.1 Introduction

The aim of this chapter is to investigate the interaction mechanisms between a cavity in subsoil layer due to karst and a dike when built over covered karst areas. The central question of the research is the evaluation of the reciprocal impact between dikes and cavities. To answer this question, this chapter investigates the influence of the dike over the cavity stability by studying the influence of the following parameters:

- The localization of the cavity relatively to the dike;
- The geometric parameters as the diameter of the cavity, the thickness of the alluvium layer, etc.);
- The geotechnical parameters.

In this chapter, an analytical model of the cavity stability that takes into account the dike will be used, according to the in-situ observations and the data for the Val d'Orléans district (France).

A mechanical model is developed to evaluate the influence of a dike over the stability of an underground cavity. It used a limit analysis approach based on a cylindrical failure surface above the cavity. A sensitivity analysis is carried out to assess the influence of the cavity position and its dimension. More specifically, the model takes into account the dike geometry and the different scenario of water level. According to the in situ observations and data for Val d'Orléans district (France) with a layer of alluvium, the localization of the cavity is exactly unknown, the impact of the cavity position along the dike cross-section is then taken into account and the factor of safety of the cavity collapse is calculated. Thereafter, the effect of the thickness of the soil (alluvium) layer was studied by taking several thickness values.

Whatever the current model doesn't take into account the non-linear behaviour of soil and dike, we will discuss the consequences of such assumptions.

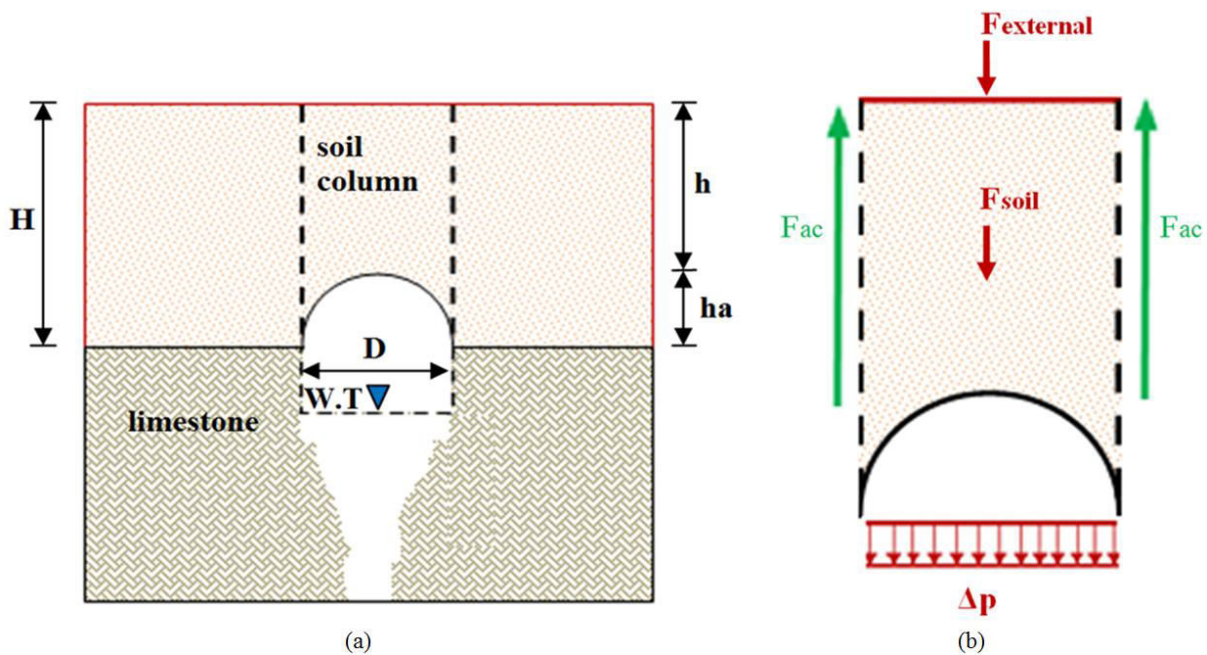
3.2 Analytical approach of cavity collapse

Several analytical and empirical methods commonly used in tunnelling, mining, and structural engineering may be relevant to this problem (Abbass-Fayed, 2004). The problem of predicting sinkhole formation resulting from the collapse of an underground cavity has, in the past, generally been approached using mainly empirical and semi-empirical approaches, (Augarde et al., 2003). However, extending those methods to the development of sinkholes in soil leads to poor predictions because of critical differences in the behaviour of soil compared to the behaviour of rock and typical structural materials (Goodings and Abdulla, 2002, Delfaut, 2007).

A mechanical model is established in this chapter to evaluate the influence of a dike on the stability of a cavity. The limit equilibrium and limit analysis for shallow cavities were

previously used to study the risk of the collapse of a cavity (Terzaghi, 1943, Keqiang et al. 2004; Zhao et al. 2011), but these models didn't take into account the influence of dike with a possible associated flooding event.

The cavity collapse adopts various geometrical forms such as conical, wedge and rectangular (Singh, 1986, Charles et al., 2003). In a coal mining context, Singh (1986) considers that a caving of 10-15 m in a weak rock formation with an equal amount of subsoil leads to cylindrical sinkhole. The cavity collapse and the sinkhole in the surface is assumed to have the shape of a column with a collapse soil column diameter above the arch roof of the cavity equal to the diameter of the cavity D (as shown in Figure 39-a). This assumption is applicable for low cohesive soil or very shallow soil layers whatever the height of soil over the cavity while in granular and cohesionless soil; this assumption could be also used according to several experimental laboratory tests especially when the soil thickness is small (Keqiang et al. 2004; Villard et al. 2009, Hassoun 2015). The cavity roof in the upper soil layers is often considered to display an arch shape especially in cohesive soil. In alluvium soil or cohesionless soil, an arch might also be formed if the soil is wet (Waltham et al. 2005).



ha refers to the height of the roof arch of the cavity, H is the thickness of the soil layer (one layer or more), h is the height of soil above the roof arch, and $W.T$ is water table level.

Figure 39 (a) Original karst cave and equilibrium roof arch of the cavity in the soil layer with D diameter (after Keqiang et al. 2004). (b) Mechanical analysis of the soil collapse column above the cavity.

To investigate the stability of a cavity, a cylindrical failure surface is considered. The static equilibrium of the cylinder is then investigated by identifying all the loading forces and resistance forces that act on the cylinder. The collapse can happen when the loading or collapse forces are more important than the resistant or anti-collapse forces (Figure 39-b). The

static forces that affect the stability of the soil cylinder above the cavity can be summarized by the three following collapse forces and one anti-collapse force:

- (1) The deadweight of the soil column (F_{soil} in Eq. 3.1).

$$F_{soil} = \gamma h \frac{\pi D^2}{4} \quad (3.1)$$

Where γ is the natural unit weight of soil layer (kN/m^3). It must be replaced by γ_{sat} (saturated unit weight) when the soil is saturated. The height of the soil column depends on the thickness of the layer (H) and the height of the arch (h_a). The height of the stable arch (h_a) of the cavity is difficult to be quantified. Keqiang et al. (2004) proposed the following formula to calculate the height of the cavity arch depending on the equilibrium arc theory:

$$h_a = 0.414 \frac{D}{\tan \varphi} \quad (3.2)$$

Where D is diameter of the cavity (m), and φ is the friction angle ($^\circ$) of the hosted soil or rock.

Some others assume that the cavity is semi-circle or hemisphere in three dimensions (Augarde et al., 2003, Long et al. 2015). We assume that height of the cavity is equal to half of the diameter in this work:

$$h_a = 0.5D \quad (3.3)$$

- (2) The external load (static load). Herein, we assume that the dike and water (in flood period) can be considered as external dead load ($F_{external}$ Figure 39-b).
- (3) The differential atmospheric pressure Δp (differential pressure between the atmospheric pressure and the relatively low pressure in the soil cave) is considered in the calculation if the water table level comes down under the level of the cavity (as shown in Figure 39-a). Its value is difficult to assess but theoretically, it is limited between 0 and 100 kPa. In China, the maximum measured value of the differential atmospheric pressure was less than 50 kPa (Keqiang et al. 2003; 2004). The forces of collapse F_c are then:

$$F_c = F_{soil} + F_{external} + \Delta p \frac{\pi D^2}{4} \quad (3.4)$$

The force of resistance or the anti-collapse force (F_{ac}) corresponds to the lateral resistance due to the friction angle (φ) and the cohesion (c). We assume that the soil may be saturated, but with no significant water pressure that can be avoided because of a natural drainage into the cavity. The anti-collapse force concerns the cylinder surface with a diameter D and height h . The lateral anti-collapse force is the strength of the soil column above the cavity, in terms of the Coulomb theory, it can be expressed as:

$$F_{ac} = (F_n \tan \varphi + ch)\pi D = \left(\frac{K\gamma h^2}{2} \tan \varphi + ch\right)\pi D \quad (3.5)$$

Where F_n is normal force, it depends of the soil weight and earth pressure coefficient K . this coefficient K depends on the friction angle and the consolidation state of the soil.

The safety factor SF can be defined as the following ratio:

$$SF = \frac{F_{ac}}{F_c} \quad (3.6)$$

$SF > 1$ corresponds to a stable configuration. $SF = 1$ corresponds to a critical configuration and $SF < 1$ corresponds to an unstable configuration leading to the occurrence of the sinkhole through the dike or the surface.

3.3 Dike effect upon the stability of cavity

Figure 40 presents a simplified 2D section of a dike over a cavity. The collapse force is changed by considering the additional weight of the dike and the flood water as external static load. Two scenarios of water level upstream are considered (normal and extreme). The water weight is assumed as an external load, and the water pressure through the dike is neglected. Therefore, the collapse force (F_c) in (Eq. 3.4) can be rewritten as follows:

$$F_c(\text{normal}) = (\gamma_{\text{sat}}(h) + \gamma(h_y) + \Delta p) \frac{\pi D^2}{4} \quad (3.7)$$

$$F_c(\text{exterm}) = (\gamma \text{ sat}_{\text{soil}}(h) + \gamma \text{ sat}_{\text{dike}}(h_y) + \gamma_w(h_d - h_y) + \Delta p) \frac{\pi D^2}{4} \quad (3.8)$$

Where γ is the natural unit weight of soil layer, γ_{sat} is the saturated unit weight, γ_w is the unit weight of water, h_y is height of the dike part above the cavity arch (m) and h_d is the maximum height of the dike (see Figure 40 & Figure 41).

$F_c(\text{extreme})$, is the collapse force for a saturated dike in the upstream section, assuming the level of water in the river reaches the top of the dike. $F_c(\text{normal})$ is the collapse force in the scenario when the level of the river water reaches the bottom level of the dike.

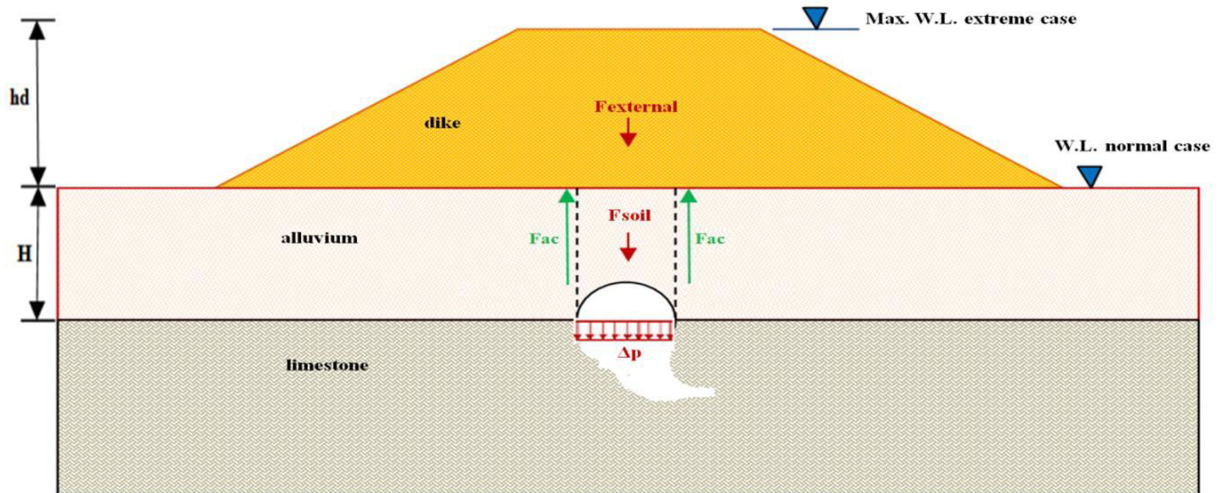


Figure 40 Sketch showing main forces that affect the stability of a cavity underneath a dike.

The same force of anti-collapse, F_{ac} , is considered (Eq. 3.5) and the safety factor can be calculated using the equation (Eq. 3.6).

3.4 Calculation of the dike effect

A typical cross-section of a Loire dike near the city of Orléans was investigated and used as reference geometry (see Figure 41). The height of dike is 6 m and its slope in the water and land sides is $1V/2H$ (vertical to horizontal). The height of arch cavity was assumed equals to the cavity radius (see Eq. 3.3). The differential atmospheric pressure Δp depends on the measured pressure in the cavity and it can become important if the water table suddenly falls by a large amplitude and this scenario could be shown after a flooding and the water table comes down under the cavity roof level. This scenario cannot present in the case of dike of Val d'Orléans because of water table due to the Loire water level always above the cavity level. Thus, the value of Δp was considered equals to zero (the pressure in the cavity equals the atmospheric pressure).

The modified mechanical model was applied to evaluate the stability of the cavity in the alluvium underneath a typical Loire dike in the Val d'Orléans area. According the database (Gombert et al. 2014) and the in-situ observations done by the authors, the following range of variables were adopted:

- The cavity position (p_i); $p_i=0$, means the cavity is under the toe of the dike and $p_i=6$ m refers to the position of the cavity under the head of the dike;
- The diameter of cavity (D from 0.5 to 2 m);
- The height of the alluvium layer (H from 3 to 10 m) with a step of 1 m; the mechanical properties of the dike and the alluvium layer were chosen from Table 3 (chapter 2) and Figure 41;
- The river water level: two scenarios; normal configuration (water level at the bottom of the dike and extreme configuration (water level at the top of the dike).

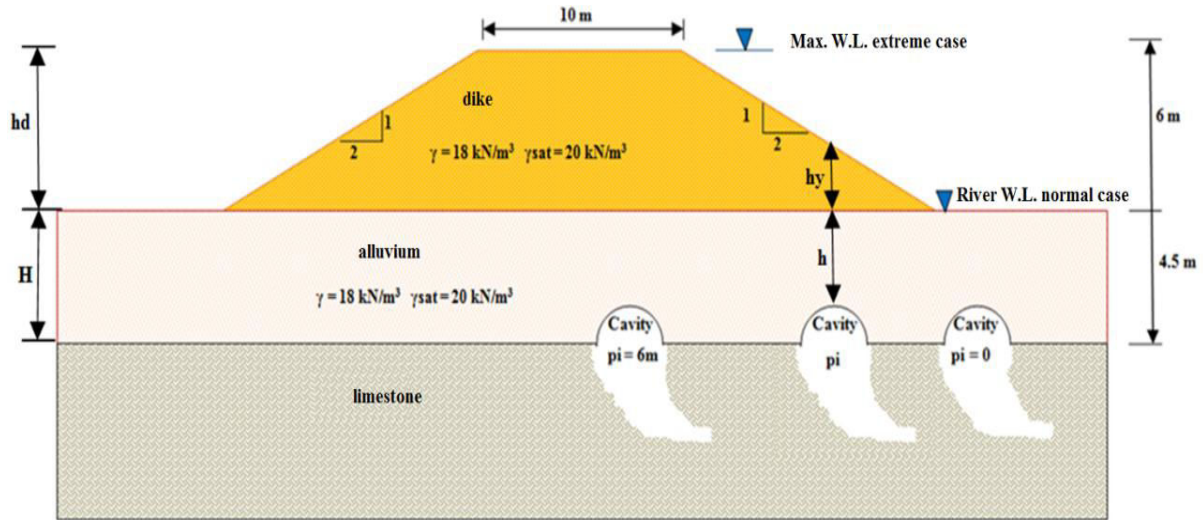


Figure 41 Scheme of the dike with different cavity positions (from under toe of the dike until centre of the dike with p_i is function of the dike above the cavity).

The following values ($c = 0$ and $\phi = 32^\circ$) were adopted because they are generally the weakest values (in saturated conditions) due to the small values of the cohesion in both the dike and the alluvium layer. Thus, the alluvium layer without cohesion ($c=0$) can be considered as the worst case scenario because the anti-collapse force (F_{ac}) will be underestimated (see Eq. 5.5).

The lateral earth pressure K is calculated using the equation of Jaky ($K = 1 - \sin \phi$) considering the soil as normal consolidation state (Mestat 1998). The result of K for a friction angle 32° was nearly to 0.5.

3.5 Results analysis and discussion

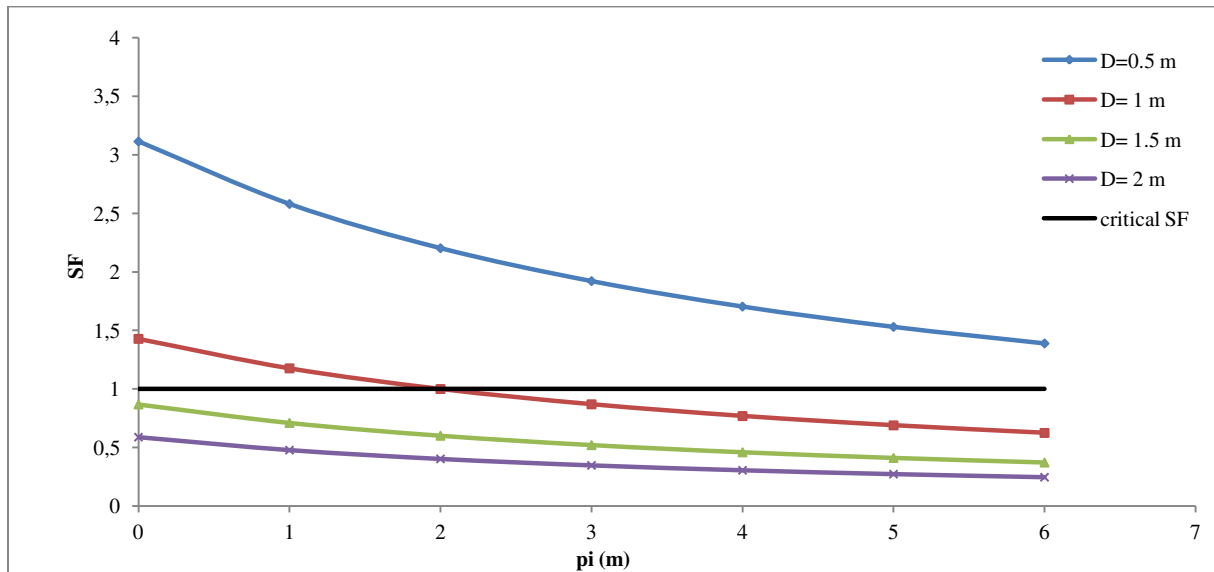
The cavity is herein considered as stable when the safety factor SF (Equation 3.6) is greater than 1. The number of stable configurations for the different studied parameters was compared. An attention was paid to determine the critical diameter of the cavity and the critical depth of the alluvium layer.

3.5.1 Effect of the position of the cavity

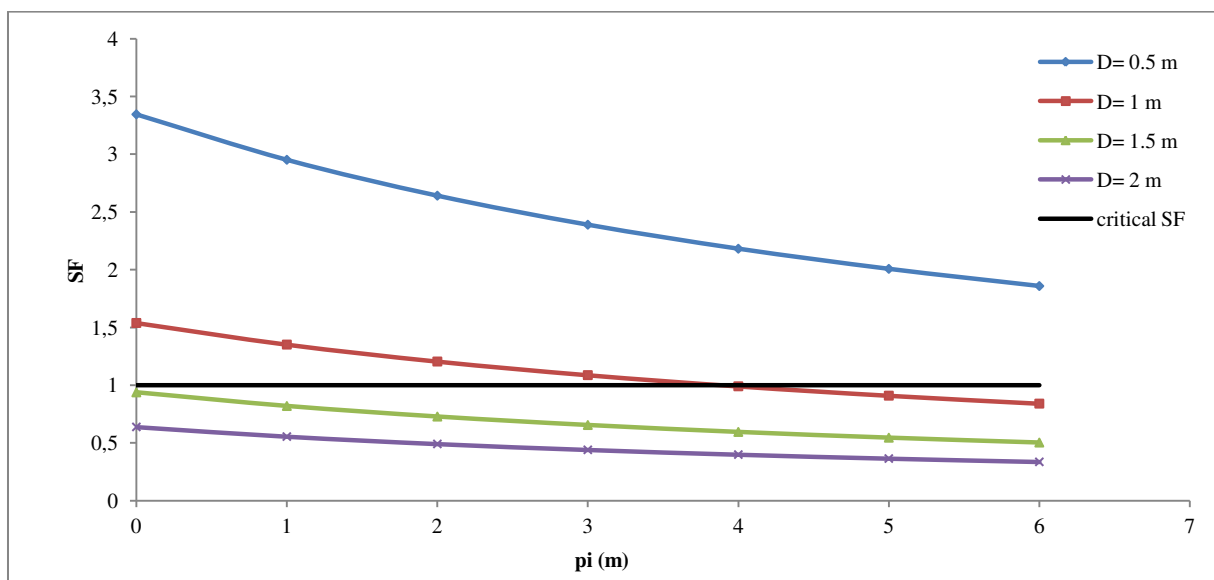
Figure 42 shows the safety factor for different diameters of the cavity (D) and different positions underneath the dike (p_i). 9 of 28 configurations (7 positions * 4 diameters) are safe ($SF > 1$) for the extreme flooding scenario (Figure 42-a) and 11 of 28 configurations for the normal flooding scenario (Figure 42-b). The results of Figure 42 show that an increase of the river water level (normal to extreme flooding scenario) leads to a decrease of the cavity stability. In other words, the water level on the upstream side of the dike adversely affects the stability of the cavity. The safety factor also decreases as function of the position ($p_i > 0$) and the diameter of the cavity.

To determine the critical diameter of the cavity which corresponds to SF=1, Figure 43 is used. It shows the effect of the cavity diameter for the two extreme positions ($\pi_i=0$ and $\pi_i=6$ m) for the extreme flooding scenario. The critical diameter ($D_{critical}$) is equal to 1.35 m for $\pi_i=0$ ($H/D=3.3$) and 1.0 m for $\pi_i=6$ m ($H/D=4.5$). The likelihood of hazard of sinkhole is more likely in the position $\pi_i=6$ m, i.e. under the head of the dike.

In this work, the effect of the dike weight was neglected for the cavities that are located somewhere far from the toe of the dike. This case is studied by the numerical model (in chapter 5).



(a) Extreme flooding scenario



(b) Normal flooding scenario

Figure 42 Relation between the cavity position (π_i) and the safety factor (SF) in two hydraulic scenarios.

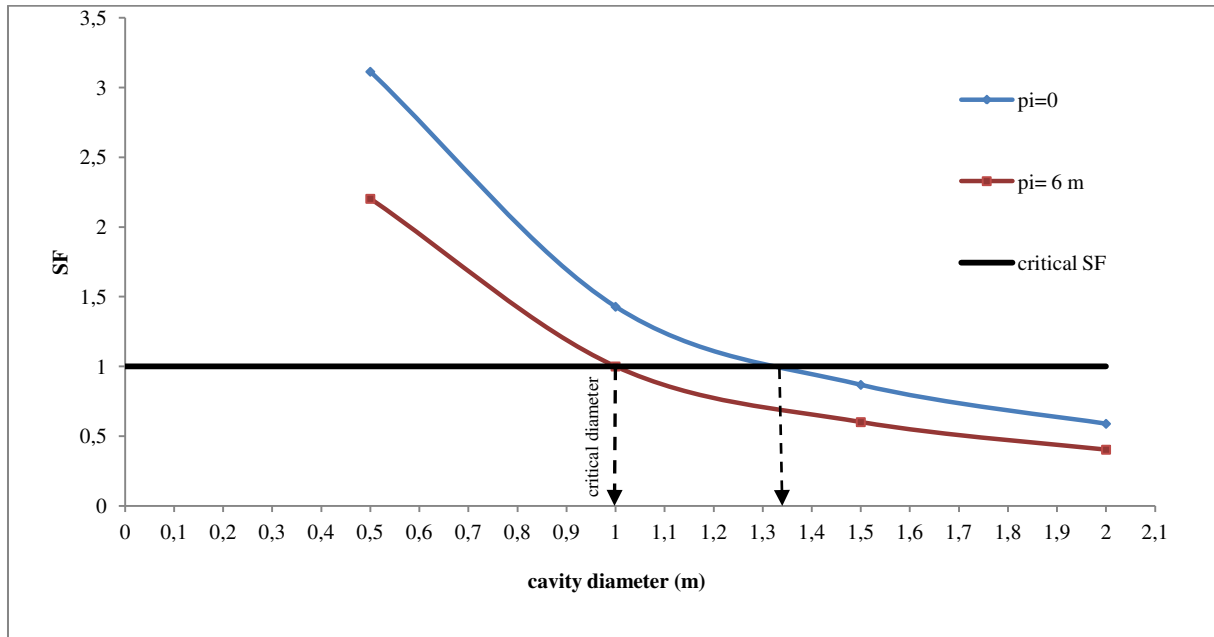


Figure 43 Safety factor (SF) due to the effect of the cavity diameter (D) for two cavity positions ($\pi=0$ and $\pi=6$ m) at extreme flooding scenario.

3.5.2 Effect of the alluvium layer thickness

To study the effect of the alluvium thickness (H), this parameter taken as a variable between 3 and 10 m according the in-situ observations (16 configurations). The height of the dike (h_d) is taken equals to $h_d=6$ m. Then we calculate the corresponding safety factor (SF) and critical diameter ($D_{critical}$ when $SF=1$) for each case for flooding state, lateral earth pressure ($K=0.5$) and when the critical cavity is underneath the head of the dike ($\pi=6$ m). Two series of calculation were carried out with two couples of cohesion and friction angle values corresponding to sand: $c=0$ and $\varphi=32^\circ$ and clay $c=36$ kPa and $\varphi=16^\circ$.

The results show (Figure 44) that the safety factor increases, and the risk of sinkhole decreases, with the increasing of alluvium layer thickness. The critical diameter goes from 0.46 m ($H=3$ m, $H/D=6.5$) to 6 m ($H=10$ m, $H/D=1.65$). The effect of increasing the cohesion is to increase the safety factor even though decreasing in the value of the friction angle. However, the increasing the value of cohesion to 36 kPa increases the value of the critical diameter (see Figure 44). While in case of alluvium thickness equals to 10 m, the increasing in cohesion led to increase in critical diameter value about twice.

The ratio critical thickness-to-cavity diameter is calculated in Table 4 in dependant on Figure 44. This table illustrated the range of the H/D ratio (height of alluvium layer to diameter). The ratio H/D varies between 1.65 (lower limit) and 6.5 (upper limit). The results can be discussed in term of risk assessment of sinkhole hazard in the Val d'Orléans area, according the obtained results:

- $SF > 1$, the likelihood of the sinkhole is negligible when the ratio $H/D > 6.5$;
- $SF < 1$, the likelihood of the sinkhole is high when the ratio $H/D < 1.65$;
- The likelihood of sinkhole is variable for the range: $1.65 \leq H/D \leq 6.5$, its probability depending on the geotechnical and geometrical parameters.

The obtained results are consistent with the literature. In fact, several analyses of experimental tests demonstrated that the cavity could not be stable for a ratio of the soil layer height H to the cavity diameter D less than 1.5 (Ellis et al. 2008; Hassoun, 2015). Surface collapse (sinkhole) tends to occur in areas where the thickness of overlying soil cover is thin. In Val d'Orléans, the knowledge of the thickness of alluvium layer can be considered as a critical data to justify the hazard map of karst induced sinkholes in the vicinity or not of a dike.

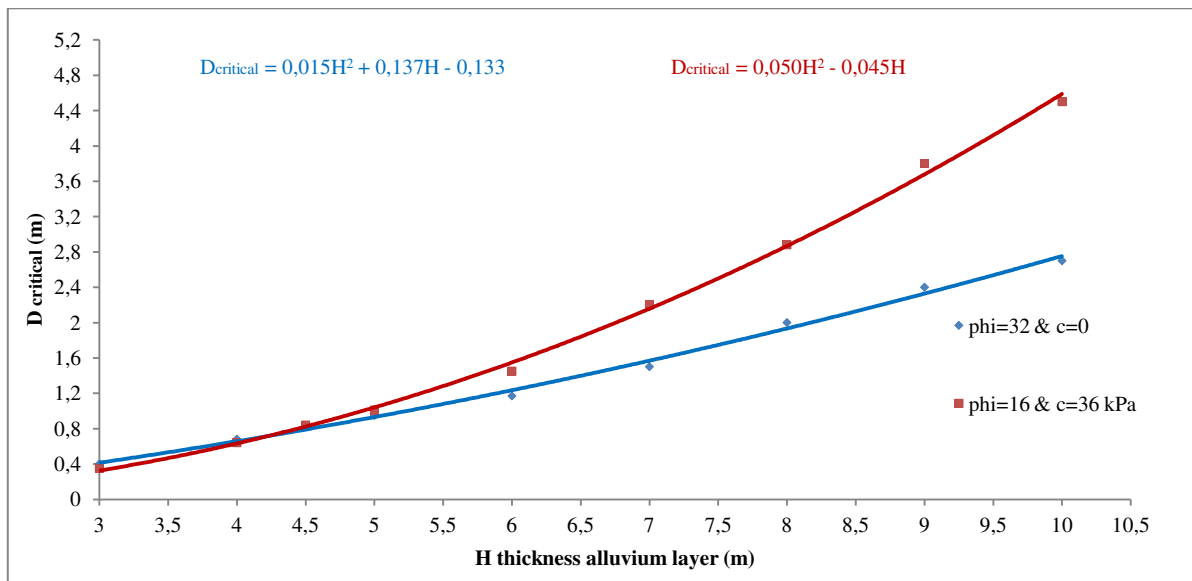


Figure 44 Relation between the alluvium thickness H underneath the dike and the critical diameter of cavity $D_{critical}$ for height of dike equals to 6 m.

Table 4 Ranges of H/D critical ratio dependent on Figure 44.

Properties of alluvium layer	H/D
$c=0$ & $\varphi = 32^\circ$	3.3-6.25
$c=36$ kPa & $\varphi = 16^\circ$	1.65-6.5

3.5.3 Effect of a sinkhole through the dike

In the theory and the application of the analytical solution, we consider the dike as an external load applied on the surface of the alluvium layer. According this assumption, the dike does not participate to the resistance force (forces anti-collapse). In this paragraph we will take into account the dike as an additional layer and the sinkhole cylinder progresses through the dike

body (Figure 45). The equilibrium and safety factor were recalculated by assuming the dike as an additional soil layer. The configuration studied herein correspond to the position $p_i=6$ m. Therefore, the effect of dike was taken into account to calculate the anti-collapse force F_{ac} (in Eq. 3.5).

Figure 46 shows that the critical diameter of the cavity is about 3.25 m (dike cohesion = 5 kPa, $\phi=32^\circ$). This critical diameter is about three times the critical diameter found when considering the dike as an external load. The previous calculation was repeated by taking minimal values of cohesion and friction angle for the dike ($c=0$ and $\phi=21^\circ$, see Table 3 in chapter 2). The critical diameter in this case is about 2.25 m, that means about two times greater than the critical diameter in case of considering the dike as an external load. In conclusion, the critical diameter of the cavity would be greater when the dike resistance is considered as an additional layer.

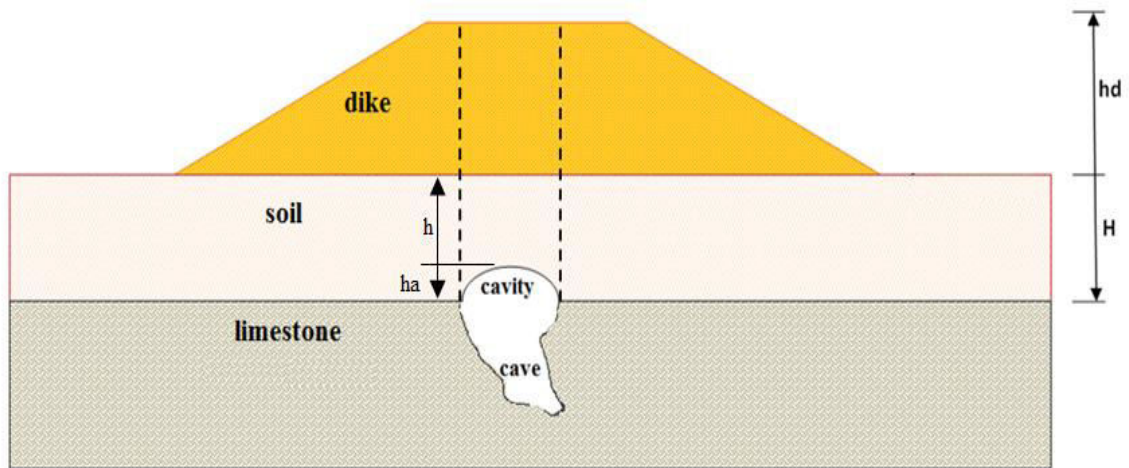


Figure 45 Sinkhole propagation through the body of dike.

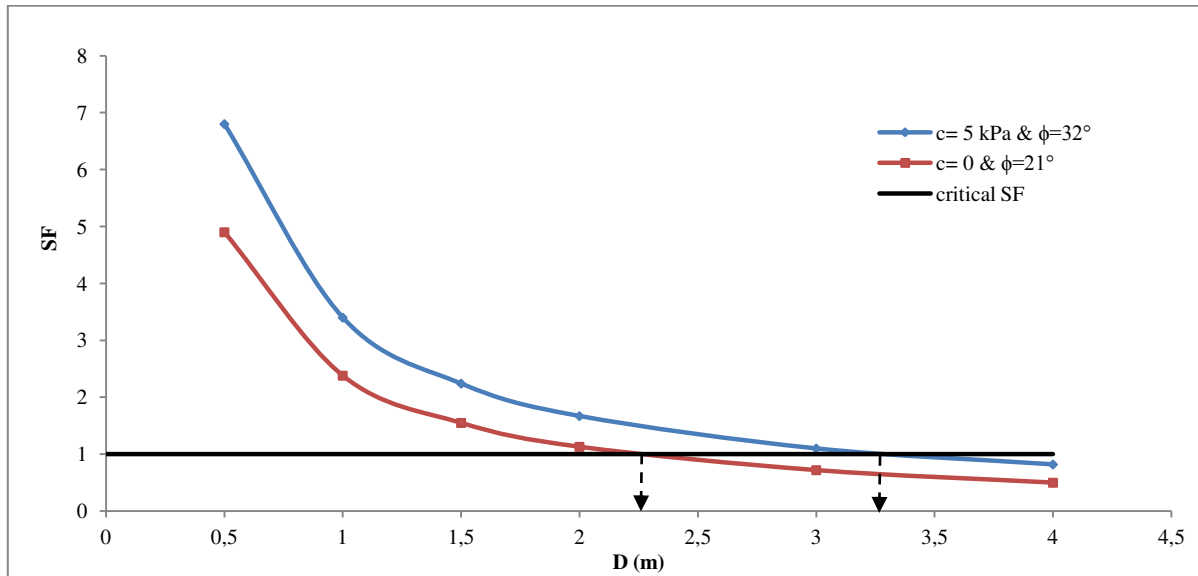


Figure 46 Safety factor for a cavity under the maximum height of the dike ($p_i=6$ m) in flood state with considering the dike resistance as an additional soil layer.

3.5.4 Critical thickness of the alluvium layer

The sinkhole is a brutal phenomenon that occurs in the surface when the thickness of the alluvium layer is critical or the cavity through the alluvium layer has a critical diameter. Set of calculations was carried out using (Eq. 3.6) for different diameters of the cavity (D from 0.5 m to 4 m). The critical thickness corresponds to a safety factor equal to 1. The height of the dike is 6 m and the position of the cavity is $p_i=6$ m. Figure 47 illustrates the relation between the critical thickness of alluvium layer above the arch of cavity ($h_{critical}$) and the diameter of the cavity. The critical depth of the alluvium layer depends on the diameter of the cavity, even for small cavity alluvium mechanical properties and thickness as shown in Figure 47.

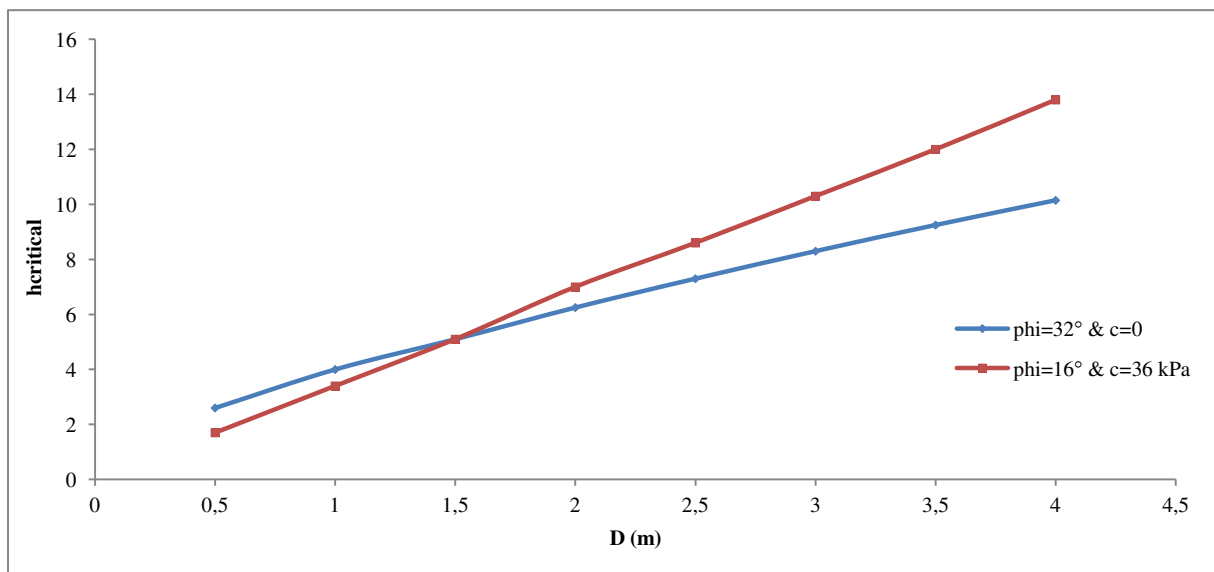


Figure 47 Relation between critical height of alluvium column above the arch of cavity ($h_{critical}$) and the diameter of cavities (D) with height of dike h_d equals 6 m.

3.5.5 Critical height of the dike

In this work, the dead weight of the dike was considered as an external load. To investigate the critical height of the dike that leads to the failure of the cavity ($SF=1$), a set of calculations was carried out using the (Eq. 3.6). This equation was applied for different values of the dike height h_d , the ratio h_d/H from 0 to 2, with considering several cavity diameter values (D from 0.5 to 2 m). The results are shown in, the critical value of h_d/H increases for small cavities, for example it is equal to 0.75 for a cavity diameter equals to 1 m (see Figure 48). In other words, for an alluvium thickness H equals to 4.5 m and with a 1 m diameter cavity underneath the dike, the critical dike height h_d would be equal to about 3.4 m.

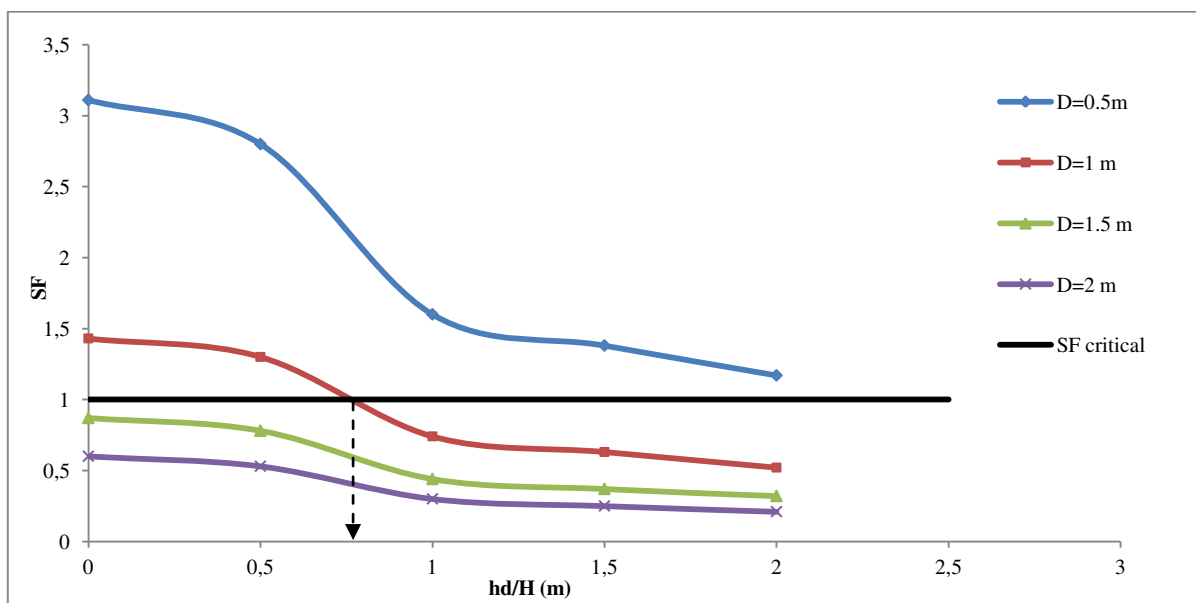


Figure 48 Safety factor for different height of dike (h_d) and different diameter of the cavity ($H=4.5$ m).

3.6 Summary

The presence of a natural cavity may induce a sinkhole in karstic regions. In this chapter, the stability of a cavity was studied taking into account the effect of the existing of a dike. The motivation resulted from the study of the sinkholes in the Val d'Orléans that occurred nearby and underneath some of the dikes of the Loire valley. An existing analytical approach based on the limit equilibrium and limit analysis was improved. The modification of the analytical approach allowed the assessment and the prediction of the risk of sinkhole due to cavity position and the dike geometry. The model was applied on the configuration of dikes of Val d'Orléans. A sensitive parameter studies were carried out based on the collected data from in situ observations and data analysis.

According to the results, the risk of the cavity collapse can be increased significantly by the effect of the dike. The collapse could occur in the extreme flood scenario for small cavity diameter of 1 m located underneath the maximum height of the dike (i.e under the head of the dike). The critical diameter of the cavity depends on the thickness of the alluvium layer and its characteristics. The analytical approach can be used to assess the hazard zone using the following parameters: diameter of the cavity (D), the thickness of the alluvium layer (H). The following ratios (H/D) maybe recommended in the case of Val d'Orléans:

- The likelihood of the sinkhole is negligible when the ratio $H/D > 6.5$;
- The likelihood of the sinkhole is high when the ratio $H/D < 1.65$;
- The likelihood of sinkhole is variable for the range: $1.65 \leq H/D \leq 6.5$.

3.7 References

- Abbass-Fayad. A., 2004. Modélisation numérique et analytique de la montée de cloche des carrières à faible profondeur. Etude de l'interaction sol-structure due aux mouvements du terrain induit par des fontis. PhD Thesis, Institut National Polytechnique de Lorraine (France).
- Augarde C.E., Lyamin A.V., and Sloan S.W., 2003. Prediction of Undrained Sinkhole Collapse, journal of geotechnical and geoenvironmental engineering, Vol. 129, No. 3, ASCE, pp 197–205.
- Delfaut A., 2007. Méthode d'évaluation des hauteurs de montée d'un fontis en sol meuble. BLPC n°266, 2007
- Ellis E., Yu K. S., G.M.C.D. Avel, A. Dawson and Thom N., 2008. Advance in transportation geotechnics. CRC Press.
- Gombert P., Orsat J., Mathon D., Alboresha R., Al Heib M., Deck O., 2014. Rôle des effondrements karstiques sur les désordres survenus sur les digues de Loire dans le Val d'Orléans (France), Bulletin of Engineering Geology and the Environment. 125–140 pp.
- Goodings D. J., Abdulla W A 2002. Stability charts for predicting sinkholes in weakly cemented sand over karst limestone. Engineering Geology 65. pp179-184.
- Hassoun M., 2015. Analytical and experimental approach in laboratory of the use of geosynthetics to reduce the risk associated with the collapse of underground cavity, master thesis, university of Grenoble.
- Keqiang H., Changli L., Sijing W., 2003. Karst collapse related to over-pumping and a criterion for its stability, Environmental Geology (2003) 43, pp 720–724.
- Keqiang H., Wang B. and Zhou D., 2004. Mechanism and mechanical model of karst collapse in an over-pumping area, Environmental Geology (2004) 46:1102–1107, pp1102-1105.
- Long J., Yan M., Zhen-de G. and Li-Peng L., 2015. Numerical simulation of karst soil cave evolution, 14th sinkhole conference, National Cave and Karst Research Institute, USA, pp493-500.
- Mestat Ph., 1998. Etat de contraintes initiales dans les sols et calcul par éléments finis, Bulletin des laboratoires des ponts et chaussées, pp15-32.
- Singh T.N., 1986. Coal mining under river beds, Workshop on Protection of Surface Features and Structures in Mining Areas, 24-29 November, CMRI, Dhanbad.
- Terzaghi, K., 1943. Theoretical Soil Mechanics. New York: John Wiley & Sons.
- Villard P., Chevalier B., Le Hello B., Combe G., 2009. Coupling between finite and discrete element methods for the modelling of earth structures reinforced by geosynthetic. Computers and Geotechnics Volume 36, Issue 5, pp. 709–717.

Waltham T., Bell F., Culshaw M., 2005. Sinkholes and subsidence, karst and cavernous rocks in engineering and construction, book, Springer, 379 pp.

Zhao H., Ma F., Guo J. 2011. Regularity and formation mechanism of large-scale abrupt karst collapse in southern China in the first half of 2010, Springer, Nat Hazards DOI 10.1007/s11069-011-9888-3. pp 1037-1054.

4.1 Introduction

Dikes are designed to protect land from flooding hazard. Different internal and external causes can affect their stability as overflow, external and internal erosion and slope instability (as they were shown in section 1.2.3 Stability of dikes). In Loire valley, historical dikes protect the land from the Loire flooding. Their substratum consists of limestone containing karstic cavities. In addition of the previous known causes, sinkhole and subsidence occur in the region due to the karstic phenomenon (collapse of the karstic cave). When an embankment (as a dike) is constructed over karstic foundation, the karstic network and associated cavities may influence the dike stability (Schaefer 2009).

In the previous chapter (3), the instability of the cavity due to the influence of the dike was studied using an analytical approach. In this chapter, the objective of the work concerns the stability of the dike when an isolated cavity/cave is present under the dike without taking into account the collapse of the cavity/cave. In another words, what is the influence of the cavity on the stability of the dike due to the stress redistribution?

In fact, the limestone layer which contains caves corresponds to the substratum. If the underlying foundation materials that support the dike become destabilized because of the karstic network, the embankment slope stability could be reduced. Slope failures can be minor or they can be significant enough to result in the failure of the dike system. The presence of a cavity underneath the dike contributes to modify the initial stresses and may weaken the stability of the dike slope. The main question herein is the evaluation of the impact of the cavity on the stability of the dike slope.

4.2 Method and objective

In fact, the initial stresses in soil layers depend mainly on the weight of the strata and the consolidation state (Mestat, 1998). If a cavity exists, the distribution of these initial stresses will be modified around the cavity (Terzaghi, 1943). By considering a circular cavity, it can be assumed that its influence over the stress field limited to a distance that can reach 10 times the diameter of the cavity (Goodman, 1989). When the distance between the dike and the cavity is less it appears crucial to take into account this stress distribution when we calculate the stability of the dike.

There are two ways to study the dike-cavity interaction: numerical and analytical methods. Each method presents certain advantages and disadvantages: data, hypotheses, time calculation, etc. The work in this chapter will focus on an analytical method because it helps us to understand easily the cavity-dike interaction and to distinguish the effect of each parameter on the calculated equilibrium forces and the final stability of the dike. Chapter 5 deals with the numerical approach.

A cavity underneath a dike could modify the stress distribution and contribute to the instability of the dike. One of the potential reasons of the instability of dikes is the slope failure. The methodology developed herein consists into two parts. Firstly, the dike (of Val d'Orléans in our case) is investigated with the Fellenius' method (Ordinary method) and the assumption of a soil without cavity underneath. Then, the second step consists in the consideration of a circular cavity located under the dike. Some analytical developments are proposed to take into account this cavity into the Fellenius' method.

The slope stability is checked by using analytical methods based on the limit equilibrium theory or slice methods. One of these methods is known as Fellenius or Ordinary method. This method was chosen because it is the most easily one in the calculations and it usually gives results more pessimistic (most conservative) which make our calculations on the safe side (Chowdhury et al. 2010).

The software (TALREN-V5)¹ was used to calculate the safety factor of the dike in normal and flooding state without existing underneath cavities. The features of this software are:

- the limit equilibrium calculation along potential failure surfaces using the Ordinary method (Fellenius) with an automatic search option for circular failure surfaces;
- the possibility to take into account hydraulic conditions as loads/forces between slices.

TALREN is based on the Fellenius method to estimate a local and global factor of safety but cannot take into consideration the cavity influence. To take into account the stress modification due to the cavity, Excel sheets were used to do the calculation with using the circular slip surface which results from the output of the software. The stress distribution around the circular cavity is calculated using Kirsch analytical solution for elastic behaviour for a circular hole in an infinity elastic medium. Thanks to the elastic assumption, the stresses induced by the cavity are added in the equilibrium equation of the ordinary method for the slope stability analysis. The factor of safety is then recalculated for normal case without flooding and flooding conditions, etc. Then, thanks to the safety factor, the comparison is done between the two configurations (with and without the cavity) in order to help assessing the likelihood of the dike instability due to the interaction between the dike and the cavity.

To facilitate the understanding of the role of the cavity, different assumptions were adopted. The calculation was carried out with a standard two-dimensional assumption, so the cavity is a cylinder and the studied section is a circle.

Thanks to elastic assumption, the stresses induced by the cavity are added in the equilibrium equation of Ordinary method of the slope, and the factor of safety can be recalculated in different scenarios of dike life: normal and flooding conditions, etc. Then, thanks to safety

¹ TALREN is ideal for checking the stability of geotechnical structures, with or without reinforcements: natural slopes, cut or fill slopes, earth dams or dikes. It takes into account various types of reinforcements such as: anchors and soil nails, piles and micropiles, geotextiles and geogrids, steel and polymer strips, more than 1100 TALREN licenses worldwide. It is available program in INERIS.

factor, the comparison can be done between the two configurations (with and without the cavity) and can help to assess the likelihood of the dike instability due to both the dike and the cavity interaction.

4.3 Slope stability analysis

The slope stability analysis is based on the limit forces equilibrium which is an analytical tool for assessing the stability of a slope by using a simple failure model. The primary objective of the stability analysis is to determine the safety factor (SF) of particular slope geometry, to predict the failure potential and to assess remedial treatments when necessary.

In many practical situations, an analytical assessment of stability can be made (Roy and Richard 2003). Slope stability analysis consists of determining and comparing the shear stress developed along the potential rupture/slipping surface with the shear strength of the soil. Limit equilibrium analysis is the basis for most the methods available for slope stability evaluations. Consideration is given to a free body of the soil mass bounded by the slope and an assumed “slip” or failure surface. Broadly slope failures are classified into 3 types (Dinesh 2008) (cf. Figure 49):

1. Face (Slope) Failure: This type of failure occurs when the slope is large and when the soil at the toe portion is strong.
2. Toe Failure: In this case the failure surface passes through the toe. This occurs when the slope is steep and homogeneous.
3. Base Failure: In this case the failure surface passes below the toe. This generally occurs when the soil below the toe is relatively weak and soft.

The common assumption to all limit equilibrium methods is to consider the potential failure surface can be divided into a finite number of slices. Equilibrium force conditions are considered for all slices. The problem is strongly indeterminate, requiring several basic assumptions regarding the location of application or resultant directions of applied forces (Roy and Richard 2003).

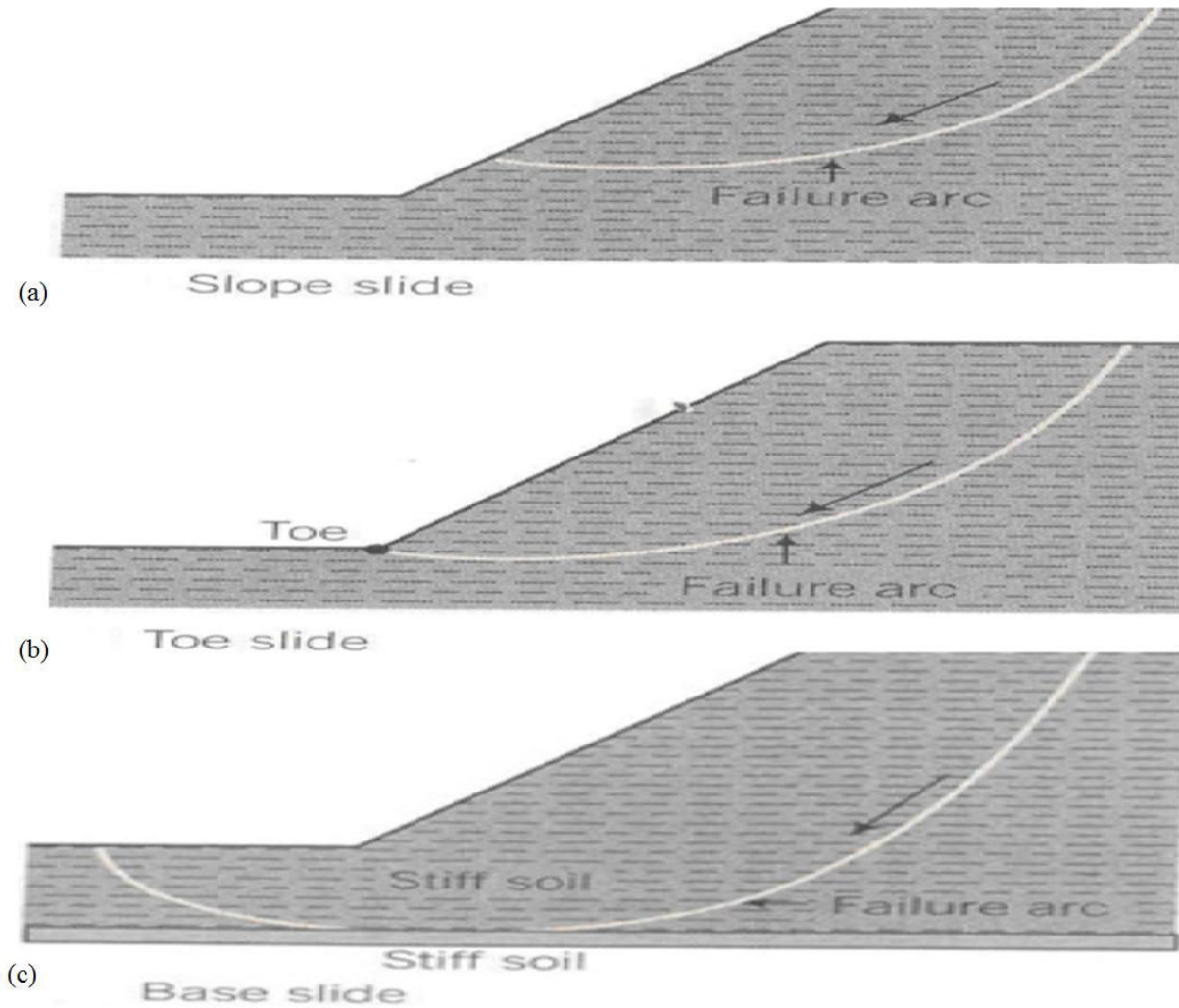


Figure 49 Types of slope sliding/failures. (a) face (slope) failure. (b) toe failure. (c) base failure (Dinesh 2008).

4.3.1 The Ordinary method of slices

We used the Ordinary method of slices, developed by Fellenius in 1936 (USACE 2003, Cheng and Lau 2008). The method assumes that resultant of side forces on each slice is collinear and acts in parallel to the failure surface, and therefore cancel each other. This method is simple to implement and generally conservative (Kitch 2012). Figure 50 shows the adopted geometry in this method while Figure 51 illustrates forces acting on each slice. The following assumptions are then made in the analysis using ordinary method of slices (Zhou 2006):

1. The available shear strength of the soil can be adequately described by the Mohr-Coulomb criterion:

$$\tau = c + \sigma \tan \phi$$

where:

τ = shear strength

c = cohesion component of shear strength

$\sigma \tan \phi$ = frictional component of shear strength

σ = normal stress on the failure surface at the base of a slice due to the weight of soil and water above the failure surface

ϕ = angle of internal friction of soil

$\tan \phi$ = coefficient of friction along failure surface

2. The factor of safety is the same for all slices.

3. The factors of safety with respect to cohesion (c) and friction ($\tan \phi$) are equal.

4. The method assumes that resultant of side forces on each slice is collinear and acts in parallel to the failure surface, and therefore cancel each other.

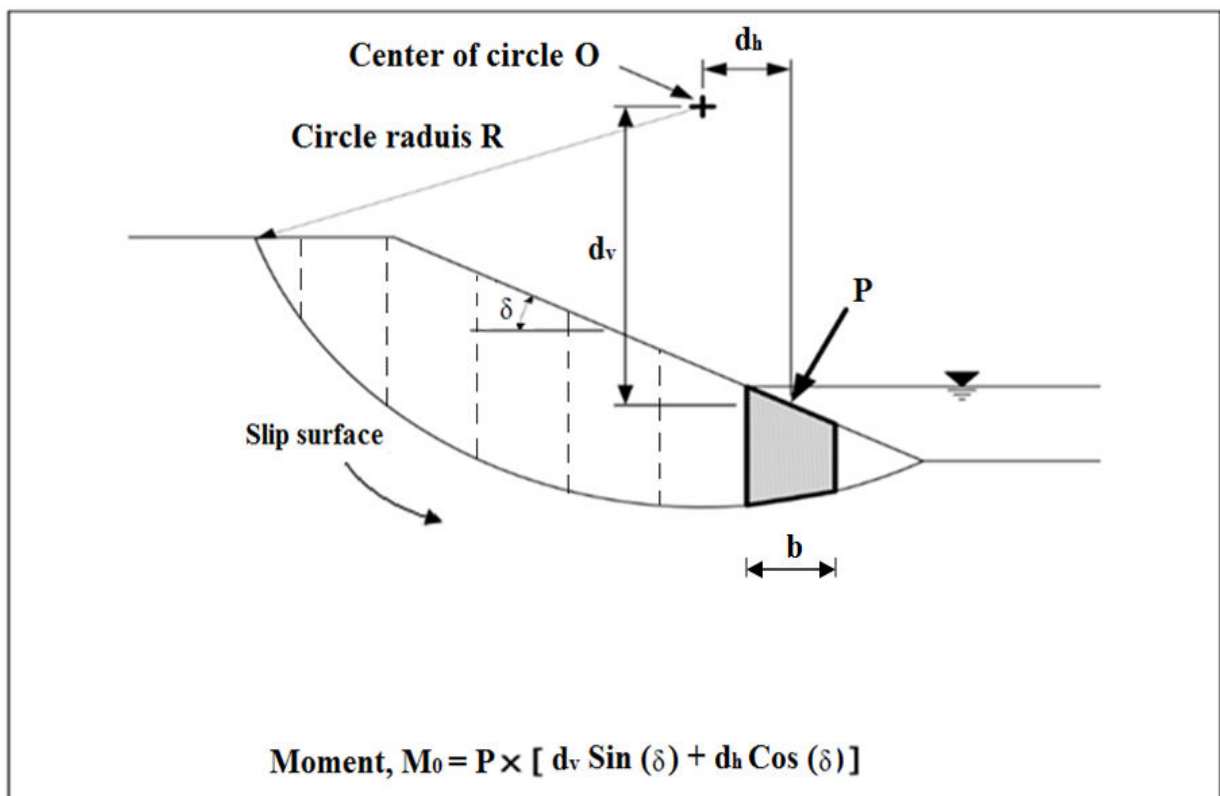


Figure 50 Geometry of Ordinary Method of Slices (after USACE 2003). Where d_v and d_h are the vertical and horizontal distance respectively between the resultant water force P over the top of the slice and the centre of the slip circle, b is the width of the slice.

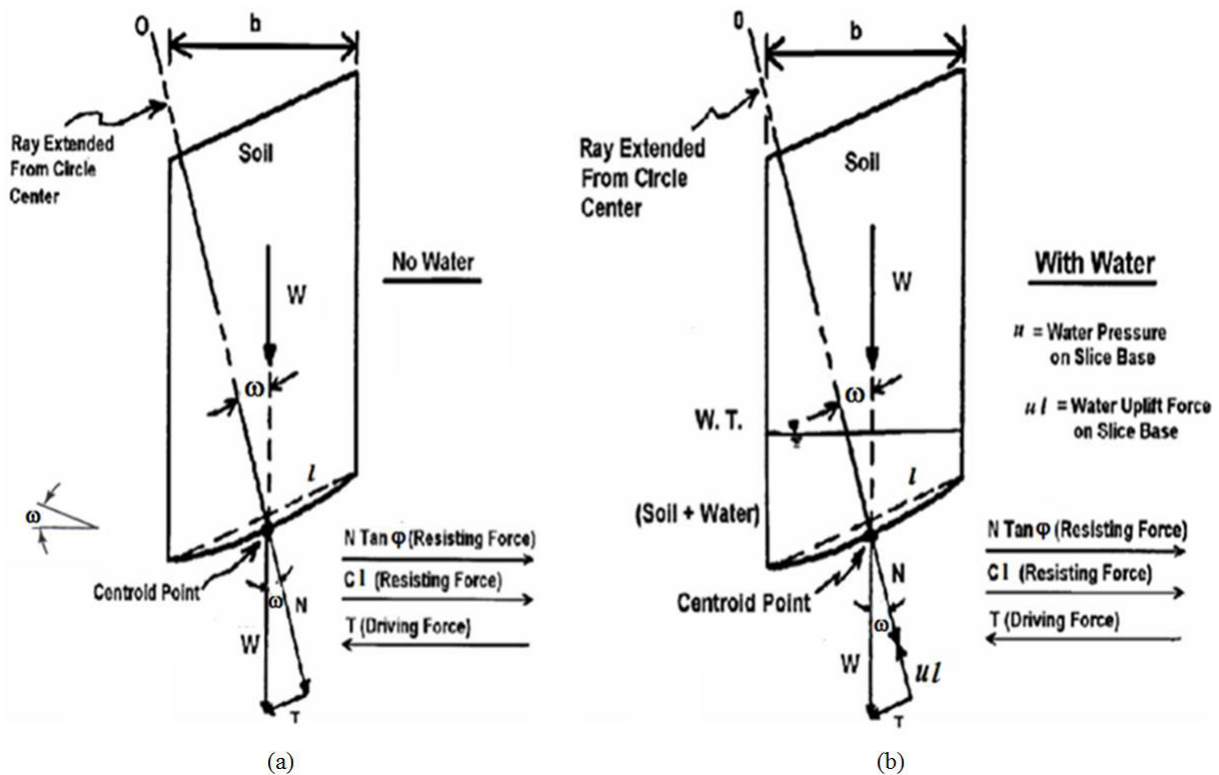


Figure 51 Forces acting on the slice in ordinary method. (a) without water case (dike is dry). (b) with water case (after Zhou 2006). W is the weight of the slice, l is the length of the bottom of the slice and ϕ is the angle of the inclination of the bottom of the slice.

The solution procedure can be summarized as follows:

- Draw a cross-section of the dike and soil foundation profile on a scale and select a circular failure surface such as shown in Figure 50.
- Divide the soil mass above the circular slip surface into convenient number of slices with width b (more than 5 are preferred according to Dinesh 2008)
- Calculate the total weight (W) of each slice;
- Calculate the force of friction resistance for each slice ($N \tan \phi$), where N is the normal force on the basis of each slice which equals the vertical component of soil weight of slice ($W \cos \omega - ul$). In dry state, the pore water pressure (u) equals to zero and vertical component of soil weight of slice would be ($W \cos \omega$);
- Calculate the tangential driving force (T) for each slice, where T is shear force on the basis of each slice equals the horizontal component of soil weight of slice ($W \sin \omega$).
- Compute the cohesive resisting force for each slice cl .
- Sum of the resisting and driving forces for all slices and calculate FS by following equation:

$$SF = \frac{\sum \text{Resisting forces}}{\sum \text{Driving forces}} = \frac{\sum N \tan \phi + \sum c l}{\sum T} = \frac{\sum (W \cos \omega - ul) \tan \phi + \sum c l}{\sum \sin \omega} \quad (4.1)$$

In the case where water loads act on the top of the slice (see Figure 50), USACE (2003) has modified the previous formula by taking into account the effect of the surface water force. Hence, Equation 4.1 must be re-written as the following:

$$SF = \frac{\sum N \tan \phi + \sum c l}{\sum T - \frac{\sum M_o}{R}} = \frac{\sum [W \cos \alpha + P \cos(\omega - \delta) - ul] \tan \phi + \sum c l}{\sum W \sin \omega - \frac{\sum M_o}{R}} \quad (4.2)$$

Where

ω is the inclination of the bottom of the slice,

u is the pore water pressure at the centre of the basis of the slice,

l is the length of the bottom of the slice ($l = \frac{b}{\cos \omega}$),

P is the resultant water force acting perpendicular to the top of the slice,

δ is the inclination of the top of the slice,

R is the radius of the slip rotation circle, and

M_o is the moment about the centre of the circle produced by the water force acting on the top of the slice, which can be calculated as is shown in Figure 50.

4.3.2 Verification of TALREN results

The original limit equilibrium method (slice method) does not take into account the cavity stress distribution influence. To overcome this point, we developed a modified method by adding the cavity effect. The calculation is carried out using Excel sheet for a slope with a cavity under the sliding surface.

To make sure that the obtained results of the safety factor are valuable, the first work done is the comparison between the TALREN (commercial software) and the modified method results for the same slope geometry and slice number (10 slices), without any cavity. In that case, the modified method is exactly the same than the Ordinary method. Figure 52 presents a schematic diagram of the slope stability problem which was taken from the guide of SLOPE/W software. The objective is to compute the minimum safety factor and locate the critical slip surface.

The slope surface is cut into two materials at 2:1 (horizontal: vertical). The upper layer is 5 m thick and the total height of the cut is 10 m. Bedrock exists 4 m below the base of the cut. The pore-water pressure conditions are depicted by the piezometric line and the soil strength parameters are listed in Figure 52.

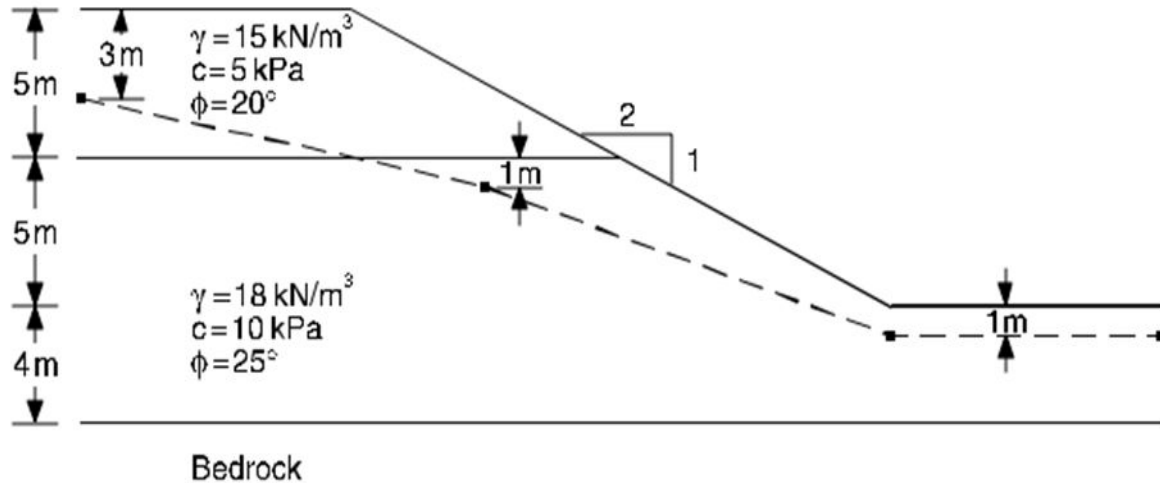


Figure 52 Sample slope stability problem (SLOPE/W, version 4).

The results obtained by TALREN and by using the Excel sheet (manual method) are compared with the original result given by SLOPE/W (Table 5). All the calculations used a number of slices equal to 10. The factor of safety which is calculated by TALREN is very close to the value obtained by SLOPE/W (+3% difference). The difference is -4% between the manual method and SLOPE/W. Therefore, the difference between the TALREN result and the modified method one is 7%. Such a low difference in the results is considered as acceptable.

Table 5 Results of verification for the example presented in the Figure 4.5.

Tool of calculation	Factor of safety	Variation
SLOPE/W	1.279	0
TALREN	1.315	3%
Manual	1.221	-4%

Another example was taken from the technical manual of TALREN (see Figure 53) to recalculate the safety factor by ordinary method manually and with TALREN for more verification of the convergence of results. The two results of safety factor by TALREN and manually calculation gave the same value of the safety factor 1.607.

From the two previous examples, it is concluded that the results difference between TALREN and method is ranging between 0% and 7%, when no cavity is taken into account.

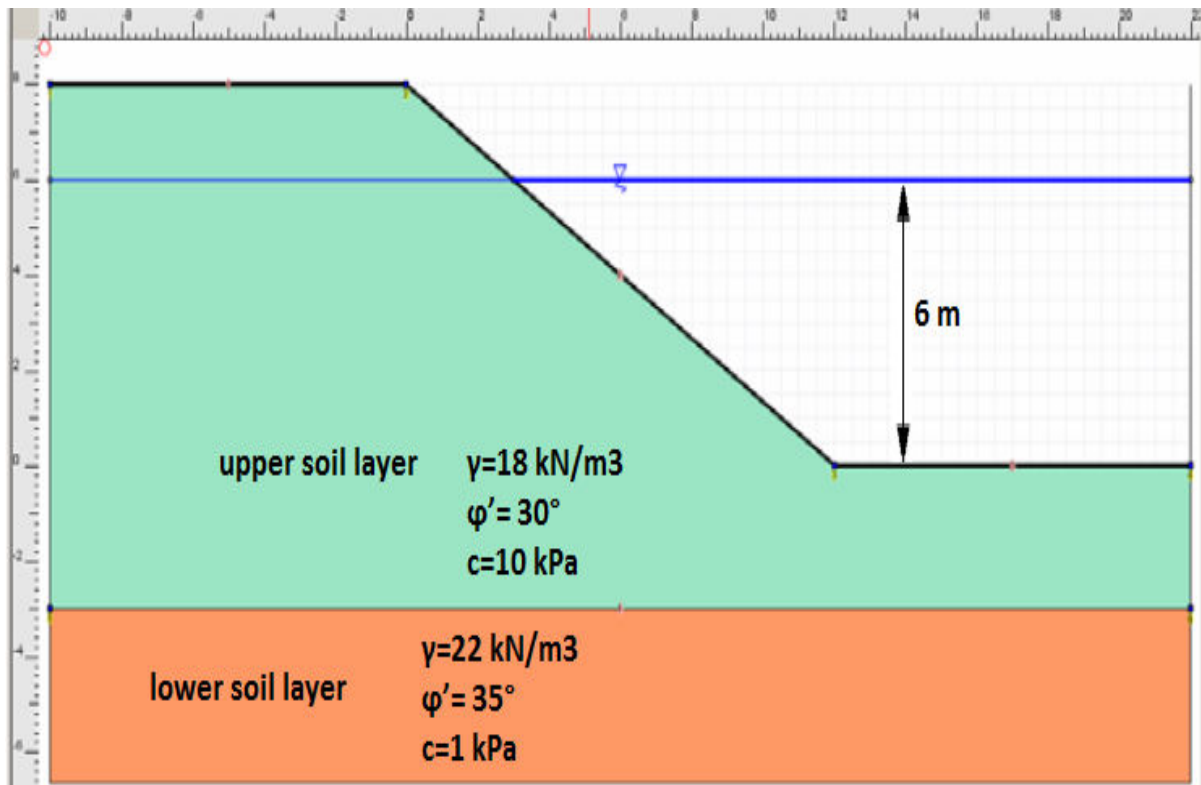


Figure 53 Slope stability problem (technical manual of TALREN, version 4).

4.3.3 Initial safety factor of the dike of Val d'Orléans (without cavity)

The geometry and the characteristics of the studied configuration are presented in Figure 54 that is mentioned as the typical cross section of the dike of Val d'Orléans (cf. chapter 3, see Figure 41). Two cases were studied to calculate the safety factor of the slope stability: without flooding and with a centennial flooding scenarios.

During flooding, the water can seep into the soil or rock and replace the air in the pore space or fractures. As a consequence, the weight of the soil will increase and a pore pressure will appear. These two consequences may significantly influence the slope stability. The weight is a force, and a force is stress divided by area, so the stress increases and this can lead to decrease slope stability (Nelson 2013, Khanmohammadi and Hosseinitoudeshki 2014).

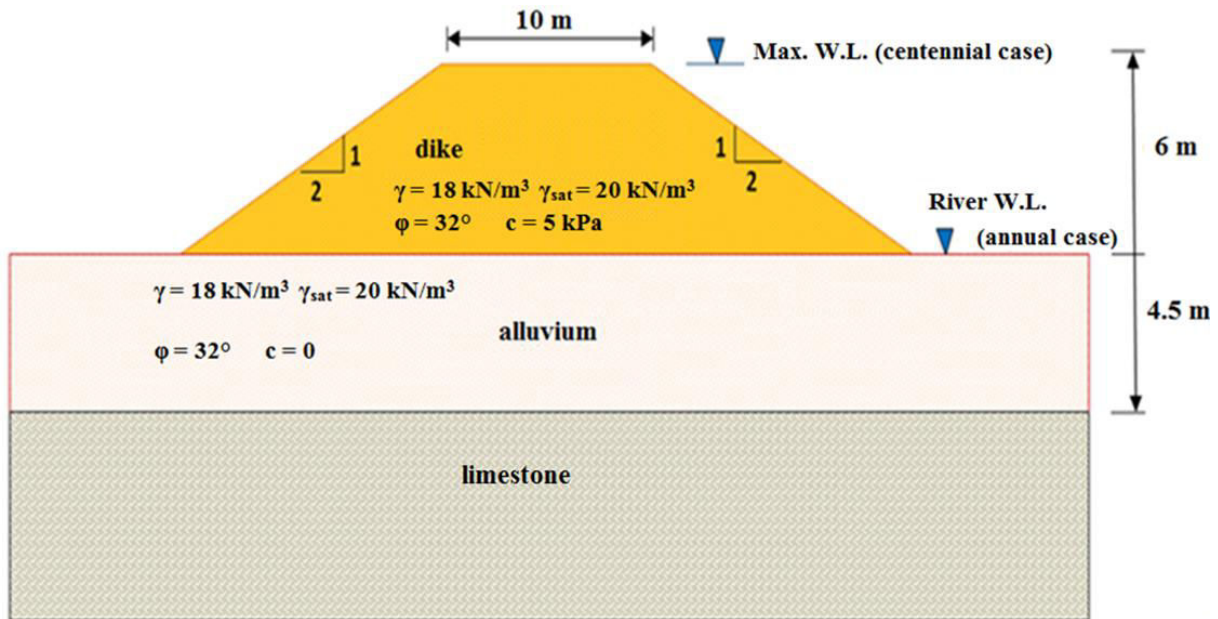


Figure 54 Scheme of the dike and underneath soils properties near Orléans (Maison Vieille, Guilly).

Water may influence the mechanical properties (friction angle and cohesion). A simple example of this effect is a sand castle on the beach. If the sand is totally dry, it is impossible to build a pile of sand with a steep face like a castle wall. If the sand is somewhat wet, one can build a vertical wall. If the sand is saturated, then it flows like a fluid and cannot remain in position as a wall (Figure 55). The scientific explanation for this physical phenomenon could be summarized by the following phrases:

- The dry grains in dry state forms a pile with a slope angle determined by the angle of repose, which is controlled by the frictional contact between the grains. In general, for dry materials, the cohesion is null and the angle of repose increases with increasing grain size, but usually lies between about 30° and 45° (Nelson 2013);
- In wet state, the partially saturated material will show a cohesion which is the consequence of the suction. When the material is fully saturated with water, the suction benefit falls to zero and the cohesion and the angle of friction are reduced until become null and the material tends to flow like a fluid.

Thus, the effect of the water upon the angle of friction and the cohesion is taken into account in this chapter.

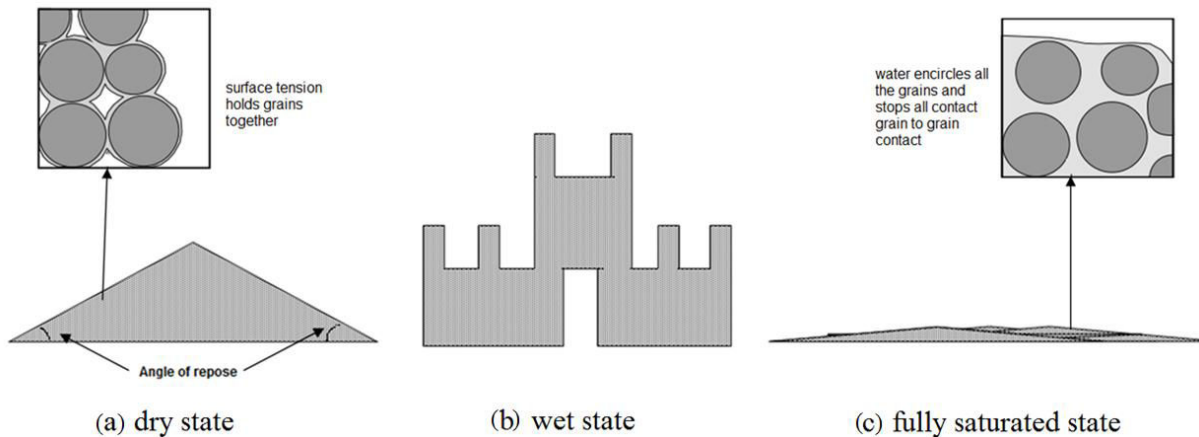


Figure 55 The effect of the water content upon the stability of cohesionless soils (sand) (after Nelson 2013).

We distinguish two scenarios (chapter 3), the first one is the dry dike state in the annual scenario that means the dike body is dry while the alluvium layer is saturated (normal state), and the second one is the saturated dike case where the water level reaches the top of the dike (extreme state). As a consequence, the characteristics of the layers will be modified to consider the water effect and the water will be considered as extra external force acting on the dike.

a- Dry state of dike (annual scenario)

The commercial software TALREN is used to determine the stability of the slope of the dike. 10 slices are considering obtaining a precise calculation and results. The results of TALREN show that the safety factor of slope stability is equal to 1.66 (Figure 56), the shape of the slip surface indicates that it is a base failure type (see Figure 49). The obtained safety factor is more than 1.5. From the long-term stability point of view, that means the dike is safe in the dry case with the properties of the dike and underneath soils, according to the soil investigations by IRSTEA as shown in Figure 54. The commercial software cannot take into account the effect of the cavity. For this reason, this effect is manually introduced with the modified method. At first, the same slip surface identified in TALREN, with a number of slices of 10 and without any cavity is investigated with the modified method. The safety factor is then equal to 1.68, which is 1% more than the safety factor value from TALREN.

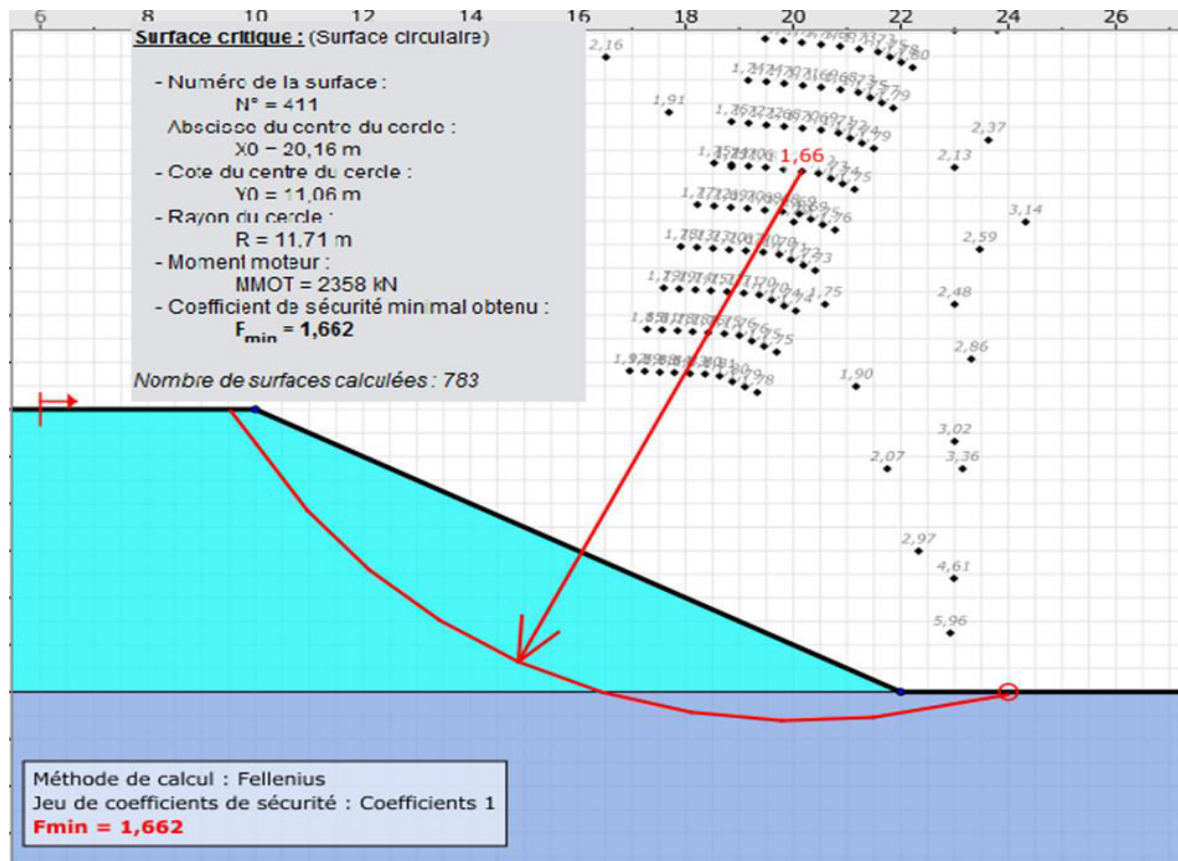


Figure 56 Dike stability - safety factor of slope stability in annual flooding scenario calculations using TALREN

b- Fully saturated state (centennial scenario)

Generally, increasing the soil water content leads to reduce the values of cohesion and internal friction angle of the soil as it mentioned previously (Arquie 1973, Kemper and Rosenau 1984, Al-Shayea 2001).

An increase of the water content may lead to a decrease of the soil proprieties: friction angle and cohesion. There are several papers studying the effect of increasing water content in cohesion soil as the clayey soil, but not many papers that studied the relation between the degree of saturation of soil and the angle of internal friction or the cohesion. Al-Shayea (2001) published an empirical relation between the internal friction angle or/and the cohesion with the degree of saturation and soil type by changing the percentage of the clay.

Al-Shayea (2001) considered that the friction angle and cohesion for a low clay content decreases in the saturated state. For a low clay content (10%), the angle of internal friction decreases with increasing water content to a certain value, beyond which it starts to increase. This increase can be attributed to the fact that excess water results in cleaning some sand particles from the adhering clay, which in turn, increases the angle of internal friction (Al-Shayea, 2001). Figure 57 illustrates the effect of the saturation degree on the internal friction angle for several soil samples. The cohesion is also increase with increasing water content,

but only to certain limits at which it reaches the maximum cohesion, above which it starts to decrease (Figure 57).

The soil of the case study of dike of Val d'Orléans in Guilly area is normally silt- sand soil but it contains some time a little of clay (Saussaye and Durand, 2015). The initial degree of saturation in the scenario of the annual river water level, when the Loire river level equals the level of the dike toe, the dike and the soil underneath ranged from 12% to 27%; therefore, the average value of 20% was taken as initial degree of saturation in the case of the dike of Guilly area. There is no accurate information about the percentage of clay in the dike and the alluvium, whereas the cohesion ranges from 0 to 5 kPa.

Therefore, the percentage of the clay is assumed 10% in the dike material (soil) and the layer of alluvium but the other clay contents in Figure 57 have been tested.

Based on the previous results and due to the absence of data about the values of the cohesion and friction angle for both the dike and soil underneath in flood state, the evolution of geotechnical parameters was assumed the same of those obtained by Al-Shayea. This assumption must be verified for the case of the Val d'Orléans dikes. From Figure 57, the initial angle of internal friction was 44° with clay percentage 10%, and it declined to 40° (decrease 9%). Therefore, the percentage of 9% was adopted in our calculation as decreasing percentage in the angle of internal friction.

For value of the friction angle, the initial value of 32° was modified to be equal to 29° with considering the angle was inclined 9% in saturated state. Figure 58 shows the effect of the saturation degree on the cohesion for different soil samples that have various percentages of clay.

For soil with 10% clay and with initial water saturation degree of 20%, the initial cohesion value was 25 kPa, and it declined to 10 kPa in saturated state that meets water saturation degree of 80% in Figure 58. Therefore, the cohesion was decreased to 15 kPa, i.e. by 60%. Therefore, the cohesion value of 5 kPa of the dike soil must be decreased by 60%, and the final cohesion value equals 2 kPa, whereas the value of the cohesion of the alluvial layer is zero and remains stable.

In this case, the river water level was taken at the top of the dike, namely it is equal to 6 m. The slope stability safety factor was calculated by TALREN (as shown in Figure 59) with modifying the friction angle of dike material and underneath alluvium soil. The safety factor value calculated by TALREN is 1.47, whereas the safety factor of the slope stability using Equation 4.2 (USACE 2003) is 1.48, which is similar to the previous value.

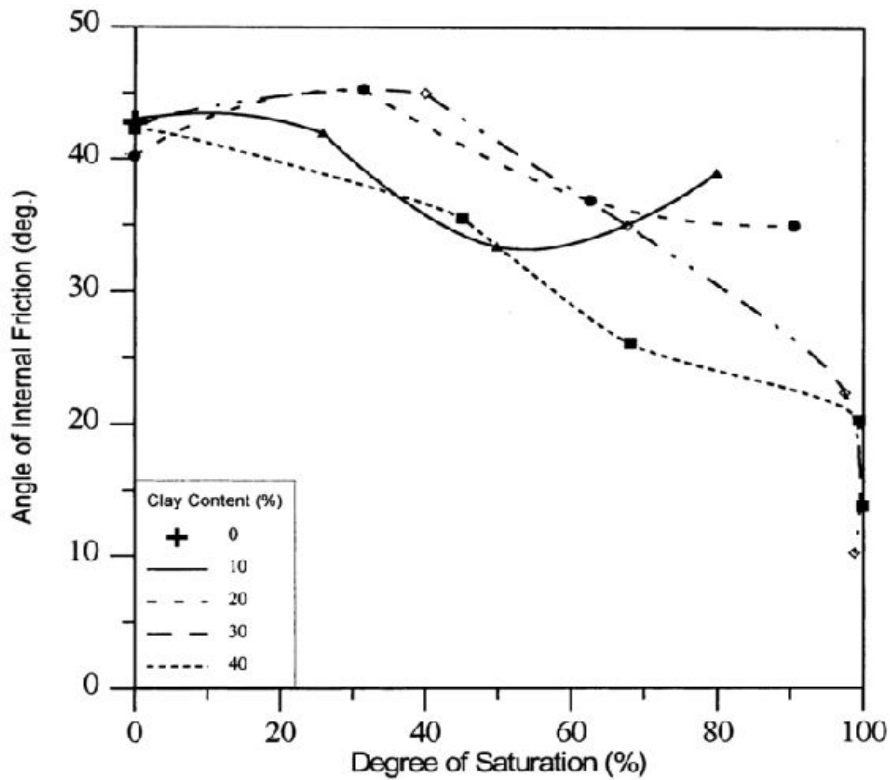


Figure 57 Combined effect of degree of saturation and clay content on the angle of internal friction (Al-Shayea 2001).

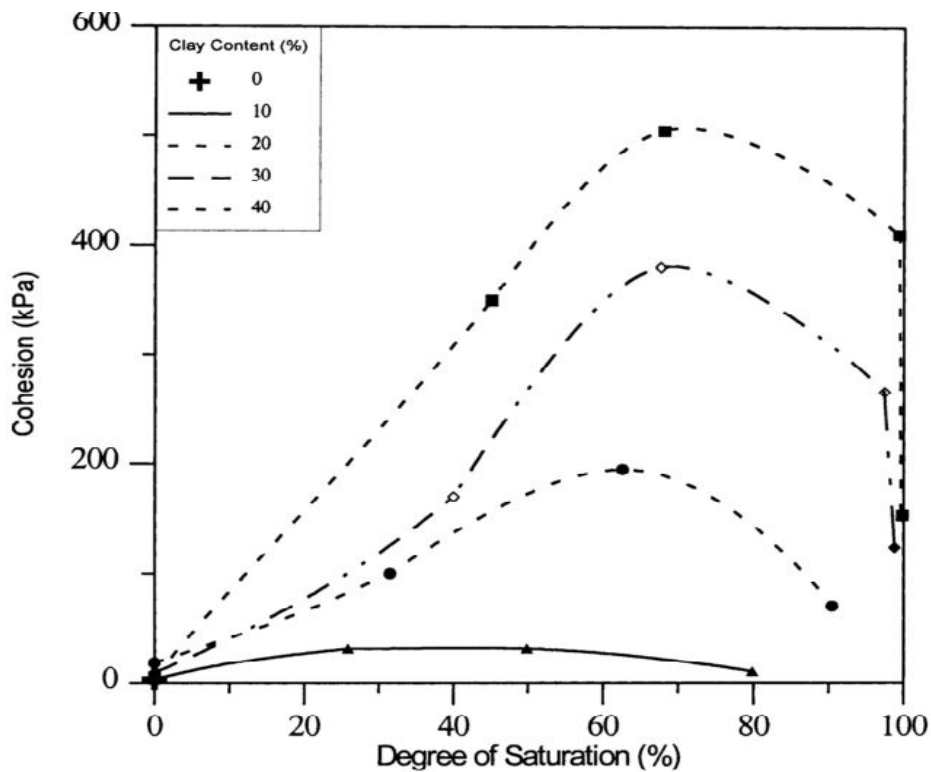


Figure 58 Combined effect of degree of saturation and clay content on the cohesion (Al-Shayea 2001).

In this case, the river water level was taken at the top of the dike, namely it is equal to 6 m. The slope stability safety factor was calculated by TALREN (as shown in Figure 59) with modifying the friction angle of dike material and underneath alluvium soil. The safety

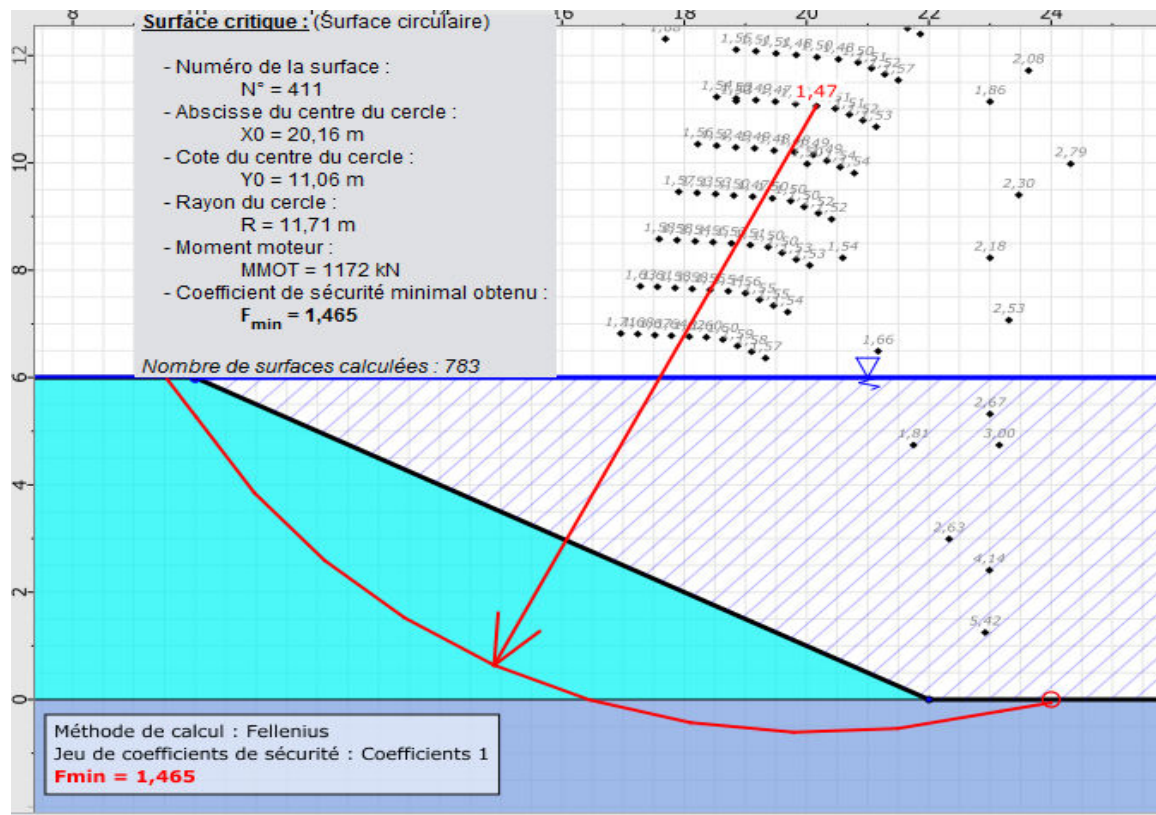


Figure 59 The result of safety factor of slope stability in flooding (centennial) case calculations in TALREN.

4.4 Modified method with a cavity underneath the dike

Let us consider a cavity located underneath the dike. To study its effect on the dike slope stability, we consider a cavity with a circular section (Figure 60). Objective of the modified method is to take into account the stresses changes due to the cavity over the safety factor of the dike. The following assumptions are made:

- We assume that the critical slip surface when a cavity is considered remains the same without the cavity. As a consequence, the new safety factor that will be calculated will not necessary be the most critical and the effect of the cavity might be underestimated.
- The cavity position is fixed under the lowest slice. This assumption is based on the idea that the influence of the cavity is maximal when it is located close to the slip surface of sliding.
- The initial stresses around the cavity are constants (isotropic or anisotropic). It will be justified that this assumption majors the effect of the cavity on the dike.

Considering the position to the lowest slice, the cavity can be moved vertically in several positions according to the distance d between the slip surface and its initial location (cf. Figure 60). We first consider that the initial stresses around the circular cavity are isotropic and equal to the weight of the soil. The soil is assumed to be a homogeneous continuum material with linearly elastic mechanical behaviour. The Kirsch solution that allows assessing the stress changes around a circular cavity in an elastic medium is then used (in: Goodman 1989). The Kirsch solution can be applied when its distance from the surface is three times larger than the hole diameter, or the Kirsch solution will be unreliable (Roylance 2001).

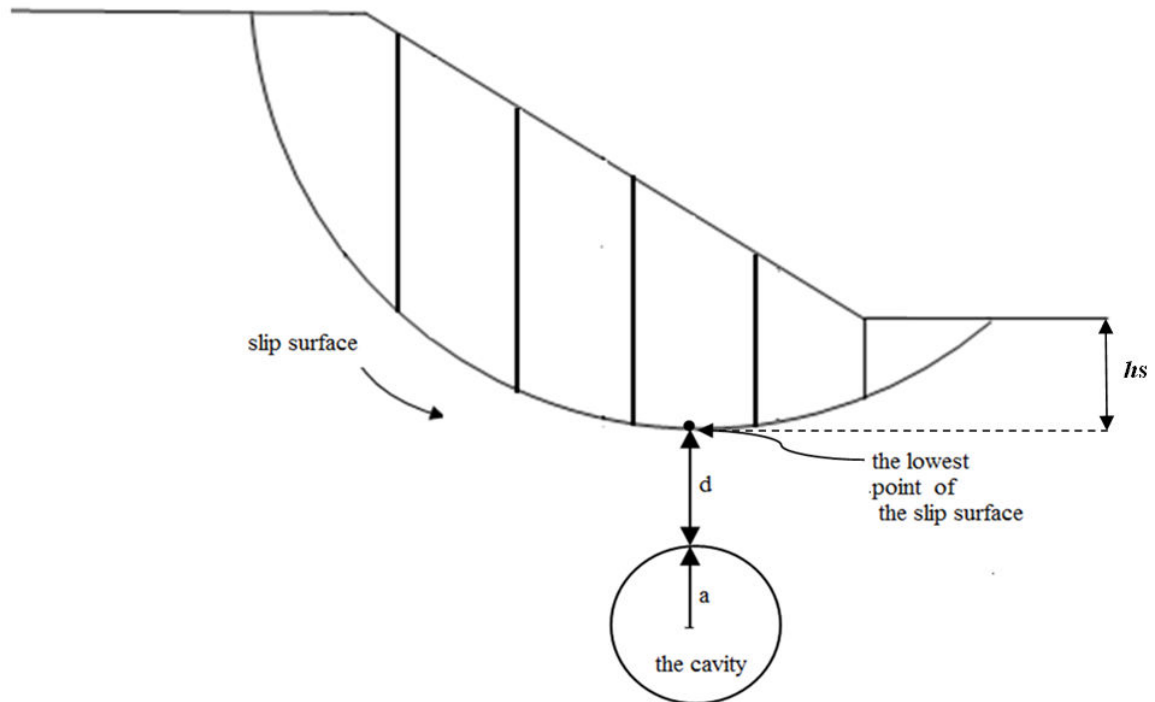


Figure 60 Presence a cavity underneath the lowest point of the slip surface, h_s is the vertical distance between the lowest point of the slip surface and the ground surface.

The solution of Kirsch is very well known and used by engineers for geotechnical problems; we will present the equations of stress distribution in the homogenous soil and isotropic initial stress. Let us consider a point into a polar coordinate system (r, θ) , near an opening with radius a , with isotropic and homogeneous initial stresses in the soil equal to σ_0 (vertical and horizontal stresses are respectively equal $\sigma_h = \sigma_v = \sigma_0$) as shown in Figure 61. The new stress state, with σ_r and σ_θ principals, induced by the cavity in the considered point can be calculated as following (Hoek and Brown (1982) and Goodman (1989),):

$$\sigma_r = \sigma_0 \left(1 - \frac{a^2}{r^2}\right) \quad (4.3)$$

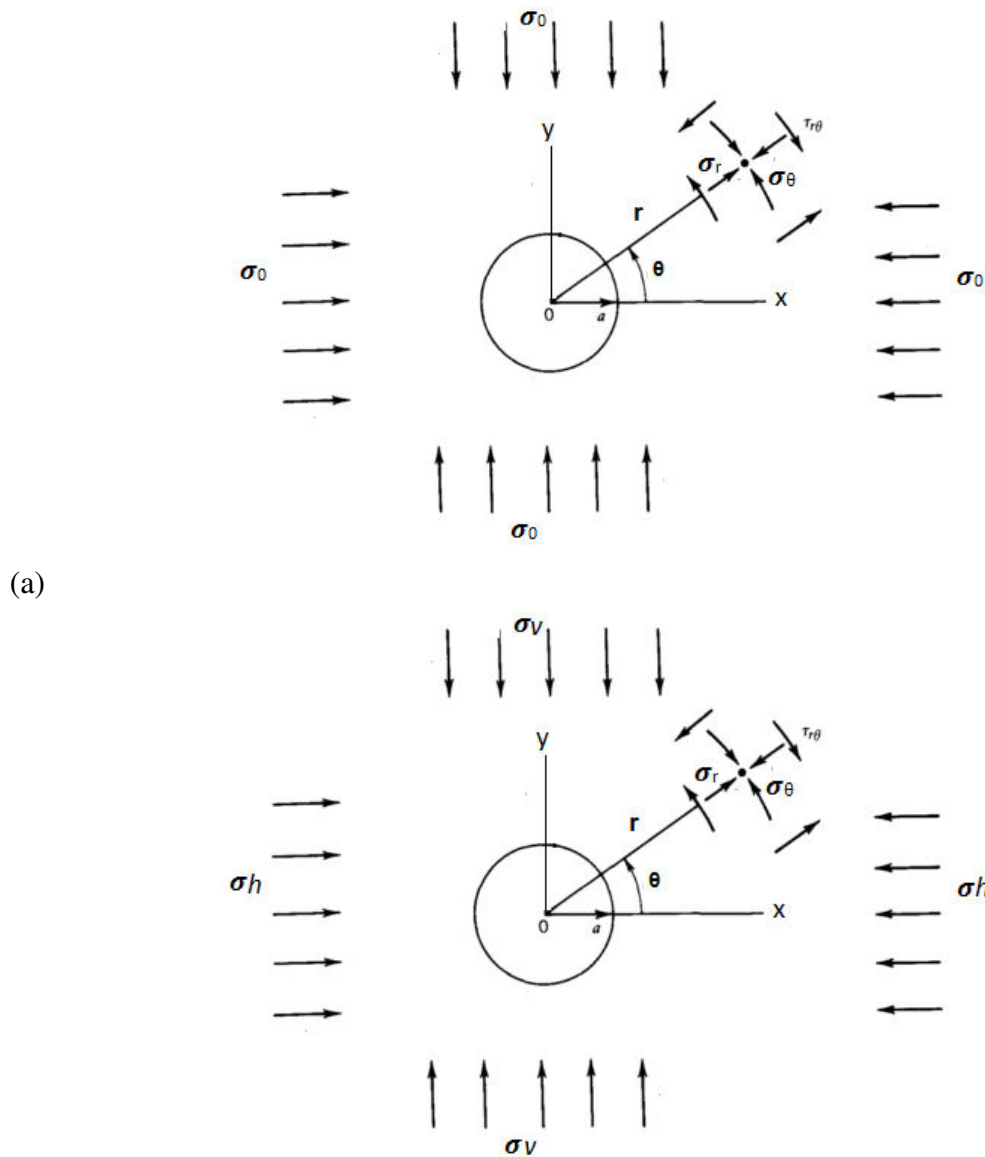
$$\sigma_\theta = \sigma_0 \left(1 + \frac{a^2}{r^2}\right) \quad (4.4)$$

In the case of an anisotropic initial stresses field, the following relations (Goodman 1989) can be used to calculate the radial and tangential stresses (σ_v and σ_h are the initial and homogeneous stresses):

$$\sigma_r = \frac{1}{2}(\sigma_h + \sigma_v) \left(1 - \frac{a^2}{r^2}\right) + \frac{1}{2}(\sigma_h - \sigma_v) \left(1 + 3\frac{a^4}{r^4} - 4\frac{a^2}{r^2}\right) \cos 2\theta \quad (4.5)$$

$$\sigma_\theta = \frac{1}{2}(\sigma_h + \sigma_v) \left(1 + \frac{a^2}{r^2}\right) - \frac{1}{2}(\sigma_h - \sigma_v) \left(1 + 3\frac{a^4}{r^4}\right) \cos 2\theta \quad (4.6)$$

Where σ_r and σ_θ are the principal stresses in the polar coordinate system (Figure 61).



(a)
(b)
Figure 61 Stresses around a circular hole in an isotropic (a) or anisotropic (b) initial stress field.

The stress variation will affect the slope stability. The modified model aims to take into account the stress variations due to the cavity over the calculation of the safety factor. The stress variation is then first assessed from the previous four equations as following:

$$\Delta\sigma_r = -\sigma_0\left(\frac{a^2}{r^2}\right) \quad (4.7)$$

$$\Delta\sigma_\theta = \sigma_0\left(\frac{a^2}{r^2}\right) \quad (4.8)$$

$$\Delta\sigma_r = -\frac{1}{2}(\sigma h + \sigma v)\left(\frac{a^2}{r^2}\right) + \frac{1}{2}(\sigma h - \sigma v)\left(3\frac{a^4}{r^4} - 4\frac{a^2}{r^2}\right)\cos 2\theta \quad (4.9)$$

$$\Delta\sigma_\theta = \frac{1}{2}(\sigma h + \sigma v)\left(\frac{a^2}{r^2}\right) - \frac{1}{2}(\sigma h - \sigma v)\left(3\frac{a^4}{r^4}\right)\cos 2\theta \quad (4.10)$$

The equations (4.7 to 4.10) are taken in term of effective stress in our calculations. In other words, $\Delta\sigma_r$, $\Delta\sigma_\theta$, σh and σv must be replaced by $\Delta\sigma'_r$, $\Delta\sigma'_\theta$, $\sigma'h$ and $\sigma'v$.

The effect of the cavity on the stability of the slope (dike) is taken into account with the influence of $\Delta\sigma'_r$ and $\Delta\sigma'_\theta$ on the normal and tangential stresses along the slip surface. The two increments of $\Delta\sigma'_r$ and $\Delta\sigma'_\theta$ lead to two increments of $\Delta\sigma'_N$ and $\Delta\sigma'_T$ where:

$$\Delta\sigma'_N = \Delta\sigma'_\theta \cos \beta'' + \Delta\sigma'_r \sin \beta'' \quad (4.11)$$

$$\Delta\sigma'_T = \Delta\sigma'_r \cos \beta'' + \Delta\sigma'_\theta \sin \beta'' \quad (4.12)$$

Where the angle β'' is shown in Figure 62.

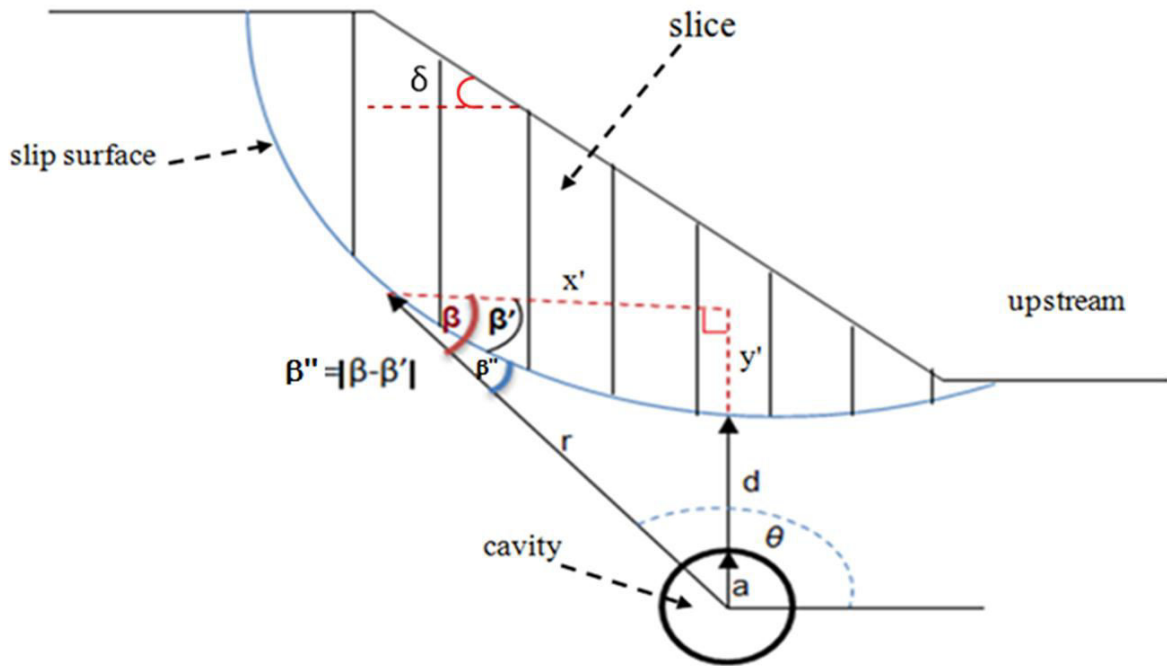


Figure 62 Scheme to clarify the angles used in the calculation of the effect of a cavity on the safety factor.

The safety factor of the slope stability is then modified with taking into account the effect of stress increments around the circular cavity. Equations 4.1 and 4.2 were then modified as following:

$$SF = \frac{\sum(W\cos\omega - ul - \Delta\sigma'N * l) \tan\phi + \sum c l}{\sum(W\sin\omega + \Delta\sigma'T * l)} \quad (4.13)$$

$$SF = \frac{\sum[(W\cos\omega + P\cos(\omega - \delta) - ul) - \Delta\sigma'N * l] \tan\phi + \sum c l}{\sum(W\sin\omega - \frac{\sum Mo}{R} + \Delta\sigma'T * l)} \quad (4.14)$$

Where the equation 4.13 represents the slope stability safety factor in a dry state with the presence of a cavity underneath the dike, while the equation 4.14 represents the slope stability safety factor in a saturated state, also with the presence of a cavity underneath the dike.

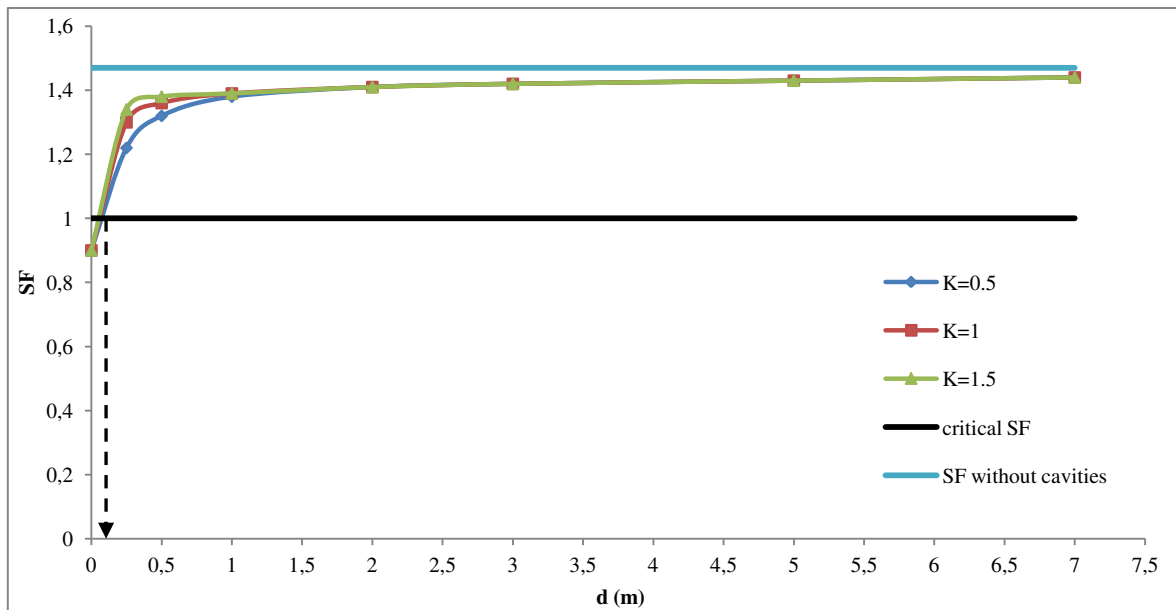
4.5 Application to the Val d'Orléans dike: safety factor of slope stability

According the database of the sinkholes (Gombert et al. 2014) and the in situ observations in the Val d'Orléans area, the diameter of cavities is assumed to range between 0.5 m and 2 m (D (2 a) from 0.5 to 2 m) were adopted to study the effect of the cavity upon the slope stability of the dike. The scenario of maximum flooding (centennial case) is considered more pessimistic than the normal scenario (annual case) according to the previous calculations for

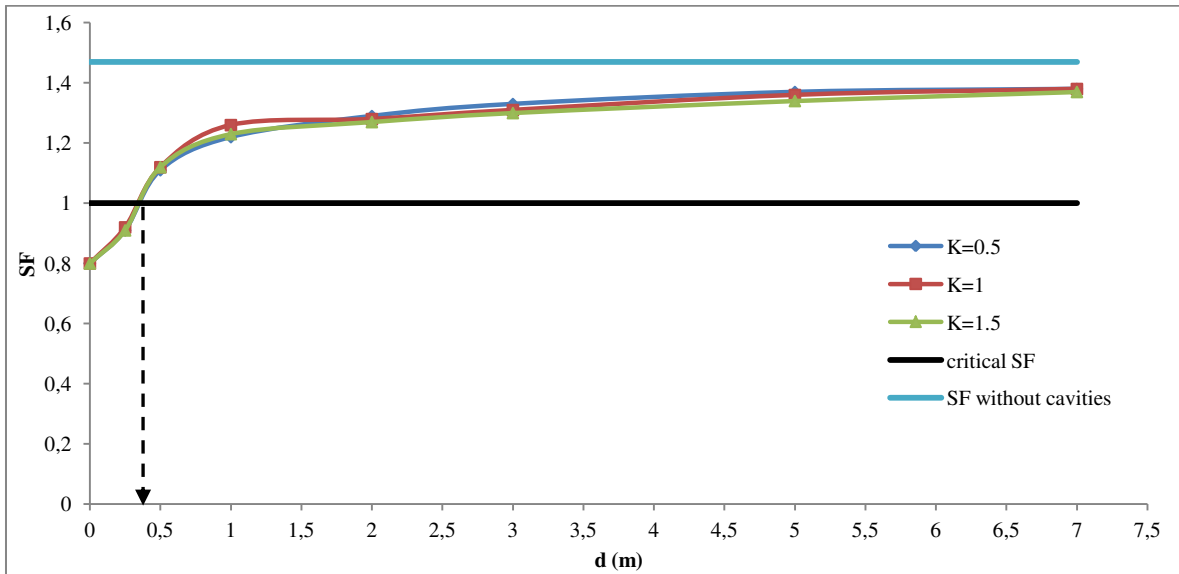
cases without cavities (cf. section 4.3.3). Hence, the calculations were done for the flooding scenario (with maximum water level) in this section.

Figure 63 and Table 6 show the values of the safety factor calculated with equations 4.13 as a function of the vertical distance between the slip surface and the cavity (d) with three different values (0.5, 1, 1.5) of the coefficient of lateral earth pressure (K) for each one of the four chosen diameters of the cavity (0.5, 1, 1.5 and 2 m).

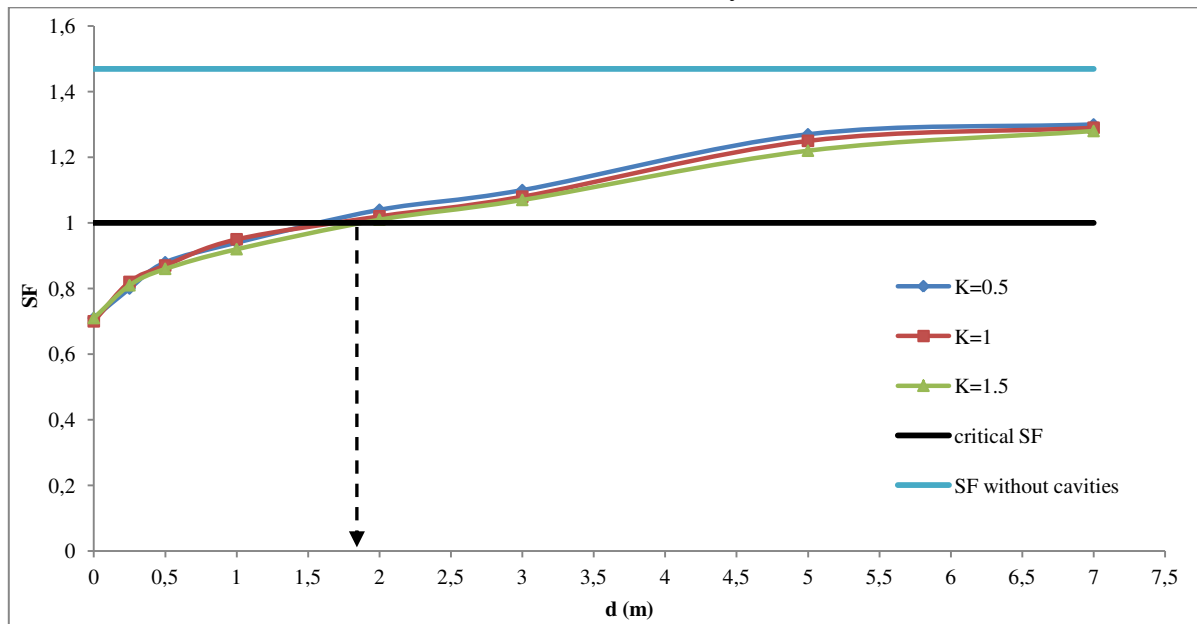
Table 6 shows the minimum vertical critical distance d at which the collapse might begin in function of the diameter of the cavity and the coefficient of lateral pressure K . The critical safety factor (SF) is considered equal to 1. The minimal critical distance “ d critical” is the distance for which the safety factor is equal 1.



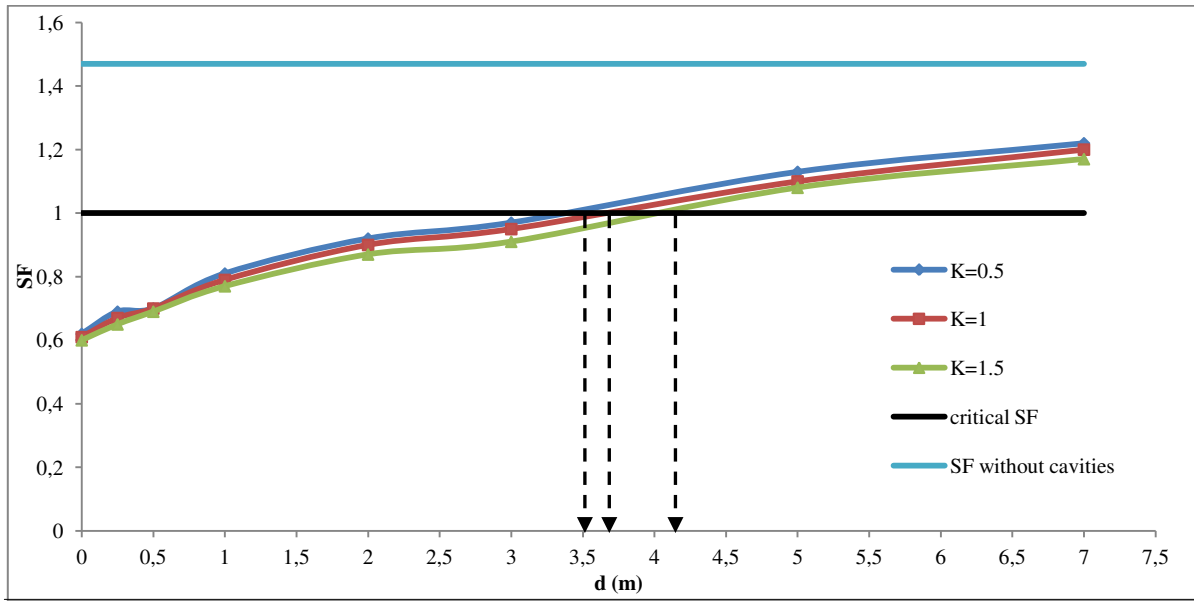
(a) Diameter of the cavity is 0.5 m.



(b) Diameter of the cavity is 1 m.



(c) Diameter of the cavity is 1.5 m.



(d) Diameter of the cavity is 2 m.

Figure 63 Safety factor (SF) function of the vertical distance between the slip surface and the cavity (d) in a centennial flooding scenario for three different states of the coefficient of lateral earth pressure (K).

Table 6 Results of the critical safety factor (SF=1) calculations for the Val d’Orléans dike.

Diameter of the cavity <i>D</i> (m)	Coefficient lateral earth pressure <i>K</i>	Min. critical distance <i>d</i> (m)
0.5	0.5	0.1
	1.0	
	1.5	
1	0.5	0.4
	1.0	
	1.5	
	0.5	

1.5	1.0	1.6
	1.5	1.8
2	0.5	3.5
	1.0	3.7
	1.5	4.2

The study results indicate that:

- (i) There is a significant effect of the cavity on the dike slope stability and
- (ii) The values of the safety factor are generally decreased with decreasing the distance d .

The safety factor is close to its initial value (value without a cavity) over a limit that we call critical distance. The safety factor for the case without a cavity is 1.48 (flooding centennial scenario with the maximal water level). The safety factor is equal to 0.9 when the cavity ($D=0.5$ m) is in direct contact with the slip surface ($d=0$), and the critical distance d is 0.1 m for the critical safety factor (equal to 1). Values of the safety factor was reduced in the three others cases with a greater cavity diameter. The safety factor value is 0.6 in the case of a 2 m diameter cavity when the cavity is in direct contact with the slip surface. In other words, the safety factor is reduced by about 33% between the two cases of cavity (diameters 0.5 and 2 m). The critical distance d was changed according to the change of the cavity diameter value and a largest value of the critical distance d is reported for the case of a 2 m diameter cavity.

Generally, and under the considered assumptions, the dike could start to collapse in the fully saturated state (centennial flooding scenario) when the distance between the cavity and the slip surface of the dike reaches about 4 m. The effect of stress variation on the safety factor is visible when the cavity is less than a about ten meters under the slip surface. In other words, for deeper cavities, the safety factor remains equal to the initial safety factor in the case of a dike without a cavity.

The coefficient of lateral earth pressure (K) has a very small influence on the results. For cases with a cavity diameter equal to 0.5 and 1 m, the critical distance d has the same value for the three cases of lateral earth K . The critical distance d shows small differences in the two other cases of the cavity diameter (1.5 and 2 m). At last, it is difficult to know the value of the coefficient of lateral earth pressure, but in recent sedimentary soil layers and small depth, it is very small and close to 0.5(Cobb 2009).

Figure 64 shows the relation between the safety factor and the vertical distance d for the four chosen diameter values (0.5, 1, 1.5, 2 m) and for an adopted coefficient of lateral earth pressure $K = 0.5$. It is clear from this figure that there is a relation between the diameter of the cavity D and the extent of its negative effect upon the slope stability. When the value of the cavity is large, its negative influence may be significant even if the vertical distance is

relatively important. As an illustration, we can highlight the difference between the two cases ($D=0.5$ m and $D=2$ m): the safety factor is found almost constant in the case of a 0.5 m cavity diameter for vertical distance d greater than 2 m, while in case of a 2 m cavity diameter, the safety factor significantly varies until the vertical distance d equals to about 11 m.

Depending on the Figure 64, we can summarize the relation between the cavity diameter D and the critical vertical distance $d_{critical}$ as it is shown in Figure 65. When the $d_{critical}$ represents the vertical distance d at which the cavity could affect the slope stability by decreased significantly the safety factor. In other words, the cavity might affect the slope stability if the vertical distance d is less than the critical vertical distance $d_{critical}$.

The results show that there is an inverse relationship between the safety factor and the cavity diameter values. In addition, these results show that a 2 m diameter cavity could cause a failure of the slope. Thanks to previous analytical calculation, the likelihood influence becomes negligible when the alluvium layer thickness is greater than 11 m.

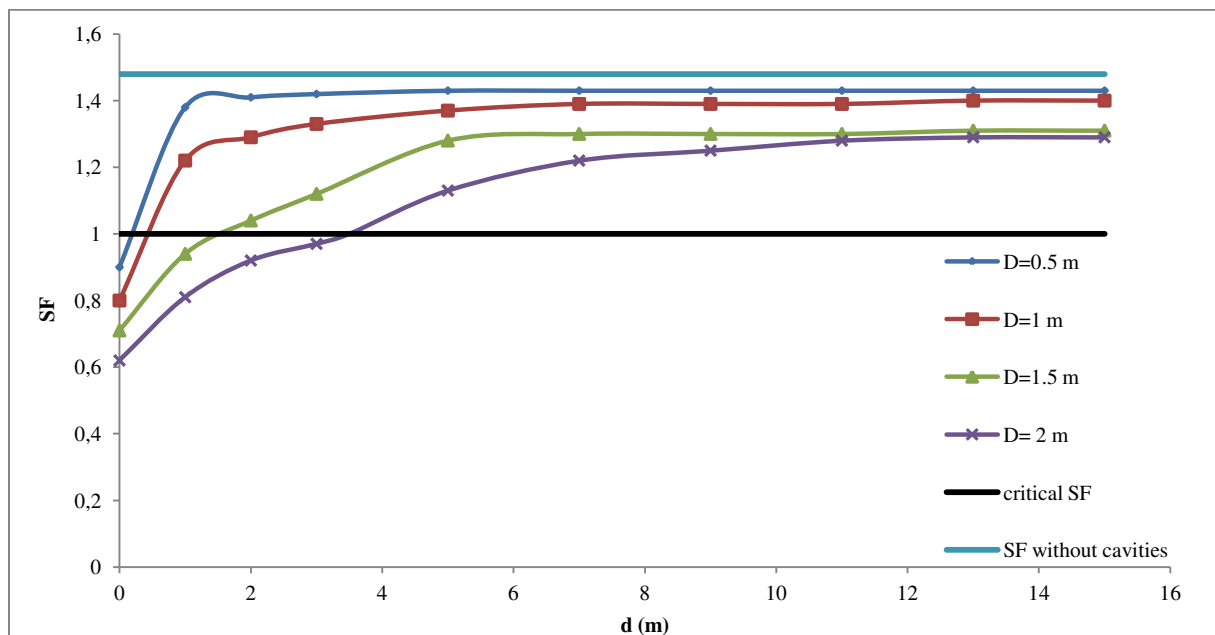


Figure 64 Safety factor (SF) function of the vertical distance (d) in a flooding scenario ($K=0.5$).

Figure 66 shows the relation between the cavity diameter and the safety factor when the coefficient of lateral earth pressure (K) is equal to 0.5. This value of K was used in the calculations of stability of the cavity in the previous chapter (chapter 3) and the position of the cavity centre was taken constant on the borderline between the limestone and the alluvium (as it explained in chapter 3). Herein, the value of the vertical distance d is calculated as the following:

$$d=H-hs-a \quad (4.15)$$

Where H is the thickness of the alluvium equal to 4.5m, hs is the vertical distance between the lowest point of the slip surface and the ground surface (cf. Figure 4.13) equal to 0.6 m and a is the radius of the cavity.

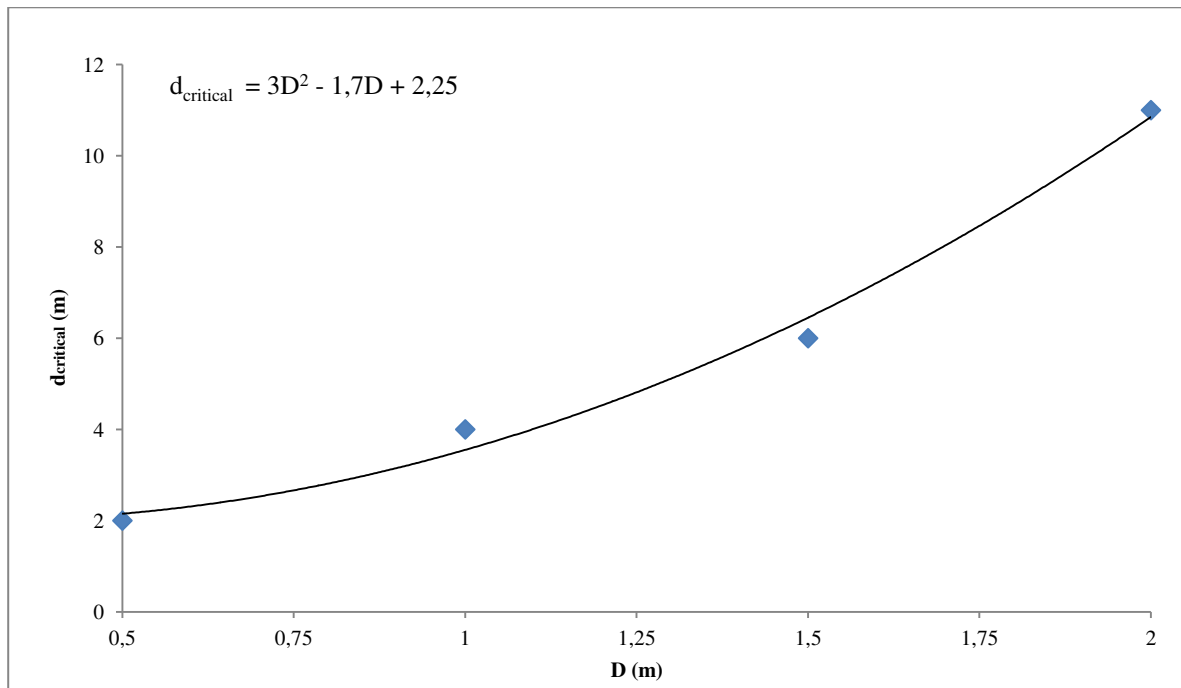


Figure 65 Relation between the critical vertical distance ($d_{critical}$) and the diameter of the cavity (D) according to the results of the Figure 64.

For a 0.5 m cavity radius ($D= 1m$), the value of the vertical distance d would be equal to 3.4 m and this value is less than the $d_{critical}$ for this value of the diameter which is equal to 4 m (cf. Figure 65). Hence, the expected impact of a cavity presence underneath the dike slope starts with a diameter equal to 1 m. On the other hand, a cavity with a diameter of 2 m could reduce the safety factor until the failure (less than 1).

Figure 67 summarizes the relation that combine the critical vertical distance ($d_{critical}$), the diameter of the cavity (D) and the safety factor (SF) in three dimensions.

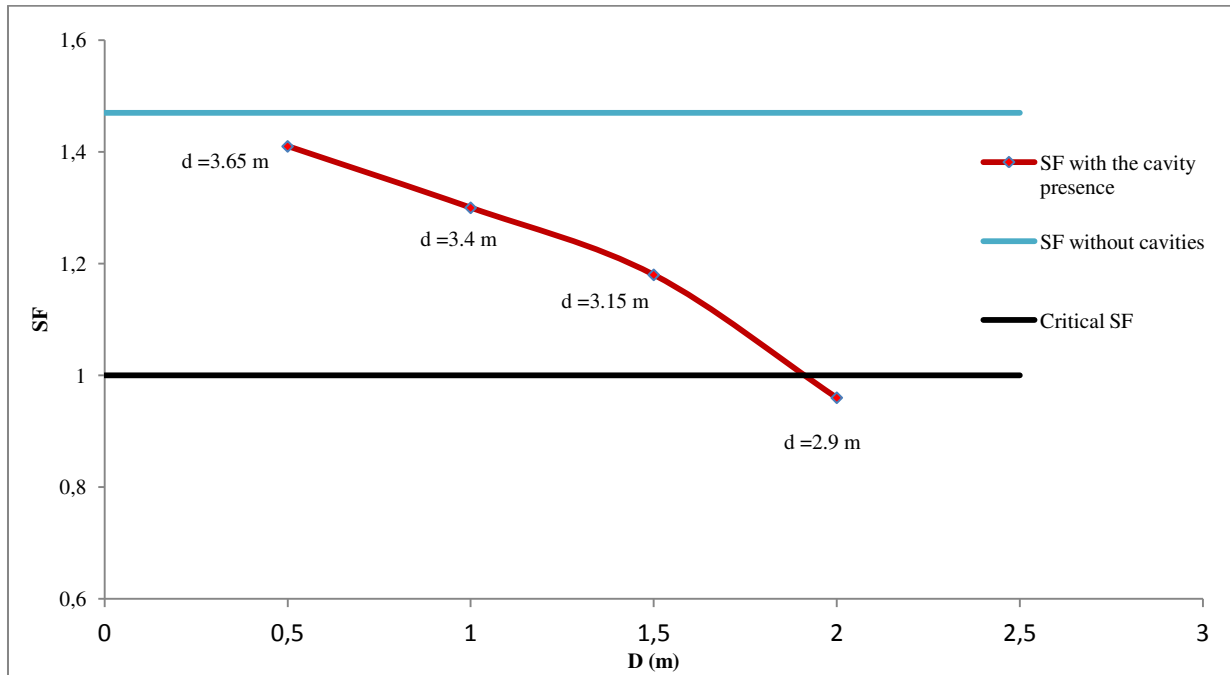


Figure 66 Safety factor (SF) function of the diameter of the cavity (D) in a flooding scenario (K=0.5). Values of d were calculated from Equation (4.15).

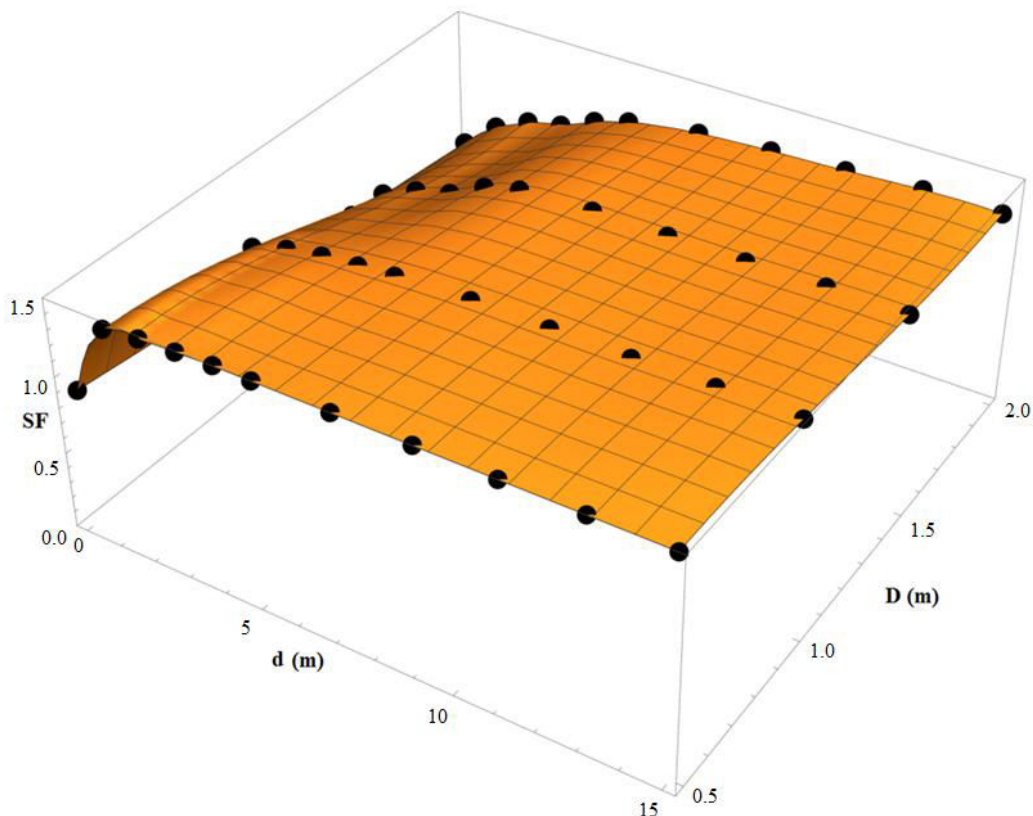


Figure 67 The critical vertical distance ($d_{critical}$), the diameter of the cavity (D) and the safety factor (SF) relation in 3D.

4.6 Summary

In this chapter the impact of the cavity was studied by using two analytical solutions for the slope stability and the cavity influence. The first is Fellenius (Ordinary) method for the slope stability analysis and the second the Kirsch solution for the stress variation around a circular hole. Different hypotheses were adopted to allow the application of the analytical solution of a circular cavity.

The safety factor equations of the slope stability were modified to take into account the modification of stresses induced by the cavity underneath the dike. The analytical solution without cavity was first verified thanks to commercial software (TALREN).

The results showed that the influence of the cavity is a reduction of the safety factor values with a significant effect on the dike slope stability, especially in the saturation state for our case study. The cavity with a diameter equals to 1 m and located at vertical distance about 3.5 m from the slip surface could reduce the slope safety factor while a cavity of 2 m of diameter and located at vertical distance about 3 m could result a failure in the dike of Val d'Orléans slope surface (for adopted coefficient of lateral earth pressure $K=0.5$).

Thanks to the analytical developments, different other configurations have been studied to assess the influence of cavities on the dike stability.

The results will be verified using a numerical modeling (in chapter 5). But the analytical approach offers an easy and simple way to assess the influence of the cavity on the dike.

4.7 References

- Al-Shayea N. A. 2001, The Combined Effect of Clay and Moisture Content on the behaviour of Remolded Unsaturated Soils, *Engineering Geology* 62(2001),319-342, pp 333-336.
- Arquie G. 1973, Théorie générale de l'influence de la teneur en eau sur les résultats du compactage, *Bulletin Liaison Laboratoire des Ponts et Chaussées*, 64, Ref. 1297, pp 145-158.
- Cheng Y.M. and Lau C.K. 2008, *Slope Stability Analysis and Stabilization; New methods and insight*, ISBN 0-203-92795-8 Master e-book ISBN, book, published by Routledge, 260 pp.
- Chowdhury R., Flentje Ph., Bhattacharya G. 2010, *Geotechnical Slope Analysis*, Taylor & Francis Group, London, UK, pp 269-270.
- Cobb F., 2009. *Structural Engineer's Pocket Book*, 2nd edition. Elsevier, 394 pp.
- Dinesh S.V. 2008, *Stability of Earth Slopes*, lecture notes for web learning, unit-6(80cv64), 4 pp.
- Gombert P., Orsat J., Mathon D., Alboresha R., Al Heib M., Deck O. 2014, Rôle des effondrements karstiques sur les désordres survenus sur les digues de Loire dans le Val d'Orléans (France), *Bull Eng Geol Environ*, DOI 10.1007/s10064-014-0594-8, pp. 125–140.
- Goodman R.E. 1989, *Introduction to Rock Mechanics*, second edition, John Wiley and Sons, pp 225-227.
- Hoek E. and Brown E.T. 1982, *Underground excavations in rock*, London: The Institution of Mining and Metallurgy, 527 pp.
- Kemper W.D. and Rosenau R.C. 1984, Soil cohesion as affected by time and water content, *Soil science society of America journal*, vol.48, pp 1001-1006.
- Khanmohammadi S. and Hosseinitoudeshki V. 2014, The effect of water level on the stability of slopes, *Journal of Novel Applied Sciences*, ISSN 2322-5149, pp 1237-1239.
- Kitch W.A. 2012, *Slope Stability Analysis Procedures*, AEG-GI SHORT course, UC Riverside, CA, 20 pp. [Online] http://www.csupomona.edu/~wakitch/arts/AEG-I_Slope_Stability_2012_0512.pdf.
- Mestat Ph. 1998, Etat de contraintes initiales dans les sols et calcul par éléments finis, *Bulletin des laboratoires des ponts et chaussées*, pp15-32.
- Nelson S.A. 2013, *Natural disasters, Slope stability*, EENS 3050, edited by Tulane university. 17 pp. http://www.tulane.edu/~sanelson/Natural_Disasters/slopestability.pdf.
- Roy E.H. and Richard J.D. 2003, *Stability of Slopes*, the *Civil Engineering Handbook*, 2nd. ed., New York: CRC press LLC, pp 1-28.

- Roylance D. 2001, Closed Form Solutions, Department of Materials Science and engineering Massachusetts Institute of Technology, Cambridge, MA 02139, pp.1-6 [online] <http://ocw.mit.edu/courses/materials-science-and-engineering/3-11-mechanics-of-materials-fall-1999/modules/airy.pdf>.
- Saussaye L. and Durand E., 2015. Levées du Val d'Orléans (45); Investigations géotechniques complémentaires- Complementary geotechnical investigations- CEREMA and DREAL Centre SLBLB- Affaire 2014-c14RB0229/C, 265 pp.
- Schaefer J.A. 2009, Risk evaluation of dams on karst foundations, 29th Annual USSD Conference Nashville, Tennessee, April 20-24, 2009, pp 541-579.
- Terzaghi K. (1943). Theoretical Soil Mechanics. New York: John Wiley & Sons.
- USACE (US Army Corps of Engineers) 2003, Slope Stability, engineering manual, Appendix c,[online] http://www.publications.usace.army.mil/Portals/76/Publications/EngineerManuals/EM_1110-2-1902.pdf.
- Zhou Y. 2006, Geotechnical Engineering: Slope Stability, Course No: G06-001, U.S. Department of Transportation, Federal Highway Administration, Publication No. FHWA NHI-06-088, chapter 6, pp 14-15.

5.1 Objective and method

The main goal of this chapter is to verify the analytical results obtained from the two previous chapters (chapters 3 and 4). Thus, the safety factors of the slope stability were recalculated with or without a cavity by using the finite element method to confirm the results of the analytical approaches. Different cavity positions and water levels are considered. Moreover, the effect of third dimension is investigated with 2D and 3D models.

The CESAR-LCPC (version 6) software is mainly used in this work. In addition, UDEC (Universal Distinct Element Code, cf. appendix A) was used just to compare the mechanisms of failure. CESAR software is based on the finite element method (FEM). This software was chosen for the following features:

- It allows both 2D and 3D calculations,
- It allows easy numerical modelling with various geometries and accurate meshes in both 2D and 3D,

The three-dimensional version (3D) allows verifying and comparing the results from the two-dimensional version (2D). Several limitations of software were met: non convergence calculation, difficulties to model spherical cavity, etc.

In order to check the stability of embankments (dikes) in FEM, the following and conventional criteria are used (Ugai1989; Griffiths and Lane, 1999; Luan et al., 2003; Zhao et al., 2003; Deng et al., 2004; Zheng et al., 2006; Zheng et al., 2008 and Jiang et al., 2015):

1- The numerical non-convergence criterion with the c - ϕ reduction method. With this method, the mechanical parameters c and ϕ are reduced as long as the calculations converge. With CESAR, three criteria are used to test the convergence. The first one is based on the residual forces; the second one is based on the displacements between two iterations and the last one about the mechanical work during one iteration (Mesta, 1998).

2- The criterion of plastic yield zone: when some elements (nodes) of the model reach the plasticity (stresses are over the elastic limit), plastic deformations occur and elements can be considered as a potential failure zones. Isovalues of the plastic deformation may be used to have an idea of the global failure shape. In the slope stability checking, plastic yield zone connects from the toe to the head of the slope during strength reduction. This situation is assumed to characterize a global failure state.

3- The total displacement criterion: when the displacement of some points on the slope surface increases suddenly sharply due to the variation of an internal or external factor, this can be used to define a change of the global behaviour.

The three previous criterions tested in this work to compare the impact of the cavity on the dike stability and vice versa. The safety factor can also be calculated with the method described in chapter 4 and the two results can then be easily compared.

The MCNL module (Module de résolution d'un problème de mécanique en comportement non linéaire) in CESAR is dedicated to the resolution of a mechanical problem exhibiting non-linear behaviour. It is possible to model elasto-plastic materials (with or without hardening) or non-linear elastic materials. MCNL module allows modifying the mechanical properties of given meshes elements to model for the replacement of a material by another during the steps of the calculation and it also allows simulating the excavation of some zones of the mesh to model the cavity.

The Mohr-Coulomb elasto-plastic criterion is adopted for the different materials. It is an elasto-plastic model without hardening (elasto-plastic perfectly plastic). The elastic part of the constitutive law is linear isotropic and specified by the input of the Young's modulus E and the Poisson's ratio ν . The Mohr-Coulomb yielding criterion is the most classically used criterion in soil mechanics. It expresses the fact that the tangential (shear) stress τ on a material face is limited by the maximum shear resistance that depends on the normal stress σ_n , which is applied on this face:

$$|\tau| \leq c + \sigma_n \tan \varphi \quad (5.1)$$

Where c is the cohesion and φ the friction angle. The Mohr-Coulomb yield criterion may also be written in term of principal stresses (Bourgeois et al., 2012):

$$F(\sigma) = (\sigma_1 - \sigma_3) - (\sigma_1 + \sigma_3) \sin \varphi - 2 c \cos \varphi \quad (5.2)$$

Where σ_1 and σ_3 represent respectively the major and the minor principal stresses, positive in compression. It should be noted that the value of the criterion does not depend on the intermediary principal stress σ_2 (Bourgeois et al., 2012).

The angle of dilation ψ controls the amount of plastic volumetric strain developed during plastic shearing and is assumed constant during plastic yielding (Eid et al., 2015; Narayanan et Jeyapriya 2015). It should be noted that when the flow rule is associated and the friction angle is non-zero, the flow rule leads to an irreversible increase in the volume controlled by the friction angle and usually not realistic for significant shear strains. In this work, the angle of dilation ψ was considered equal to the friction angle φ considering the soils as an associated material according to recommendation of the theoretical manual of CESAR especially if the flow rule is associated.

Two modes of calculations are possible in the CESAR-LCPC software. The first one is the "Standard" mode that can be used to evaluate the movements, the plastic deformations and the stresses in the model for a given set of mechanical properties. The second is the "C-phi reduction" mode that can be used to assess the safety factor.

We decided to use the safety factor criterion to compare the results; we firstly started with the c-phi reduction method which gives the safety factor value directly contrary to the standard mode.

The appendix A and UDEC manual (Itasca, 2000) present in details the code UDEC and some applications in geotechnical domain.

5.2 General description of the dike of Val d’Orléans model in CESAR-LCPC

Based on the description of the dike of Val d’Orléans in the chapter 2, the numerical model was carried out to verify its stability. The layer of limestone was assumed equal to 10 m and the width in upstream and downstream side was chosen equal to 40 m as it is shown in Figure 68. The mechanical properties of the dike, alluvium and limestone layers are shown in Table 7. The layer of limestone was considered in elastic state to neglect the lower part of the cavity (cave) and to focus only on the upper part in soil layer. Young’s modulus values were assumed due to the soil type and its properties. The dimensions of the model are enough to avoid any negative consequences of the boundary conditions on the results.

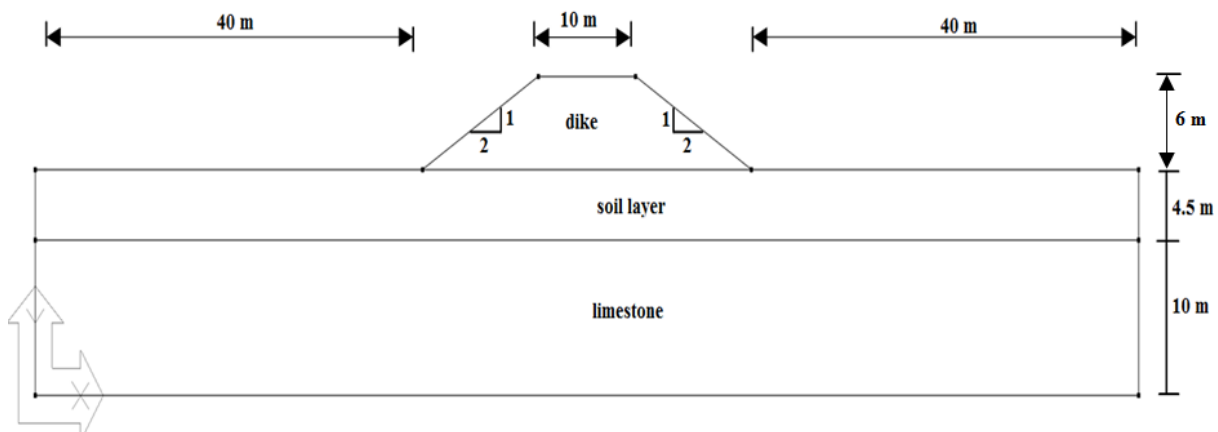


Figure 68 Dimensions of the FEM numerical model of the dike of Val d’Orléans, soil and limestone layers.

Table 7 Mechanical properties of the soil, limestone and the dike materials.

	Dike	Alluvium layer	Limestone (karst) layer
Young’s modulus (MPa)	70	50	100
Poisson’s ratio	0.33	0.33	0.2
Unit weight (kN/m ³)	18	20	22
Friction and dilation angles (°)	32	32	in elastic state
Cohesion (kPa)	5	0	

The boundary conditions of the 2D and 3D models are illustrated in Figure 69. A zero normal displacement is applied on the lower and lateral boundaries of the model. Where u_i , v_i and w_i

are the displacements in x, y and z directions respectively and when one of each is assumed equals to zero that means this boundary is fixed or no allowed displacements. Figure 70 shows the general parameters are used in CESAR with the MCNL module to solve the non-linear problem. The maximum iterations number is equal to 1000 and the tolerance value for the convergence criteria is 0.01. Quadratic interpolation elements (meshes) are used: six-node triangular elements in 2D and tetrahedron shape in 3D. The algorithm used to solve the problems is the multi-frontal type.

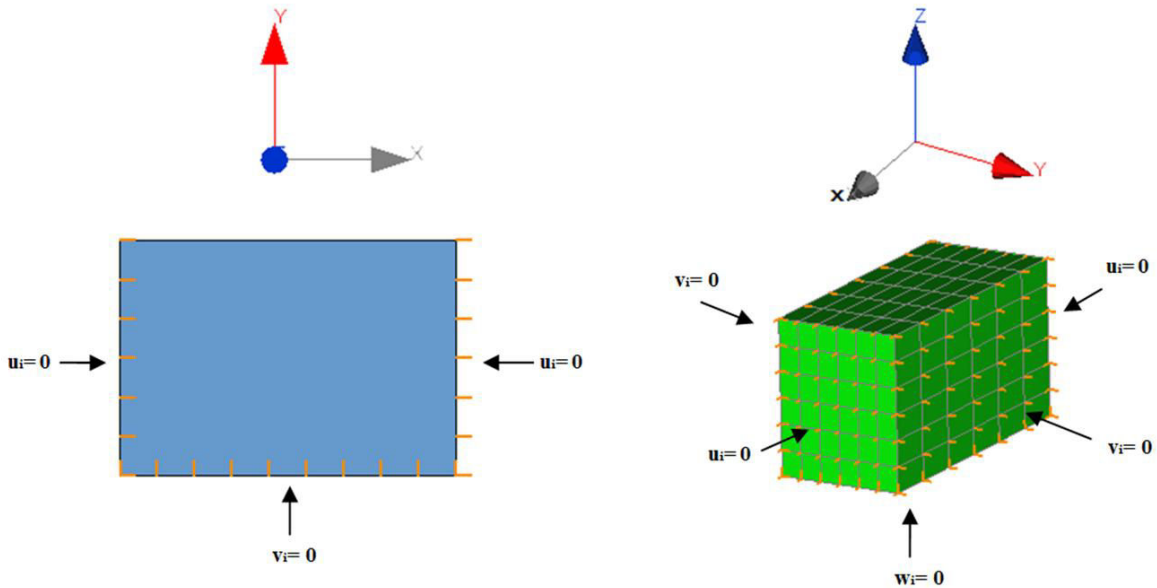
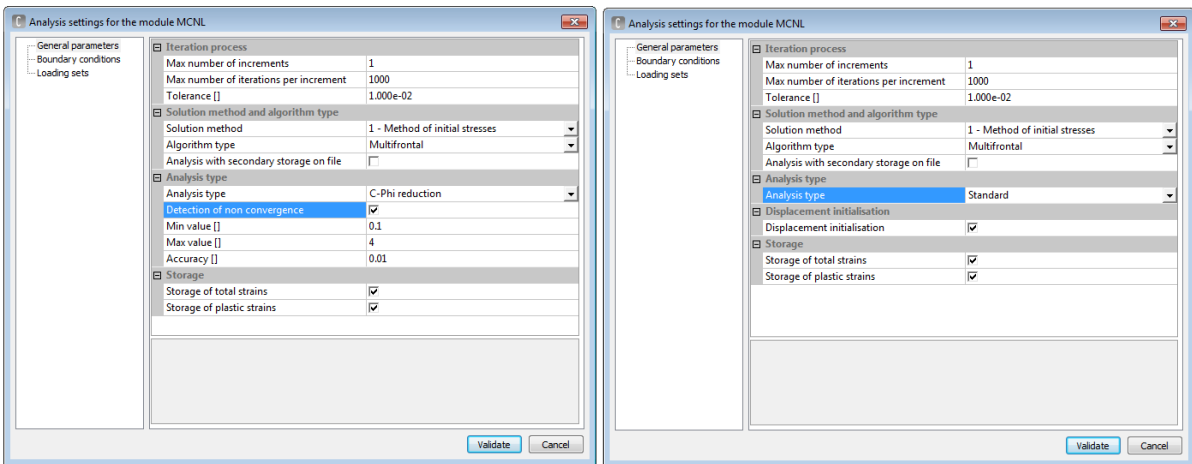


Figure 69 Boundary conditions used for CESAR 2D (u: horizontal and v: vertical displacement) & 3D models (u and v: horizontal and w: vertical displacement).



(b) C-phi reduction method parameters. (b) Standard method parameters.

Figure 70 General parameters for the MCNL module calculation in CESAR-V6.

The simplest way to compare the results of the analytical approach (chapter 3&4) with the numerical model results is the safety factor value. Hence, the first criterion must be used in CESAR-LCPC is the safety factor value of the slope stability obtained by the c-phi reduction

method. Then, this result can be compared to the previous results, which were obtained from the analytical approach (chapter 4). According to the results, we could decide to continue with this mode of calculation in CESAR or if we must use the other standard calculation option.

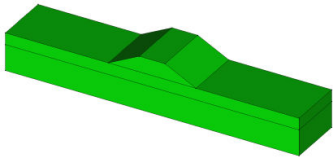
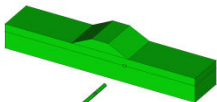
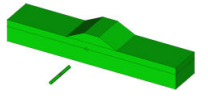
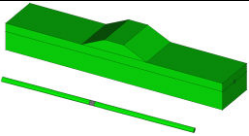
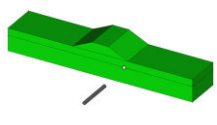
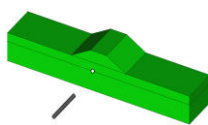
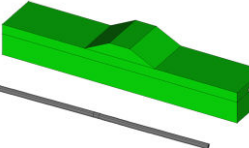
Table 8 presents the different models and steps carried out to achieve the study of dike – cavity interaction. Firstly, the dike of Val d’Orléans is modelled in 2D by using:

- C-phi reduction method to calculate the safety factor of the dike slope stability without presence of cavities; and
- The standard method to study: the effect of the cavity upon the dike; and the effect of the dike on the stability of the cavity (for a cavity underneath the maximum height of the dike and cavities beside the dike).

While the model of 3D is used to:

- Compare its results with the 2D results;
- Compare between the presence of a local cavity and a conduit underneath the dike (effect of the third dimension); and
- Study the effect of the direction of the (cavity or conduit) relative to the direction of the dike.

Table 8 Methodology for investigating the dike-cavity interaction in CESAR.

		Standard method		
		With a cavity		
2D	Slope stability (c-phi reduction method)			
	Without cavities	cavity under the slope	cavity under the dike head	cavity beside the dike
3D		parallel to the dike axis		perpendicular to the dike axis
		(local cavity /conduit) under the slope	(local cavity /conduit) under the dike head	(local cavity /conduit) under the dike head
				
				

5.3 Slope stability calculation by the c-phi reduction method

5.3.1 The theoretical bases of the method

The c-phi reduction method became recently a popular numerical method to evaluate the safety factor in geomechanic problems and it is used widely in the context of Mohr-Coulomb material (Dawson and Roth, 1999; and Griffiths and Lane, 1999).

The principle of c-phi reduction method is reducing shear strength parameters of soils in a slope. Thus, cohesion c and friction angle ϕ are reduced to assess the slope stability. The main output of this type of analysis is the factor of safety.

The ratio of the true strength to the computed minimum strength required for the equilibrium is the safety factor that is conventionally used in soil mechanics. By introducing the standard Coulomb condition, the initial cohesion and the tangent of the friction angle are reduced in the same proportion until non-convergence of the numerical calculation (Baba et al., 2012; Rabie, 2013; Jiang et al., 2015):

$$RF = \frac{c}{cr} = \frac{\tan\phi}{\tan\phi_r} \quad (5.3)$$

Where RF is the reduction factor at any stage during the calculations, c and ϕ are the input strength parameters while the parameters cr and ϕ_r reduced strength parameters that are just large enough to maintain equilibrium.

The resulting yield surface is shown in Figure 71 in which c and ϕ are scaled down to cr and ϕ_r respectively. The reduction of strength parameters is controlled by the strength reduction factor RF. This parameter is increased in a step-by-step procedure until failure occurs (non-convergence of the calculation). The safety factor is then defined as the value of RF at failure. This method in MCNL module computes the highest RF coefficient that divides the strengths parameters of soil bodies while achieving convergence of the elasto-plastic calculation, i.e. stability (for the given number of the iterations and tolerance). In order to obtain a true factor of safety, the strength reduction factor RF needs to be gradually increased until the reduced strength parameters (cr and ϕ_r) bring the slope into the failure state. At that time, the factor of safety for the slope is equal to the strength reduction factor, i.e., $SF = RF$ (Jiang et al., 2014).

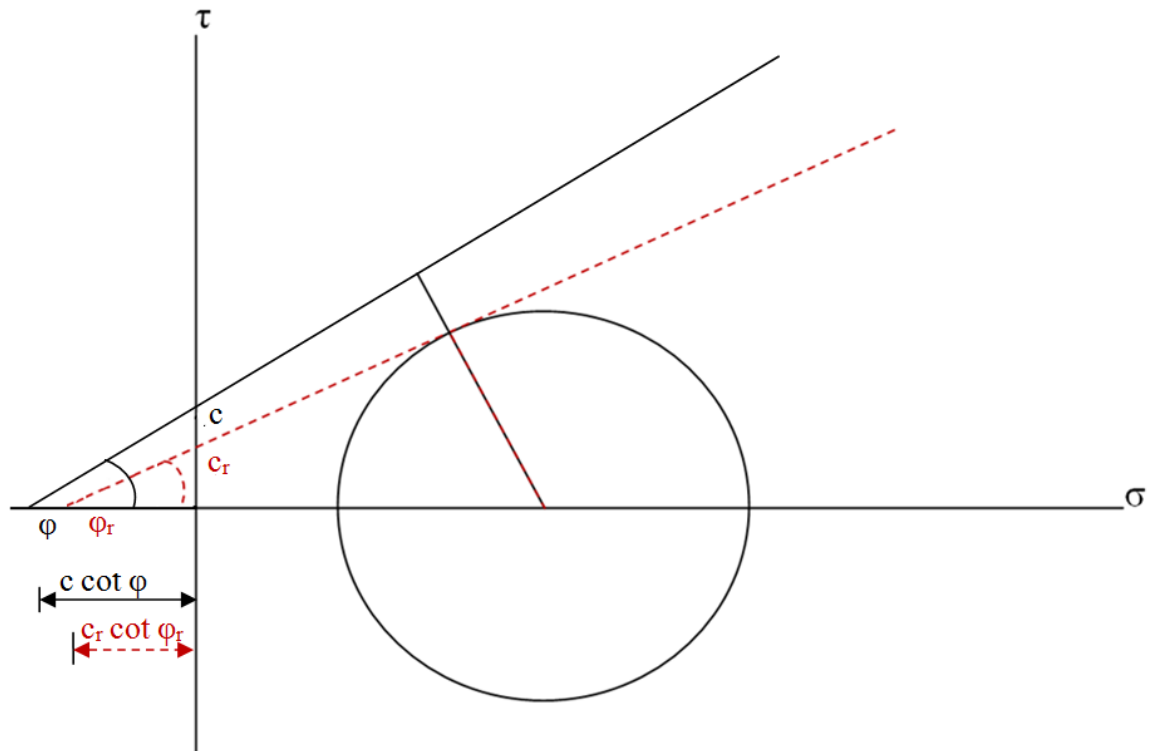


Figure 71 Mohr-Coulomb yield surface after strength reduction, c and ϕ are the initial cohesion and friction angle, c_r and ϕ_r are the reduced cohesion and friction angle.

The c - ϕ reduction method has several advantages (Baba et al., 2012). It allows to model slopes with a degree of very high realism (complex geometry, sequences of loading, presence of material for reinforcement, action of water) and to better visualize the deformations in soils in place. We don't need to give the sliding surface as a data of the calculation. In FEM, the final result of c - ϕ reduction method is considered as failure state according to the numerical non-convergence criterion.

5.3.2 Slope stability calculation for the dike without cavities

This section aims to verify the slope safety factor result of the dike of Val d'Orléans without cavities and in the normal state and compare this result with previous results that were calculated by the ordinary limit equilibrium method in chapter 4. The geometry in Figure 68 was modelled with CESAR (18660 finite elements) and UDEC and the c - ϕ reduction method was applied. The results are summarized in Table 9.

From the results of Table 9, the SF values got with the FEM were generally greater than those got with the ordinary methods (Fellenius and Bishop). This difference may be explained by the influence of the mesh dimensions and the algorithms performances (CESAR and UDEC). The value of SF decreases with reducing the dimensions of the elements (meshes). Thus, the mesh dimensions are considered in the next calculations equal to 0.5 m (Figure 72).

The result of the safety factor in CESAR with finite elements equal to 0.5 m is shown in Figure 73, with the isovalues of the plastic strain norm in micro deformation (10^{-6}). The white zone in the figure means the elements are still in the elastic state. The dotted lines in this

figure were added to illustrate the range of the potential failure surface. The slip surface which was obtained from the ordinary method (TALREN software) is in the range of the dotted lines. The two results are then consistent.

Table 9 Results of the safety factor SF of the dike of Val d'Orléans in dry state by using the ordinary method (Fellenius and Bishop) and a numerical method (c-phi reduction method), FE: finite element method, FD: finite difference method.

Method and software	SF
FE (CESAR-V6) (meshes 0.5 m)	1.96
FE (CESAR-V6) (meshes 1 m)	2
FD (UDEC) (meshes 0.5 m)	1.84
FD (UDEC) (meshes 1 m)	1.93
Bishop (TALREN)	1.83
Fellenius (TALREN ²)	1.66
Fellenius (manually ^{1 3})	1.68

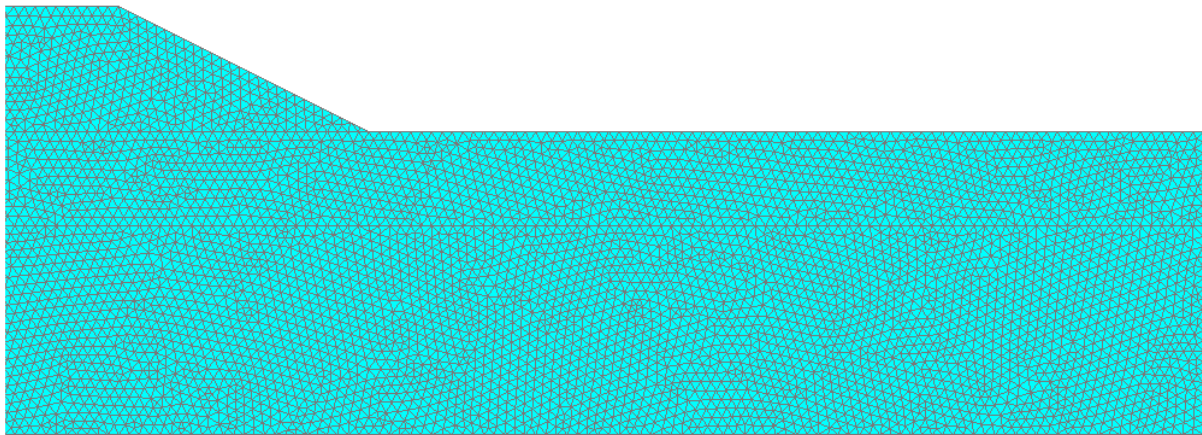


Figure 72 Cross section of the dike of Val d'Orléans with finite element dimensions equal to 0.5 m.

² Cf. chapter 4.

³ Using Excel sheet for ordinary equilibrium method.



Figure 73 Isovalues of the plastic strain norm for the dike of Val d'Orléans by using the c-phi reduction method in CESAR with finite element dimensions equal to 0.5 m. The dotted lines refer to the range of potential failure surface, while the red line refers to the failure surface got from the ordinary method (TALREN software).

5.3.3 Slope stability calculation for the dike with cavities

The c-phi reduction method is generally used to check and calculate the safety factor of the embankment structure. It is efficient and gives a potential failure slip in one or the two sides of the dike. Its application to a case with a cavity leads to some difficulties. In fact, the result of the method is dependent on the weakest area of the model. When a cavity or any hole is present in the model, the bordure of the cavity may become the weakest point. The c-phi reduction method will then give results that correspond to the safety factor of the cavity rather than the one of the slope. The mesh dimensions on the roof of the cavity are considered equal to 0.05 m.

For the purpose of neglecting the effect of yielding around the cavity and to avoid its impact on the final value of the slope safety factor; the zone around the cavity was taken modelled with elastic properties and the safety factor with the c-phi reduction method was then possible to calculate. Two assumptions were tested for the elastic zone around the cavity. The first assumption assumes a thin circular elastic zone around the cavity (thin circular shell equals to 1m). The second assumes an elastic behaviour for the lower 2 m of the alluvium layer. Both the two assumptions give the same final result (see Appendix B).

From the results, we found that the cavity doesn't influence the safety factor. However, this approach is not suitable to assess the influence of a cavity close to the dike, since the elastic zone around the cavity may interact with the failure surface.

We can interpret that the c - ϕ reduction method takes into account only the zones in case of elasto-plastic. Hence, its results not affected by the zones of elastic in the model. We can then conclude that a distant cavity doesn't affect the stability, but we can't conclude for a close cavity.

This method of safety factor with CESAR did not give us a good vision to continue studding cavity-dike interaction. Thus, the standard method in CESAR will be used.

5.4 Calculation by standard method

With the standard method of calculation in CESAR, the model is carried out without reducing the values of the materials properties. Herein, we will use the standard method to study:

- The effect of the cavity on the slope stability by using only the plastic strain zone as collapse criterion because of the safety factor criterion was already tested in previous section by using c - ϕ reduction method.
- The effect of the dike on the cavity stability by testing three criterions (the safety factor, the vertical displacement and the plastic strain).
- The effect of the dike on the existing cavity a little away from the dike toe due to this case was not studied in the analytical approach.

5.4.1 Effect of the cavity on the slope stability

Herein, the evolution of plastic strain zone was adopted as a criterion to identify the unstable zone and compare the results in term of slope and cavity interaction.

It is difficult to distinguish effects of the dike upon the cavity stability from the impact of the cavity upon the slope stability. Hence, the progress of plastic strain zone until it contacts the expected slope slip surface failure could consider as the consequence due to the presence of the cavity underneath it. A possible solution is to assume that the plastic zone around the cavity should be linked to the plastic zone of the slope to consider that the cavity has an effect on the slope stability.

Several values of diameter of the cavity were studied with the same properties conditions and the same position of the cavity in the alluvium layer (Figure 74). The slip surfaces that got from the analytical approach (chapter 4) remain in the range of potential failure slips in CESAR as it is shown in Figure 73. Hence, the cavity is taken in the same position that was considered in the analytical approach. This position corresponds to the lowest position of the failure surface.

Two scenarios were considered relative to the water level in the river; normal state and flooding state (cf. chapter 4). The flooding state refers to the maximum water level in the upstream side of the dike, equal to the level of the dike head (6 m). While the level of water for the normal state is equal to the dike toe level (0 m). Table 10 shows the procedure of the

calculations that it is used in CESAR to study the effect of an existing cavity upon the slope stability.

It is worth mentioning that all calculations with the presence of the cavity didn't converge (in normal state) due to the properties of alluvium (especially the cohesion that is equal to 0). The calculation didn't converge unless the cohesion value of the alluvium layer is replaced by 10 kPa. However, we used the final results that appeared for $c = 0$ to identify the shape of the failure. The maximum number of iterations is then equal to 1000. The shape of the plastic strain zone remains the same for a greater number of iterations (5000).

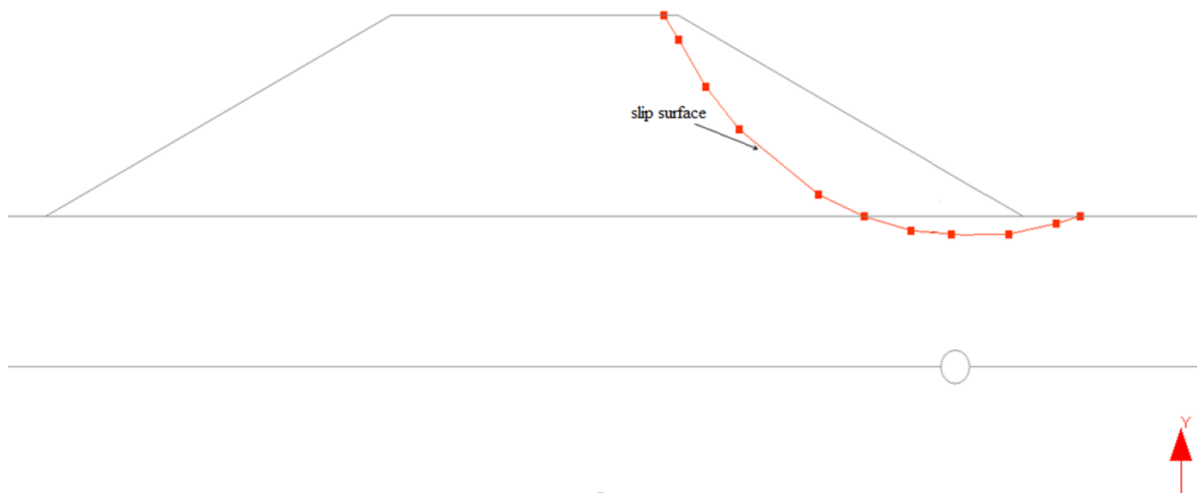
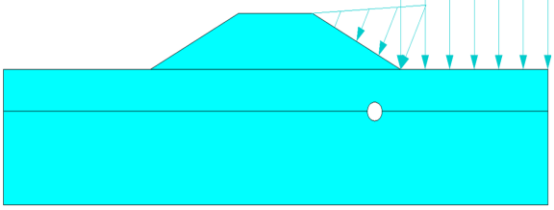


Figure 74 Position of the cavity relative to the dike slope by assuming the same slip surface that the one got from the analytical approach.

Table 10 Steps to study the effect of the cavity upon the dike slope in CESAR.

Steps	Configuration	Boundary and load conditions
1		Weight of alluvium and limestone due to the gravity force: An initial stress tensor is obtained
2		Adding the weight of the dike and the consolidation displacements are initialised.
3		Excavation of the cavity. 1. Cavity excavated in one step ($l=1$, see appendix C). 2. The initialization of the dike displacements.

4	 <p>The diagram shows a cross-section of a dike with a trapezoidal top. A horizontal line represents the ground surface, and a white circle below it represents a cavity. The area above the ground surface is shaded light blue, and the area below is shaded dark blue. A series of downward-pointing arrows of varying lengths are positioned above the dike, representing a water load. The arrows are tallest on the right side of the dike and decrease in height towards the left.</p>	<p>In flooding scenario, two loads are considered:</p> <ol style="list-style-type: none"> 1. The water load due to the gravity force with a height equal to the height of the dike (the cavity is empty from water). 2. An extra load due to the soil saturation in the dike only (with initialization of the dike displacements).
---	--	--

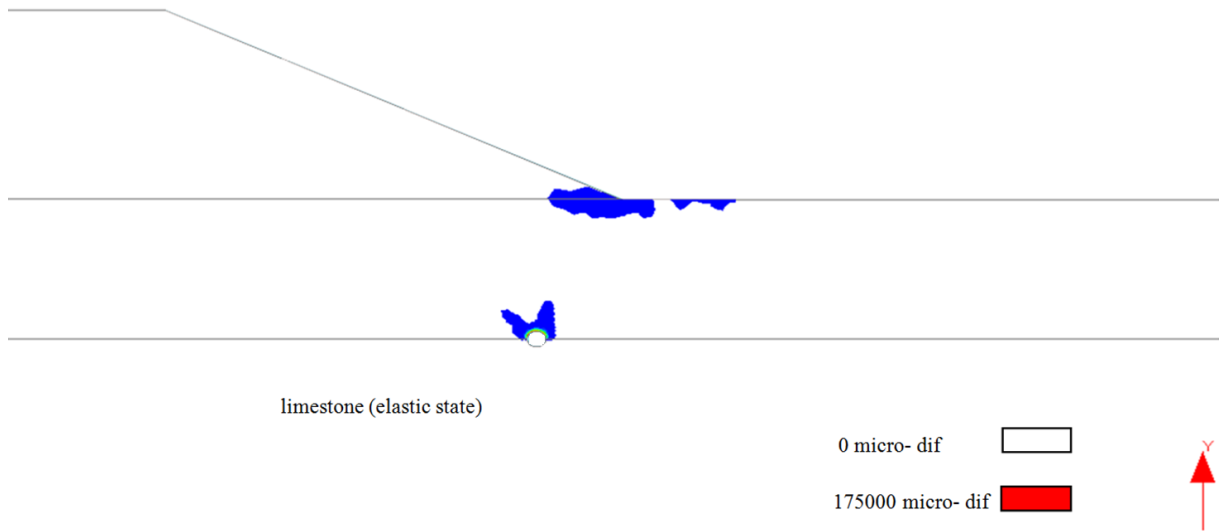
Isovalues of the plastic strain norm are shown in Figures (Figure 75-Figure 78) for the normal and flood states and for different diameters of the cavity. It can be observed that the plastic strain zone increases with increasing the cavity diameter. The plastic strain zone around the cavity and near the slope is connected for a cavity diameter greater than 1 m. The water in the flooding scenario increases (slightly) the values of the plastic strain and the dimension of the plastic zone. Hence, the cavity diameter is more influential parameter than the water on the plastic zone increasing.

The results highlighted that a cavity under the slope of the dike could affect its stability, when the cavity diameter is greater than 1 m. A cavity with a 2 m diameter leads to a very large plasticity zone, that may lead to a possible failure of the slope (see Figure 78).

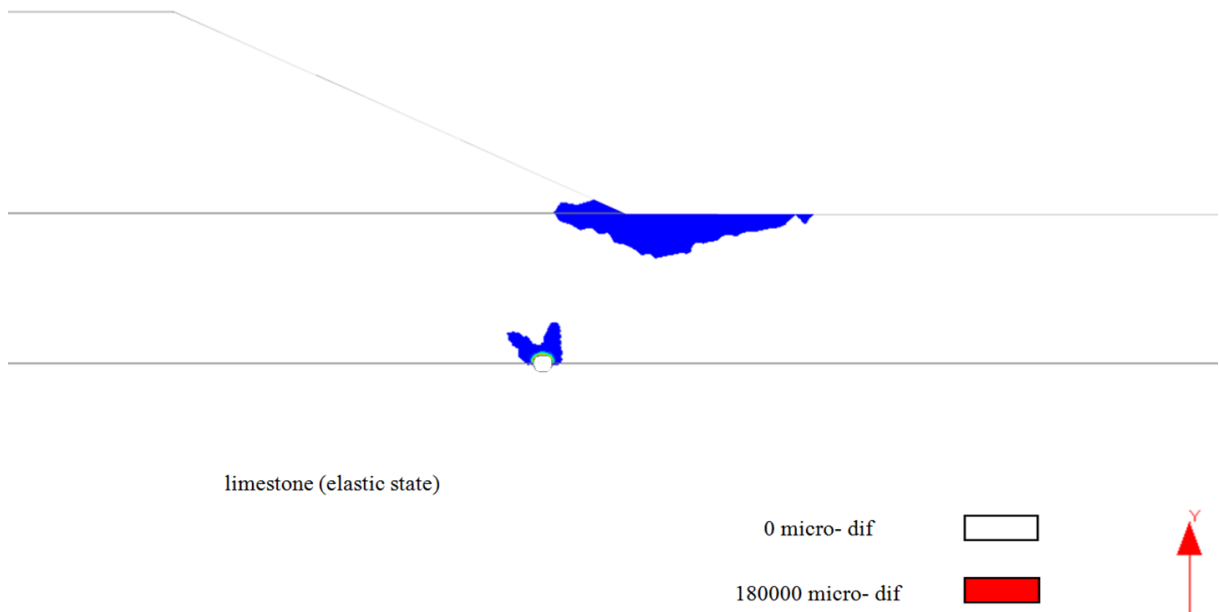
In addition, the direction of the expected failure propagation above the cavity, based on the form of the plastic zone, is inclined and not vertical. It takes a frustum shape, which is different than the assumption of a vertical column (in chapter 3).

In addition, results are summarized in Table 11. From this table, we can see that the plastic strain value increases due to the cavity diameter increasing and due to the effect of water pressure (in flood state). All calculations converged in the flood state contrarily to the normal state. For the same number of iterations, the maximum plastic increases between the normal and flood state.

As a conclusion, results are consistent with those of the analytical approach (chapter 4). The expected impact of a cavity presence underneath the dike slope starts with a diameter equal to 1 m (Figure 76). On the other hand, a cavity with a diameter of 2 m could reduce the safety factor until the failure (less than 1).

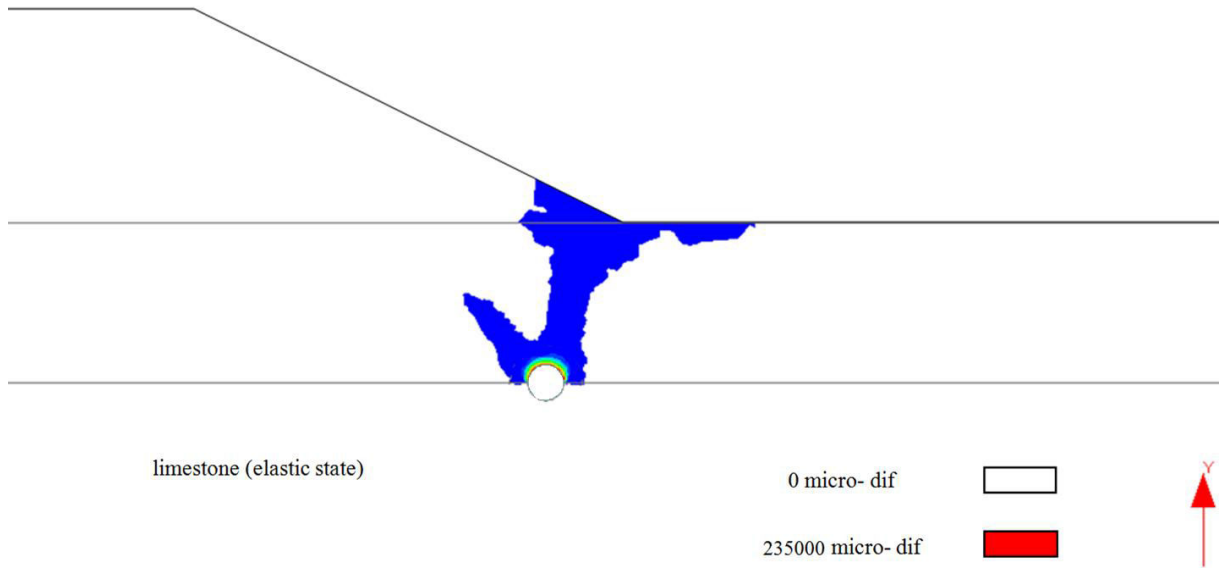


(a) Normal state.

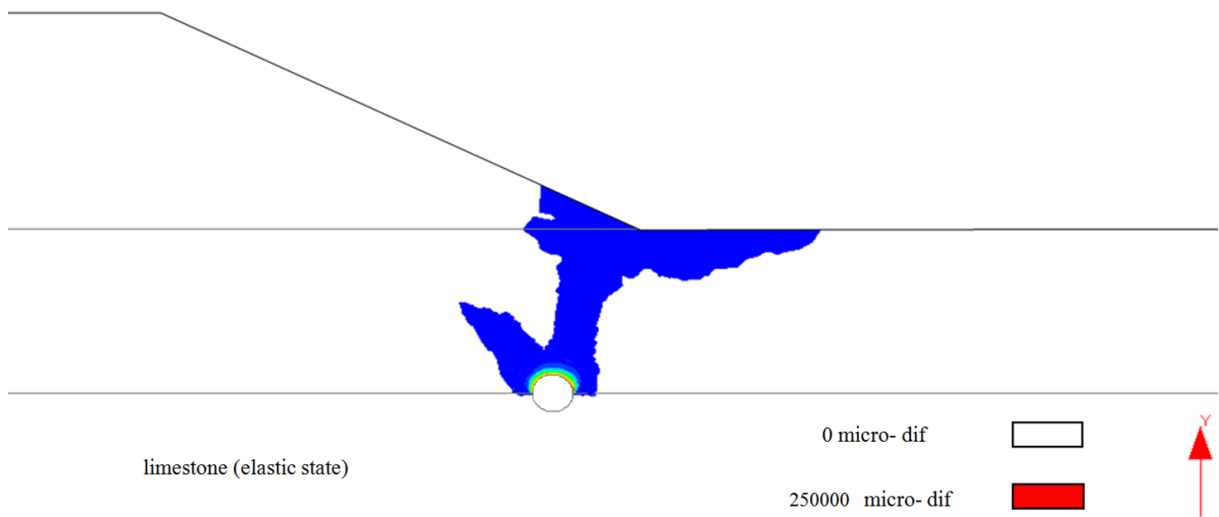


(b) Flooding state.

Figure 75 Plastic strain norm results of a cavity with a 0.5 m diameter, underneath the slope of the dike.

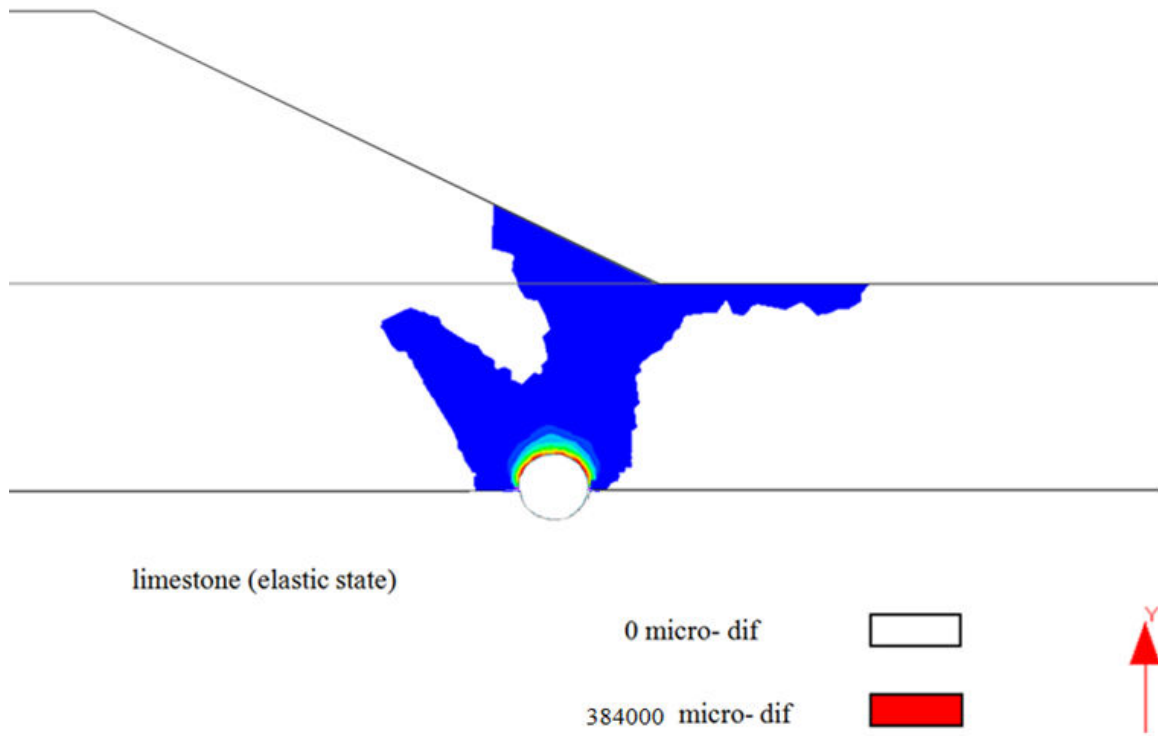


(c) Normal state.

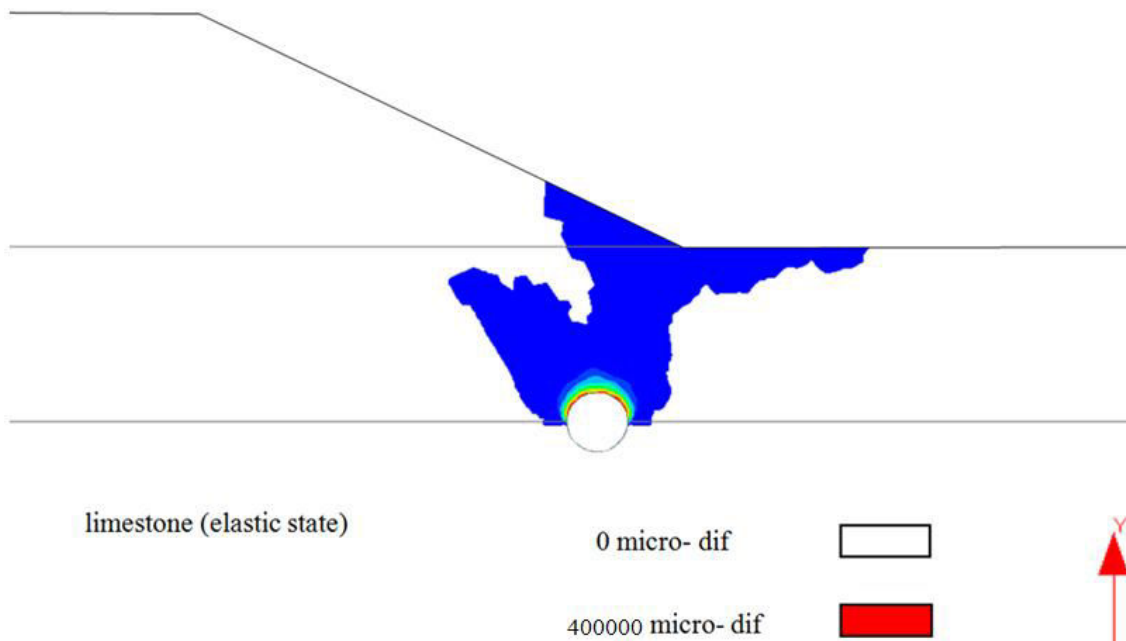


(d) Flooding state.

Figure 76 Plastic strain norm results of a cavity with a 1 m diameter, underneath the slope of the dike.

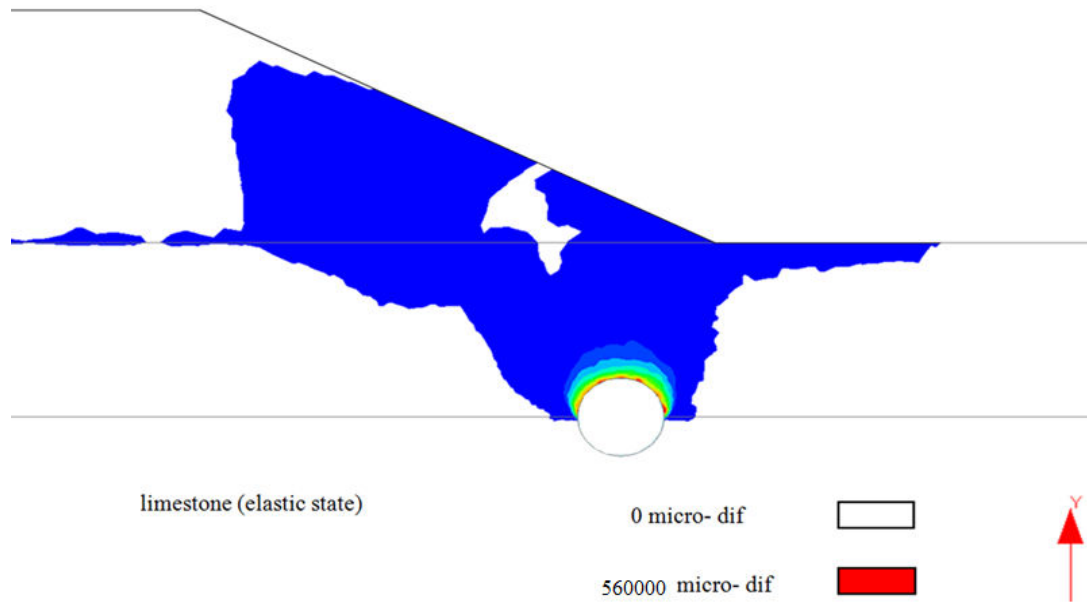


(a) Normal state.

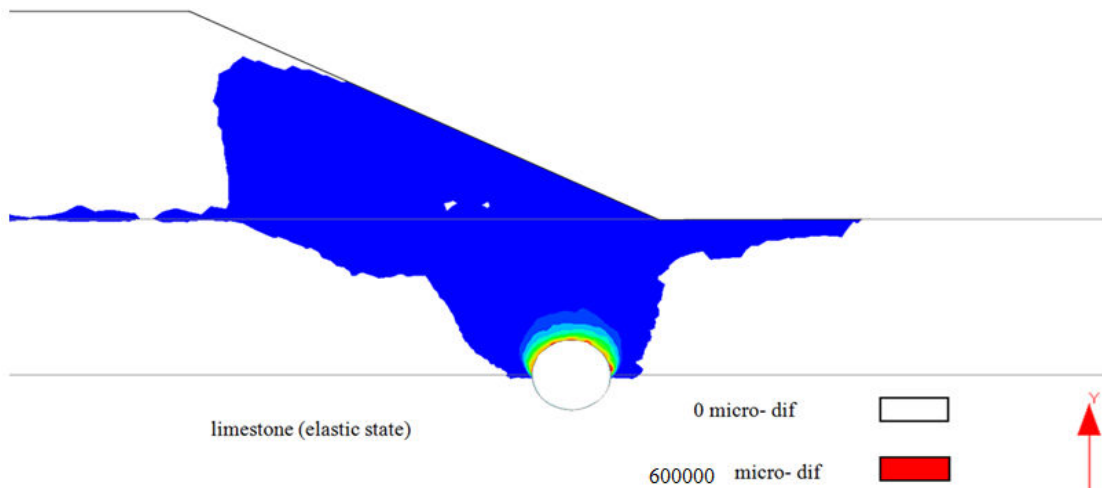


(b) Flooding state.

Figure 77 Plastic strain norm results of a cavity with a 1.5 m diameter, underneath the slope of the dike.



(c) Normal state.



(d) Flooding state.

Figure 78 Plastic strain norm results of a cavity with a 2 m diameter, underneath the slope of the dike.

Table 11 Summary of the numerical calculation results of the cavity effect on the dike slope from CESAR. The plastic strain is in micro-deformation.

NS: Normal water state, FS: Flooding water state.

Diameter (m)	Max. plastic strain norm (normal state NS)	Max. plastic strain norm (flooding state FS)	Difference (FS-NS)	Cavity-slope interaction
Without cavity	0	800	800	
0.5	175000	180000	5000	-
1	235000	250000	15000	+
1.5	384000	400000	16000	++
2	560000	600000	40000	++++

5.4.2 Effect of the dike upon the cavity stability

The following three criteria are used to study the effect of the dike upon the stability of the cavity: the safety factor criterion, the vertical displacement criterion and the plastic strain criterion.

a- Safety factor criterion

In order to investigate the effect of the dike upon the stability of the cavity with safety factor criterion, a cavity with different diameters is studied through three specific cases. The first one with the cavity underneath the centre of the dike in normal case, the second in flood case and the third one when the dike above the cavity is neglected (in normal case). Stresses are monitored in some specific nodes of the model, in the roof of the cavity for the three scenarios (without dike, with a cavity and a dike in normal state and with a cavity and a dike in flooded state). Thanks to Mohr-Coulomb criterion and the tensor of stress, a local safety factor of the node can be obtained; the safety factor is defined as the difference between the radius of Mohr circle in elastic state the radius of Mohr circle in elasto-plastic state. The radius of Mohr circle in elasto-plastic state is assumed equal to the perpendicular distance between the centre of Mohr circle (in elastic state) and the yielding criteria. All results from CESAR would be compared with results of the analytical approach (chapter 3).

To highlight this method, two points have been selected near the cavity for the purpose of calculating principal stresses. The first point is located at the top of the cavity roof, while the second is located at a vertical distance from the first point equal to the radius of the cavity a (Figure 79). The goals of selecting the two points are:

- To discuss the adding effect of the dike upon the stability of each point around the cavity in difference scenarios (normal and flooding scenarios);
- To test the efficiency of using the safety factor method for each point by drawing Mohr circles.

The equation of safety factor for each chosen point can be written as the following:

$$SF = \frac{df}{ac} = \frac{\left(\sigma_1 + \frac{1}{2}(\sigma_2 - \sigma_1)\right) \sin \varphi}{\frac{1}{2}(\sigma_2 - \sigma_1)} \quad (5.4)$$

Where

σ_1 and σ_2 are the minimum and maximum principal stresses, respectively,

df is the perpendicular distance between the centre of the Mohr circle and the envelope of failure that is equal to the radius of the Mohr circle in elasto-plastic state (Figure 80), and

ac is the radius of Mohr circle in elastic state with assuming the centre of the circle remain the same in the two state (elastic and elasto-plastic). When ac traverses perpendicularly the

envelope of failure and equals to the radius of the Mohr circle by assuming the soils in elastic state (see Figure 80).

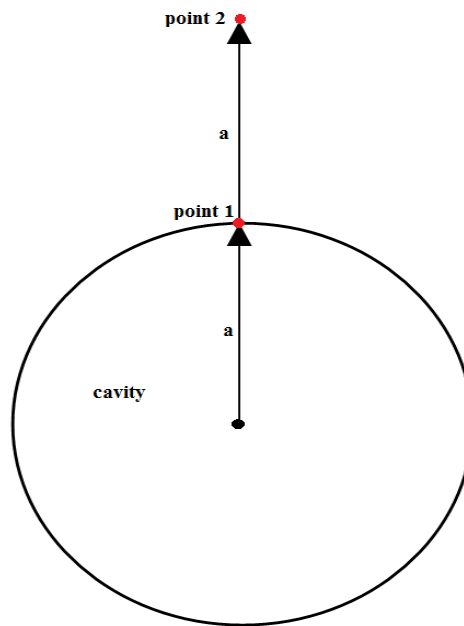
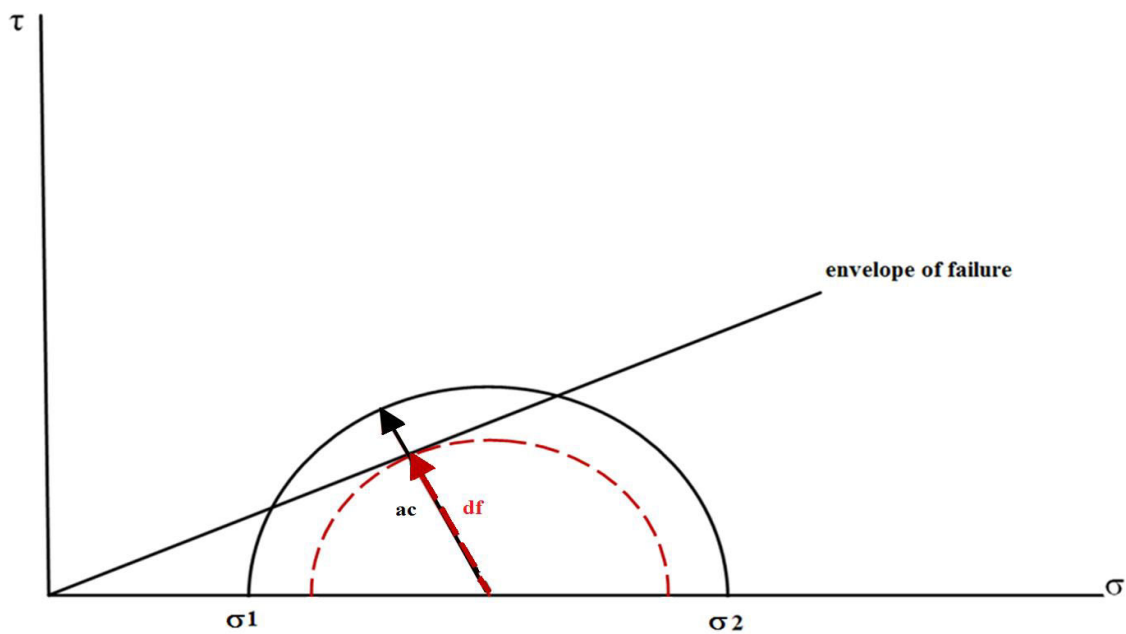


Figure 79 Positions of the two points used to calculate SF by Mohr circle method.



ac: the radius of Mohr circle in elastic state. **df:** the radius of the Mohr circle in elasto-plastic state.

Figure 80 Mohr circle in elastic state with minimum and maximum principal stresses σ_1 and σ_2 , respectively. The envelope of failure for the cohesionless alluvium layer ($c = 0$).

Results in Table 12 only give local information of the safety factor for the two points around the cavity. Those values are constant or slightly increase with the increase of the diameter of the cavity for cases of the dike presence, while the safety factor decreases with the increase of

the cavity diameter for cases without cavity. The safety factor for the point 1 is constant. The dike presence and the cavity diameter seem to have no influence on the safety factor. Results for the point 2 show that the dike presence decreases the safety factor for cavity diameter less than 1 m.

Table 12 Results of the safety factor calculation from the Mohr circle method in elastic state. Point 1 & 2 are shown in Figure 79.

Point 1						
D (m)	without the dike			with the dike		
	σ_1 (kN/m ²)	σ_2 (kN/m ²)	SF	σ_1 (kN/m ²)	σ_2 (kN/m ²)	SF
0.5	1.3	36.3	0.57	1.0	25.1	0.57
1	1.2	33.7	0.57	0.85	20.50	0.57
1.5	0.98	30.4	0.57	0.63	15.5	0.57
2	0.88	27.1	0.57	0.2	9.2	0.55
Point 2						
D (m)	without the dike			with the dike		
	σ_1 (kN/m ²)	σ_2 (kN/m ²)	SF	σ_1 (kN/m ²)	σ_2 (kN/m ²)	SF
0.5	43.6	51.8	6.2	81.3	105.8	4.1
1	37.8	47.6	4.6	73.6	95	4.2
1.5	29.5	39	3.8	70.9	90.3	4.4
2	25	33.2	3.75	68.3	85.2	4.81

We can explain the case of safety factor value of less than 1 (point 1), it means already had dropped. Then, we should look for points were presented above it that have critical safety factor (equals to 1). These points represent the critical points at which the roof of the cavity provisionally stable waiting for other factors that could cause collapse (flood waves, dynamic factors, etc.). Figure 81 shows an example of the results synthesized in Table 12 for the point 1 when the cavity diameter is equal to 2 m. From this figure; the centre of the circle is not the same in the two states (elastic and elasto-plastic) and then the assumption about the fixed position of the Mohr circle is not realistic.

However, this method of the safety factor is not practical to adopt because of it is can be applied only in the elastic state because of the results of safety factor always equal to 1 in elasto-plastic state (the circle is tangent the envelope of failure). Moreover, it needs to accuracy in calculations for each point that depends on element dimensions and the convergence of the calculations.

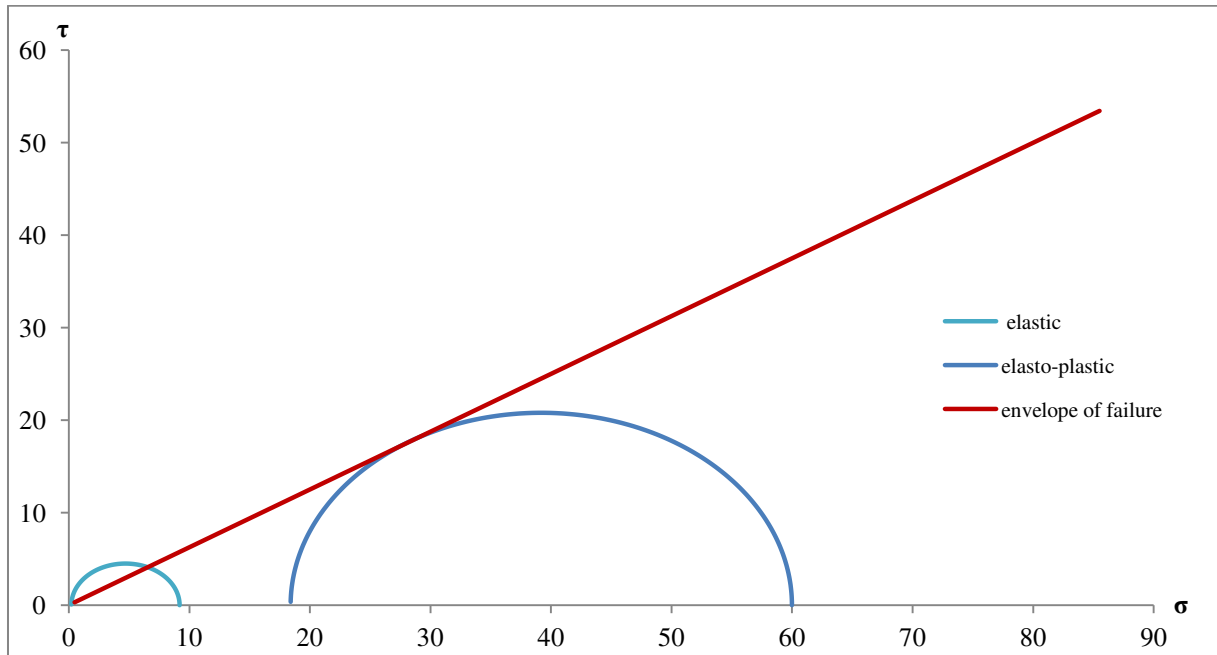


Figure 81 Mohr circle in elastic and elasto-plastic states for the point 1 in case of a cavity diameter equal to 2 m underneath the dike.

b- Vertical displacement criterion

The displacement criterion is used to investigate the effect of the dike on the cavity stability. Several points on and through the dike were chosen to compare the displacement in each point for different cavity positions (Figure 82). Two positions of the cavity were assumed in this study; the first one under the slope in the position already used in chapter 4 (see Figure 74) and the second under the centre of the dike (chapter 3). The vertical displacement is monitored in six points (A, B, C, D, 1 and 2). The calculations are for elasto-plastic state. The point A is located on the slope above the cavity centre in case of the cavity position under the slope; the point B is located on the centre of the slope, the point C in the corner between the slope and the head of the dike and the point D is located in the centre of the dike head (Figure 5.15-b). The positions of the two points 1 and 2 are the same than previously (cf. Figure 79).

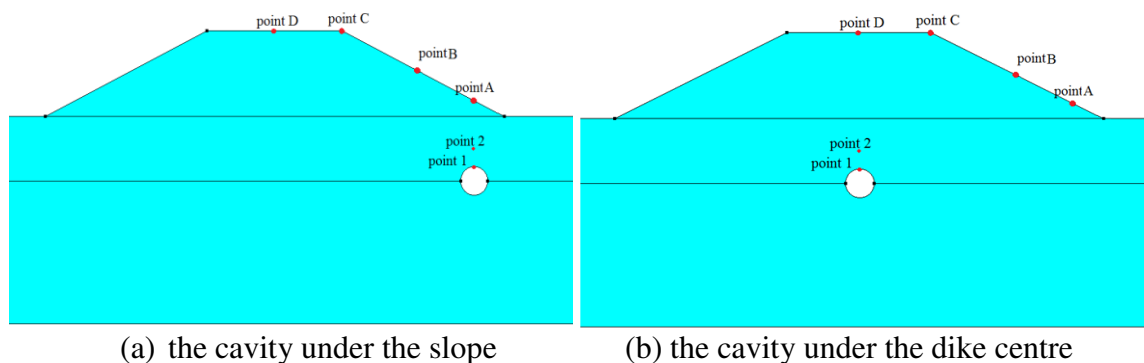


Figure 82 The chosen points used to monitor the vertical displacement.

Table 13 (a and b) shows the vertical displacement of these points. It can be observed that the vertical displacement of each point increases with the increase of the cavity diameter D and decreases when the distance between the cavity and the point is larger.

Results of the point A (Figure 82-a) and point D (Figure 82-b), when the cavity is respectively located under the points A and D are compared. The displacement in the two points increases with the increasing of the cavity diameter (Table 13). The point D has larger values of displacement than point A for the same cavity diameter (e.g. 8mm for the point D and 6 mm for the point A, for a cavity diameter of 2 m). This difference in the results between the two points A and D (for the same cavity diameter) is due to the difference in the height of the part of the dike above the cavity (i.e. 6 m in case of point D above the cavity while 1.1 m in case of the point A above the cavity). Hence, the cavity underneath the maximum height of the dike (under the dike centre) leads to a largest displacement of the dike surface.

Table 13 Results of the vertical displacement.

(a) The cavity under the slope (under the point A).

D (m)	Vertical displacement (mm)					
	point A	point B	point C	point D	point 1	point 2
0.5	0.17	0.10	0.03	0	16	1.2
1	0.60	0.40	0.10	0.03	39.50	3.50
1.5	3	1.20	0.40	0.10	91	7.50
2	6	2.30	0.75	0.16	177	28

(b) The cavity under the dike centre (under the point D).

D (m)	Vertical displacement (mm)					
	point A	point B	point C	point D	point 1	point 2
0.5	0	0	0.13	0.25	49	3
1	0	0	0.15	0.75	135	24
1.5	0	0	0.80	4.40	150	27
2	0	0.12	3	8	255	35

These results show little consequences of the cavity on the dike surface with a maximum vertical displacement equal to 3.5 mm for the point D (with a cavity diameter is equal to 2 m under the dike centre) while the vertical displacement for the same case on the top of the cavity (point 1) was 255 mm. In other words, the effect of the cavity ($D=2$ m) upon the dike surface vertical displacement in point D is less than 1% of its effect in point 1.

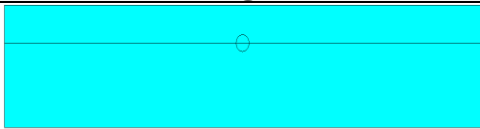
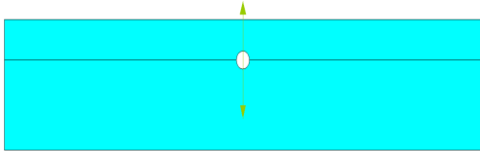
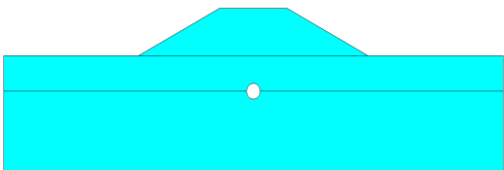
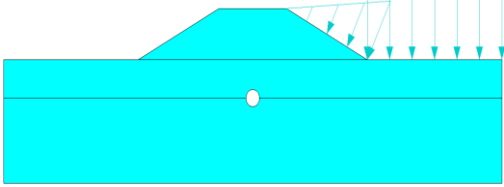
The displacement in elasto-plastic state could be considered as a local effect. Also, the large vertical displacement for a point refers to a failure (plastic behaviour) in this point only. In this work; we look for an impact of the presence of the cavity on all points around the cavity and its consequence on the dike. Hence, it is not practical (in CESAR) to calculate and analysis all the points to know the effect of the cavity for each point.

For this reason, we can consider the displacement criterion as secondary criterion to compare and test the stability of selected points.

a- Plastic strain criterion

Different values of diameter of the cavity were taken for two extreme positions; the first position corresponds to a cavity under the maximum height of the dike and the second position to a cavity far from the dike (without dike). Table 14 shows the procedure of the calculations that it is used in CESAR to study the effect of the dike upon the stability of the cavity in CESAR.

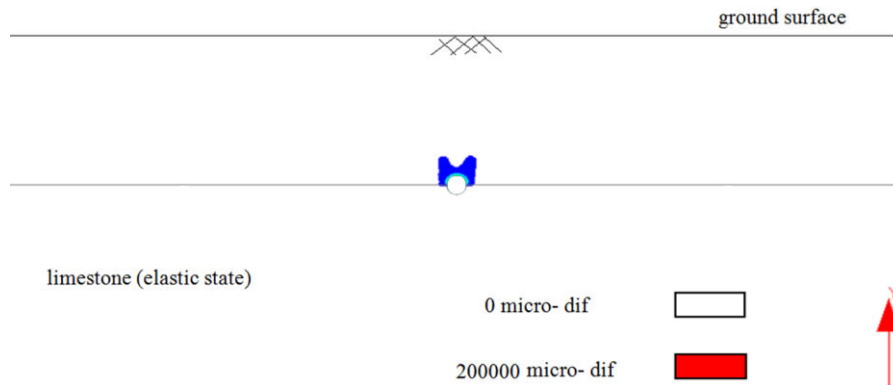
Table 14 Steps of calculation to study the effect of the dike upon the cavity stability in CESAR.

Step	Configuration	Load and boundary conditions
1		Weight of alluvium and limestone due to the gravity load. An initial stress tensor is obtained.
2		Excavation of the cavity. 3. Cavity excavated in one step ($l=1$, see appendix C). 4. The initialization of the dike displacements.
3		Adding the weight of the dike only with the initialization the consolidation displacements.
4		In flooding scenario, two loads are considered: 3. The water load due to the gravity force with a height equal to the height of the dike (the cavity is empty from water). 4. An extra load due to the soil saturation in the dike only (with initialization of the dike displacements).

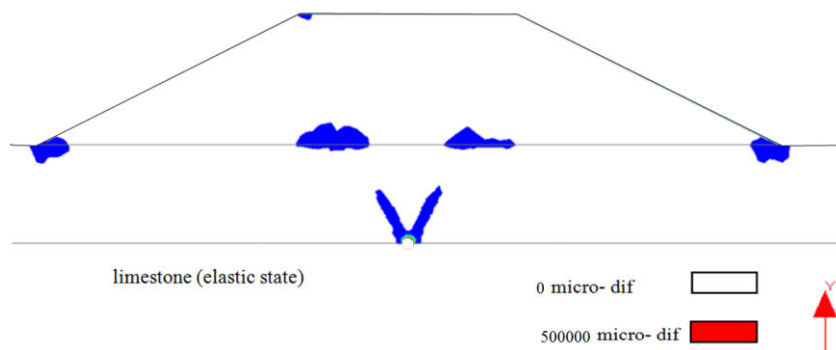
Figures (Figure 83-Figure 86) show the plastic yield zone for the stage 2 (cavity only), the step 3 (dike and cavity) and step 4 (dike, cavity and water) and for 4 diameters (from 0.5 to 2m). Results show the isovalues of the plastic strain norm. The plastic yield zone increases proportionally with the diameter of the cavity located underneath the dike. The plasticity area is located near the cavity for the small diameter, but reaches the dike surface for the largest. The comparison between the two steps 2 and 3 when without the dike or with the dike shows that the dike may have a significant effect on the plastic zone around the cavity. Even if the diameter of the cavity is small (0.5 m), there is a significant modification of the plastic zone around the cavity (Figure 83).

We can see that the plastic zone climbs upward almost vertically for the step 2 (without the dike), while it takes an inclined shape for the step 2 (with the dike). The plastic zone is slightly modified due to the water effect in flooding state, especially in the head and toe of the dike surfaces.

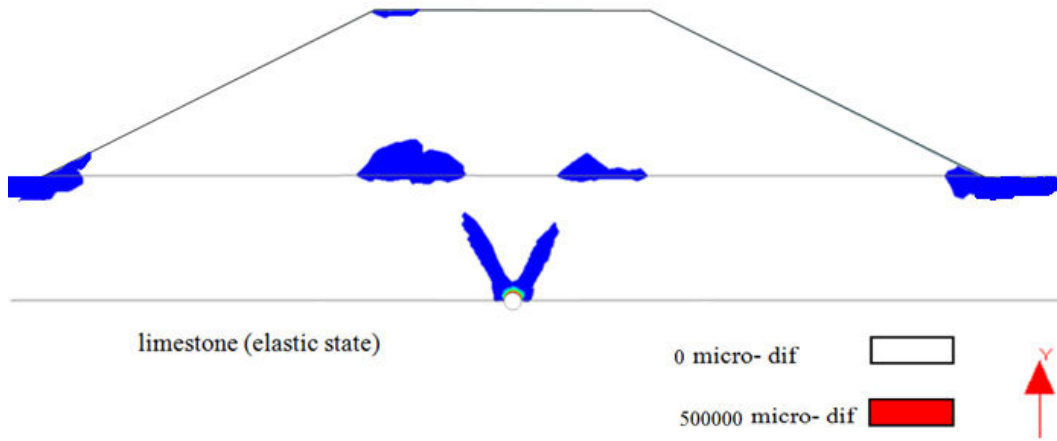
The shape of the plastic zone shows a diagonal progression in the alluvium layer and a vertical one in the dike. This difference in the shape of the plastic deformation between the two soils is the consequence of the mechanical properties of the soils. The alluvium is cohesionless soil ($c=0$) while the soil dike has a small value of cohesion ($c= 5$ kPa).



(a) Cavity without any dike.

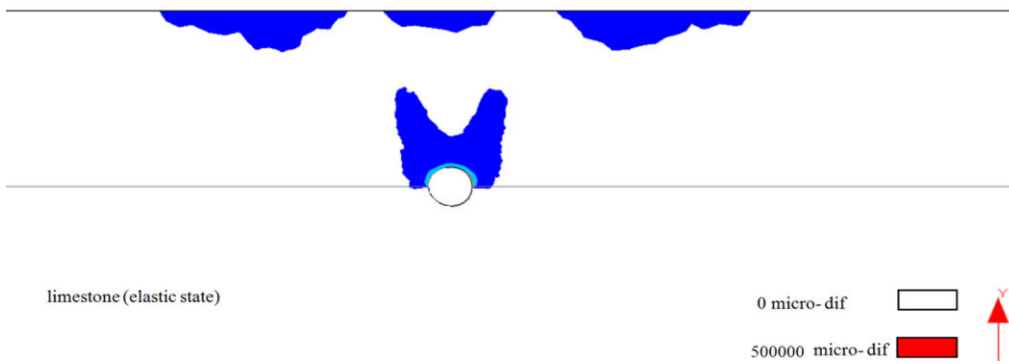


(b) Cavity underneath the dike in normal state.

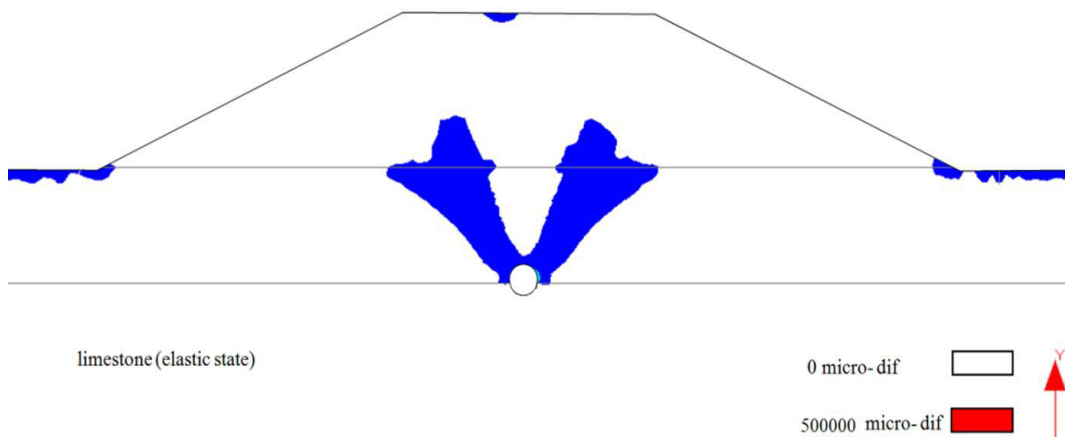


(c) Cavity underneath the dike in flooding state.

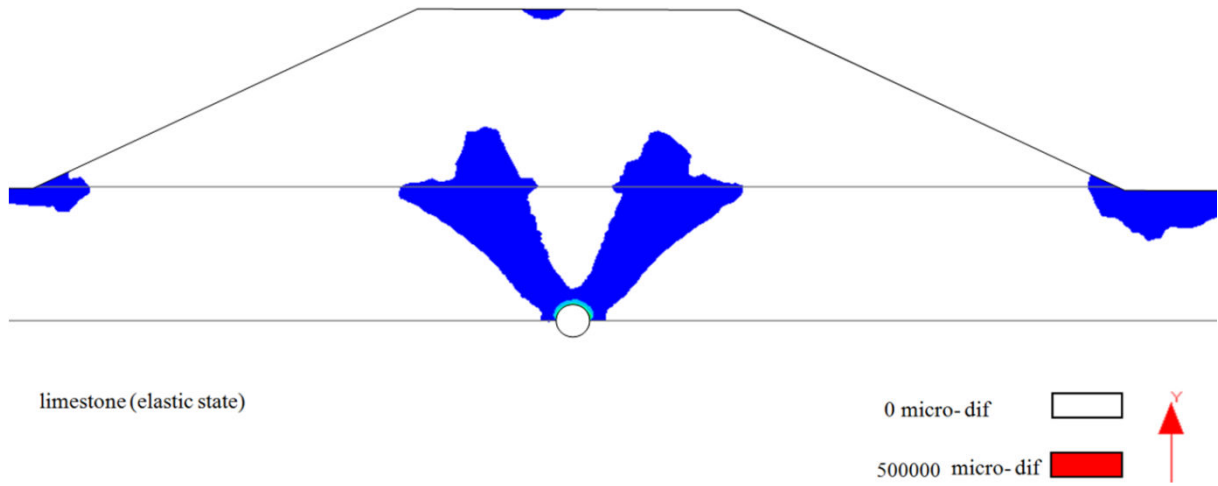
Figure 83 Isovalues of the plastic strain norm for a pre-existed cavity with a 0.5 m.



(a) Cavity without existence the dike.

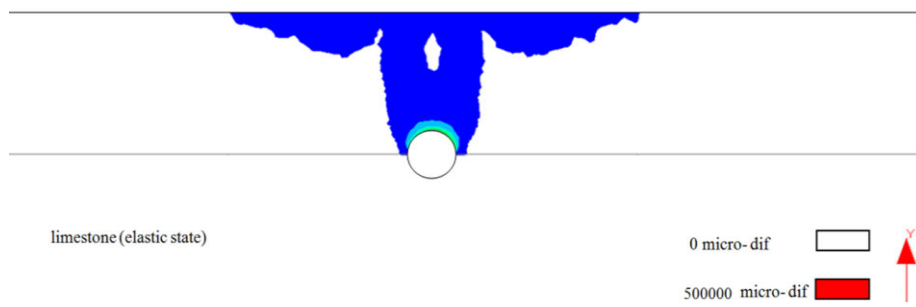


(b) Cavity underneath the dike in normal state.

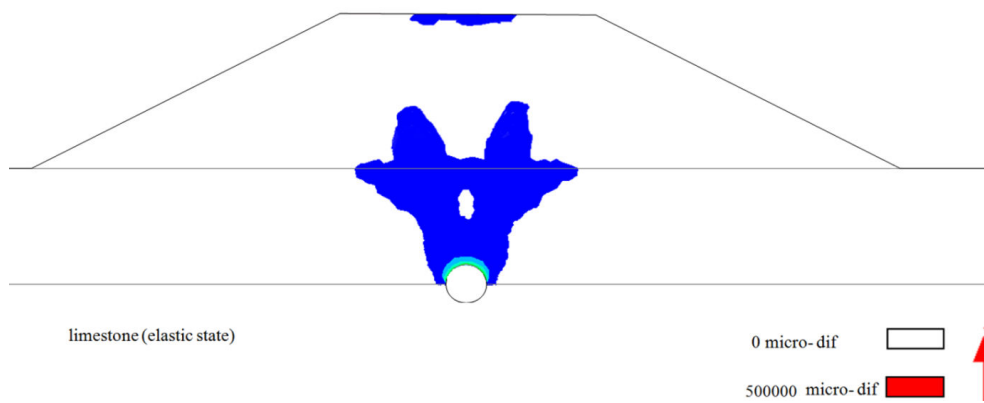


(c) Cavity underneath the dike in flooding state.

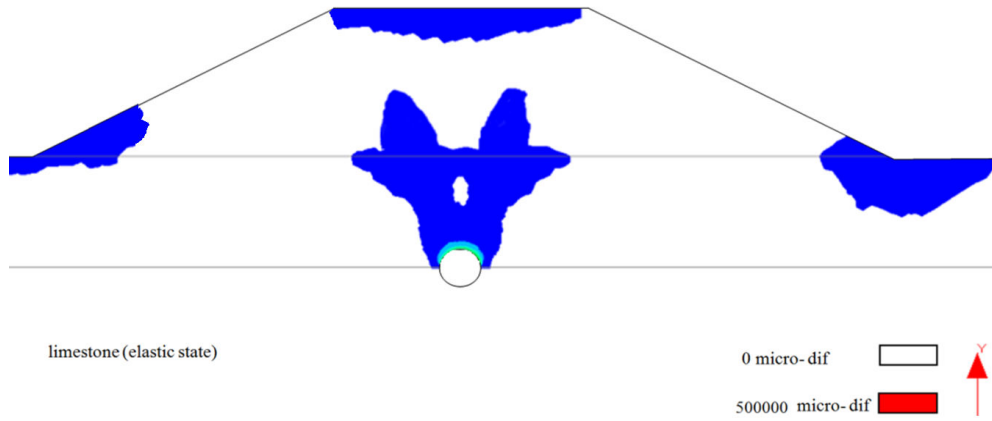
Figure 84 Isovalues of the plastic strain norm for a pre-existed cavity with a 1 m.



(a) Cavity without existence the dike.

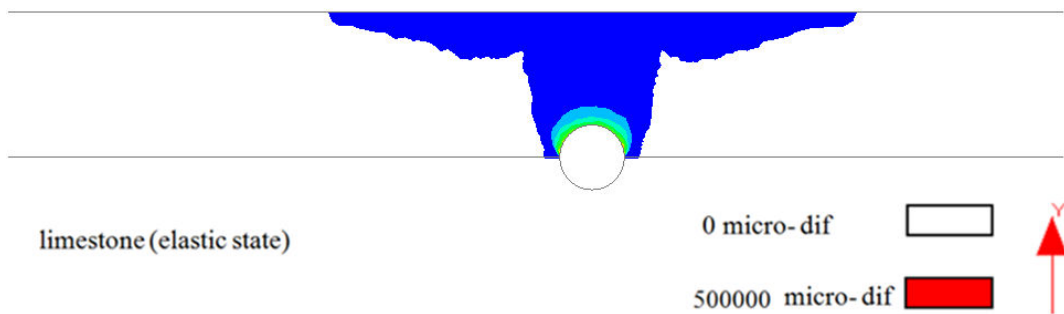


(b) Cavity underneath the dike in normal state.

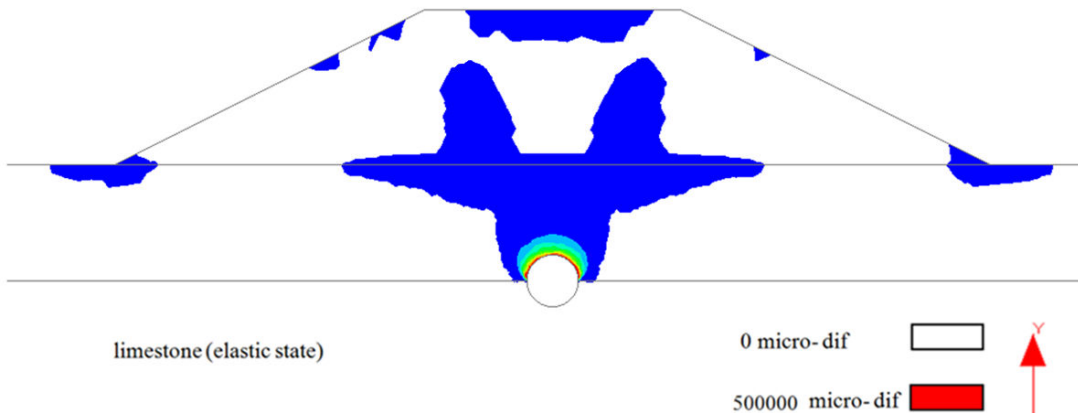


(c) Cavity underneath the dike in flooding state.

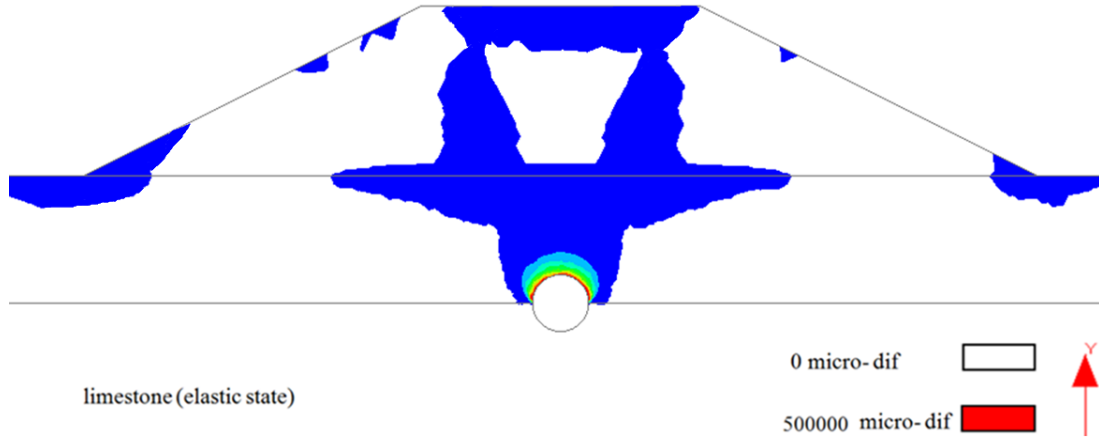
Figure 85 Isovalues of the plastic strain norm for a pre-existed cavity with a 1.5 m.



(a) Cavity without existence the dike.



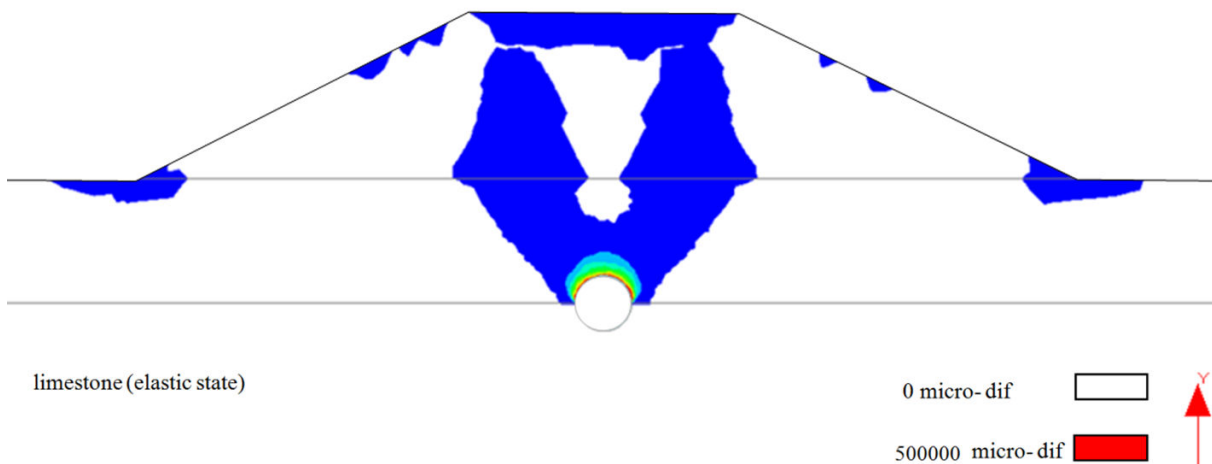
(b) Cavity underneath the dike in normal state.



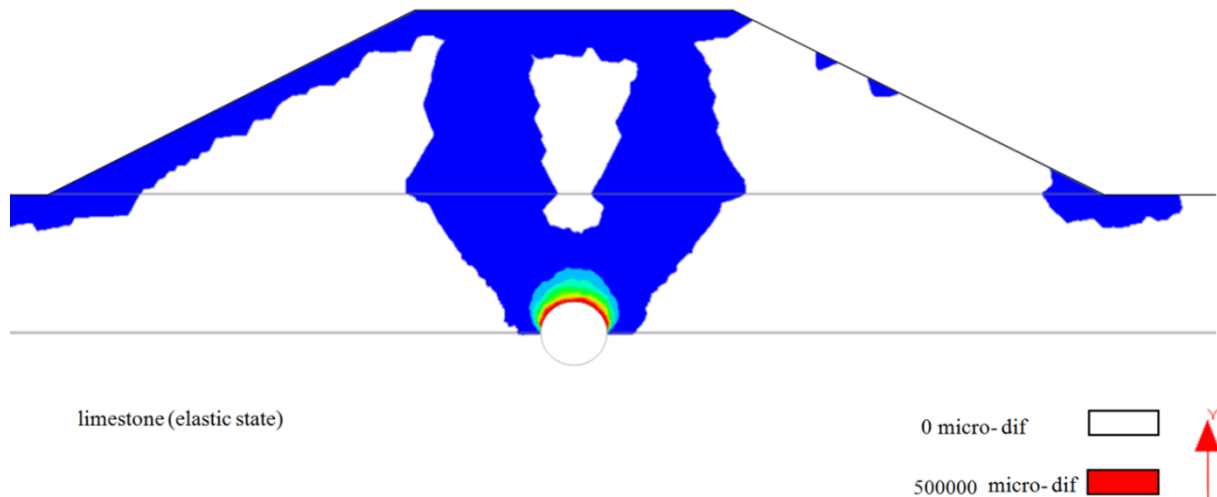
(c) Cavity underneath the dike in flooding state.

Figure 86 Isovalues of the plastic strain norm for a pre-existed cavity with a 2 m.

To compare the consequences of the presence of a cavity before or after the construction of the dike, the case of a cavity with a diameter equal to 2 m in Figure 86 was repeated with the steps used in Table 10. In other words, the cavity is created under an existing dike instead of the assumption that considered the cavity is existed and then the dike will be added in Table 14. Figure 87 shows the results of this case for the steps 3 and 4. From the two Figures (Figure 86 and Figure 87), we can see the difference between the plastic strain zones. The maximum value of the plastic strain norm for the flooding state was about 750 000 micro-strain (10^{-6}) in case of Figure 86 while it was about 850 000 micro-deformation in case of Figure 87. It is important to recall that the two numerical calculations in the Figures (Figure 86 and Figure 87) didn't converge in normal state. However, the two cases show that the plastic zone about the cavity with diameter 2 m can reach the dike head or in other words the sinkhole will appear in the dike head with vertical column shape through the dike.



(a) Cavity underneath the dike in normal state.



(b) Cavity underneath the dike in flooding state.

Figure 87 Isovalues of the plastic strain norm for a cavity with a 2 m diameter underneath the mid of the dike (the cavity is later than the dike).

From the previous results and discussions in sections (5.4.1 & 5.4.2) that concern the Standard method in CESAR; the plastic deformation zone could be considered as the failure indicator while the displacement criterion as secondary criterion.

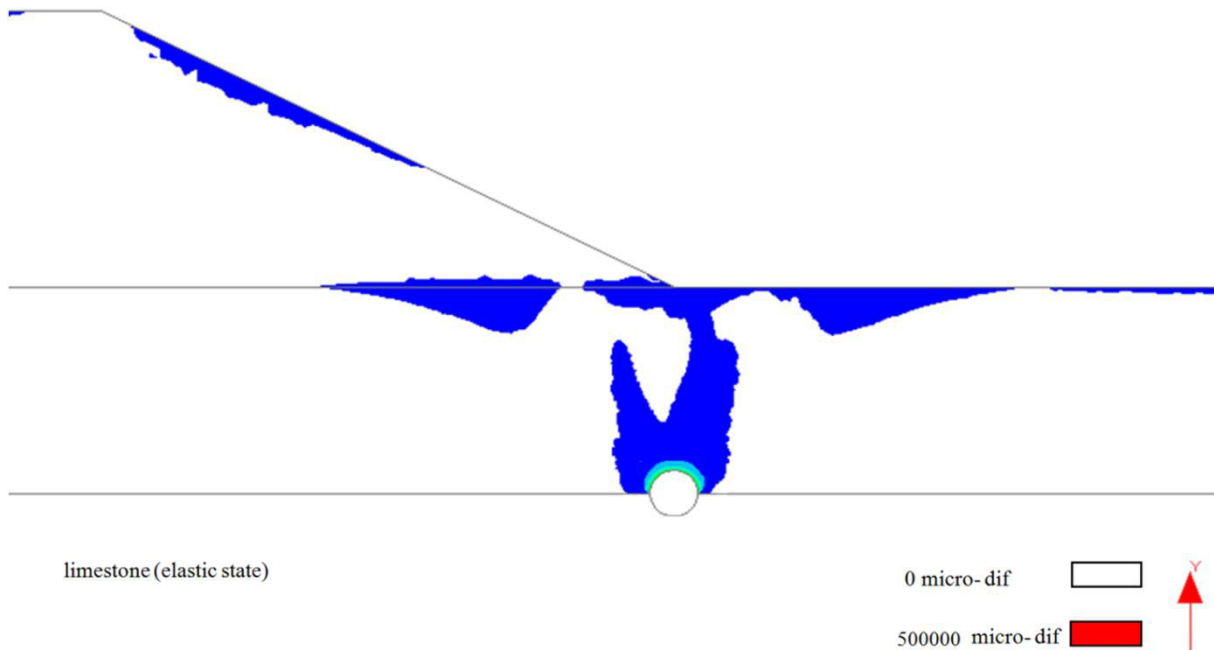
5.4.3 Effect of the dike on the existing cavity a little away from the dike toe

Cavities may exist a little away from the dike toe. This case couldn't be studied in the analytical approach (chapter 3) because the dike was only considered as an external load above the cavity and has then no effect over a cavity away from it. Hence, this case was studied with CESAR.

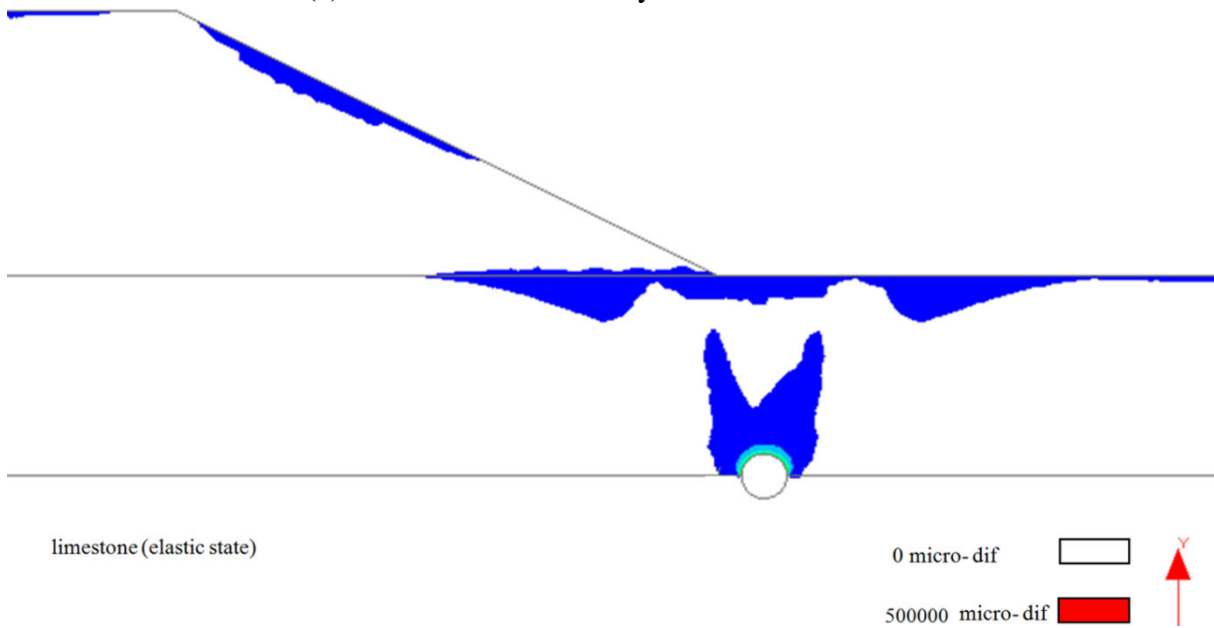
Figure 88 shows the results of the plastic strain zone for a cavity with a diameter equal to 1 m under the dike toe or a little away from it in normal state (from 0 to 4 m, see Figure 88). The plastic strain zone over the cavity located under the toe (Figure 88-a) is clearly modified compare to the case of the same cavity without the dike (see Figure 84-a). There is now a connection between the plastic zone which is above the cavity and the one that is located near the dike toe. Others cases for different diameters in the Figure 88 (from b to e) are also modified without contact with the plastic yield zone around the dike toe.

In order to compare cases of Figure 88, the vertical displacement in the crest of the cavity arch due to the dike presence was collected from CESAR results for each case and these results are shown in Figure 89. The results show that there is an effect inversely proportional to the horizontal distance from the dike toe ranging from 13 mm to 1.5 mm. There is a slightly effect of the dike upon the cavity even if the horizontal distance is equal to 4 m from the dike toe. In that case, the vertical distance between the crest of the arch and the land surface (4 m) is equal to the horizontal distance. The same vertical displacement for a similar cavity under the centre of the dike in normal state was founded equal to 135 mm (point

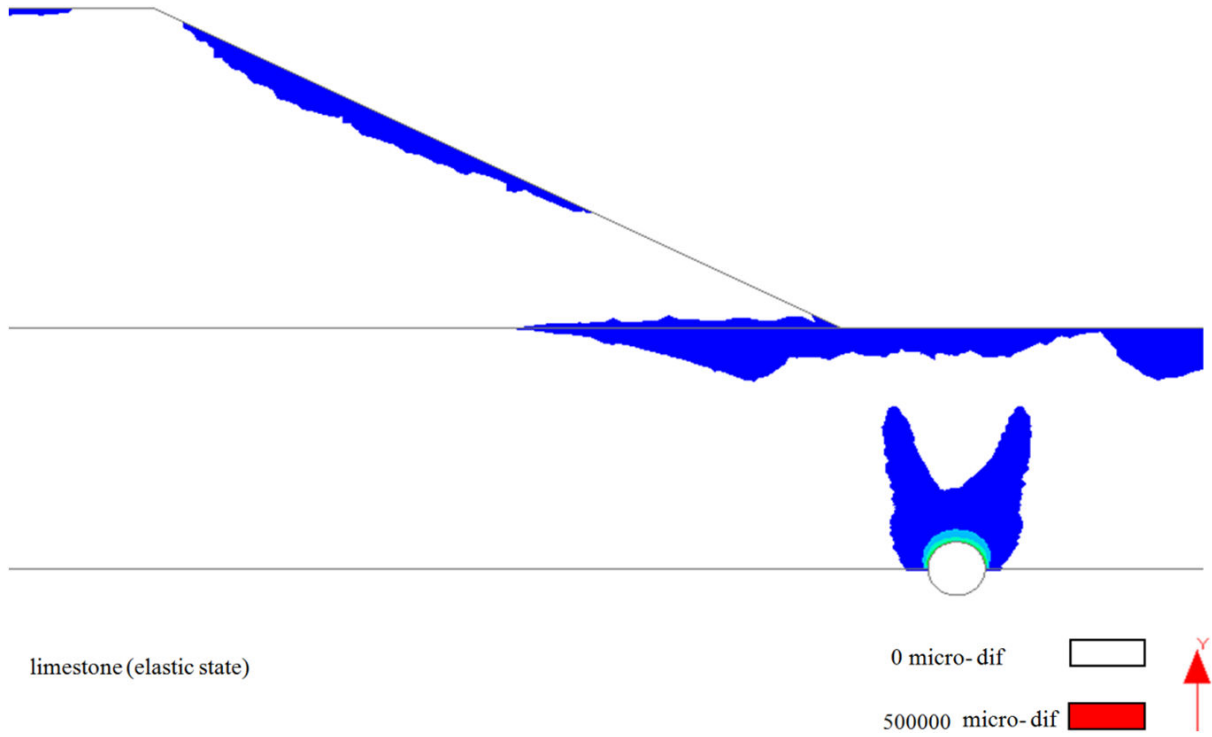
1 in Figure 82-b). It can be then concluded that the vertical displacement in the crest of the cavity arch that is due to the dike presence is reduced by 90 % due to the decreasing in the height of the dike from 6 m to 0m.



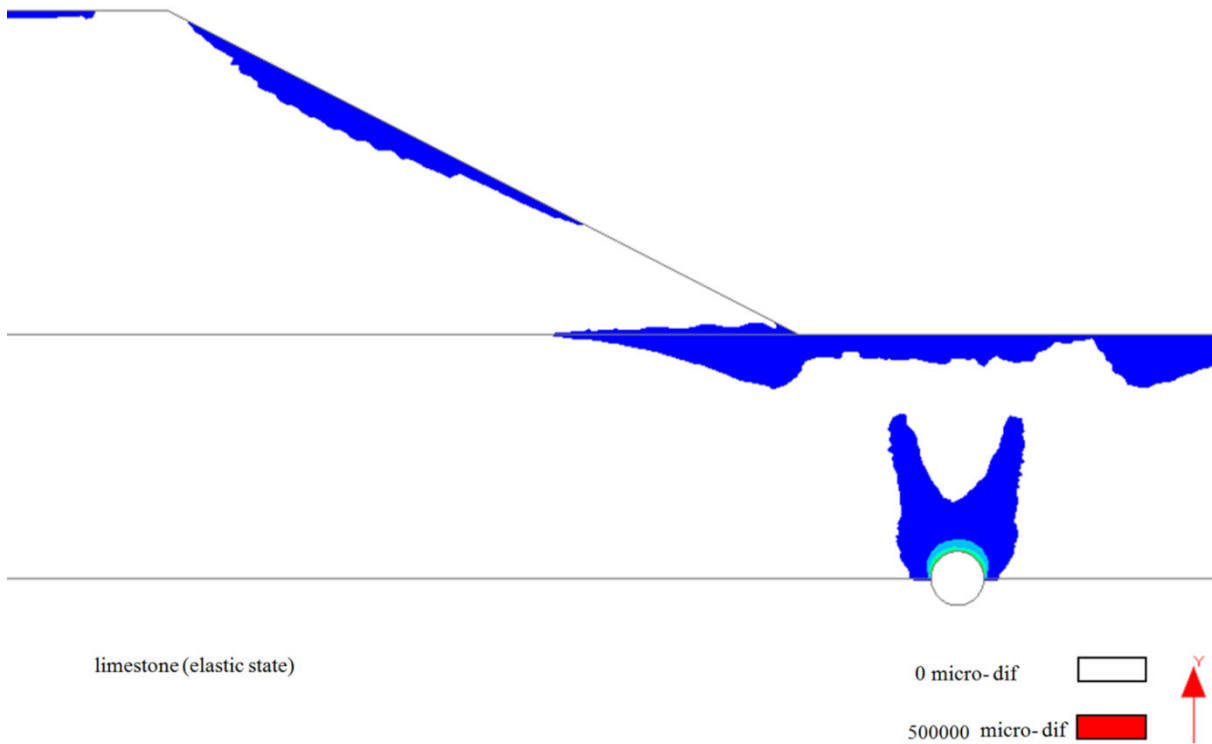
(a) The centre of the cavity underneath the dike toe.



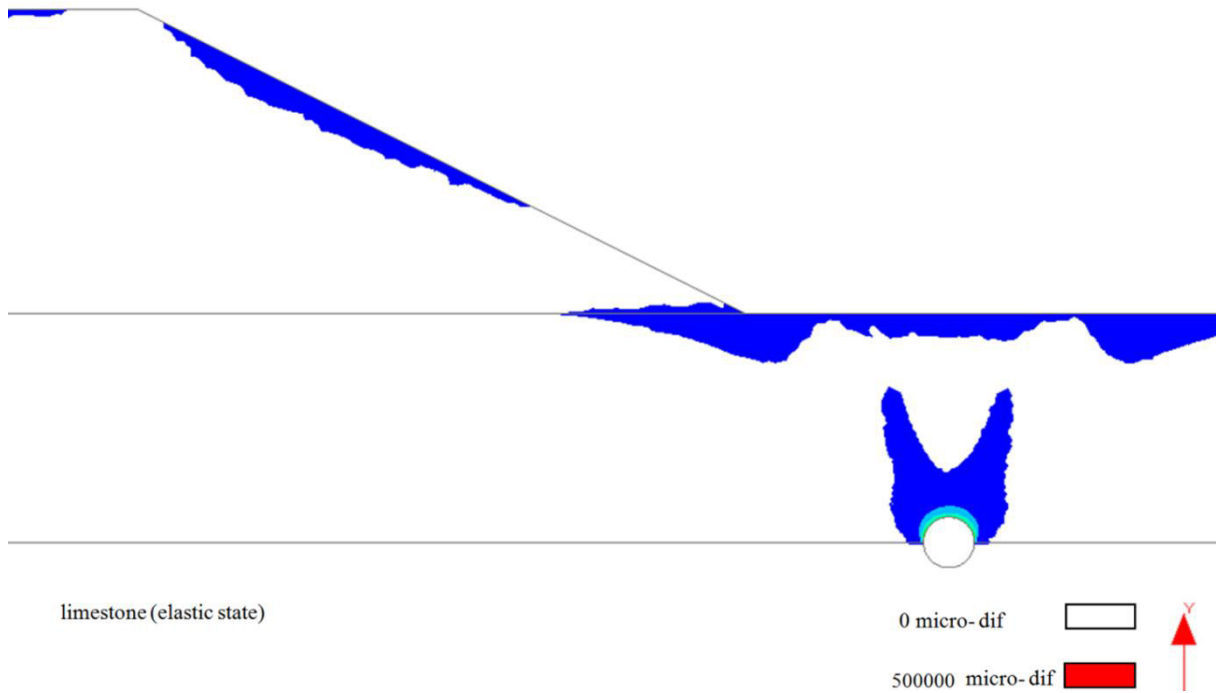
(b) The centre of the cavity exists 1m horizontally away from the toe.



(c) The centre of the cavity exists 2 m horizontally away from the toe.



(d) The centre of the cavity exists 3 m horizontally away from the toe.



(e) The centre of the cavity exists 4 m horizontally away from the toe.

Figure 88 Effect of the dike presence on the isovalues of the plastic strain norm for a 1 m diameter cavity and different positions away from the dike toe.

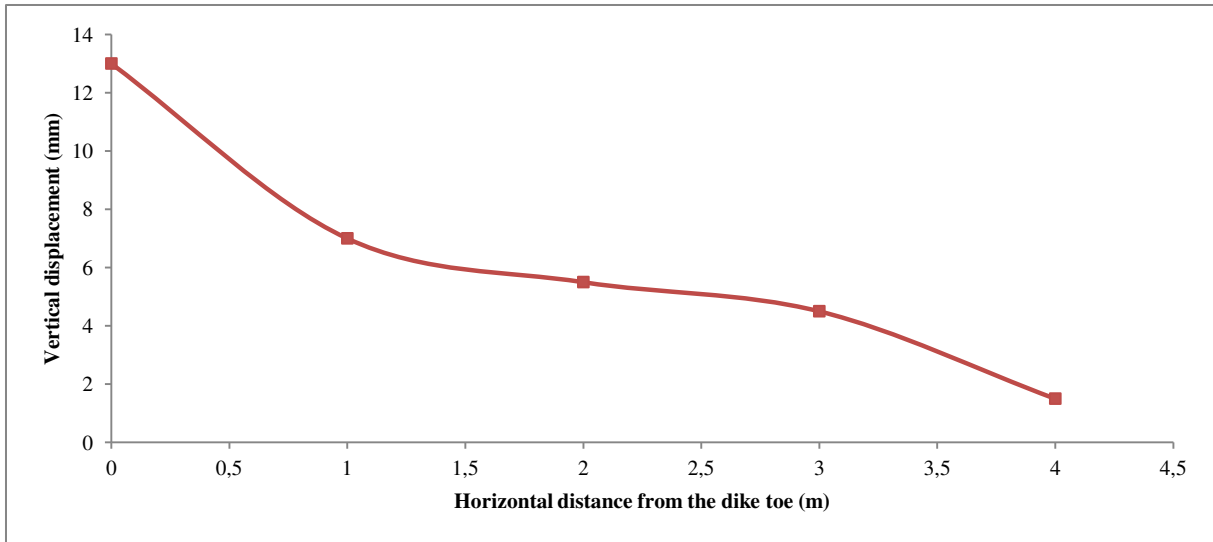


Figure 89 Relation between the position of the cavity with 1 m of the diameter relative to the dike toe and the vertical displacement due to the dike presence in the crest point of the arch of the cavity.

In conclusion, the results of the numerical models with CESAR-2D are consistent with the results that were obtained from the analytical methods especially in case of the effect of the cavity upon the dike slope stability. The results of the numerical and analytical methods indicated that a cavity with a diameter equal to 2 m could affect the dike slope stability. While

the results of the dike effect upon the cavity stability underneath the centre of the dike showed the roof of the cavity with a 0.5 m of the diameter could be collapse whereas the effect of the cavity with a 2 m of the diameter could reach the head of the dike.

The case of a cavity beside the dike was also studied and the results show there is a slight effect of the dike upon the cavity when the horizontal distance is less than the depth of the cavity.

5.5 Simulation of the dike of Val d’Orléans in CESAR 3D

The numerical model carried out in the first part of the chapter investigates the problem using CESAR-2D with some assumptions concerning the geometry of the dike and the cavity. The same problem was studied with CESAR-3D with 1360300 tetrahedron elements (instead of only 18660 in 2D). Objectives of the 3D simulations and the methods that are used in CESAR are summarised in Table 15.

The 3D model has the same boundary conditions than the 2D model, and use finite elements with dimension equal to 0.5 m. The third dimension of the dike was assumed equal to 20 m (cf. Figure 90).

The safety factor of the dike (without the cavity) in 3D is 5.5% greater than in 2D (i.e. SF=2.07 in 3D and 1.96 in 2D). Hence, this result indicates that the results in 2D are more conservatives than those obtained with 3D. Generally, the 2D analysis results yield a conservative estimation of the safety factor because of the end effects is not included in 2D estimation of safety factor (Duncan 1996; Kondalamahanthy and Alekhya 2013).

To study the interaction between the cavity and the dike in 3D, some 2D models are selected. From a practical point of view, it is difficult to model a spherical cavity because of the mesh generation with the current tools. Hence, the cavity was considered as a section of cylindrical with a length equal to the cavity diameter D (cf. Figure 91).

Table 15 Objectives of the 3D simulations in CESAR and the methods that are used.

Objective	Method
Recalculate the safety factor of the dike by using c-phi reduction method to show the effect of the third dimension upon the results.	C-phi reduction
Determine the effect of the third dimension upon the plastic deformation around the cavity and in the dike; and	Standard
Test the effect of the cavity direction (parallel or perpendicular to the dike direction) for a chosen case.	Standard

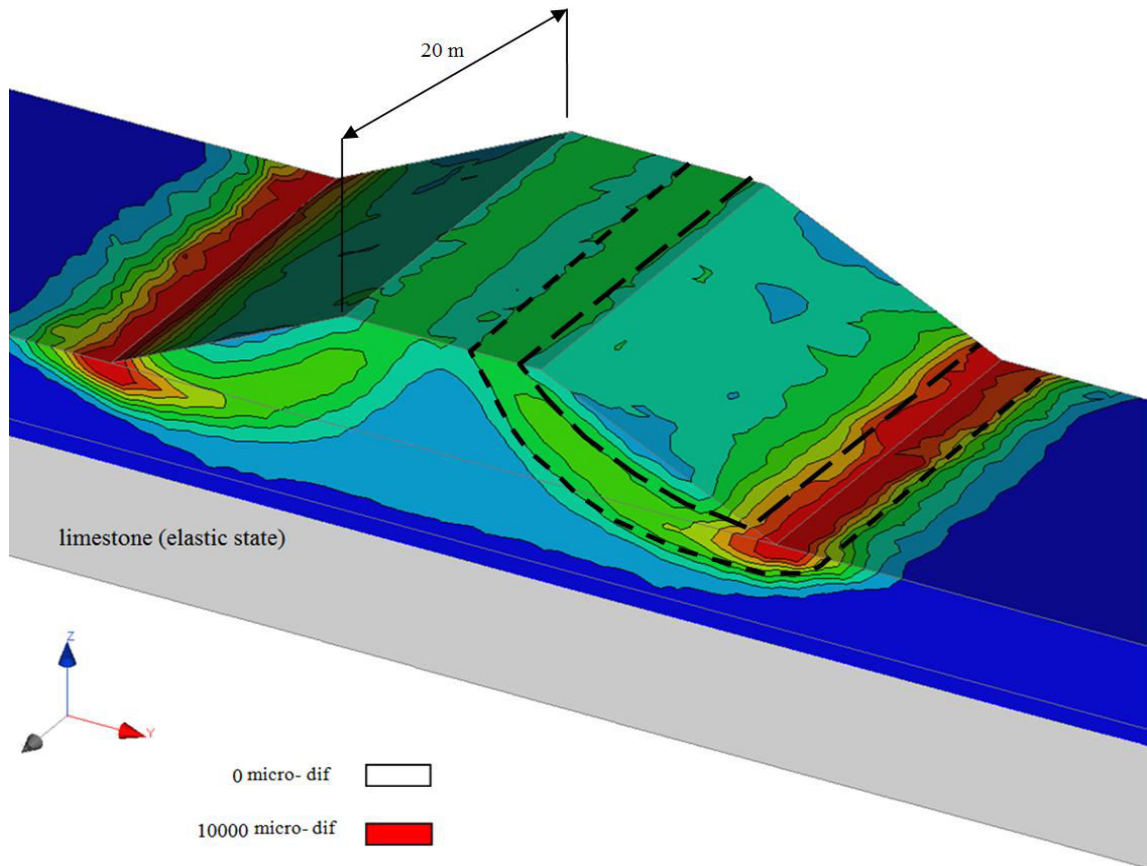


Figure 90 Isovalues of the plastic strain norm of the dike of Val d’Orléans with using the c-phi reduction method in CESAR-3D. The dotted lines show the position of potential failure surfaces.

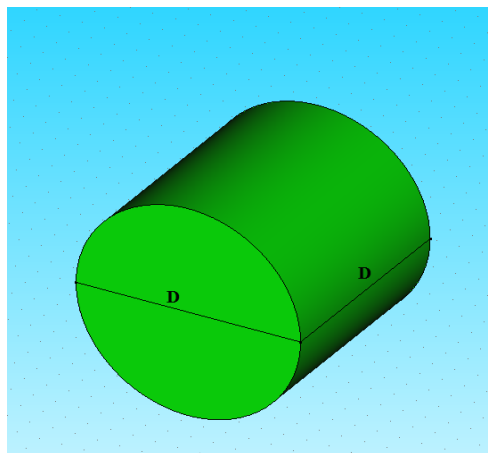


Figure 91 Considered shape of the cavity in CESAR/ 3D. D refers to the diameter of the cavity.

A cavity with a diameter equal to 1 m was selected to simulate the problem of the dike with a cavity underneath its centre. This value of the cavity diameter was chosen dependant on the critical cavity diameter from the results of the analytical approach (chapter 3). Results are then compared with the 2D results for the same case. A cavity with a diameter equal to 2 m was selected to simulate the problem of the dike with a cavity underneath the slope and its value of the cavity diameter was selected due to this value represents the critical cavity

diameter from analytical approach (chapter 4). Then, its results are compared with the 2D results for the same case. The cavity in two previous cases was repeated by considering it as a conduit to see the effect of the third direction on the results and to compare this case with the equivalent case of the cavity.

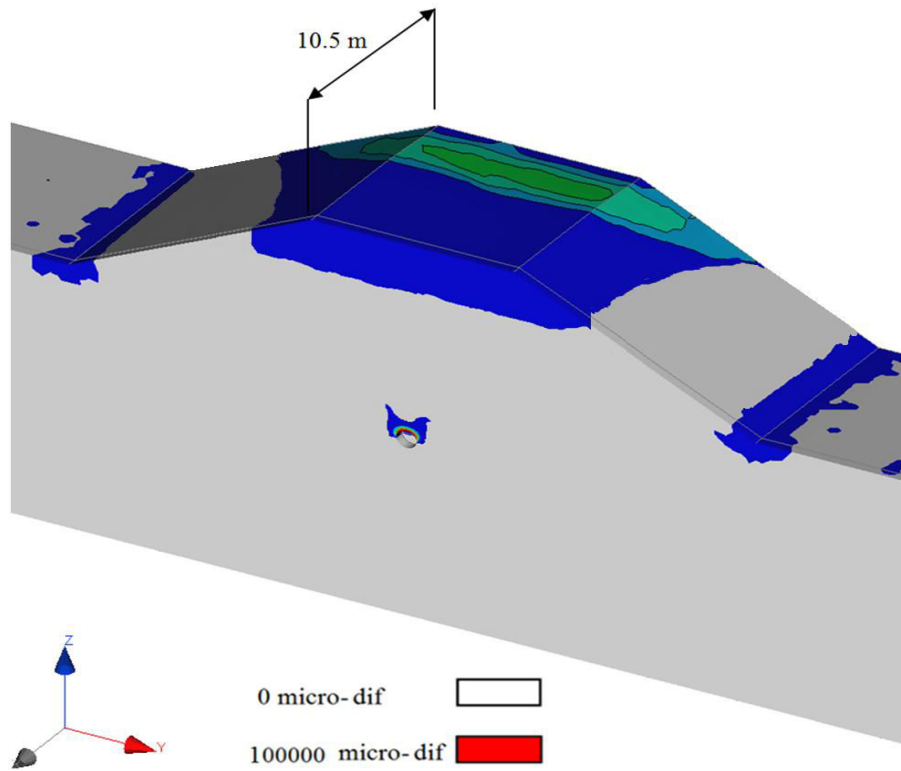
The effect of the cavity direction was tested for a chosen case by considering the direction of the cavity extension perpendicular to the dike direction. The integration of the cavity in the model in CESAR-3D corresponds of a slice form equals to the cavity diameter D in the middle of the dike model in the third dimension. Hence, the third dimension in the Figure 90 (20 m) will be $(20\text{ m} + D)$.

As in the previous 2D calculations with the standard method, all 3D calculations didn't converge after adding the cavity (in normal state) even if the number of maximum iterations increases until 2000 instead of 1000. The shape of the plastic strain zone remains the same even if the iterations number is changed. Hence, the number of maximum iterations (1000) was adopted.

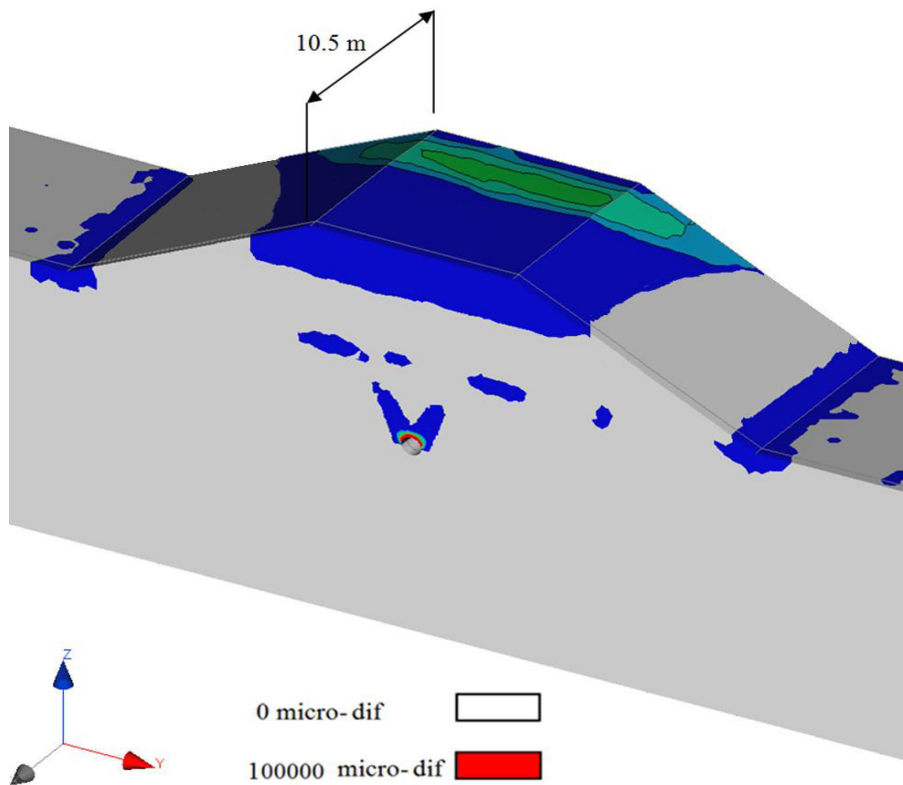
5.5.1 Cavity underneath the centre of the dike

The model of a cavity with a diameter equal to 1 m under the centre of the dike was established with the same procedures which were used in 2D as it was shown in Table 14. In addition, the same finite element dimension (0.5 m) was used. For the purpose of comparison; the model in normal scenario is used (without water behind the dike). Figure 92-a shows the results of the plastic strains. The dimension of the plastic strain zone around the cavity is smaller than the one in 2D (cf. Figure 84-b). In other word, the cavity in 3D is less affected by the dike than a cylindrical cavity modeled in 2D. The vertical displacement on the top of the cavity arch centre (equivalent point 1 in 2D) is equal to 115 mm while it was equal to 135 mm in the 2D configuration. Hence, the vertical displacement was reduced about 15%. While the Figure 92-b shows the results of plastic deformations and the shape of these deformations about a conduit with 1 m instead of the cavity. Herein, the plastic deformations around the conduit are more closely to those in the 2D configuration.

Hence, we can say the 'confinement due to boundary conditions and the axial dimension of the model' of the soils on the cavity in the 3D reduces the plastic deformations or it helps the cavity to be more stable. Adversely to the case in 2D, the plastic deformations herein cover the dike surface due to the ends effect and the calculation doesn't converge with a maximum number of iterations equal to 1000 (even if 2000 iterations).



a- Cavity with diameter equals to 1 m under the centre of the dike.

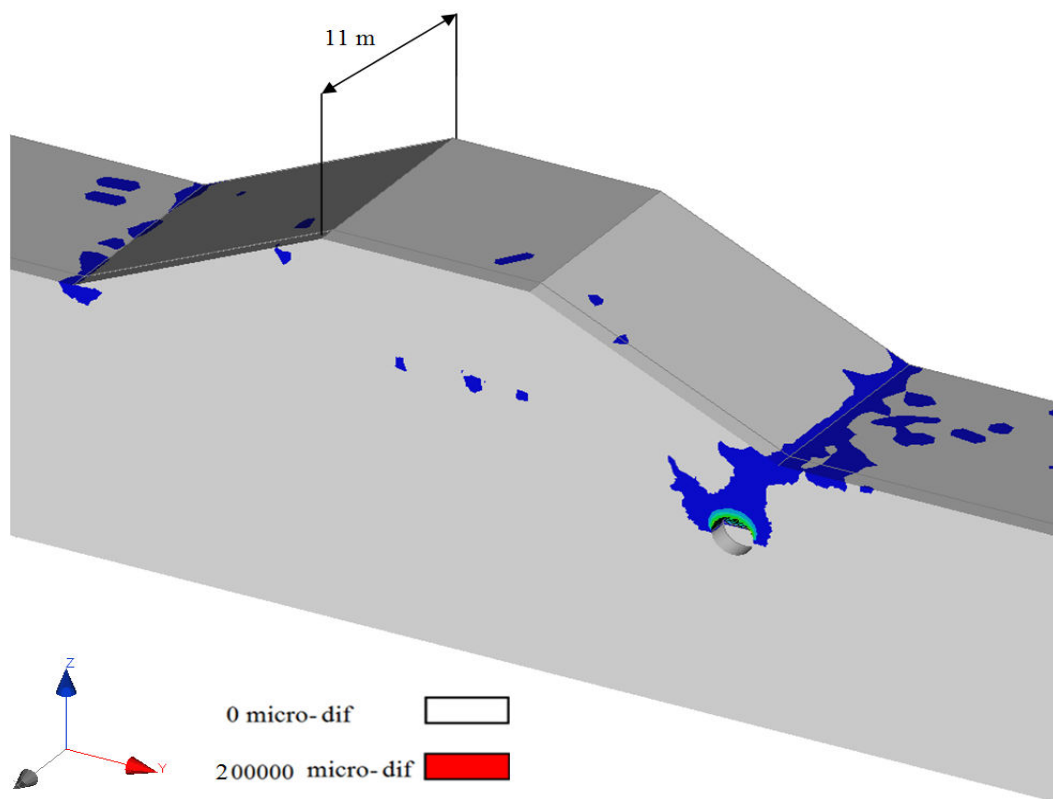


b- Conduit with diameter equals to 1 m under the centre of the dike.

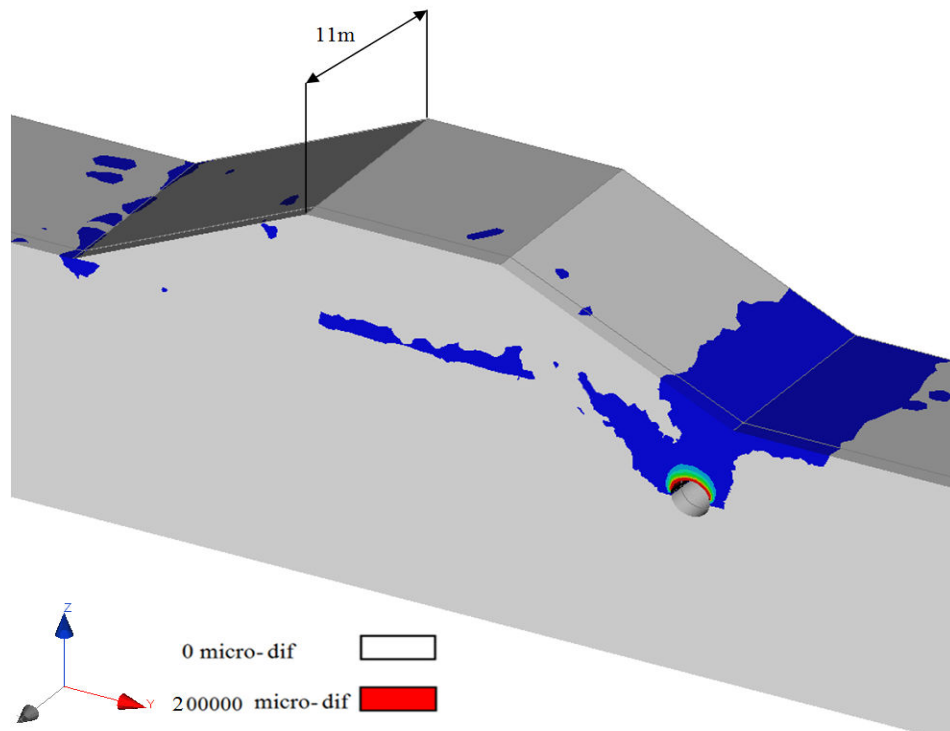
Figure 92 Isovalues of the plastic strain norm for a longitudinal section of the dike model in CESAR-3D in normal scenario (only half of the 3D model is shown).

5.5.2 Cavity underneath the dike slope

The model of the cavity with a diameter equal to 2 m underneath the dike slope in the same position which was modeled in 2D (cf. Figure 74) was carried out. The result of the plastic deformations (Figure 93-a) shows a reduction of the deformation zone around the cavity and of the maximum value of the micro deformation compared to the 2D results (cf. Figure 78-a). The vertical displacement is reduced by about 20 % between the 3D and the 2D models (137 mm in 3D in instead of 177 mm in 2D). Figure 93-b shows the results of the plastic deformations and the shape of these deformations around a 2m diameter conduit. Herein, the plastic deformations around the conduit are more closely to those in the 2D state. Hence, we can conclude that the ‘confinement’ of the cavity in the 3D model reduces the plastic deformations and then helps the cavity to be more stable.



(a) Cavity with a diameter cavity equals to 2 m under the dike slope.



(b) Conduit with a diameter cavity equals to 2 m under the dike slope.

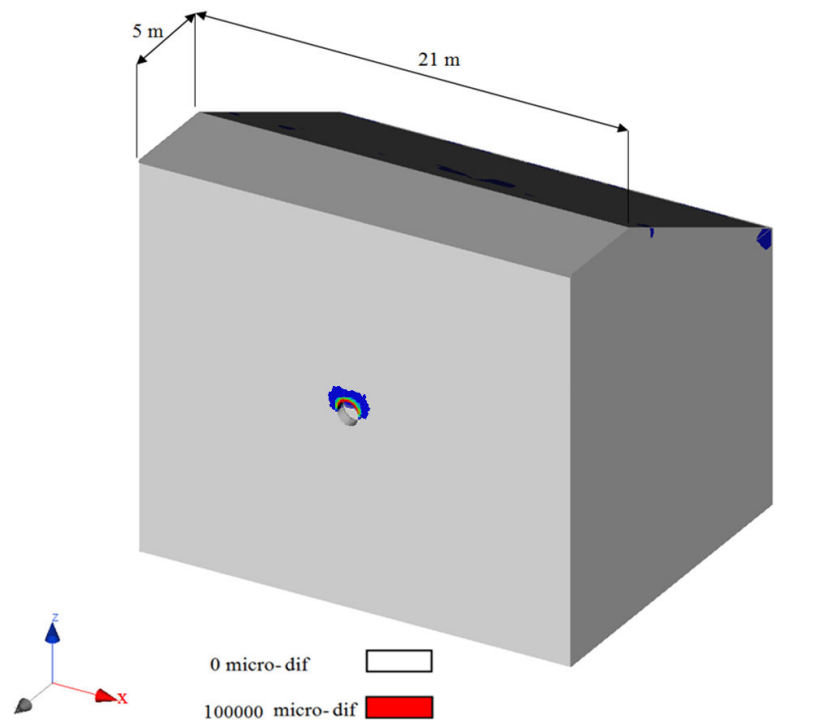
Figure 93 Isovalues of the plastic strain norm for a longitudinal section of the dike model in CESAR-3D in normal scenario (half of the 3D model is shown).

5.5.3 Effect of the direction of the cavity

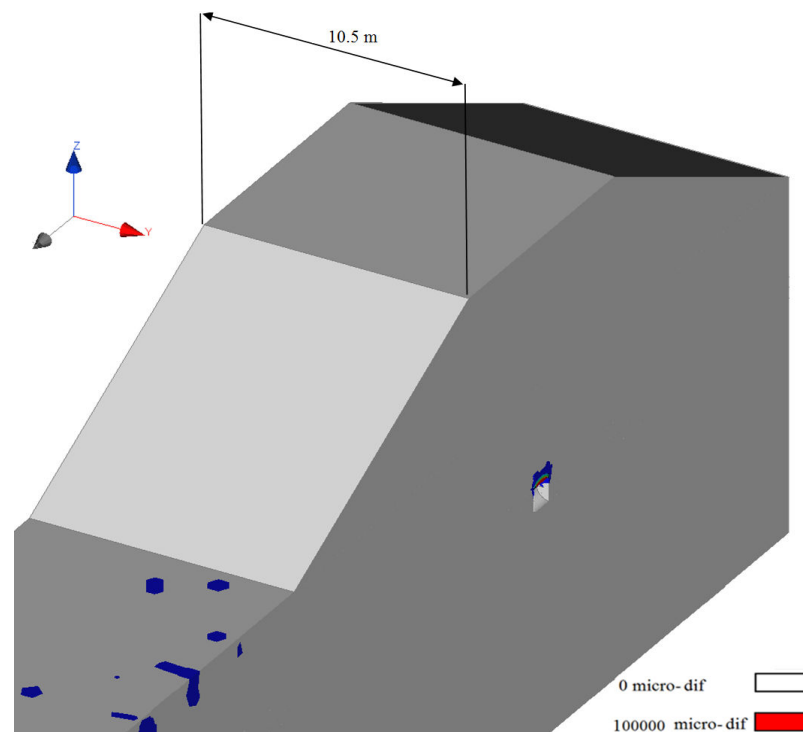
The models in section 5.5.1 were repeated by changing the direction of the cavity (or the conduit) perpendicularly to the dike axis (x) to see if there is an effect of the direction or not. A conduit with a diameter equal to 1 m underneath the dike was investigated to see this effect. Figures Figure 94 and Figure 95 show the plastic deformations around the cavity and the conduit that located perpendicularly to the dike axis (x). These deformations are similar to the ones in case of the cavity and conduit parallel to the dike axis (x) in Figure 92. Some differences in the results may be observed because the calculations didn't converge due to the alluvium properties as we mentioned it previously. It is difficult to keep the same numbers and shapes of the elements in both perpendicular and parallel models and then some differences in the final results between the two models may appear.

The difference in stresses distribution around the cavity between the two cavity cases (perpendicular and parallel to the dike axis) due to the assumption of the cavity as cylindrical segment results. The calculations in 3D more complicated and it is need to simulate the cavity as aspheric shape to obtain real distribution of the forces and stresses around the cavity. However, this study in 3D is given an initial perception about the impact of the third dimension on the results and it was generally lower than the 2D.

For the purpose of testing and investigating the dike safety; the 2D calculations are adopted due to their simplicity and because their results are more conservative. For that, the results of the CESAR-2D are adopted to be compared with those from the analytical methods.

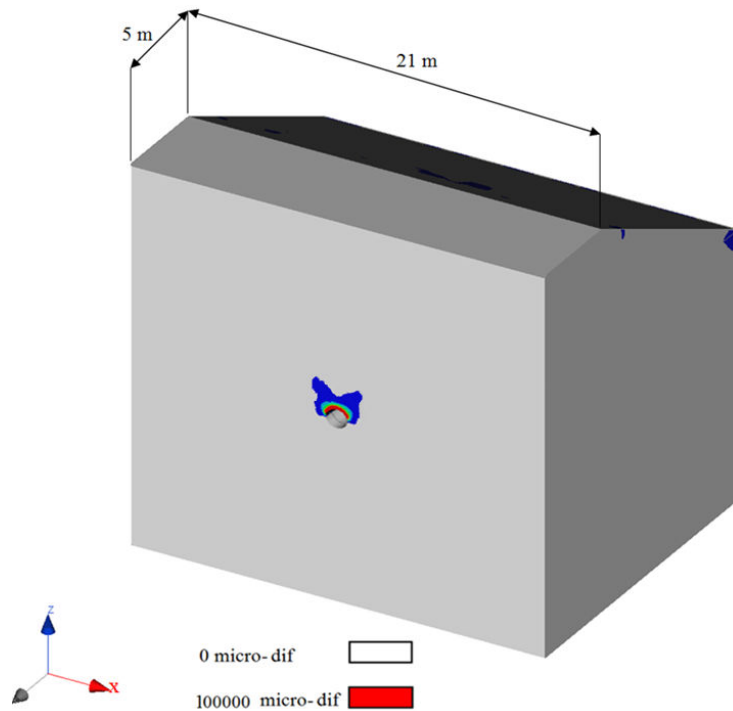


(a) Longitudinal section of the dike.

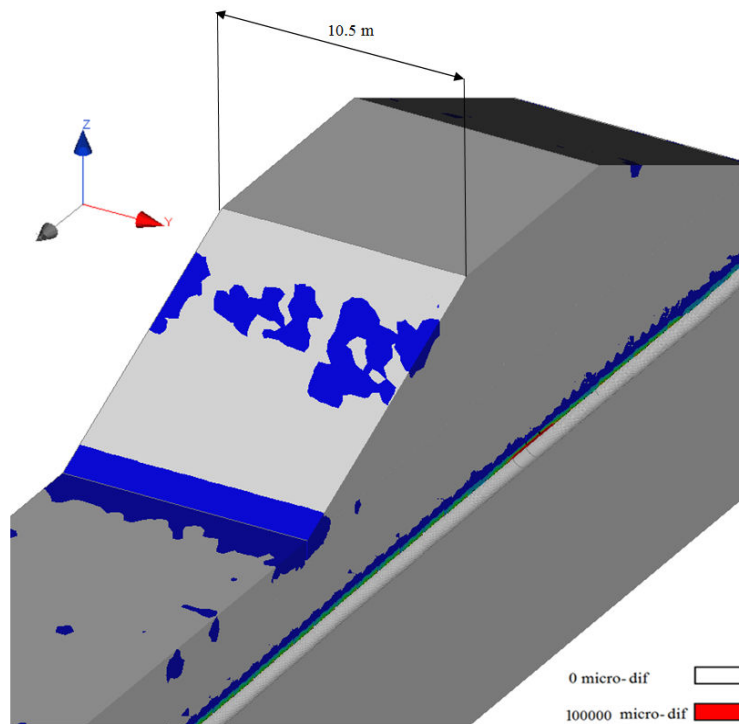


(b) Cross- section of the dike.

Figure 94 Isovalues of the plastic strain norm for the dike model in CESAR 3D in normal scenario. The cavity is perpendicular to the dike axis (x-axis).



(a) Longitudinal section of the dike.



(b) Cross- section of the dike.

Figure 95 Isovalues of the plastic strain norm for the dike model in CESAR-3D in normal scenario. The conduit is perpendicular to the dike axis (x-axis).

5.6 Comparison between the analytical and numerical results

5.6.1 Cavity stability and collapse shape

The results of the analytical approach (chapter 3) gave a critical diameter at which the cavity starts to collapse equal to 1 m. The results of the numerical method (CESAR 2D) did not give a specific value of the critical diameter of the cavity, the development of the plastic deformations around the cavity in relation to its diameter was considered as an indicator. The plasticity zone could reach the dike head when the cavity diameter is equal to 2 m but at the same time there is a plastic zone about the cavity which is resulted due to the dike presence with a diameter equals to only 0.5 m (cf. Figure 78 and Figure 82). In reference to Table 13-b, the arch cavity already came down in case of a cavity diameter equal to 0.5 m (with a vertical displacement of 49 mm). Hence, in the numerical model there is two types of cavity collapse scenario; the first one is the collapse of the roof of the cavity (arch of the cavity) and the second one is the collapse of the soil column above the cavity (the parts of alluvium and the dike). The soil column can reach the dike and propagate until to the surface to form a sinkhole (see chapter 6). In other words, the roof of the cavity collapse could start with a diameter equals to 0.5 m while the collapse of the soil above the cavity could start with a diameter equal to 2 m.

The collapse of the cavity in the analytical solution (chapter 3) is considered as a total collapse of the cavity arch and the soil above it. In fact, the value of the 0.5 m critical diameter could be considered as the first collapse of the cavity arch and doesn't always lead to a total collapse because the collapsed soil volume above the cavity depends on the capacity of the cavity and the karstic cave underneath it. Hence, the collapse of a cavity roof with a small cavity diameter (0.5 m) may result small the collapsed soil that can fall down in the cavity. The consequence of the cavity collapse on the dike head is a sinkhole or a subsidence. The volume of the karstic cave plays an important role to increase the collapse process of the soil above the cavity; if the cave could contain all the collapsed soil or not (as it is discussed in chapter 6).

The analytical solution is based on the equilibrium between the anti-collapse forces and collapse forces above the cavity to test its stability (chapter 3). This solution assumes that the collapse displays a cylindrical form. However, the numerical models using CESAR showed an expected frustum collapse form by assuming that the form of the collapse is similar the plastic deformation zone. This assumption agrees with the results of Gombert et al. (2016). They simulated two cavities with diameters equal to 5 and 20 m respectively in elasto-plastic state with using a finite element software (Plaxis 2D) and their results shown that the plastic zone around and above the cavity displays a frustum shape through the sand ($c=0$) and it climbs about vertically as a cylindrical column through the clayey soil and the dike. In addition, numerical modelling using UDEC (Universal Distinct Element Code) was used to study and to discuss the choice of the collapse mode of the alluvium layer above the cavity and dike (Al Heib, 2016).

The soil materials are assumed like granular material, corresponding to small 2D blocks. In CESAR (in finite element methods) the soil is continuous assumption. The advantage of discontinuous behaviour, one can observe the instability mechanisms. To verify this assumption in the case of alluvium (soil); we simulated the soil by particle elements with the same properties and global dimension than the alluvium layer in the continuous model used in this thesis. We divided a limited alluvium zone by rectangular and equal particles; the dimensions of the particle are 20*20 cm that is small enough to observe the failure surface and the collapse when the cavity is created. The analytical solution considers the failure surface is vertical (cf. chapter 3). We considered the soil granular layer width in surface equal 15 m, 3 times the diameter of the cavity (5 m). Two simulations were carried out: vertical and inclined plans. The results shown clearly herein that the inclined plan has not a direct effect on the failure mode; we still obtain a cylindrical failure mode with a swelling of the particles as presented in Figure 96 and Figure 97. In the both cases, a sinkhole created in the surface.

A numerical model was carried out taking into account the cavity underneath the dike (at the centre position). The soil and the dike presented also as particles in the total surface of the dike and the zone of interest of the alluvium layer. The geometry of the dike is identical to the typical Val d'Orléans dike. The alluvium layer thickness is equal to 5 m, and the width of the cavity is also equal to 5 m.

The existing of the cavity under the dike, the alluvium layer starts slid into the cavity and the movement or the sinkhole propagates through the dike (Figure 98). The sinkhole propagates through the alluvium layer and the dike body. The form of the sinkhole at the surface depends on the buckling of the soil (extension of the volume). The cylindrical form of collapse is also obtained (Figure 97). The results of UDEC confirm that assumption which was used in the analytical approach concerning the collapse mode as a cylindrical column.

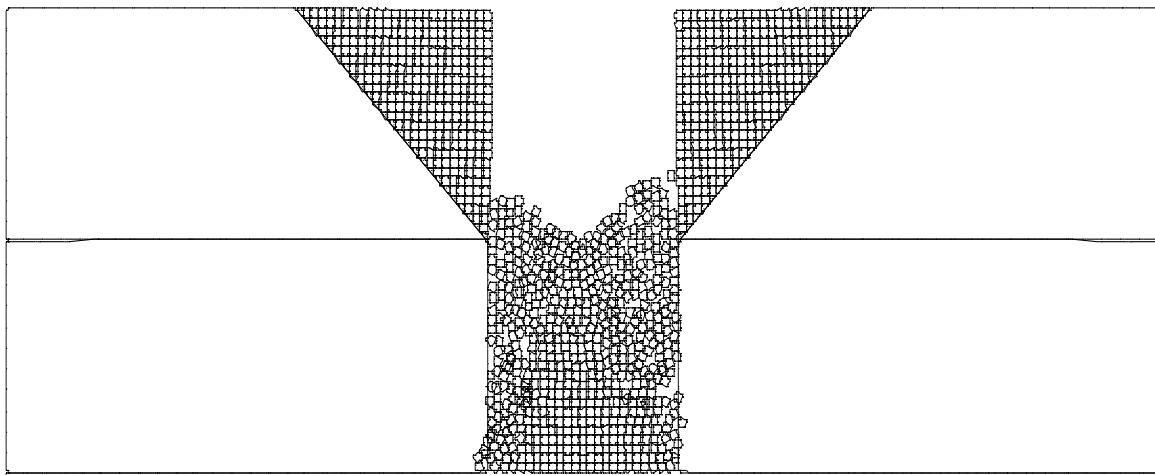


Figure 96 Instability and failure collapse in the case of inclined surfaces and particle zone.

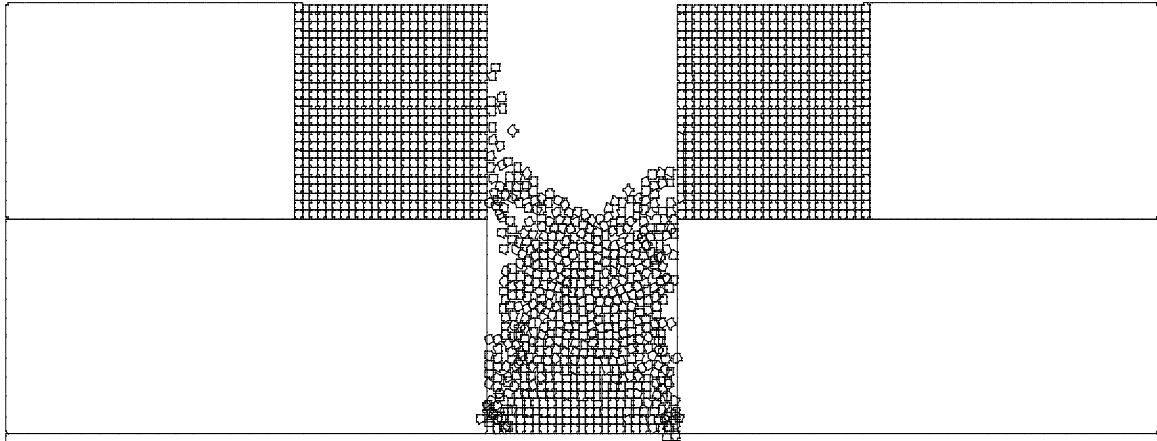


Figure 97 Instability and failure collapse in the case of vertical discontinuities and particle zone.

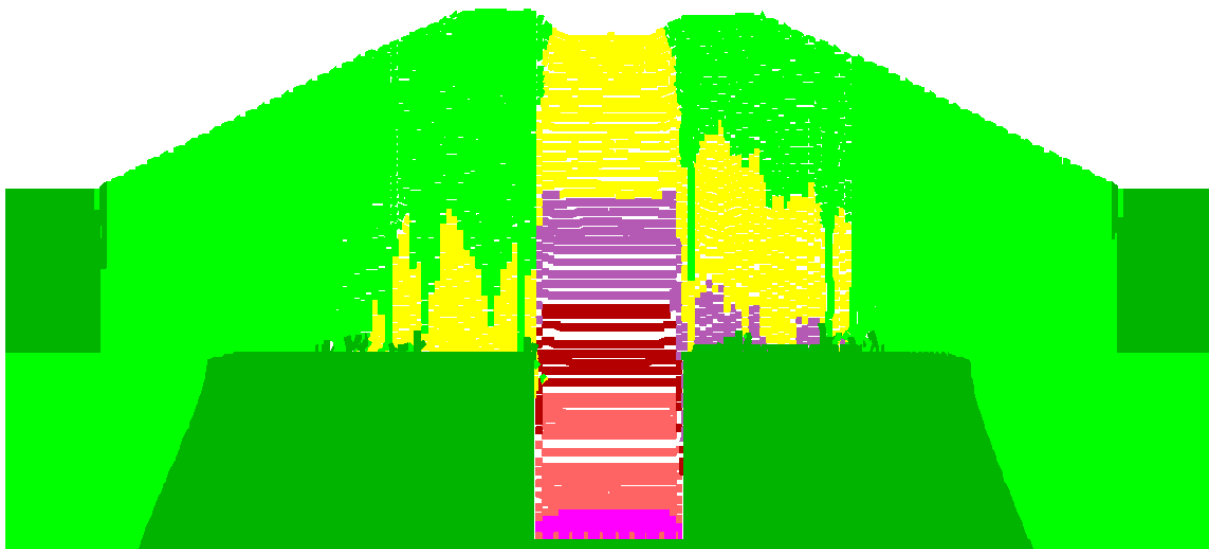


Figure 98 Vertical displacements due to the cavity and the collapse of the dike and the alluvium layer (max. vertical displacement = 5 m, min. vertical displacement = 0 m), the sinkhole on the surface = 2 m.

The results of the analytical approach, CESAR and UDEC can help to better justify the assumption and strength the results analysis. The different methods have common results that the dike increases the likelihood of the collapse both the cavity in the dike. Each method presents a specific indicator, the analytical method in term of safety factor, the finite element method in term of the plastic strain and the distinct element method in term of collapse. we can explain the difference in the shape of the failure due to the assumption of the soil material as a block that led to appear a frustum collapse shape (in CESAR). However, the assumption of the collapse force and the resistance force concerning the cylindrical column soil above the arch of the cavity is acceptable in all cases and we could consider the cavity extends upwards in frustum shape (after the roof is collapsed).

In other words, the assumption of main collapse and resistance forces due to the cylindrical column of soil above the cavity is favorable to test the stability of the cavity arch but the form of the cavity propagation upward after the arch collapse is difficult to expect and the properties of soil materials play an important role in identifying the final shape of the collapse. Thus, the form of propagation of cavity collapse is assumed grow vertically as a soil column through the cohesive soil (the dike) while it grows as frustum form through the cohesiveness (the alluvium) in next chapter (chapter 6). This interpretation compatible with the observed sinkhole as that is shown the Figure 99 with diameter equals about 2 m on the head of the dike. It is clear that each method presents advantages and disadvantages, but we can consider the analytical tool presents an engineering tool to assess the risk of cavity-dike collapse in the karstic region.



Figure 99 Sinkhole on the head of the dike of Val d'Orléans in area of Jargeau (Dore and Mathon 2011).

5.6.2 Cavity effect upon the dike slope stability

The results of the analytical approach (chapter 4) showed a 1 m diameter of the cavity could affect the slope stability of the dike (but SF remains >1) while a 2 m of the diameter of the cavity results failure of the slope stability (SF < 1). In the 2D numerical model, the plastic zone was considered as a failure indicator. When the two plastic zones around the dike slope and around the cavity are connected, the cavity is considered to have an influence over the slope stability. The results of the numerical model (2D) give similar results of the analytical approach. Hence, the two results of the analytical and numerical methods are in agreement.

5.7 Summary

In this chapter, the numerical modelling was carried out to 1- verify the results of the analytical models in previous chapters (chapter 3 and 4) and to 2- analyses the cavity dike interaction mechanisms. The CESAR-V6 (2D and 3D) finite element software was used.

The 2D calculations are adopted to compare their results with those from the analytical methods due to their simplicity and also their results more conservative.

Different approaches were discussed to analyses the results of the numerical model (stress, displacement and plastic deformation strain). The plastic deformation criterion was adopted as a principle failure indicator while the vertical displacement criterion was used as a secondary failure indicator.

Most of the numerical calculation results confirm the analytical results especially in case of the effect of the cavity upon the dike slope. Hence, the results of the numerical and analytical methods indicated that a cavity with diameter equals to the 2 m could affect the dike slope stability. While the results of the dike effect upon the cavity stability underneath the centre of the dike showed the roof of the cavity with a 0.5 m of the diameter could be collapse whereas the effect of the cavity with a 2 m of the diameter could reach the head of the dike.

The cavity failure mechanism results from the numerical model could be divided into two parts, the first one collapse of the immediate roof of the cavity and the second one is the failure of column soil above it which may be in phases until the failure reaches the surface (dike surface) and a sinkhole appears.

The critical diameter of the cavity underneath the centre of the dike from the analytical method (chapter 3) equals to 1 m. Hence, this value is in the range of the numerical results but it could be considered as the critical diameter at which the roof of the cavity starts collapse. However, the use analytical methods could be considered practical (particularly in the field of initial assessment of the engineering structures) because they often give quick results and not need to high experience. On other hand, the numerical model needs to experience and practice to establish and analyse the problem in addition to the time and the cost.

The results highlighted that the cavity position under the centre of the dike is more critical than that presents under the slope (for the same diameter). In this configuration, the plastic deformation around the cavity increases due to the effect of the additional weight of the dike. The water in flooding state can increase the plastic zone about the cavity and on the surface of the dike which can accelerate the collapse propagation until the surface.

The numerical methods (as finite elements method in CESAR) needs to the accuracy in the selection of the meshes dimensions and also the results depend on convergences that are affected by the mechanical properties of the materials. Thus, these methods need to high practice and experience.

The numerical modelling calculations in 3D more complicated and the cavity was simulated as spherical shape instead of the cylindrical form (as it was assumed in the calculations) to obtain uniform distribution of the forces and stresses around the cavity. However, this study in 3D is given an initial perception about the impact of the third dimension on the results and they are generally lower than the 2D results (stresses and strains).

5.8 Reference

- Baba Kh., Bahi L., Ouadif L., Akhssas A., 2012. Slope Stability Evaluations by Limit Equilibrium and Finite Element Methods Applied to a Railway in the Moroccan Rif, *Open Journal of Civil Engineering*, 2. pp. 27-32.
- Bourgeois E., Mestat Ph., Pucheu M., 2012. Abridged theoretical manual; CESAR-LCPC. IFSTAR-itech. 42 pp.
- Dawson, E. M., W. H. Roth and Drescher A., 1999. Slope Stability Analysis by Strength Reduction” *Géotechnique*, 49(6). pp. 835-840.
- Deng J.H., Wei J.B., Min H., 2004. 3D stability analysis of landslides based on strength reduction (I): back analysis for the shear strength of sliding soils. *Rock Soil Mech* 6: pp. 896–900.
- Dore L., Mathon D., 2011. Essai de cartographie de l'aléa «effondrement karstique» dans le Val d'Orléans. 08 au 10 novembre. Journées National Géotechnique et Géologie de l'Ingénieur. 21 pp.
- Duncan, J. M., 1996. State of the art: Limit equilibrium and finite-element analysis of slopes, *J. Geotech. Geoenviron. Eng.*,122(7). pp.577–596.
- Eid Mona M., Ahmed Ali A. A., Hefnyand Ashraf M., EL-Attar Ahmed N., 2015. Tunneling effect on the adjacent pile footings. *J Am Sci (Journal of American Science)* 2015;11(1). ISSN:1545-1003. pp. 88-98.
- Gombert P., Alboresha R., Treffot M, Al Heib M., Deck O., 2016. Impact du changement climatique sur l'aléa « effondrement karstique » dans le Val d'Orléans (Loiret) et risque induit sur les digues de Loire. *Géologues* 187.pp 26-30.
- Griffiths D.V., Lane P.A., 1999. Slope stability analysis by finite elements. *Geotechnique* 49(3):387–403.
- Itasca, 2000. UDEC Universal Distinct Elements Code Manual. Continuously yielding joint model. Itasca Consulting Group Inc., pp. 1–16.
- Jiang Q., Zufang Qi., Wei Wei Zhou C., 2015. Stability assessment of a high rock slope by strength reduction finite element method. *Bull Eng Geol Environ* (2015) 74:1153–1162 DOI 10.1007/s10064-014-0698-1.
- Kondalamahanthy, Alekhya K., 2013. 2D and 3D Back Analysis of the Forest City Landslide (South Dakota). Master thesis. Iowa State University (USA). 73 pp.
- Luan M.T., Wu YJ, Nian T.K., 2003. A criterion for evaluating slope stability based on development of plastic zone by shear strength reduction FEM. *J Disaster Prev Mitig Eng* 23(3): pp.1–8.

- Mesta P., 1998. Modèles d'éléments finis et problèmes de convergence en comportement non linéaire. Bulletin des laboratoires des ponts et chaussées, pp. 45-60.
- Narayanan P. S., Jeyapriya S.P., 2015. Numerical modeling and development of empirical correlations for prediction of plane strain properties of cohesionless soils. The Electronic Journal of Geotechnical Engineering Vol. 20. pp. 6169-6183.
- Rabie M., 2013. Comparison study between traditional and finite element methods for slopes under heavy rainfall. HBRC Journal Volume 10, Issue 2, August 2014, pp. 160–168.
- Ugai K., 1989. A method of calculation of total factor of safety of slopes by elasto-plastic FEM. Soils Found 29(2): pp. 190–195.
- Zhao S.Y., Zheng Y.R., Deng W.Z., 2003. Stability analysis on jointed rock slope by strength reduction FEM. Chin J Rock Mech Eng 22(2): pp.254–260.
- Zheng H., Liu D.F., Li C.G., 2008. On the assessment of failure in slope stability analysis by the finite element method. Rock Mech Rock Eng 41(4): pp. 629–639.
- Zheng Y.R., Zhao S.Y., Deng C.J., 2006. Development of finite element limit analysis method and its applications in geotechnical engineering. China Eng Sci 8(12): pp. 39–61.

6.1 Introduction

This chapter presents an operational feedback of the cavity collapse underneath a dike in the karstic zones. Thanks to previous analytical studies and analysis, the stability of a cavity underneath the dike could be predicted, but the form and mechanism of collapse after the arch (roof) of the cavity reached the failure state ($FS < 1$) were not enough discussed. Thus, we are able to suggest, in this chapter, several scenarios for expected behaviour or action in critical case of a cavity underneath the centre of a dike (underneath the highest elevation of soil column) in flooding state. In other word, the objective is to predict what may happen when the cavity arch (roof) reaches the point of failure and when the soil column starts collapsing. The dike modifies and increases the collapse forces that affect the roof of the cavity (see chapter 3) and it also increases the volume of collapsed soil, which fall in the karstic cave or conduit.

These scenarios can be classified according to the properties of the dike and the soil layers under it. They may also depend whether the karstic cave is connected with a karstic conduit or not. To describe and illustrate these scenarios, the dike is considered as constituted by a cohesive soil ($c > 0$). We consider that the alluvium layer under the dike can be divided into one or two sub-layers. The main factors that influence the form of the collapse propagation from the cave toward the surface (cylindrical chimney or frustum) are the soil properties of alluvium, especially the cohesion. When the soil is cohesive ($c > 0$) the prolongation of opening will have a cylindrical shape while the prolongation of the opening in the cohesionless soil is approximated by a frustum, according the results of Drumm et al. (1990). These authors studied the stability of sinkholes, indicating that the included angle is very nearly $45^\circ - \varphi/2$ (angle with vertical axis, φ average friction angle of soil layers). The main force responsible for soil mass movement is gravity in the vertical opening (chimney). In our study, the inclined line of the open frustum above the cavity was assumed vertical for a cohesive ground or inclined at an angle (α) with the horizontal axis for a cohesionless ground.

The scenarios of failure propagation through the alluvium and the dike will be divided into two principle groups (each one of them having several subgroups): scenario for isolated karstic caves and for karstic caves connected with a karstic conduit.

The term isolated cave is used here to describe an underground void which has no conduits connecting it to the input and output boundaries of the aquifer (Dreybrodt and Siemers, 2000). Thus, the effect of water flow in the karst can be neglected.

6.2 Scenario of isolated karstic caves

In this case, there is no connection between the karstic cave and a neighboring karstic conduit, or such a conduit is absent: for example, this can be happened for ghost-karstification (Quinif & Bruxelles 2011, Dubois et al. 2014) that result of the in situ dissolution of limestone in a drowned environment that preserves the surrounding structure and a generally crushed

structure is usually found (Vergari & Quinif, 1997). Three general scenarios of the cavity-sinkhole propagation can be illustrated herein:

6.2.1 Scenario for one cohesionless alluvium layer

If a single cohesionless alluvium layer exists between the dike and the limestone layer where a cavity exists, then the expected shape of the void propagation after the collapse of the arch in the limestone layer is a frustum form with an angle of the failure lines (α). The diameter of the moving ground under the dike may be very large. Because the dike is made with cohesive ground the failure shape into the dike is assumed to be cylindrical (see Figure 100). A subsidence of the dike head is then expected and the likelihood of overflow in flood period will increase as a result the subsidence of a dike head level.

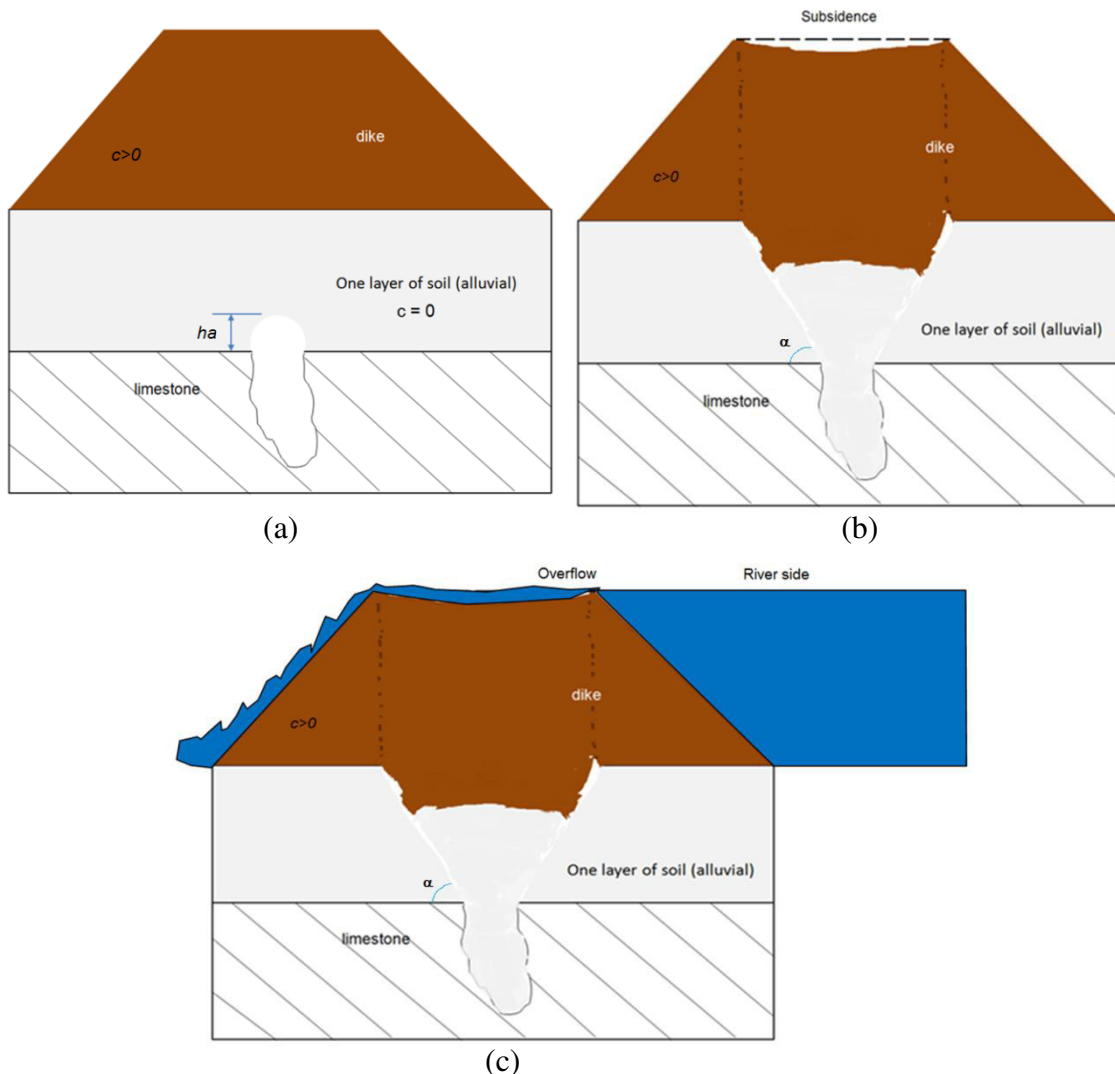


Figure 100 Isolated karstic cave scenario with one cohesionless soil layer. (a) initial state: formation of the cavity; (b) final state: frustum shape propagation in the cohesionless soil layer and subsidence of the dike head; (c) likelihood of overflow due to the subsidence in flood period. h_a is the height of the cavity arch, c is the cohesion and ϕ is the friction angle of soils.

6.2.2 Scenario for one cohesive alluvium layer

If a single cohesive alluvium layer exists between the dike and the limestone layer where a cavity exists, then the expected shape of the void propagation after the collapse of the arch in the limestone layer is a cylindrical chimney with a diameter nearly equal to the diameter of the critical cavity. Because the dike is made with cohesive ground the failure shape into the dike is assumed to remain the same (see Figure 101). The depth of the sinkhole depends upon the volume of the karstic cave. A large cave will cause a deep sinkhole. The presence of the sinkhole is then assumed to decrease the dike strength in flood period.

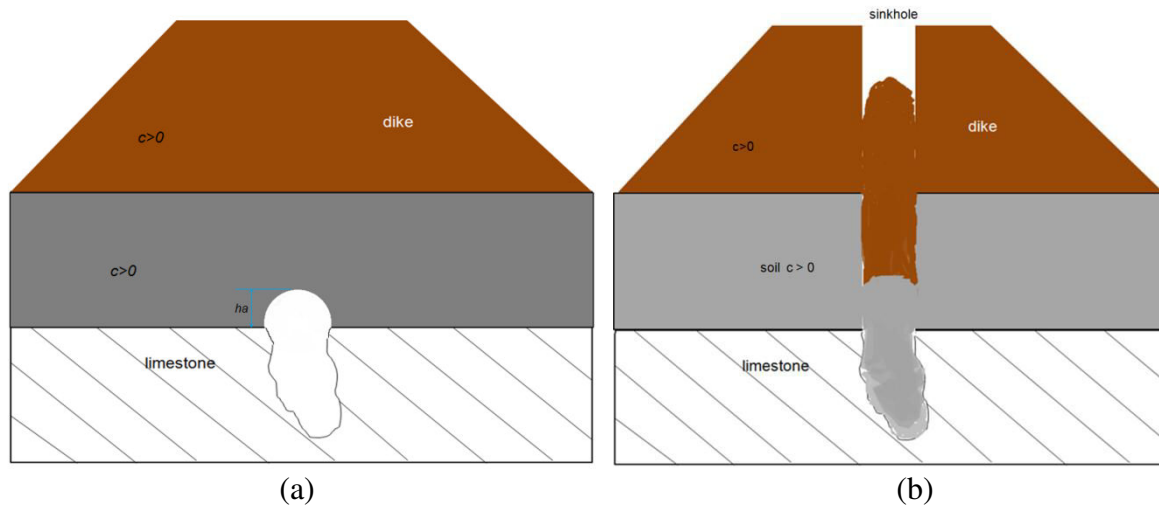


Figure 101 Isolated karstic cave scenario with one cohesive soil layer; (a) initial state: formation of the cavity; (b) final state: cylindrical propagation in the cohesive layers.

6.2.3 Scenario for two alluvium layers

Two alluvium layers are considered underneath the dike. A cohesive soil layer is assumed directly above the karst or the stratum layer and a cohesionless layer above it (see Figure 102). When the arch or roof of the cavity failed, the propagation will take a cylindrical chimney shape in the first cohesive layer. When it propagates through the cohesionless soil layer the chimney will enlarge and take a frustum shape with an angle α . Generally, the dike is built with cohesive soil and the void propagation is then expected to take again a cylindrical chimney shape in the dike.

The most expected result is the subsidence in dike surface. It is because the limiting of cave volume and the final shape of expansion, as a result of the transition from loose soil (cohesionless alluvium layer) to the dense soil (cohesion alluvium layer). This process returns a cylindrical opening shape with diameter equal to the diameter of the upper frustum. So, the soil in the dike cannot be continued landslides as a unit block but it will slide inside the frustum under the influence of gravity in small blocks until the karstic cave be totally full. A subsidence of the dike head is then expected and the likelihood of overflow in flood period will increase as a result the subsidence of a dike head level.

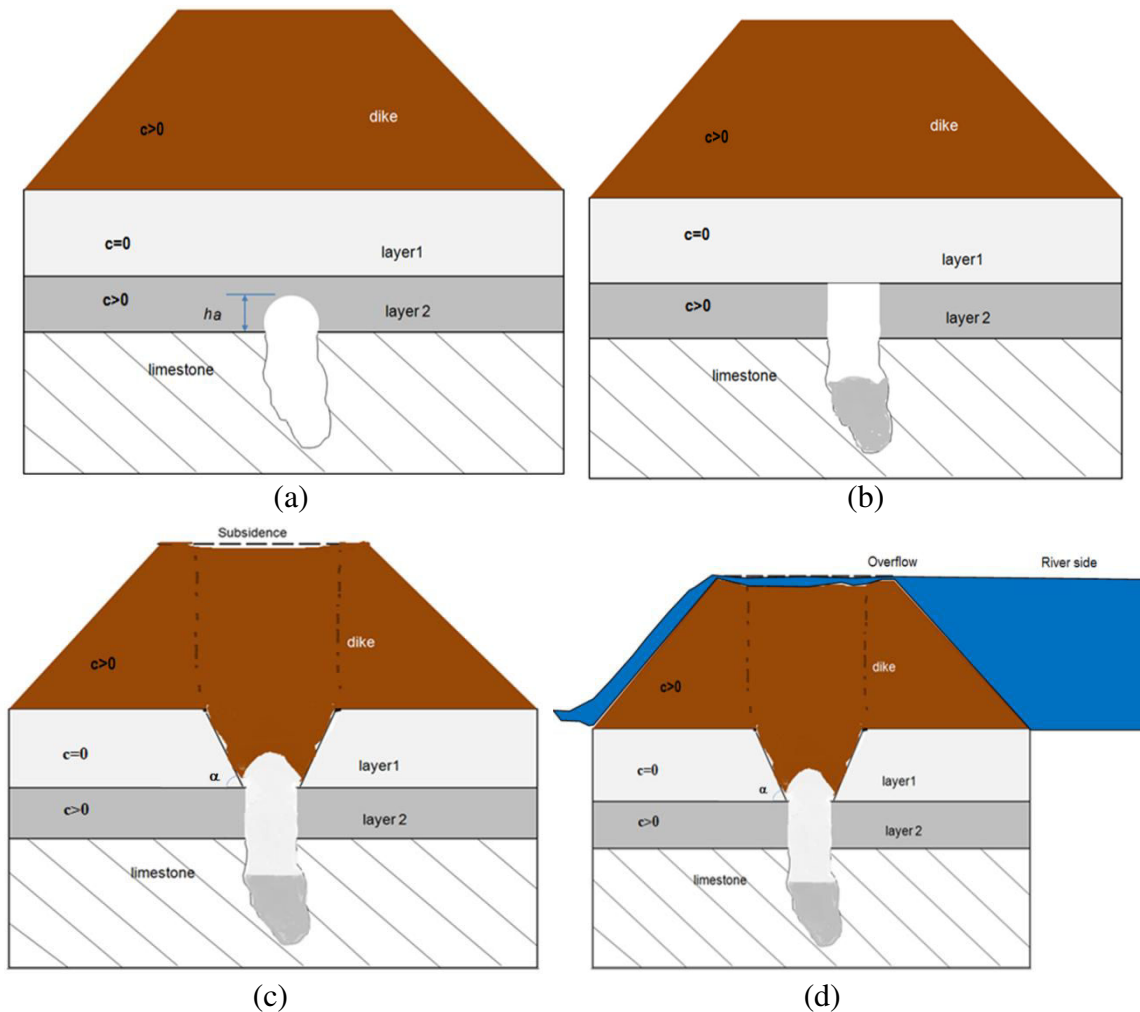


Figure 102 Isolated karstic cave scenario with two soil layers (with and without cohesion). (a) initial state: formation of the cavity; (b) cylindrical propagation into the cohesive soil layer; (c) final state: frustum shape propagation in the cohesionless soil layer and subsidence of the dike head; d- likelihood of overflow due to the subsidence in flood period. h_a is the height of the cavity arch, c is the cohesion and ϕ is the friction angle of soils.

6.3 Scenario for cave connected to a karstic conduit

In this case, there is a vertical connection between the karstic cave and a neighboring karstic conduit. Karstic conduit is assumed to be filled with water due to the water level in the river (Loire) that is always higher than the level of cavity arch (principle of the communicating vessels). Water in the cave may have a significant influence since its level may quickly change and the flow into the karstic conduits may evacuate all collapsed materials that fall from the roof into the cave. Collapsed materials will then never fill the cavity.

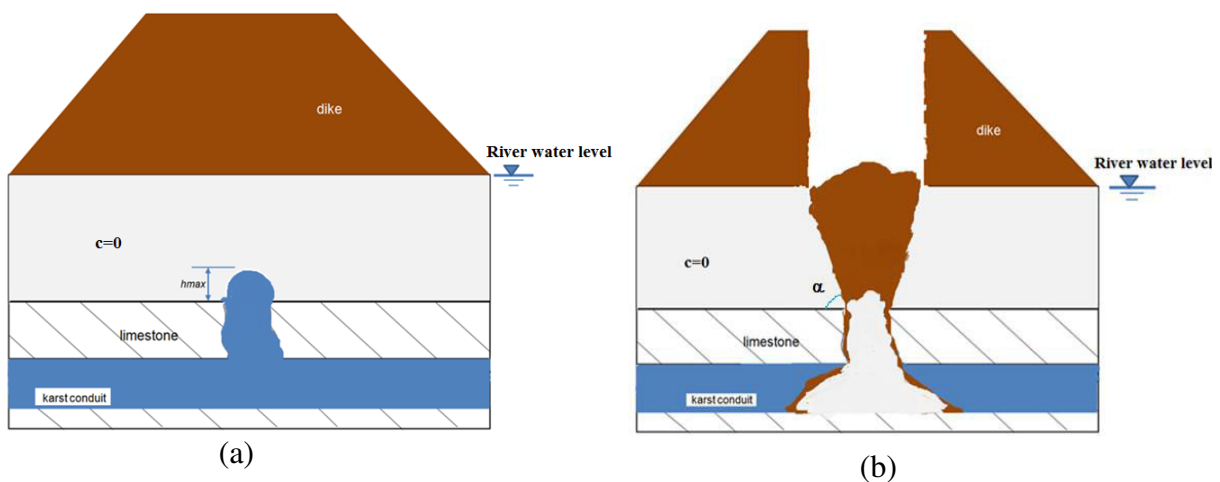
6.3.1 Scenario for one cohesionless alluvium layer

In state of presence of a cohesionless soil layer between the dike and the karstic zone, the vertical soil column over the arch of the cavity collapses as frustum shape in the cohesionless soil area. Then it continues upwards through the dike by taking cylindrical form until the

surface. Thus, the perspective final result is a sinkhole in the land surface of the dike (as shown in Figure 103).

An intermediate step may be observed as the previous state (with two soil layers) and also its presence depends on the volume of the karstic conduit cross section underneath the cavity. If the prospective frustum volume of collapsed soil mass in the karstic conduit (V_2) is less than the total volume of the vertical chimney (V_1); an intermediate step could be observed (Figure 104). Herein, the collapsed soil was considered as one block due to the surface tension between and around the grains that increases the shear strength. The duration of this step depends on the water flow force value in the karstic conduit and the property of the collapsed soil in the conduit. When the water flow force value is more than the friction resistance force between the soil block inside the conduit and surface of the karstic conduit, the flow water force will push the soil block and then the duration of the intermediate step will be short. The opposite case when the flow water force value is less than the resistance friction force: the duration of the intermediate step might take longer (maybe several days or months) as function of the collapsed soil properties (especially the permeability and soil gradation) that effect upon the water seepage through the soil block overtime.

Thereafter, the soil block will be divided as several blocks and flow water would can carry the small buoyant soil blocks. They were resulted to the liquefaction occurs when loose soils becomes oversaturated with water and individual grains loose grain to grain connected to with one another as water gets between them. The other soil mass in the upper part in the chimney will be replaced in place of the displaced soil block and this operation would be repeated several times until all soil in the chimney would be dropped and carried by water stream in the conduit.



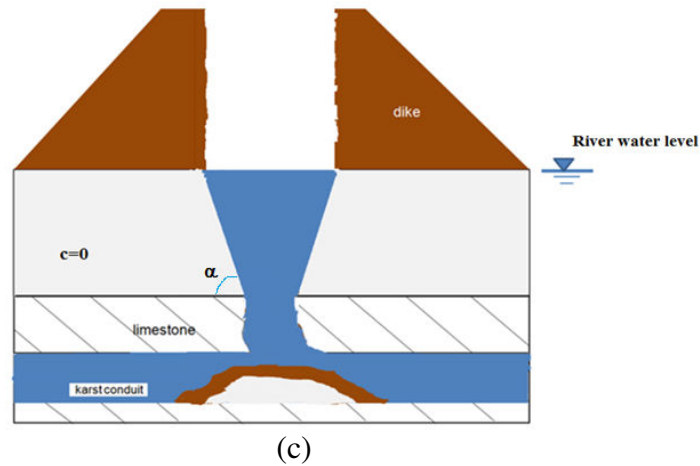


Figure 103 karstic cave connected to a karstic conduit scenario with one cohesionless soil layer (a) initial state: formation of the cavity; (b) final state: with crammed chimney by the collapsed soil; (c) final state: without collapsed soil in the chimney.

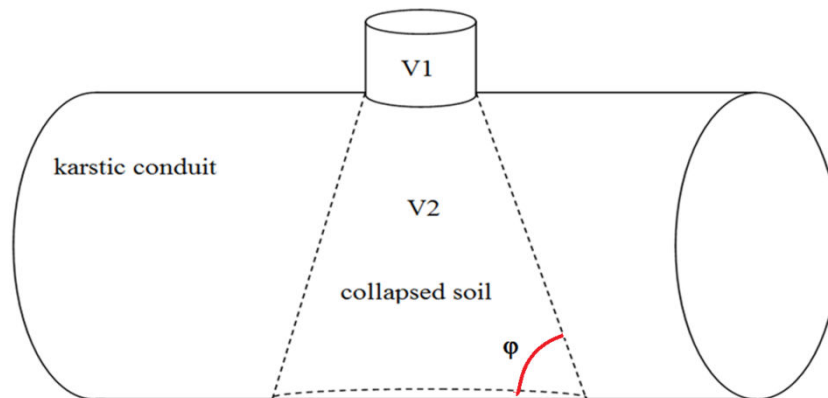


Figure 104 Sketch used to illustrate hypothesis of comparison between the volume of collapsed soil V1 from the chimney and the expected volume to be filled of the karstic conduit underneath the cavity V2.

6.3.2 Scenario for one cohesive alluvium layer

When a cohesive soil layer exists between the dike and the limestone, the chimney takes a cylindrical shape and a diameter equals to the diameter of the critical cavity (see Figure 105). This development continues vertically until the surface of the dike due to the cohesion property in the soil of the alluvium layer and the dike. As for the previous case, the depth of the sinkhole may be important is the water flow in the conduit is enough to evacuate the collapsed materials.

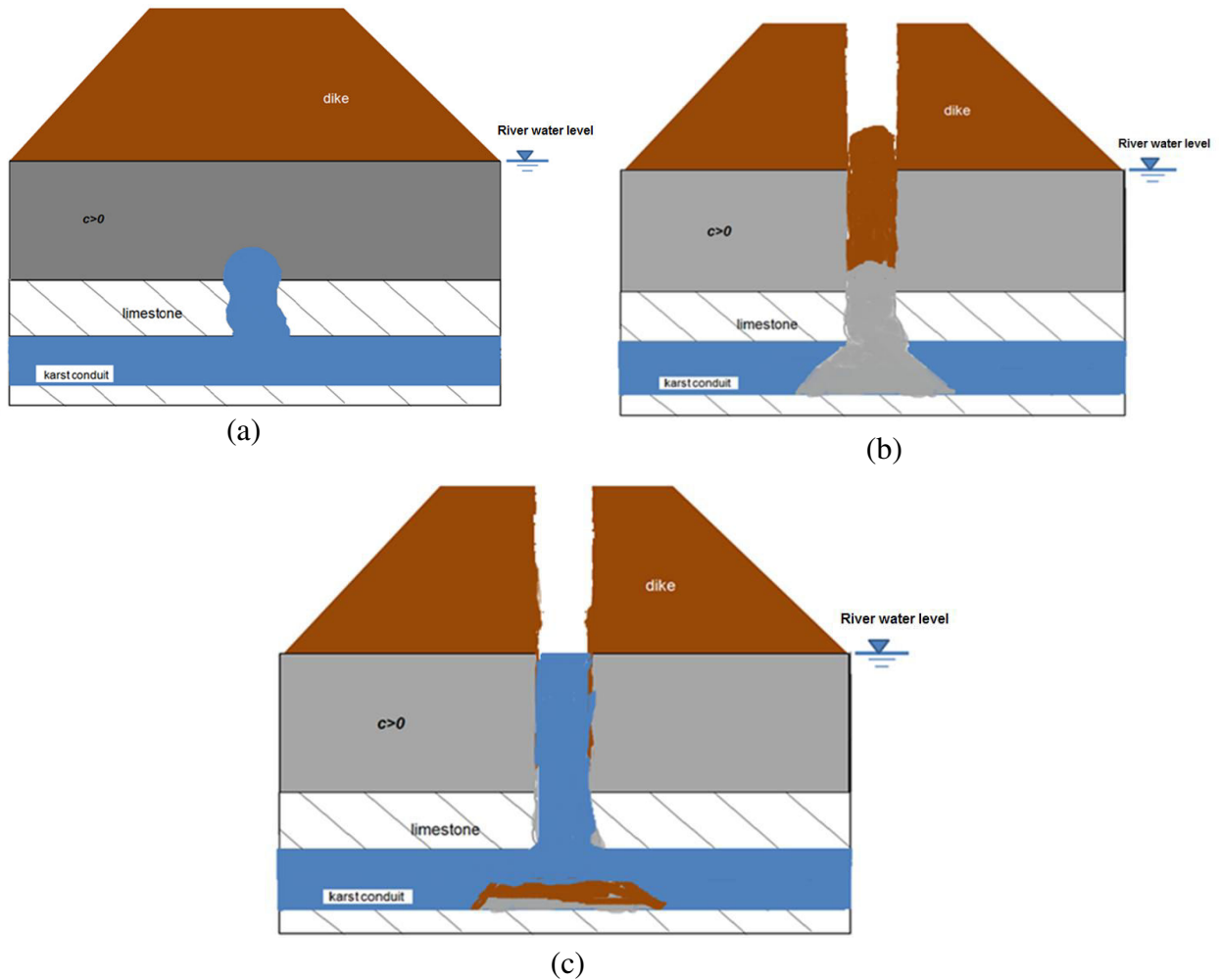


Figure 105 karstic cave connected to a karstic conduit scenario with one cohesive soil layer (a) initial state: formation of the cavity; (b) final state: with crammed chimney by the collapsed soil; (c) final state: without collapsed soil in the chimney.

6.3.3 Scenario for two alluvium layers

After the collapse of the arch cavity, the opening above it will take a frustum shape in cohesionless layers and a cylindrical shape in cohesive layers, as for isolated karstic cave scenario but with a difference in expected results in current state due to the connection between the karstic conduit and the cave: the soil blocks would breakdown in the conduit (see Figure 106). An intermediate step may be observed when a part of collapsed soil blocks is arrived inside the conduit and the residual of soils remain through the vertical opening and the chimney. If the resistance of friction force between the soil blocks inside the conduit and surface of the karstic conduit is more than the flow water force through the conduit, the water could not push the soil block. Then, the water will try to seep through the soil block and the small grains are subjected to the effect of suffusion. This operation might result in gradual landing in the soil blocks that are present through the chimney, and it can displace the removed grains of soil. When the water flow force is greater than the friction resistance force of the block soil in the conduit, the vertical opening will continue until the conduit (or in the other word, the sinkhole) will continue to open into the karstic conduit. The intermediate step

also might disappear in case of large karstic conduit cross section when the volume of the soil column is less than the volume of the karstic conduit cross section underneath the cavity or if there is a sufficient flow rate in the karstic conduit (as illustrated in Figure 104).

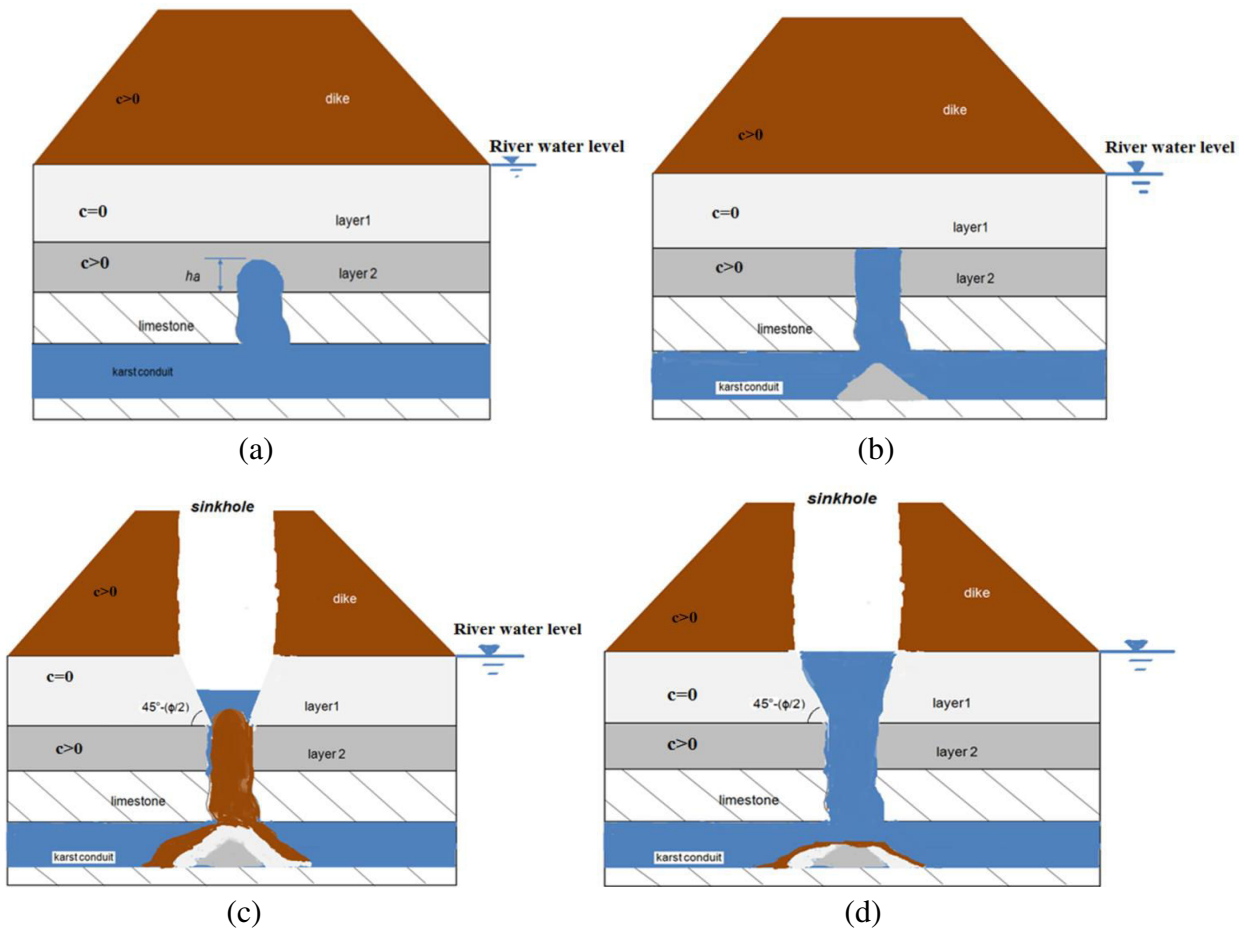


Figure 106 karstic cave connected to a karstic conduit scenario with one cohesionless soil layer; (a) initial state: formation of the cavity; (b) intermediate state: upward progression in the soil layers after the arch falling; (c) first expected final state: sinkhole occurrence at the surface of the dike with partially filled chimney by the collapsed soil. d- second expected final state: sinkhole with opened chimney.

6.4 Water pressure effect and the final form of the cavity collapse

The quick and brutal falling of soil mass due to the collapse of the cavity roof into the karstic conduit may trigger a ‘water hammer’ effect in the karstic conduit system (Lei et al. 2010 and 2013, Gao et al. 2013). When flowing water is suddenly stopped by the filling, its kinetic energy must be dissipated (Jian 1988).

Water hammer or valve closure phenomenon is so called because it is usually observed as banging sounds in pipes or conduits when a valve is suddenly closed. It is caused by sudden changes in fluid velocity and is associated to an increase of the pressure.

For estimate the form of collapse caused by the falling of roof of the cavity (sinkhole, subsidence), in state of the karstic cave connected to with the karstic conduit, the phenomenon of valve closure is considered, thinks to dynamic equilibrium between the forces, (see Figure 107) and the employment of the following simple equations:

$$\frac{F}{F_f} \geq 1 \Rightarrow \text{open sinkhole connected to the karstic conduit} \quad (6.1)$$

$$\frac{F}{F_f} < 1 \Rightarrow \text{subsidence or open sinkhole not connected to the karstic conduit} \quad (6.2)$$

Where

F is the water flow force that trying to drive the collapsed soil mass in the conduit, and Ff is the resistance force against the water flow; it depends on the mass of the soil and the surface of the karstic conduit.

6.4.1 Resistance force against the water flow Ff

The resistance force against le water flow is calculated with the Coulomb theory by multiplying the vertical load by the friction angle. As a first approximation, effect of uplift water pressure is neglected and the total weight of soil is calculated as the following:

Weight of the collapsed soil mass (W) = (total volume of chimney) * (saturated unit weight of soil)

$$W = \frac{\pi}{4} D^2 (H_d + H) \gamma_{\text{sat}} \quad (6.3)$$

The resistance force Ff against the water flow in the conduit is considered as the force due to the friction resistance. There is two friction surfaces that must be taken into account to assess the force Ff (cf. Figure 108). The first one is between the lower surface of the conduit and the collapsed soil (friction limestone-soil), while the second is between the collapsed soil itself at the top of the conduit (friction soil-soil). Hence, the resistance force Ff can be calculated by:

$$F_f = f_k W + f_s (W - V_2 \gamma_{\text{sat}}) \quad (6.4)$$

Where fk is the coefficient of friction (static) between the limestone (karst) and the soil and fs is the coefficient of friction (static) in the soil. The value of (V2γsat) refers to the weight of the collapsed soil mass in the karstic conduit V2γsat (cf. Figure 104). The force of water F, which is produced by the water flow in the karstic conduit, must be greater than Ff to push and carry out the collapsed soil mass (see Figure 108).

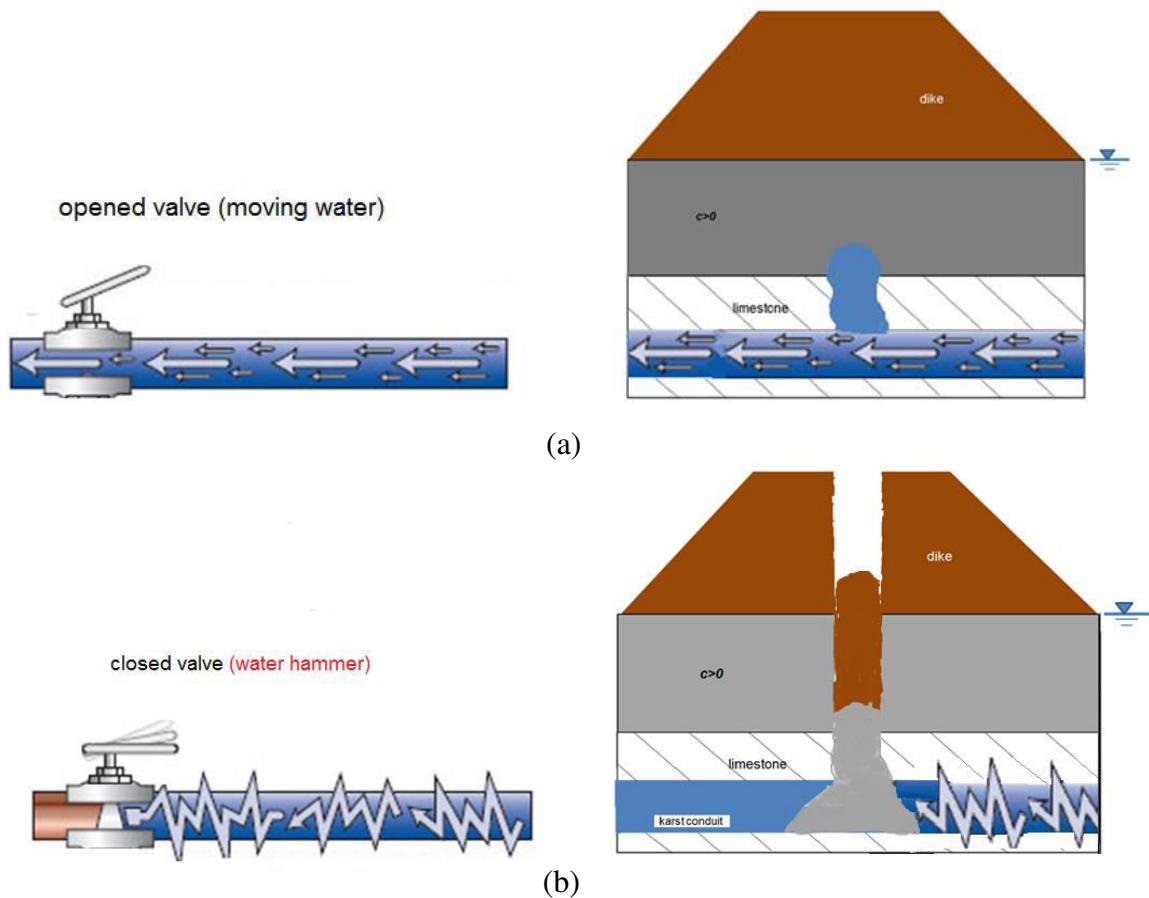


Figure 107 The phenomenon of valve closure applied in the karstic conduit. (a) before the collapse of the cavity roof. (b) after the collapse of the cavity roof and falling in the conduit.

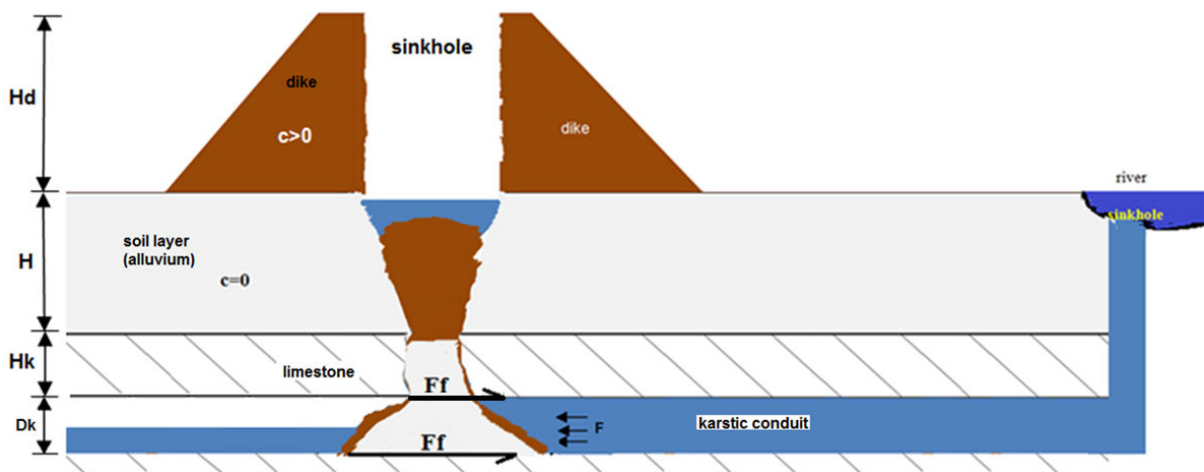


Figure 108 Scheme illustrated the forces that effect upon the collapsed soil mass in the karstic conduit.

6.4.2 water flow force F

Before the soil mass is collapsed, the water is flowing at a steady velocity of v in the conduit. When the soil mass is collapsing, the velocity decreases from v to zero in t time. The flow in

rigid conduit was considered, and the phenomenon can be described in terms of rigid column theory (Douglas 2005, Ord 2006):

$$\Delta F = ma = \rho LA \frac{dv}{dt} \quad (6.5)$$

Assuming constant deceleration of the water column ($dv/dt = v/t$), gives:

$$\Delta F = \frac{\rho LA v}{t} \quad (6.6)$$

The initial water flow force (F_i) before the collapse of the cavity can be calculated as:

$$F_i = PA \quad (6.7)$$

P = pressure in the upstream of the conduit, Pa

So, the total flow water force F :

$$F = F_i + \Delta F \quad (6.8)$$

Where:

ΔF = force due to water hammer, N

m = mass of the water column, kg

a = acceleration, m/s^2

A = conduit cross section, m^2

ρ = water density, kg/m^3

L = conduit length until the position of soil mass collapsed, m

v = water velocity, m/s

t = falling soil mass time, s

The equation 6.8 can be used to calculate the force at the moment of the collapse under the cavity in the conduit by assuming a value for the time t in equation 6.6.

6.4.3 Application to the Val d'Orléans case

To apply the previous method to the case of dike of Val d'Orléans, the shape of soil failure above the cavity was considered as a cylindrical column as shown in Figure 109. Despite the alluvium is cohesiveless underneath the dike of Val d'Orléans, the assumption of the vertical column is acceptable for small soil layer(s) thickness (Keqiang et al. 2004; Villard et al. 2009, Hassoun 2015). Moreover, this assumption is more conservative than the frustum shape assumption because the volume of failed soil in the last one would be greater and the resistance friction force F_f would increase.

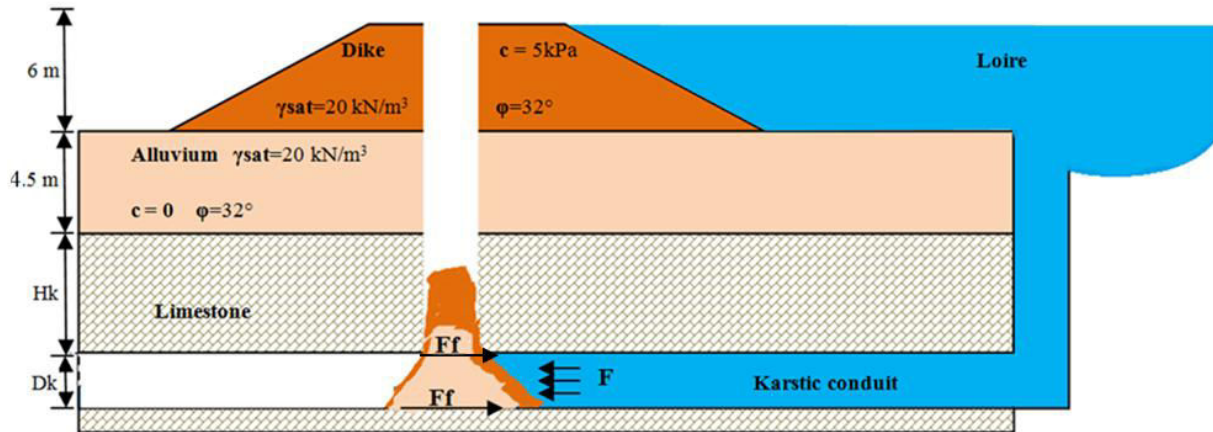


Figure 109 Considered geometry and properties to assess the force of the water flow on the collapsed soil into a karstic conduit.

Firstly, the F_f must be calculated by using (equations 6.3-6.5) and, from results of chapter 3, the critical diameter of the cavity is 1 m (maximal diameter for a stable cavity). Thus, the cavity diameter D is taken equal to 1 m to use a value that gives the greatest volume of collapsed soil. The coefficient of friction f_k of (limestone-soil) is taken equal to 0.65 and for soil, equal to the tangent of internal angle of friction ($\tan \phi$). Taking into account the dimension of the dike ($H_d=6$ m) and the alluvium layer ($H=4.5$ m) and by applying equations 6.3 to 6.5, F_f is calculated as following:

$$W = \frac{\pi}{4} D^2 (H_d + H) * \gamma_{sat} = \frac{\pi}{4} 1^2 (6 + 4.5) * 20 = \mathbf{165 \text{ kN}}$$

$$\text{Then } F_f = f_k W + f_s (W - V_2 \gamma_{sat})$$

Where V_2 (volume of the frustum fall in the conduit) can be taken equal to the volume of the cylindrical with a diameter equals to the diameter of the conduit D_k and the length is the average length of the two friction surface (D and $D+2 (D_k/\tan\phi)$). Then, the average length is equal to $(D+ D_k/\tan\phi)$.

Hence, V_2 can be calculated by assuming that the diameter of the conduit is equal to 1 m as following:

$$V_2 = \frac{\pi}{4} D_k^2 \left(D + \frac{D_k}{\tan\phi} \right)$$

$$V_2 = \frac{\pi}{4} 1^2 \left(1 + \frac{1}{\tan 32}\right)$$

$$V_2 = 2 \text{ m}^3$$

So, the resistance friction force F_f can be calculated as:

$$F_f = 0.65 * 165 + \tan(32) * (165 - 2 * 20) = \mathbf{185 \text{ kN}}$$

The hydrostatic water pressure in the karstic conduit P depends on two parameters: the depth of the karstic network, which is in the Val d'Orléans, near the Loire, from 10 to 25 m, equivalent to 100 to 250 kPa (Gombert et al. 2014) and the maximum water level during flooding that is equal to the maximum height of the dike (6 m in the Val d'Orléans). Thus, the values of pressure in the conduit are calculated with different depth of the karstic network (10, 15, 20 and 25 m). Herein, the conduit was assumed connected to Loire river with one sinkhole and with negligence any other opening in the karstic network.

Velocity values in karst are very uncertain. Measurements are quite impossible and the easiest solution is to estimate the flow velocity based on the geometry of karstic conduits. For example, in White Lady cave (UK), the calculated flow velocity is 1.21 m/s for a cross-sectional area of 7.6 m², equivalent to 3.1 m diameter (Kresic 2006). Jeannin (2001) has calculated a flow velocity of 1.3-2.0 m/s in Hölloch cave for a karstic conduit of 3.6 m² of cross-sectional area (equivalent to 2.10 m diameter). We then consider an order of magnitude of karstic flow velocity in high flow conditions around 1-2 m/s.

Thus, the velocity is taken equal to 1 and 2 m/s. The length L is assumed equal to 100 m, the diameter of the conduit D_k equal to 1 m and the time t equal to 5 sec.

By using the equations 6.6 to 6.8, the water flow force that affects the soil mass can be calculated. To show an example of the calculations, the following case is considered with a velocity taken equal to 2 m/s, a depth of the karstic network equal to 10 m and the water level of the Loire equal to the maximum level of the dike (6m). The pressure reaches then the value 160 kPa:

$$\Delta F = \frac{\rho L A v}{t} = \frac{1000 * 100 * \frac{\pi}{4} 1^2 * 2}{5} = 31.4 \text{ kN}$$

$$F_i = P A = 160 * \frac{\pi}{4} 1^2 = \mathbf{125 \text{ kN}}$$

$$\text{So, } F = F_i + \Delta F = 125 + 31.4 = \mathbf{156.4 \text{ kN}}$$

$$\frac{F}{F_f} = \frac{156.4}{185} = 0.84 < 1 \text{ (subsidence or open sinkhole not connected to the karstic conduit)}$$

Thus, a 1 m diameter karstic conduit do not lead to a water flow force that is able to push a collapsed soil mass, which resulted from the fall of a 1 m diameter soil column in the cavity.

The previous calculations were repeated for four values of the karstic network depth (10, 15, 20 and 25 m), with two values of the water velocity through it (1 and 2 m/s) and two values of the conduit diameter ($D_k = 1$ and 1.25 m). The final results of F/F_f are shown in Table 16 and Table 17. The results of Table 6.1, when the karstic conduit diameter is equal to 1 m, show

that for all the cases the water pressure is greater than the soil resistance. This leads to an open sinkhole connected to the karstic conduit (Equation 6.1). It can be observed that the initial force F_i is greater than the friction force F_f ($F_i > F_f$) for all the cases when the depth is more than 20 m. The previous result remains greater than 1 even when the force due to the water hammer ΔF is neglected. While the results show that for cases with a depth less than 15 m lead to a subsidence or open sinkhole not connected to the karstic conduit (equation 2).

When the karstic conduit D_k is equal to 1.25m (Table 17), the equations 6.3 and 6.4 were repeated to calculate the resistance friction force F_f which is then equal to 170 kN. It can be observed that all the cases the water pressure is greater than the soil resistance. This leads to an open sinkhole connected to the karstic conduit (equation 6.1). It can be observed that the initial force F_i is greater than the friction force F_f ($F_i > F_f$) for all the cases. In other words, the previous result remains greater than 1 even when the force due to the water hammer ΔF is neglected.

Hence, the decrease of the karstic conduit leads to increase the resistance friction force F_f due to the increase of the soil volume that remains in the vertical chimney which increases the friction between the soil particles in upper of the collapsed soil in the conduit. In other words; the second part of the Equation (6.4) will increase.

Table 16 the results of (F/F_f) calculations when the karstic conduit D_k is equal to 1 m ($F_f=185$ kN).

Karstic network (karstic conduit) depth (m)	P (kPa)	F _i (kN)	V=1m/s (ΔF=15.7 kN)		V=2m/s (ΔF=31.4 kN)	
			F	F/F _f	F	F/F _f
10	160	125	140.7	0.76	156.4	0.84
15	210	165	179.7	0.97	195.4	1.05
20	260	204	219.7	1.18	235.4	1.27
25	310	243.4	259.2	1.4	274.9	1.48

Table 17 the results of (F/F_f) calculations when the karstic conduit D_k is equal to 1.25 m ($F_f=170$ kN).

Karstic network (karstic conduit) depth (m)	P (kPa)	F _i (kN)	V=1m/s (ΔF=24.4 kN)		V=2m/s (ΔF=48.8 kN)	
			F	F/F _f	F	F/F _f
10	160	195.2	219.6	1.3	244	1.43
15	210	256.2	280.6	1.65	305	1.79
20	260	317.2	341.6	2	366	2.15
25	310	378.2	402.6	2.36	427	2.5

By reference to the equation (6.6), we can see that the force due to water hammer ΔF increases proportionally with length, square of diameter of the conduit and the velocity of water flow through it. Conversely, ΔF decreases with increasing the time of collapse. Thus, the diameter of the conduit (cross section area of the conduit) has the most important role in the calculation of ΔF and also in the calculation of initial water flow force F_i (see equation 6.8). Doubling the diameter value of the karstic conduit leads to increase the ΔF and F_i values four times (the other parameters are constant).

The resistance friction force F_f increases directly proportional with the height of collapsed soil column ($H+H_d$), tangent of friction angle of the collapsed soils and the square of vertical chimney diameter (D^2) as shown in equations (6.3 and 6.4). Thus, we can also say that the effect of the vertical chimney diameter is most significant. Hence, doubling the value of the vertical chimney diameter will increase the resistance friction forces F_f four times (the other parameters are constant). In other hand, we can say the karstic conduit with a diameter equals to or more than 1 m would result open sinkhole connected to the karstic conduit (with the same conditions and values that were used in our case study).

6.5 Summary

In this chapter, a methodology was proposed to estimate several possible scenarios for expected behaviour or action in critical case of a cavity underneath the centre of a dike underneath a dike. These scenarios are based on hypothesis depending on two factors: the first one is the soil type underneath the dike (cohesive or not cohesive) and the second one is the connection between the cavity and the karstic conduit. The dike was considered as formed by a cohesive soil.

The scenarios with a karstic cave connected to a karstic conduit may lead to sinkholes with a significant impact at the surface of the dike because the collapsed soil may be evacuated by the water flow in the karstic conduit. The scenarios and their consequences can be summarizing as shown in the Table 18.

Several equations are detailed to calculate the water force that act on the collapsed soil mass in the case of a cavity linked with a karstic conduit. These equations could be used to assess the water pressure whether is enough to push the collapsed soil mass in the karstic conduit or not.

Table 18 Summary of the proposed scenarios and their consequences.

Karstic cave state	Scenario of alluvium layer(s)	Consequence
Isolated (absence of the karstic conduit or not connect with it)	-Two layers (one cohesionless and one cohesive).	- A subsidence at the head of the dike may be appeared. - Likelihood of overflow in flood period.
	- One cohesionless layer.	
	- One cohesive layer.	- Failure in the head of the dike with open sinkhole, which diameter is equal to the diameter of the original collapsed cavity and depth depending on the karstic cave volume.
Connected to a karstic conduit underneath	- Two layers (one cohesionless and one cohesive).	Failure in the head of the dike with open sinkhole, which diameter is more than the diameter of the original collapsed cavity: -It is <u>not connected</u> to the karstic conduit (If the collapsed soils in the karstic conduit can't be evacuated by flow). -It is <u>connected</u> to the karstic conduit (if all collapsed soils dropped in the conduit due to force of water flow in the conduit).
	-One cohesionless layer.	
	- One cohesive layer.	Failure in the head of the dike with open sinkhole, which diameter is equal to the diameter of the original collapsed cavity: -It is <u>not connected</u> to the karstic conduit (If the collapsed soils in the karstic conduit can't be evacuated by flow). -It is <u>connected</u> to the karstic conduit (if all collapsed soils dropped in the conduit due to force of water flow in the conduit).

6.6 References

- D.D.T. Haute-Garonne Service Risques et Gestion de crise 2014, Plan de prévention des risques inondations- Vallée De L'Hers-Mort, GRONTMIJ environnement et infrastructures agence de Montpellier, Dossier GEI O 001 08 077, 40 pp.
- Douglas J. F., Gasoriek J. M., Swaffield J., Jack L., 2005, Fluid Mechanics (5th Edition), Pitman Publishing Limited, England, Ch. 20, pp. 674-715.
- Dreybrodt, W., Siemers, J., 2000, Cave evolution on two-dimensional networks of primary fractures in limestone. In: Klimchouk, A.B., Ford, D.C., Palmer, A., Dreybrodt, W. (Eds.). Speleogenesis: Evolution of Karst Aquifers. National Speleological Society, Huntsville, pp. 201–211.
- Drumm E.C., Kane W.F. and Yoon C.J., 1990, Limit plasticity to the stability of sinkholes, *Engineering Geology*, 29, Elsevier, pp 213-225.
- Dubois C., Quinif Y., Baele J.-M., Barriquand L., Bini A., Bruxelles L., Dandurand G., Havron C., Kaufmann O., Lans B., Maire R., Martin J., Rodet J., Rowberry M.D., Tognini P., Vergari A., 2014, The process of ghost-rock karstification and its role in the formation of cave systems. *Earth-Science Reviews*, Volume 131, April 2014, Pages 116–148, doi:10.1016/j.earscirev.2014.01.006
- Gao Y., Luo W., Jiang X., Lei M., Dai J., 2013, Investigations of large scale sinkhole collapses, Laibin, Guangxi (China), 13th sinkhole conference, New Mexico, USA, pp 327-331.
- Gombert P., Orsat J., Mathon D., Alboresha R., Al Heib M., Deck O., 2014, Rôle des effondrements karstiques sur les désordres survenus sur les digues de Loire dans le Val d'Orléans (France). *Bull Eng Geol Environ*, DOI 10.1007/s10064-014-0594-8. pp. 125–140.
- Hassoun M. 2015, Analytical and experimental approach in laboratory of the use of geosynthetics to reduce the risk associated with the collapse of underground cavity, master thesis, university of Grenoble.
- Jeannin P.Y., 2001, Modelling flow in phreatic and epiphreatic karst conduits in the Hölloch cave (Muotatal, Switzerland). *Water resources research*, vol. 37, n°. 2, 191-200.
- Jian C., 1988, Karst collapse in cities and mining areas, china, *Environmental Geology and Water Sciences* Vol. 12, No. 1, pp. 29-35.
- Keqiang H, Wang B, Zhou D 2004, Mechanism and mechanical model of karst collapse in an over-pumping area, *Environmental Geology* (2004) 46, pp 1102-1105.
- Kresic N., 2006, *Hydrogeology and Groundwater Modeling*, Second Edition CRC Press, USA.

- Lei M., Jiang X., Guan Z., 2013, Emergency investigation of extremely large sinkholes, Maohe, Guangxi, China, pp. 293-297.
- Lei M., Jiang X., Li Y., Meng Y., Dai J., Gao Y., 2010, Predicting sinkhole collapse by long-term monitoring of karst water pressure in Zhemu (China), *Geologically Active: Proceedings of the 11th IAEG Congress*, Auckland, New Zealand, pp 355-362.
- Mesta P., 1998. Modèles d'éléments finis et problèmes de convergence en comportement non linéaire. *Bulletin des laboratoires des ponts et chaussées*, pp. 45-60.
- Ord S.C., 2006, How to predict it and prevent it damaging pipelines and equipment, symposium series no. 151, IChemE, UK, 20 pp.
- Quinif Y. & Bruxelles L., 2011, L'altération de type « fantôme de roche » : processus, évolution et implications pour la karstification, *Géomorphologie : relief, processus, environnement*, 4/2011 | 2011, URL : <http://geomorphologie.revues.org/9555> ; DOI : 10.4000/geomorphologie.9555.
- Vergari A., Quinif Y. 1997, Les paléokarsts du Hainaut (Belgique). *Geodinamica Acta*, 10, 4, 175-187.
- Villard P., Chevalier B., Le Hello B., Combe G. 2009, Coupling between finite and discrete element methods for the modelling of earth structures reinforced by geosynthetic. *Computers and Geotechnics* Volume 36, Issue 5, pp. 709–717

7.1 General conclusion

The main objective of this thesis is to investigate the interaction mechanisms between a cavity and an earthen dike (levee) constructed above the karstic area. The numerical data are based on the in situ observations from Val d'Orléans area, located in the Loire valley (France). This is a karstic area where several hundreds of sinkholes appeared due to a highly karstified limestone layer. As this layer is overlain by several meters of alluvium, the underground cavities cannot be known at the surface until they collapse. This urbanized area is protected from the river floods by dikes. The sinkholes have already affected houses, highways and dikes.

The flood of the valley due to the collapse of the dike presents a major hazard for land use and the population. The role of the karst in such event is still questionable due to the different uncertainties and unknown factors. Nowadays, the risk assessment of the dike “study of dangers” was carried out without taking into account the role of the cavities underneath the dike.

Herein, we aim to understand the role of the cavity in the instability scenario and to evaluate the reverse impact between the dike and the cavity. In addition, we worked to propose an analytical tool (engineering and operational tool) allowing the assessment of the hazard level when the likelihood of a cavity is considering as high level.

To fulfil these objectives, the state of the art showed the complexity of the mechanism involved in the cavity collapse, the role of water presence, and the nature of the alluvium layer and the bed rock. The sinkhole mechanism was considered as the main issue and both the mechanical behaviour and the water effect were studied.

The stability of both the cavity and the dike were analysed using analytical approaches. Moreover, the numerical modelling (2D and 3D) was carried out to highlight the cavity-dike interaction. The data concerning the mechanical properties was collected from different in situ investigations and laboratory tests. The average values of the geotechnical parameters were adopted to be able to generalize the results.

The study was divided into two main topics:

- The first topic aimed to: i) Investigate the influence of the dike on the cavity stability, ii) Modify an analytical model used to assess the stability of an isolated cavity stability by taking into account the influence of the dike load, and iii) Investigate the influence of the location of the cavity relatively to the dike, the geometric and geotechnical parameters of the alluvium soil and the diameter of the cavity.
- The second topic aimed to: i) Evaluate the impact of the cavity on the stability of the slope dike by studying the influence of the presence of a cavity underneath the dike, ii) Modify the Fellenius method used to assess the stability of the dike by taking into account the influence

of a cavity in the vicinity of the dike, and iii) Calculate the safety factor of the slope stability by taking into account the stresses modification induced by the cavity underneath the dike.

Thanks to the analytical studies, the sinkhole hazard and the slope instability were identified and highlighted.

After that, some numerical modelling was carried out to verify the validity of the assumptions and to trust results got from the analytical models. The finite element CESAR-V6 (2D and 3D) software was used. We compared three approaches to assess the interaction between the dike and the cavity based on stresses, displacements and the plastic strain norm. The plastic strain norm presents the best and most global indicator for quantifying the influence of the cavity on the dike and the dike-cavity interaction.

The main achievements and results of this thesis are summarized as follow:

Impact of the dike on the cavity stability:

- The risk of the cavity collapse can be increased significantly by the presence of the dike. The collapse could occur in the extreme flood scenario for small cavity diameter of 1 m located underneath the maximum height of the dike (i.e. under the head of the dike). The critical diameter of the cavity depends on the thickness of the alluvium layer and its mechanical characteristics.
- The analytical approach can be recommended to assess the hazard zone using the following parameters: diameter of the cavity (D), the thickness of the alluvium layer (H). The following ratios (H/D) may be recommended in the case of Val d'Orléans:
 - The likelihood of the sinkhole is negligible when the ratio $H/D > 6.5$;
 - The likelihood of the sinkhole is high when the ratio $H/D < 1.65$;
 - The likelihood of sinkhole is variable for the range: $1.65 \leq H/D \leq 6.5$.

Impact of the cavity on the dike slope stability:

- The presence of the cavity underneath the dike slope reduces the safety factor of the dike slope stability, especially in the saturation state (i.e. during a major flood) in our case study.
- A cavity of 1 m diameter and located at a vertical distance about 3.5 m from the slip surface could reduce the slope safety factor, while a cavity of 2 m of diameter and located at a vertical distance about 3 m could lead to a slope failure in the dike of Val d'Orléans (for adopted coefficient of lateral earth pressure $K= 0.5$).

Numerical modelling:

- Most of the numerical calculation results match the analytical results especially in the case of the cavity effect upon the dike slope. Hence, the results of the numerical and analytical methods indicate that a cavity with diameter equals to 2 m and located at vertical distance about 3 m could affect the dike slope stability.
- The results of the dike effect upon the stability of a cavity located underneath the dike centre showed that the roof of the cavity with a 0.5 m of the diameter could collapse whereas the effect of the cavity with a 2 m diameter could reach the head of the dike.
- The cavity failure mechanism resulting from the numerical model could be divided into two parts: the first one is the collapse of the immediate roof of the cavity, and the second one is the failure of the soil above the roof of the cavity that may occurred in several phases until the failure reaches the (dike) surface and the sinkhole appears.
- The results of the dike effect on the cavity stability demonstrated that the cavity position under the centre of the dike is more dangerous than under its slope (for the same diameter). In addition, the plastic strains around a cavity increase due to the dike presence above it due to the effect of its additional weight. The water in flooding scenario can increase the plastic strain zone around the cavity as well as on the surface of the dike, which can accelerate the collapse phenomenon.
- The numerical methods (as finite elements method in CESAR) require an accurate selection of the mesh dimensions and a careful interpretation of the results. Some calculations may not converge. Thus, these methods need high practice and experience.

Expected scenarios due to the collapse of a cavity underneath a dike:

Several collapse scenarios are expected, for an existing critical cavity underneath the centre of a dike built with a cohesive material. These scenarios are based on hypothesis depending on two different factors: i) the soil type underneath the dike (cohesive or non-cohesive), and ii) the presence of a connection between the cavity and the karstic conduit.

- The scenarios with a karstic cave connected to a karstic conduit may lead to sinkholes with a significant impact at the surface of the dike, because the collapsed soil may be evacuated by the water flow in the karstic conduit.
- Several equations are detailed to calculate the water force that acts on the collapsed soil mass in the case of a cavity linked with a karstic conduit. These equations could be used to assess whether the water pressure is enough to push the collapsed soil mass in the karstic conduit or not.

7.2 Perspectives

Even if a progress has been achieved during the thesis, different aspects always need to be investigated to determine the influence of the cavity upon the dike stability. We tried herein to list some possible perspectives:

- Improve the knowledge of the dike-cavity interaction using a physical model that includes a dike and a cavity. Large experience exists for studying the dams and dikes but without the cavity influence.
- There is not enough information about the karstic conduits under the dike, so it is important to investigate their properties (dimensions, water velocity, length, etc.).
- Geophysical and in-situ investigation should be used to compare the analytical results with the real dimensions of cavities, dikes and the alluvium thickness.
- Study the influence of the dynamic loads (e.g. the cars movement on the dike when it is used as a road) in the future to develop the analytical approaches, because the current study neglected them.
- The 3D modelling assumes that the cavity is a cylindrical segment rather than spherical. Influence of thus choice could be investigated by modelling a spherical cavity to check the results of the 2D and 3D models.
- Thanks to the numerical modelling capabilities, the influence of the cavity shape (e.g. ellipse) should be studied and compared with the circular shape to establish a specific model for all cavity shapes.
- The mitigation techniques are also a major topic following the understanding of the phenomenon. The reinforcement of the dike foundation, that aims reducing the risk, should be integrated in such an analysis.

7.1 Conclusion générale

L'objectif principal de cette thèse est d'étudier les mécanismes d'interaction entre une cavité d'origine karstique et une digue en terre (levée) construit sur des terrains karstifiés. Les données numériques sont basées sur les observations in situ du Val d'Orléans, situé dans la vallée de la Loire (France). La zone urbanisée du Val d'Orléans est protégée contre les crues du fleuve par des digues. C'est une zone urbanisée, où plusieurs centaines de fontis sont apparus en raison d'une couche de calcaire très karstifiée. Comme cette couche est recouverte de plusieurs mètres d'alluvions, les cavités souterraines ne peuvent être facilement identifiées depuis la surface jusqu'à ce qu'elles s'effondrent.

L'inondation du Val d'Orléans en raison de l'effondrement de la digue peut présenter un risque majeur pour l'utilisation des terrains et la sécurité de la population. L'influence du karst sur l'efficacité et la résistance des digues est encore discutable en raison des différentes incertitudes et facteurs inconnus. Actuellement, "l'étude de dangers" de la digue a été effectuée sans tenir compte du rôle des cavités potentiellement situées en dessous de la digue.

Ici, nous cherchons à comprendre le rôle d'une cavité dans le scénario d'instabilité de la digue et d'évaluer l'impact inverse entre la digue et la cavité. Par ailleurs, nous proposons un outil d'analyse opérationnel permettant d'évaluer le niveau de danger lorsque la probabilité de présence d'une cavité est jugée significative.

Pour pouvoir réaliser ces objectifs, l'état de l'art a montré la complexité des mécanismes impliqués dans l'effondrement d'une cavité, le rôle de la présence de l'eau et l'influence de la nature de la couche d'alluvions et de la roche sous-jacente. Le mécanisme de fontis a été considéré comme le principal problème. Il a été étudié du point de vue de leur comportement mécanique et de l'effet de l'eau.

La stabilité de la cavité et la digue ont été analysés en utilisant des approches analytiques. Par ailleurs, la modélisation numérique (2D et 3D) a été utilisée pour mettre en évidence l'interaction entre la cavité et la digue. Les données concernant les propriétés mécaniques ont été collectées à partir de différentes investigations in situ et de tests en laboratoire. Les valeurs moyennes des paramètres géotechniques ont été adoptées pour pouvoir généraliser les résultats.

L'étude a été divisée en deux thèmes principaux :

- Le premier thème vise à : i) Etudier l'influence de la digue sur la stabilité de la cavité, ii) Modifier un modèle analytique utilisé pour évaluer la stabilité d'une cavité isolée en tenant compte de l'influence de la charge de la digue, et iii) Etudier l'influence de la localisation de la cavité par rapport à la digue, des paramètres géométriques et géotechniques du sol alluvial et du diamètre de la cavité.

- Le deuxième thème vise à : i) Evaluer l'impact de la cavité sur la stabilité de la pente de la digue, ii) Modifier la méthode de Fellenius utilisée pour évaluer la stabilité de la digue en tenant compte de l'influence d'une cavité au voisinage de la digue, et iii) Calculer le

coefficient de sécurité de la pente en prenant en compte la modification des contraintes induites par la cavité au-dessous de la digue.

Les résultats de ces études analytiques ont permis de mettre en évidence la possibilité de remontée d'un fontis et son influence sur la stabilité de la pente de la digue.

Ensuite, une modélisation numérique a été effectuée pour vérifier la validité des hypothèses et comparer les résultats à ceux obtenus à partir des modèles analytiques. Le logiciel aux éléments finis CESAR-V6 (2D et 3D) a été utilisé. Nous avons comparé trois critères pour évaluer l'interaction entre la digue et la cavité : les contraintes, les déplacements et la norme de la déformation plastique. La norme de la déformation plastique apparaît le meilleur indicateur pour quantifier l'influence de la cavité sur la digue et l'interaction digue-cavité.

Les principales réalisations et les résultats de cette thèse sont les suivants :

Impact de la digue sur la stabilité de la cavité :

- Le risque d'effondrement de la cavité peut être considérablement augmenté par la présence de la digue. L'effondrement pourrait se produire dans le scénario de crue extrême pour des diamètres de la cavité de 1 m situés sous la hauteur maximale de la digue (sous la tête de la digue). Le diamètre critique de la cavité dépend de l'épaisseur de la couche d'alluvions et de ses caractéristiques mécaniques.
- La méthode d'analyse peut être recommandée pour évaluer la zone de danger en utilisant les paramètres suivants : le diamètre de la cavité (D), l'épaisseur de la couche d'alluvions (H). Les rapports suivants (H / D) peuvent être recommandés dans le cas du Val d'Orléans :
 - La probabilité de remontée des fontis est négligeable lorsque le rapport $H/D > 6.5$;
 - La probabilité de remontée des fontis est élevée lorsque le rapport $H/D < 1.65$;
 - La probabilité de remontée des fontis est variable pour la gamme $1.65 \leq H/D \leq 6.5$.

Impact de la cavité sur la stabilité de la pente de la digue :

- La présence de la cavité sous la pente de la digue réduit le facteur de sécurité de la pente, en particulier dans l'état saturé (par exemple au cours d'une inondation majeure) dans notre étude de cas.
- Une cavité de 1 m de diamètre, située à une distance verticale d'environ 3,5 m de la surface de glissement pourrait réduire le facteur de sécurité de la pente, tandis qu'une cavité de 2 m de diamètre située à une distance verticale d'environ 3 m peut conduire à un effondrement de la pente de la digue du Val d'Orléans (pour un coefficient de poussée adopté de $K = 0.5$).

La modélisation numérique :

- La plupart des résultats des calculs numériques sont cohérents avec les résultats analytiques en particulier dans le cas de l'effet d'une cavité sur la pente de la digue. Au final, les résultats des méthodes numériques et analytiques indiquent qu'une cavité

avec un diamètre est égal à 2 m et situé à une distance verticale d'environ 3 m pourrait affecter la stabilité de la pente de la digue.

- Les résultats de l'effet de la digue sur la stabilité d'une cavité située au-dessous du centre de la digue ont montré que le toit d'une cavité de 0,5 m de diamètre pourrait s'effondrer tandis que l'effet d'une de 2 m de diamètre pourrait atteindre la tête de la digue.
- Le mécanisme de rupture de la cavité résultant de la modélisation numérique pourrait être divisé en deux parties : la première est l'effondrement du toit immédiat de la cavité, et le second est l'effondrement du sol au-dessus du toit de la cavité qui peut se produire en plusieurs phases jusqu'à ce que l'effondrement atteigne la surface de la digue.
- Les résultats de l'effet de la digue sur la stabilité de la cavité ont démontré que la position de la cavité sous le centre de la digue est plus dangereuse que sous sa pente (pour le même diamètre). En plus, les déformations plastiques autour d'une cavité augmentent en raison de la présence de la digue et de l'effet de son poids supplémentaire. L'eau dans le scénario d'inondation peut augmenter la zone de déformation plastique autour de la cavité ainsi que sur la surface de la digue, ce qui peut accélérer le phénomène de l'effondrement.
- Les méthodes numériques (comme méthode des éléments finis dans CESAR) nécessitent une sélection précise des dimensions du maillage et une interprétation attentive des résultats. Certains calculs peuvent ne pas converger. Par conséquent, l'utilisation de ces méthodes requiert une grande pratique et de l'expérience.

Scénarios prévus en raison de l'effondrement d'une cavité sous une digue :

Plusieurs scénarios d'effondrement sont attendus, pour une cavité critique existante sous le centre d'une digue construite avec un matériau cohésif. Ces scénarios sont basés sur des hypothèses en fonction de deux facteurs : i) la nature cohérent ou non cohérent du sol sous la digue, et ii) la présence d'un lien entre la cavité et le conduit karstique.

- Les scénarios avec une cavité karstique reliée à un conduit karstique aboutissent à des fontis ayant un impact significatif sur la surface de la digue. Dans ce cas, le sol effondré peut être évacué par l'écoulement de l'eau dans le conduit karstique.
- Plusieurs équations sont détaillées pour calculer la force de l'eau qui agit sur la masse du sol effondré dans le cas d'une cavité reliée à un conduit karstique. Ces équations peuvent être utilisées pour évaluer si la pression d'eau est suffisante pour pousser la masse de sol effondré dans le conduit karstique ou non.

7.2 Perspectives

Même si des progrès ont été réalisés au cours de la thèse, différents aspects doivent toujours être étudiés pour déterminer l'influence de la cavité sur la stabilité de la digue. Nous avons formulé quelques perspectives possibles :

- Améliorer la connaissance de l'interaction digue-cavité à l'aide d'un modèle physique qui comprend une digue et une cavité. Des exemples nombreux existent pour l'étude des barrages et des digues, mais sans l'influence de la cavité.
- Il n'y a pas suffisamment d'informations sur les conduits karstiques sous la digue, il est donc important d'étudier leurs propriétés (dimensions, la vitesse de l'eau, longueur, etc.).
- Des investigations géophysiques in-situ devraient être utilisées pour comparer les résultats de l'analyse avec les dimensions réelles des cavités, des digues et l'épaisseur des alluvions.
- Etudier l'influence des charges dynamiques, comme par exemple l'influence de la circulation de voitures sur la digue quand elle est utilisée comme une route.
- La modélisation 3D suppose que la cavité est un segment cylindrique au lieu d'une cavité sphérique. L'influence de ce choix pourrait être étudiée par la modélisation d'une cavité sphérique pour vérifier les résultats des modèles 2D et 3D.
- Grâce aux capacités de modélisation numérique, l'influence de la forme de la cavité (par exemple de l'ellipse) devrait être étudiée et comparée avec la forme circulaire afin d'établir un modèle spécifique pour toutes les formes de cavité.
- Les techniques de remédiation sont également un sujet majeur suite à la compréhension du phénomène. Le renforcement de la fondation de la digue, qui vise la réduction du risque, devrait être intégré dans une telle analyse.

A.1 Presentation of UDEC

UDEC (Universal Distinct Element Code) is based on the discrete element method. The material is presented by an assembly of independent blocks. They can be rigid or deformable blocks.

The representation of the interface between blocks relies on sets of point contacts (Figure A-1 and Figure A-2). Adjacent blocks can touch along a common edge segment or at discrete points where a corner meets an edge or another corner. At each contact (joint), the mechanical behaviour of contacts and blocks is represented by force-displacement relationships. The blocks can be displaced and rotated. The contact displacements are defined as the relative displacement between two blocks at the contact point. In the elastic range, contact forces and displacements are related through the contact stiffness parameters (normal and shear stiffness).

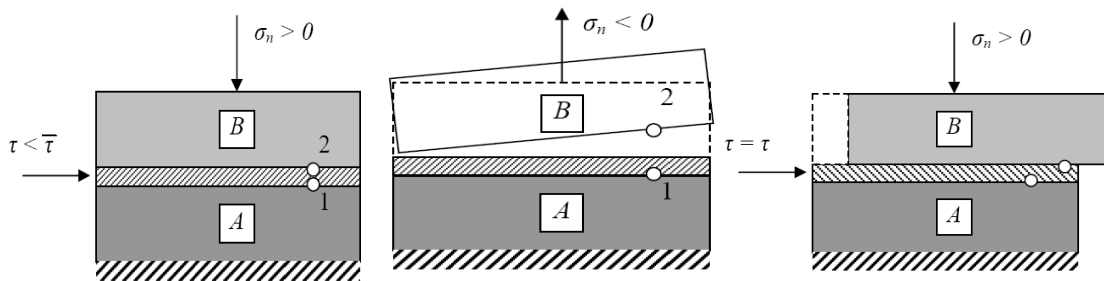


Figure A-1 Coulomb slip model with residual strength (shear and normal behaviour).

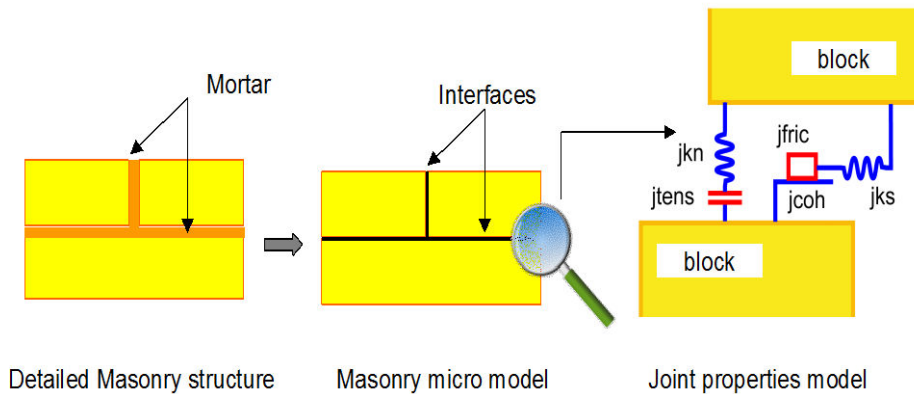


Figure A-2 Interface model code (jkn: joint normal stiffness, jks joint shear stiffness, jcoh: joint cohesion, jf ric: joint friction angle and jtens joint tensile strength).

The mechanical behaviour of joints is described as follows, (Itasca, 2000):

The response to normal loading is expressed by the normal stiffness, jkn and normal displacement Δu_n :

$$\Delta \sigma_n = j_{kn} \Delta u_n \quad (\text{A-1})$$

The shear stress increment is calculated as:

$$\Delta\tau = jks \Delta us \quad (A-2)$$

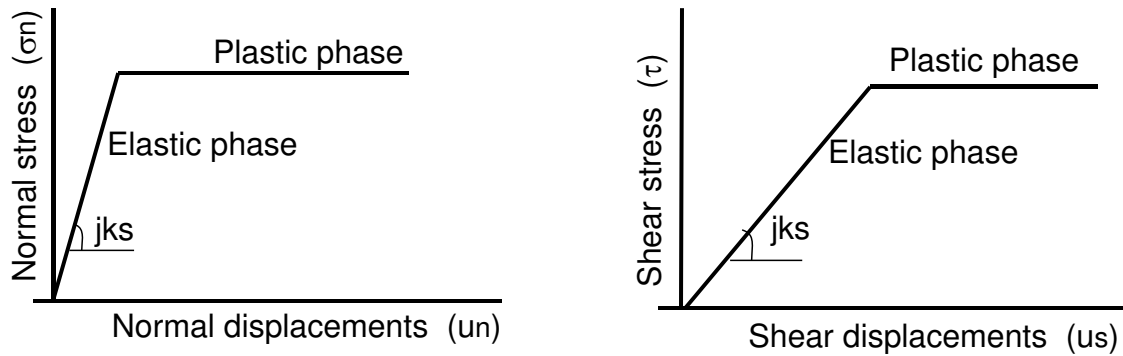


Figure A-3. Joint behaviour (respectively) under normal and shear loads.

Where jks , jkn are joint (contact) shear stiffness and normal stiffness and Δus and Δun are shear displacement and normal displacement of joint. The value of jkn will depends on the contact area ratio between the two joint surfaces and the relevant properties of the joint filing material, if present (Souley, 1993). The value of jks depends on the roughness of the joint surface, which can be determined by the distribution, amplitude, and inclination of the asperities on the friction along the joint, the cohesion due to interlocking, and the strength of the filing material, if present. Figure A-3 shows the evolution of joint behaviour under normal and shear loads. The following parameters are used to define the mechanical behaviour of the contacts: the normal stiffness (kn), shear stiffness (ks), friction angle (ϕ), cohesion (c) and tensile strength (Rt). To approximate a displacement-weakening response, the Coulomb slip model with residual strength (Figure A-4) is used.

$$\tau = coh + \sigma_n \tan fric \quad (A-3)$$

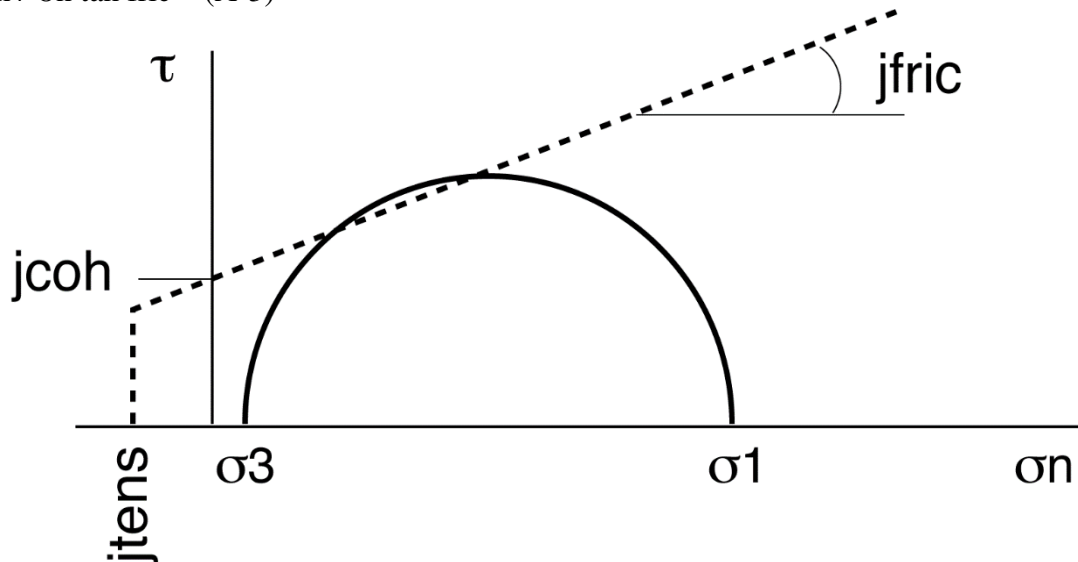


Figure A-4. Elasto-plastic Mohr-Coulomb joint model, code ($jcoh$: joint cohesion, $jfric$: joint friction angle and $jtens$ joint tensile strength) (Itasca, 2000, UDEC).

When the forces (stresses) are over the Mohr-Coulomb criteria, the blocs can separate or slide. Blocs can be deformed if the deformable blocks option is adopted.

A.2 References

Itasca, 2000. UDEC Universal Distinct Elements Code Manual. Continuously yielding joint model. Itasca Consulting Group Inc., pp. 1–16.

Souley M., 1993. Modelling of jointed rock masses by distinct element method, influence of the discontinuities constitutive laws upon the stability excavation. Doctoral thesis of (Institut national poly technique de Lorraine), pp.75-136.

The c-phi reduction method was used to calculate the safety factor (SF) of slope stability by using CESAR software (version 6). Several models have been formed by adding a cavity to show the effect of cavity upon the slope stability with using the case study in this work (dike of Val d'Orléans). The cavity was adding in elastic zone to neglect the effect of plasticity around the cavity on the safety factor value. The results indicated that the c-phi reduction method not take into account the impact of elastic zones. Thus, the value of safety factor is for the elastic-plastic zone. All the following results are in form of deformation plastic zone to show the slip slope surface.

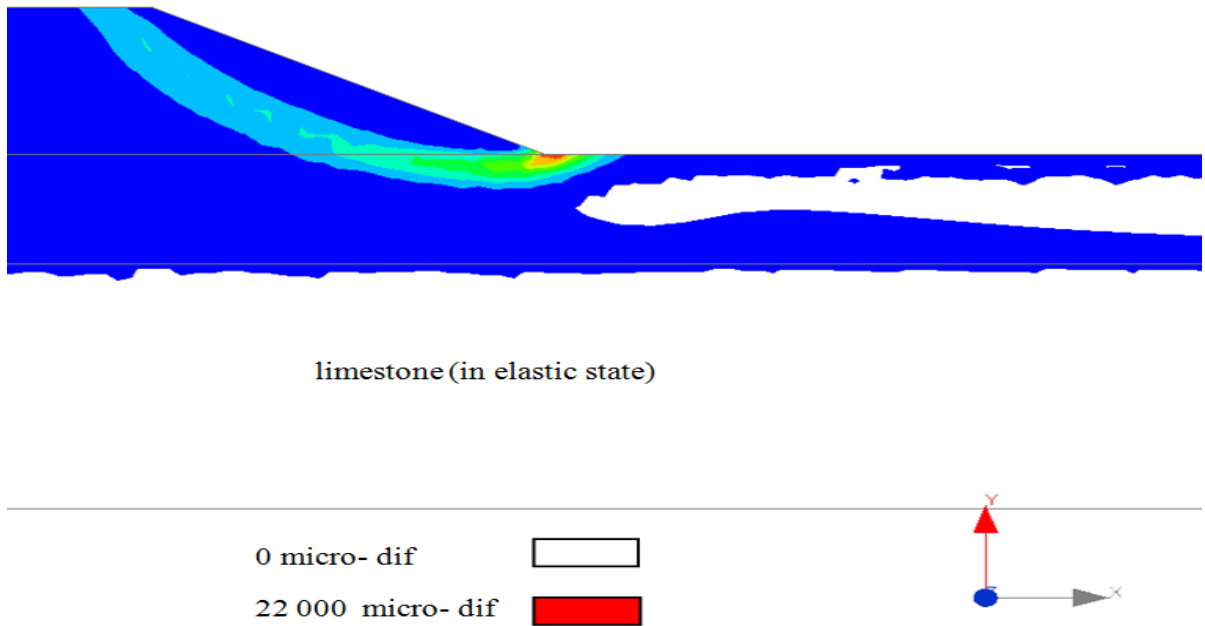
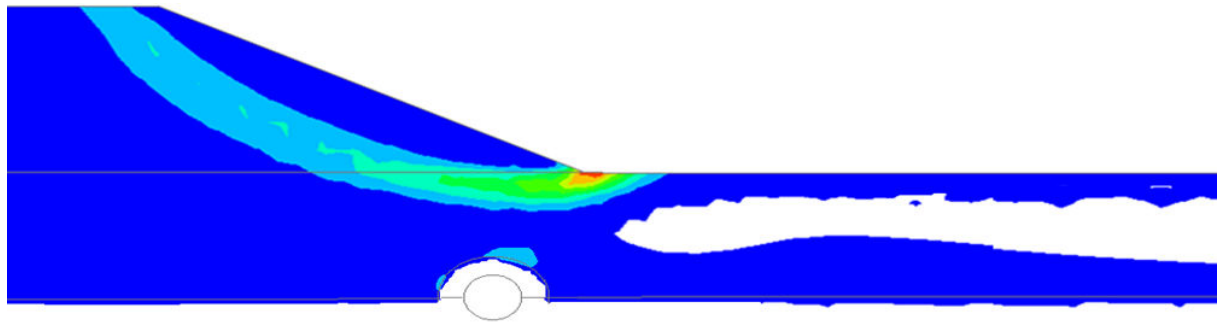



Figure B-1 Result of deformation plastic strain of dike of Val d'Orléans in normal state (without cavity) and the SF= 1.96



limestone (in elastic state)

0 micro- dif 

22 000 micro- dif 

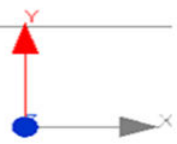
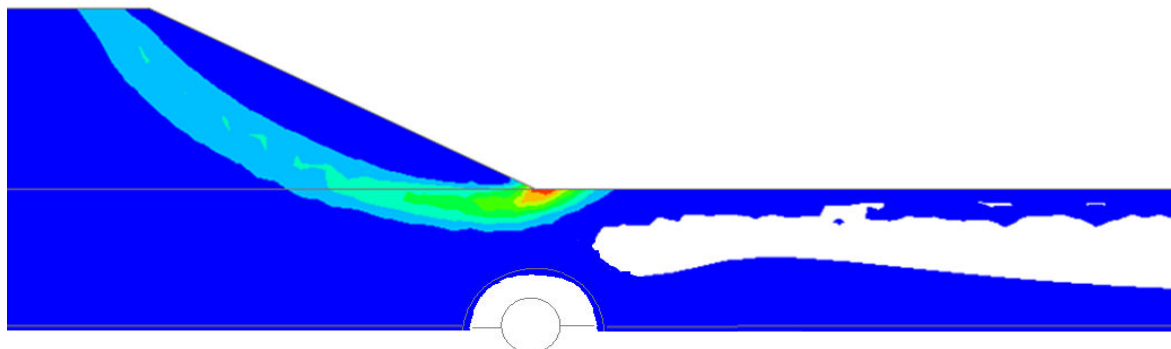



Figure B-2 Cavity 2 m of the diameter underneath the dike slope nearby the toe in with thin elastic zone around the cavity (1 m) and SF= 1.97.



limestone (in elastic state)

0 micro- dif 

22 000 micro- dif 

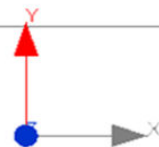
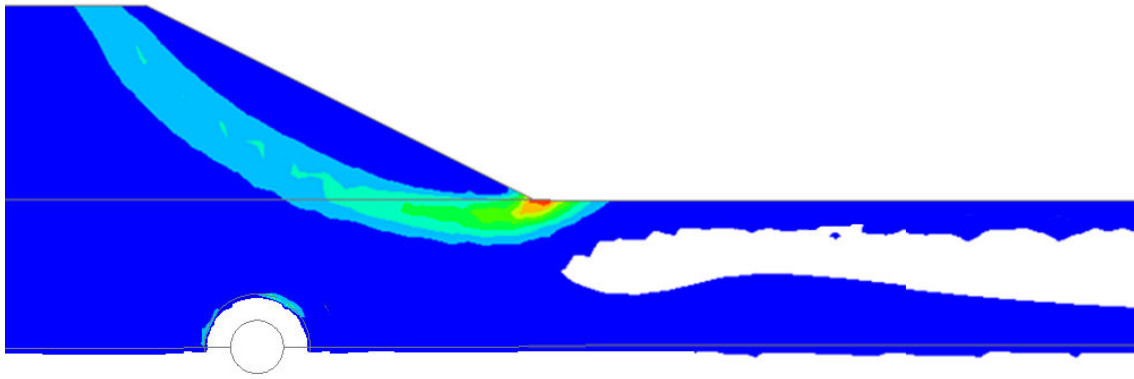


Figure B-3 Cavity 2 m of the diameter underneath the dike slope under the toe with elastic zone around the cavity (1 m) and SF= 1.96.



limestone (in elastic state)

0 micro- dif



22 000 micro- dif

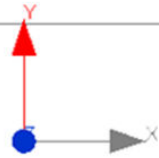
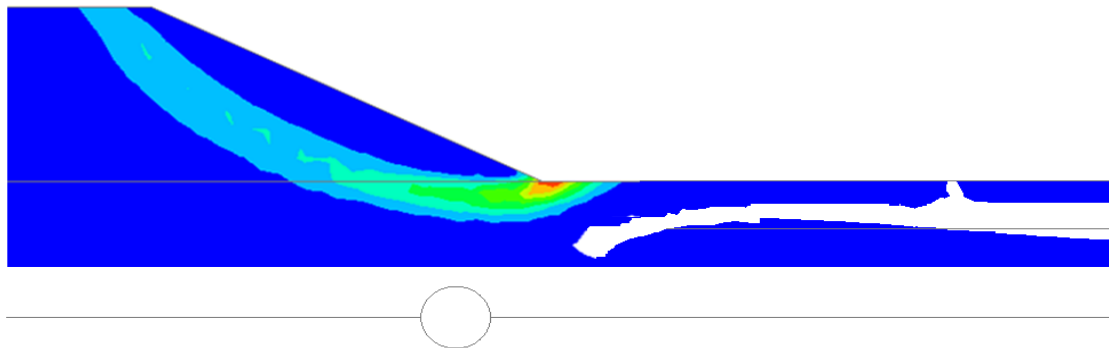
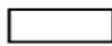


Figure B-4 Cavity 2 m of the diameter underneath the middle of dike slope with elastic zone (1 m) around the cavity and SF= 1.97.



limestone (in elastic state)

0 micro- dif



22 000 micro- dif

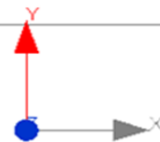


Figure B-5 Cavity 2 m of the diameter underneath the dike slope nearby the toe with strip elastic zone (2 m) in the alluvium layer and SF= 1.97.

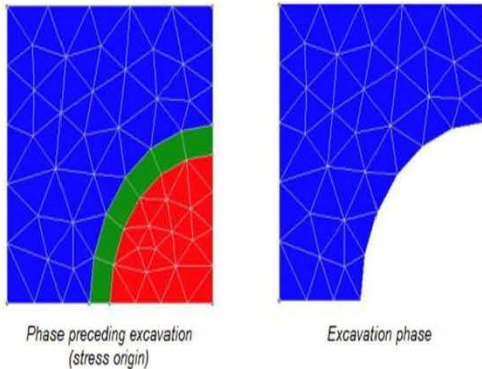
The lambda option in CESAR is very useful to excavate a cavity and apply stresses from a previous calculation. The appendix was taken from the (Help) of CESAR-V5 to explain the main idea of the option. We used it for the creation of the cavity under the dike. The lambda option needs to use MCNL option in the calculation.

Mechanics: Confining stress removal

This tool enables assigning "confinement-removal"-type surface forces on external segments of visible regions.

The tool is only activated for load cases associated with a "Phasing"-type model.

Confinement-removal forces are used to model the influence of an excavation on the adjacent soil.

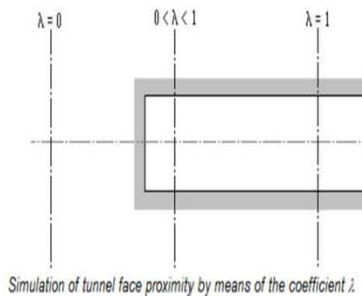


In order to model an excavation, one conventional method consists of applying surface forces on the set of segments that become "external" during the excavation-simulation phase (i.e. the Excavation Phase). These applicable surface forces can be expressed as follows:

$$\begin{Bmatrix} T_x \\ T_y \end{Bmatrix} = -\lambda \begin{Bmatrix} \sigma_{xx}^0 n_x + \sigma_{xy}^0 n_y \\ \sigma_{yx}^0 n_x + \sigma_{yy}^0 n_y \end{Bmatrix}$$

with:

- T_x, T_y : Surface force vector components (confinement-removal) applicable at a point of a segment that has become external during the excavation-simulation phase;
 - σ_{ij}^0 : "Initial" stress tensor components expressed at this same point and existing in the soil prior to excavation.
- These "initial" stresses can be defined in one of two ways:
- Result of the phase preceding the excavation,
 - Initial stresses of the geostatic type defined during initialization of the first phase.
- n_x, n_y : Components of the vector normal to the given segment at this point;
 - λ : Coefficient with a value of between 0 and 1. This coefficient λ serves to apply a portion of the confinement-removal forces in order to simulate eventual tunnel face proximity.



- ! In the event the given coefficient is not set equal to 1 during the excavation phase, it would then become necessary to include the "complement" of these surface forces within a subsequent phase (tunnel face placed at infinity).
- ! It should be noted herein that this tool remains inactive in the special case where the model corresponds with Phase 1 and where initial stresses during this phase are zero.

Evaluation of the impact of a cavity upon an earth dike (analytical and numerical approaches) Application to the Val d'Orléans area (France)

The objective of this thesis is to study the interaction mechanisms between a cavity resulting from a karst collapse and a fluvial dike. The question that arises here is to evaluate the potential role of cavities beneath the dikes and their impact on the dike stability in normal and extreme flood conditions. Therefore, the first main point of the present work is to create a method to assess the influence of a dike on the stability of a cavity beneath it. Thereafter the second main point is to evaluate the stability of the dike slope when a cavity appears underneath without taking into account the collapse of the cavity.

To achieve the objectives of the thesis, the dike effect on the cavity stability was investigated by studying the influence of the cavity location relatively to the dike and the interaction mechanisms, in the way to prioritize the geometric and geotechnical parameters for a better evaluation of the risk of dike failure. Numerical and analytical approaches were used. An application is described based on the in situ observations and data for the Val d'Orléans area (France). This area is protected against the Loire's floods by 52 km of earth dikes (levees), in this area, more than 600 karstic sinkholes from 0.5 to 20 m diameter have been identified.

The first results of the analytical method show that the cavity instability can significantly increase when the cavity is located under the centre of the dike, and this can affect the stability of the dike when the cavity is sufficiently close to it. We also show that there is a significant effect of the cavity on the dike slope stability, especially in the saturation state (i.e. during extreme floods): cavity collapse can then contribute to dike collapse. A nonlinear numerical modeling (2D and 3D) was used to validate the analytical approach, and to highlight the influence of the different geometrical and geotechnical parameters of the dike and the cavity. The results of the numerical modeling confirmed those of the analytical method.

As operational conclusion, the results of the analytical model can be used to help assessing hazard due to the dike collapse taking into account the likelihood of an existing cavity, its position and diameter, and the thickness of the alluvium layer, regarding the data from the Val d'Orléans area.

Keywords: dike, karst, cavity, instability, analytical approach, modeling, Val d'Orléans, France.

Évaluation de l'impact d'une cavité sur une digue en terre (approches analytiques et numériques) Application au cas du Val d'Orléans (France)

L'objectif de cette thèse est d'étudier les mécanismes d'interaction entre une cavité résultant d'un effondrement karstique et une digue fluviale. Il s'agit d'évaluer le rôle potentiel des cavités sous les digues et leurs effets sur ces dernières dans des conditions hydrologiques normales et extrêmes. Par conséquent, le premier point est de proposer une méthode pour évaluer l'influence d'une digue sur la stabilité d'une cavité sous-jacente. Le deuxième point concerne la stabilité de la pente de la digue quand une cavité est présente à proximité, sans prise en compte de l'effondrement de la cavité.

Afin d'atteindre les objectifs de la thèse, les influences respectives du positionnement de la cavité par rapport à la digue et des paramètres géométriques et géotechniques ont été étudiées, par des approches analytiques et numériques, pour une meilleure évaluation du risque de rupture de la digue. Une application est proposée, basée sur des observations in situ et des données disponibles pour le secteur du Val d'Orléans (France). Cette zone est protégée des crues de la Loire par 52 km de digues fluviales (les levées), il y a été recensé plus de 600 effondrements karstiques (fontis) de 0,5 à 20 m de diamètre.

Les premiers résultats obtenus par la méthode analytique montrent que l'instabilité de la cavité peut augmenter de manière significative lorsqu'elle est se trouve sous le centre de la digue et que cela peut affecter la stabilité de la digue lorsqu'elle en est suffisamment proche. Nous montrons aussi que le risque d'instabilité de la digue augmente en raison de l'apparition des fontis provenant de l'effondrement de cavités karstiques. Ces résultats indiquent qu'il y a un effet significatif de la cavité sur la stabilité de la pente, surtout dans le cas de matériaux saturés (c'est-à-dire en période de forte crue de la Loire) : autrement dit, l'effondrement de la cavité peut contribuer à la rupture de la digue.

Une modélisation numérique non linéaire (2D et 3D) a été utilisée pour valider l'approche analytique et permettre la compréhension de l'influence des différents paramètres géométriques et géotechniques de la digue et de la cavité. Les résultats de la modélisation numérique ont confirmé ceux de la méthode analytique. Ces derniers peuvent donc être utilisés dans l'évaluation du risque de rupture de la digue en tenant compte de la probabilité d'existence d'une cavité sous-jacente, de sa position, de son diamètre, mais aussi de l'épaisseur de la couche d'alluvions. Les données numériques prises en compte sont celles du Val d'Orléans.

Mots-clés : digue, karst, cavité, instabilité, approche analytique, modélisation, Val d'Orléans.